



UNIVERSITEIT VAN PRETORIA
UNIVERSITY OF PRETORIA
YUNIBESITHI YA PRETORIA

SINKHOLE FORMATION DUE TO SUBSURFACE EROSION ABOVE UNDERMINED GROUND

JACOBUS BREYL

A dissertation submitted in partial fulfilment of the requirements for the degree of

MASTER OF ENGINEERING (GEOTECHNICAL ENGINEERING)

In the

FACULTY OF ENGINEERING

UNIVERSITY OF PRETORIA

December 2019

DISSERTATION SUMMARY

SINKHOLE FORMATION DUE TO SUBSURFACE EROSION ABOVE UNDERMINED GROUND

JACOBUS BREYL

Supervisor:	Professor SW Jacobsz
Department:	Civil Engineering
University:	University of Pretoria
Degree:	Master of Engineering (Geotechnical Engineering)

In November 2016, 38 sinkholes formed due to subsurface erosion above undermined ground on Donkerhoek farm near Sasolburg. The fact that the sinkholes formed more than 24 years after mining in the area ceased, emphasised the need for a method to predict the likelihood of sinkhole formation due to subsurface erosion. This is especially relevant for mining houses required to quantify their mine closure risks.

The purpose of this study was to investigate the mechanisms and soil properties involved in the formation of the 38 sinkholes on Donkerhoek farm through a fieldwork and laboratory testing programme and develop a method to predict the likelihood of sinkhole formation.

Three areas were selected for test pit excavation: an area with large sinkholes, one with small sinkholes and a third with no sinkholes but with a history of subsidence crack formation. The same mechanism of sinkhole formation was observed in both the large and small sinkhole areas: at the soil-rock interface, soil was being eroded into a subsidence crack in the rock, resulting in an upwards migrating cavity and the eventual formation of a sinkhole on surface when the cover over the cavity collapsed. This was the first time that this mechanism was observed in the Sasolburg area, having previously only been identified in the Secunda area.

The laboratory tests, carried out on samples obtained during the fieldwork, included foundation indicator, dispersivity, XRF and XRD, soil water retention curves, consolidated undrained triaxial and permeability tests. By comparison of the results from the different study areas, it was concluded that the larger sinkholes form in areas with highly dispersive soils, higher clay content, higher swell potential and a higher capacity to retain suctions when wetted.

The following soil properties and factors were identified as the main contributors to sinkhole formation:

- The strength of the lid, which is highly influenced by the unsaturated behaviour of the lid material. The lid strength determines the sinkhole diameter;
- The erodibility of the material which is influenced by dispersivity and the material obtaining a crumb structure due to desiccation;
- The activity of the soil, which influences the volume changes during drying and thereby the width and depth of desiccation cracks; and
- The thickness of the soil layer overlying the rockhead.

With the critical factors identified, the Van der Merwe method to predict sinkhole size was used as basis to develop an index method to predict the likelihood of sinkhole formation due to subsurface erosion above undermined ground. The method considers combinations of the following factor groups to express a high or low likelihood of the formation of large or small sinkholes in a particular area:

- The strength of the lid material, mainly influenced by the unsaturated behaviour of the soil;
- The capacity for cavity formation (CCF), which combines the dispersivity, erodibility and activity of the soil; and
- The influence of the thickness of the soil layer overlying the rock, evaluated by calculating the ratio between crack width in the rock and the soil layer thickness.

DECLARATION

I, the undersigned, hereby declare that:

- I understand what plagiarism is and I am aware of the University's policy in this regard;
- The work contained in this dissertation is my own original work;
- I did not refer to work of current or previous students, lecture notes, handbooks or any other study material without proper referencing;
- Where other people's work has been used this has been properly acknowledged and referenced;
- I have not allowed anyone to copy any part of my thesis;
- I have not previously in its entirety or in part submitted this thesis at any university for a degree.

Signature of student:



Name of student: **Jacobus Breyl**

Student number: **24462022**

Date: **9 December 2019**

ACKNOWLEDGEMENTS

I wish to express my appreciation to the following persons and organisations who made this dissertation possible:

- a) My Heavenly Father, for His provision and guidance throughout the project.
- b) My wife and two children for their encouragement, support and affording me the opportunity to carry out this work by giving up so much family time.
- c) My parents and my parents-in-law, for their interest, support and encouragement.
- d) Sasol Mining, especially Mr Trevor Davids, Mr Pierre Jordaan and the late Mr Chris Scheppel, for the research grant to carry out the project.
- e) Mrs Tharina van Rooy for granting permission for the fieldwork to be carried out on Donkerhoek and De Pan farms, Mr Douw Crous for providing information around the November 2016 sinkhole formation and Mr Mokkie Fourie for his assistance in the fieldwork.
- f) Professor SW Jacobsz for his enthusiasm, support and advice.
- g) Professor Nielen van der Merwe for sharing his experience and knowledge on the topic with me and for reviewing the initial results of the study.
- h) Dr Phil Paige-Green for assistance in the dispersivity analysis.
- i) Jones & Wagener for granting permission to carry out the study - especially Mrs Beth Steenekamp for typing the soil profiles and Mr Mzwakhe Dlamini and Mr Louis Geldenhuys for their assistance during the fieldwork.
- j) The staff at the civil engineering laboratory at the University of Pretoria.

TABLE OF CONTENTS

1	INTRODUCTION	1-1
1.1	Background.....	1-1
1.2	Objectives of the Study.....	1-2
1.3	Scope of the Study	1-3
1.4	Methodology.....	1-4
1.5	Organisation of the report.....	1-4
2	LITERATURE REVIEW.....	2-1
2.1	Introduction	2-1
2.2	Classification and terminology	2-1
2.3	SSE resulting in sinkholes above undermined ground in South Africa.....	2-3
2.3.1	Introduction	2-3
2.3.2	Historical occurrences of sinkholes due to SSE above undermined ground.....	2-3
2.3.3	Current understanding of the SSE and sinkhole formation process	2-7
2.3.4	Predictive model for undermining related SSE sinkhole size.....	2-21
2.3.5	Remaining questions about the SSE process in SA.....	2-26
2.4	SSE and sinkhole formation unrelated to undermining	2-28
2.4.1	Introduction	2-28
2.4.2	Factors influencing and mechanisms involved in SSE.....	2-28
2.4.3	Factors influencing and mechanisms involved in sinkhole formation.....	2-34
2.5	Further factors contributing to SSE and sinkhole formation	2-42
2.5.1	Erodibility and Dispersivity.....	2-42
2.5.2	Unsaturated nature of soils and suction measurement.....	2-48
2.6	Summary.....	2-51
3	FIELDWORK	3-1
3.1	Introduction	3-1
3.2	Site location and regional geology	3-1
3.3	Methodology.....	3-3
3.3.1	Selection of investigation areas	3-3
3.3.2	Investigation methods and positions.....	3-5
3.4	Results	3-11
3.4.1	Soil profiles.....	3-11
3.4.2	Observations	3-11

3.4.3	Discussion with farmers	3-25
3.4.4	Coarse Ash backfilling as remedial method	3-25
3.5	Summary of fieldwork results	3-26
4	EXPERIMENTAL PROGRAMME	4-1
4.1	Introduction	4-1
4.2	Laboratory tests and results	4-1
4.2.1	Grading and foundation indicator results.....	4-4
4.2.2	Dispersivity tests.....	4-7
4.2.3	XRD and XRF tests	4-13
4.2.4	Consolidated undrained triaxial and triaxial permeability tests.....	4-15
4.2.5	Soil water retention curves	4-16
4.3	Summary of laboratory test results	4-32
5	DISCUSSION	5-1
5.1	Introduction	5-1
5.2	Identification of critical soil parameters	5-1
5.2.1	Area 1 vs Area 3	5-3
5.2.2	Area 1 vs Area 2	5-5
5.2.3	Summary.....	5-7
5.3	Mechanisms involved in SSE and sinkhole formation	5-7
5.4	Evaluation of the Van der Merwe method.....	5-10
5.4.1	Application of method to the sinkhole at TP02	5-11
5.4.2	General comments on the Van der Merwe method	5-12
5.5	Proposed new method to predict likelihood	5-17
5.5.1	The revised method to predict the likelihood of sinkhole formation.....	5-17
5.5.2	Application to the three study areas.....	5-24
5.5.3	Application to the sinkholes in the Secunda area	5-25
5.6	Additional comments on observations.....	5-26
5.6.1	Subsidence is necessary for SSE to occur	5-26
5.6.2	Formation of V-shapes necessary for larger sinkhole formation.....	5-26
5.6.3	Crack vs fracture zone	5-26
5.6.4	Possibility of saturated soil below an unsaturated lid.....	5-28
5.6.5	Clamped rock at top of crack at TP06 and TP07.....	5-29
5.6.6	Termite activity at sinkhole positions.....	5-30
6	CONCLUSIONS AND RECOMMENDATIONS	6-1

6.1	Conclusions	6-1
6.2	Recommendations.....	6-3
7	REFERENCES.....	7-1

APPENDIX A: FIELDWORK RESULTS

APPENDIX B: LABORATORY TEST RESULTS

LIST OF TABLES

Table 2-1: Bell and Walker (2000) dispersivity rating system	2-48
Table 3-1: Summary of all investigation positions	3-6
Table 3-2: Fall duration for pebbles in to crack at TP06	3-23
Table 3-3: Summary of fieldwork results from three study areas	3-27
Table 4-1: Samples submitted for laboratory testing and tests carried out.....	4-2
Table 4-2: Distribution of tests between hillwash and residual sandstone	4-4
Table 4-3: Foundation indicators and soil classification for hillwash samples	4-5
Table 4-4: Foundation indicators and soil classification for residual sandstone samples.....	4-6
Table 4-5: Classification of residual sandstone samples	4-7
Table 4-6: Summary of dispersion test results on hillwash samples	4-8
Table 4-7: Hillwash results according to the Bell and Walker (2000) rating system	4-10
Table 4-8: Summary of dispersion test results on residual sandstone samples	4-11
Table 4-9: Residual sandstone results according to the Bell and Walker (2000) rating system.....	4-13
Table 4-10: XRD – Estimated mineralogical percentage by weight	4-14
Table 4-11: Consolidated undrained triaxial and triaxial permeability results	4-15
Table 4-12: Summary of suction measurement specimens and results of filter paper tests	4-20
Table 4-13: Decrease in matric suction from in-situ moisture content to saturation.....	4-29
Table 4-14: Summary of laboratory test results from the three study areas.	4-32
Table 5-1: Summary of fieldwork and laboratory test results for study areas.....	5-3
Table 5-2: Back calculated tensile strengths from TP02	5-11
Table 5-3: Likelihood of sinkhole formation based on factor combinations.....	5-22

LIST OF FIGURES

Figure 1-1: The largest sinkhole found in November 2016 (Van der Merwe, 2017a).....	1-1
Figure 2-1: Classification scheme for sinkholes based on the predominant process of their formation (White and White, 1992).	2-2
Figure 2-2: Photo of the first sinkhole at Sigma Colliery (left) and subterranean tunnel (right) (Van der Merwe, 1990).....	2-4
Figure 2-3: Strip like sinkholes with the soil arch above the subterranean tunnel (Van der Merwe, 1990).	2-5
Figure 2-4: Positions of sinkhole features relative to longwall panels at Sigma Colliery (Adapted from Van der Merwe, 1990).	2-6
Figure 2-5: Process of SSE resulting in sinkholes (adapted from Van der Merwe, 2017a and Van der Merwe and Madden, 2010).	2-9
Figure 2-6: Cross section through longwall panel showing subsidence and surface cracks as adapted from Van der Merwe, 2017a.....	2-10
Figure 2-7: Surface cracks as a result of tensile strain shortly after mining (Van der Merwe and Madden, 2010).....	2-11
Figure 2-8: Displaced open crack in rock with no crack in soil above (Wagener <i>et al.</i> , 1990).....	2-13
Figure 2-9: Cavities below ground surface with soil filled crack in rock below (Van der Merwe, 2018).	2-15
Figure 2-10: SSE schematic as found in Van der Merwe (2017a).....	2-16
Figure 2-11: Development of local depression in homogenous profile (Wagener <i>et al.</i> , 1990).....	2-17
Figure 2-12: Development of sinkhole in stratified profile (Wagener <i>et al.</i> , 1990).	2-18
Figure 2-13: Progressive failure of the cover to the subterranean cavity (Van der Merwe, 2018)....	2-20
Figure 2-14: Cross section through SSE sinkhole (Van der Merwe, 2018).....	2-23
Figure 2-15: Sinkhole cover failure modes (Van der Merwe, 2018).....	2-25
Figure 2-16: Image of soil pipes (Beckedahl, 1998).....	2-29
Figure 2-17: Shrinkage crack in cultivated field (Marr, 1955).....	2-31
Figure 2-18: Enlargement of shrinkage crack by tunnel erosion (Dunne, 1990).....	2-33

Figure 2-19: Sinkholes due to SSE in Arizona, USA (Hoffmann <i>et al.</i> , 1998).	2-35
Figure 2-20: Progressive failure mechanisms (Oberholzer, 2017).	2-38
Figure 2-21: Head drop for hydraulic fracture vs rate of head drop (Tharp, 2003).	2-39
Figure 2-22: Location of some of the crack outlets in the hillside slope (Xu <i>et al.</i> , 2011).	2-40
Figure 2-23: Diagram of determination of dispersion potential as a function of ESP and CEC per 100g clay (Gerber and Harmse, 1987).	2-46
Figure 2-24: Potential dispersivity based on TDS and percentage sodium (Sherard <i>et al.</i> 1976a)....	2-47
Figure 2-25: The SWRC framework and terminology from Al Haj and Standing (2016).	2-50
Figure 3-1: Location of Donkerhoek and De Pan farms near Sasolburg with investigation portions indicated.	3-2
Figure 3-2: Location of sinkholes on Donkerhoek farm.	3-3
Figure 3-3: Location of sinkholes on De Pan farm.	3-4
Figure 3-4: Location of area with subsidence cracks, but no record of sinkholes.	3-5
Figure 3-5: Location of all investigation positions on Donkerhoek farm.	3-7
Figure 3-6: Location of all investigation positions on De Pan farm.	3-7
Figure 3-7: 20 ton excavator excavating at TP06.	3-8
Figure 3-8: Location of three selected study areas on Donkerhoek farm.	3-9
Figure 3-9: Percussion borehole rig drilling BH01.	3-10
Figure 3-10: Test pit layout in Area 1.	3-12
Figure 3-11: Looking downwards into TP01 showing the infilled cracks in the residual sandstone and rock below.	3-13
Figure 3-12: The partially collapsed sinkhole at TP02.	3-14
Figure 3-13: V-shaped zone in TP03 above the collapsed tunnel and crack in the rock below.	3-15
Figure 3-14: View downwards into TP18 showing the subterranean tunnel running from right to left.	3-15
Figure 3-15: Cross section through each test pit in Area 1.	3-16
Figure 3-16: Layout of test pits and boreholes in Area 2.	3-17
Figure 3-17: Trench in Area 2 at TP10 and hillwash infilled crack in the residual sandstone.	3-18
Figure 3-18: Layout of test pits in Area 3.	3-19

Figure 3-19: Typical sinkhole (0,3m diameter) in Area 3 and subterranean tunnel (0,45m deep)....	3-20
Figure 3-20: V-shape infilled with coarse ash above crack in sandstone rock in Area 3.	3-21
Figure 3-21: Looking down into the empty V-shape of the sinkhole at TP06.....	3-22
Figure 3-22: Crack in the rock at TP06 covered with sandstone and open below.....	3-22
Figure 3-23: Termite activity in the side of sinkhole DSC109 (left) and TP10 (right).	3-24
Figure 3-24: Historical sinkhole backfilled with ash (TP15).....	3-26
Figure 4-1: Grading curves for hillwash in Area 1, 2 and 3 and two test pits on De Pan.....	4-4
Figure 4-2: Grading curves for residual sandstone in Area 1, 2 and 3.	4-6
Figure 4-3: ESP versus CEC per 100g clay for hillwash samples.	4-9
Figure 4-4: %Na versus TDS for hillwash samples.....	4-9
Figure 4-5: ESP versus CEC per 100g clay for residual sandstone samples.	4-11
Figure 4-6: %Na versus TDS for residual sandstone samples.	4-12
Figure 4-7: Specimen carved out from clock sample into oedometer ring.....	4-17
Figure 4-8: Wetting of specimens to target moisture content.....	4-18
Figure 4-9: Swelling of the specimen upon wetting.	4-19
Figure 4-10: Specimens after the completion of the wetting curve tests.....	4-19
Figure 4-11: Primary drying curves for residual sandstone specimens.	4-21
Figure 4-12: Primary wetting curves for residual sandstone specimens.....	4-21
Figure 4-13: Primary drying and wetting curves for Area 1.....	4-21
Figure 4-14: Primary drying and wetting curves for Area 2.....	4-22
Figure 4-15: Primary drying and wetting curves for Area 3.....	4-22
Figure 4-16: Slurry paste used to seal tensiometer into drilled hole.....	4-24
Figure 4-17: Experimental set-up to measure primary drying curves with tensiometers.	4-24
Figure 4-18: Matric suction and total mass change for specimen C6 (Area 2).	4-25
Figure 4-19: Primary drying curve from tensiometer data with filter paper results for Area 1.....	4-26
Figure 4-20: Primary drying curve from tensiometer data with filter paper results for Area 2.....	4-26
Figure 4-21: Primary drying curve from tensiometer data with filter paper results for Area 3.....	4-27
Figure 4-22: All primary drying curves from tensiometer tests combined.....	4-27

Figure 4-23: Tensiometer PDCs with filter paper PWC and moisture content variation added.....	4-29
Figure 4-24: Hydraulic conductivity for change in matric suction for the three study areas.....	4-31
Figure 5-1: Cross sections through each test pit in Area 1.	5-8
Figure 5-2: Arching support along the perimeter of the lid.	5-13
Figure 5-3: Sinkhole width for circular and rectangular shapes for varying crack width.....	5-15
Figure 5-4: Rectangular and circular shape of sinkhole formation.....	5-16
Figure 5-5: Relationship between w_h and w_o/t_s for rectangular and circular cavities for a crack depth of 25m.	5-19
Figure 5-6: Relationship between w_h and w_o/t_s for rectangular and circular cavities for a crack depth of 5m.	5-20
Figure 5-7: Relationship between w_h and w_o/t_s for rectangular and circular cavities for a crack depth of 5m and lid thickness equal to zero.....	5-21
Figure 5-8: Axis system for graphical representation of factor combinations.....	5-22
Figure 5-9: Combinations 1 and 5 showing a high likelihood of large sinkholes (left) and a high likelihood of small sinkholes (right).	5-23
Figure 5-10: Combinations 2, 3, 6 and 7 showing a low likelihood for large sinkholes (left) and a low likelihood for small sinkholes (right).....	5-23
Figure 5-11: Combinations 4 and 8 showing both large (left) and small (right) sinkholes are unlikely.	5-24
Figure 5-12: The fracture zone at the bottom of TP15.	5-27
Figure 5-13: Possible mechanism for clamping of rock fragment in top of crack.....	5-29
Figure 5-14: Termite activity within hillwash infilled crack in residual sandstone at TP10.	5-30

LIST OF SYMBOLS

w_h = cavity width (m)

t_s = thickness of soil layer above rock (m)

t_l = thickness of the lid covering the subterranean cavity (m)

t_c = depth of crack in the rock (m)

w_c = width of crack in the rock (m)

α = inclination of the V-Shape sides above the horizontal ($^\circ$).

S_m = maximum amount of subsidence in the centre of the mining panel (m)

σ_t = tensile strength of the cover material (kPa)

F = point load (kN)

ν = Poisson's ratio

r = radius of the sinkhole (m)

γ = unit distributed weight of the cover material ($\rho g t_l$)

r = radius of the cavity (m)

c = cohesion of the upper soil layer (kPa)

ϕ = angle of internal friction of the soil

ρ = density of the material (kg/m^3)

S_r = degree of saturation (%)

1 INTRODUCTION

1.1 BACKGROUND

In November 2016, 38 sinkholes were noticed in a corn field on the farm Donkerhoek, located to the south-west of Sasolburg (Van der Merwe, 2017a). The largest sinkhole was 1,6m deep with a diameter of 1,5m as shown in Figure 1-1. At the time, the question was asked whether the sinkholes were the result of subsurface erosion due to undermining. Subsurface erosion is a process which occurs when material below natural ground level is transported to a deeper underlying cavity resulting in a shallow cavity below ground level. Once the cover of the cavity collapses, a sinkhole is formed. In this case, the deeper lying cavity could have been the result of undermining activity in the area.



Figure 1-1: The largest sinkhole found in November 2016 (Van der Merwe, 2017a)

The suspicion that subsurface erosion due to undermining was the cause of the sinkholes was substantiated by the history of subsurface erosion related sinkholes in the area. During the 1980s and 1990s, Donkerhoek and the adjacent farms were undermined for coal extraction

purposes as part of the operations of Sigma Colliery (Van der Merwe, 2017a). When sinkholes formed during this period, investigations indicated a positive link between the sinkhole formation, subsurface erosion and the undermining (Van der Merwe, 1990).

To answer the question about the cause of the November 2016 sinkholes, a specialist investigation was carried out which found evidence of a positive link to subsurface erosion as the cause (Van der Merwe, 2017a).

Sinkhole formation by subsurface erosion is a time dependant phenomenon. In some cases sinkholes have formed up to 100 years after mining (Van der Merwe, 2018). All coal extraction operations at Sigma Colliery have ceased, and in the area underlying the November 2016 sinkholes, the last coal was extracted in 1992 (Scheppel, 2017b). The appearance of the sinkholes 24 years after mining leads to the question of which other areas of Sigma Colliery are at risk of subsurface erosion and sinkhole formation; a question which can only be answered if, as a starting point, a method for predicting the likelihood of sinkhole formation is available.

Although Van der Merwe (2018) presented a method to estimate the maximum width of a sinkhole due to subsurface erosion above undermined ground, “many important questions that cannot be answered with the current level of knowledge” remain (Van der Merwe, 2017a). As such, a method to predict the likelihood of sinkhole formation due to subsurface erosion has not been developed. The formation of the November 2016 sinkholes presented an ideal opportunity for the further investigation of the subsurface erosion phenomenon to assist in developing a prediction method.

This research project aimed to develop such a method by identifying the critical mechanisms and soil parameters relevant to the process through a fieldwork and laboratory testing programme.

1.2 OBJECTIVES OF THE STUDY

The goal of this research project was to improve the understanding of subsurface erosion resulting in sinkholes above undermined ground and develop a method to predict the likelihood of future sinkhole formation. To achieve this, the following objectives were set out:

- Identification of the mechanism at work which results in the sinkholes by excavating test pits through existing sinkholes.

- Understanding and identifying the critical soil properties involved in subsurface erosion and sinkhole formation through laboratory tests carried out on samples obtained from the test pits. The laboratory tests included foundation indicator tests and grading analyses, consolidated undrained triaxial tests, flexible wall permeability tests, mineralogy, dispersivity and determination of soil water retention curves (suction response to changes in moisture content).

For comparative purposes, tests were also carried out on samples collected from areas with similar undermining and subsidence characteristics, but with no records of sinkhole formation.

- Evaluation of the current published method to predict the maximum sinkhole size against the results of the field work and laboratory testing and, where applicable, building on the current method to develop a method to predict the likelihood of sinkhole formation.

1.3 SCOPE OF THE STUDY

The scope of this research project was limited to subsurface erosion and sinkhole formation caused by undermining related subsidence. The fieldwork and experimental programme included an assessment of only some of the sinkholes which appeared on Donkerhoek farm in November 2016. Although some test pits were excavated on De Pan (the neighbouring farm to the south) these results were not evaluated and discussed in detail. The study focussed on the properties of the soil profile only and the properties of the underlying bedrock were not investigated.

Furthermore, the following aspects were excluded from the scope of the study:

- Undermining stability assessments and subsidence calculations – reliance was made on reports by others to obtain the relevant information.
- Rainfall data analysis
- Topographical analysis
- Groundwater analysis
- A detailed assessment of the influence of plant roots on the tensile strength of the uppermost soil layer.

1.4 METHODOLOGY

To investigate the mechanism and soil properties involved in subsurface erosion and sinkhole formation, a four-phase methodology was employed.

Firstly, a literature review was carried out to study the history of subsurface erosion above undermined ground in South Africa, subsurface erosion in general including the mechanisms and soil properties involved, the mechanisms of sinkhole formation in general and a study of the non-standardised laboratory tests to evaluate dispersivity and soil water retention curves.

The literature review was followed by the fieldwork component in which test pits were excavated to observe the mechanisms involved and to collect samples for laboratory testing.

Thirdly, the laboratory testing programme was carried out to determine the soil properties of the samples collected during the fieldwork.

The last phase comprised the analysis of the fieldwork and laboratory test results and the development of a prediction method.

1.5 ORGANISATION OF THE REPORT

The report consists of the following chapters and appendices:

- Chapter 1 serves as introduction to the report.
- Chapter 2 contains a review of the literature available on the topic to substantiate the fieldwork and laboratory tests.
- Chapter 3 describes the fieldwork carried out, presents the results and includes a limited discussion thereof needed to understand the scope of the laboratory testing in the following chapter.
- Chapter 4 comprises a description of the experimental programme and laboratory testing carried out, presents the results and offers a brief discussion to summarise to results.
- Chapter 5 includes a discussion of the fieldwork and laboratory test results, an evaluation of the existing prediction method against the results and the description of a new method to predict the likelihood of sinkhole formation.
- Chapter 6 contains the conclusions of the study and recommendations for further research.

A list of references and the Appendices are included at the end of the report. The Appendices are as follows:

- Appendix A: Fieldwork results
- Appendix B: Laboratory test results.

2 LITERATURE REVIEW

2.1 INTRODUCTION

This chapter provides a review of literature on the research topic to contextualise the problem and ensure the focus and relevancy of the fieldwork and experimental programme. In section 2.2 the process of subsurface erosion (hereafter referred to as SSE) resulting in sinkholes is first classified within the broader framework of sinkhole formation to provide context. Section 2.3 focusses solely on SSE resulting in sinkholes *above undermined ground in South Africa*; an account of the historical occurrences is given, a detailed discussion of the current understanding of the process is presented and a method to predict the maximum sinkhole size is described.

As the phenomenon of SSE resulting in sinkholes is not only limited to undermined areas in South Africa, the net is cast wider in section 2.4 where factors and mechanisms involved in the process elsewhere in South Africa and beyond are presented. Specific attention is paid to the mechanisms of sinkhole formation. In the last two sections of this chapter, a review of soil dispersion theory and the related laboratory tests are given followed by a short description of the behaviour of unsaturated soils. The chapter concludes with the hypothesis.

2.2 CLASSIFICATION AND TERMINOLOGY

The process of SSE and the formation of sinkholes as described by Van der Merwe (2017a and 2018) essentially comprises two separate processes – each with their own mechanisms: the removal of material below ground level to another location and the upwards migration of the cavity which eventually results in a sinkhole on surface.

It is important to note that not all examples of subsurface erosion result in sinkholes. Beckedahl (1998) and Jones (1981) described several types of subsurface erosion where no sinkholes are formed. The formation of “soil pipes” through earth embankments (Elges, 1985) also illustrated this point. Conversely, many types of sinkholes are caused by other factors than subsurface erosion, as detailed in Waltham and Fookes (2003).

Both processes have been independently researched and published on extensively. Yet, this research project deals with the combination of the two, a topic which is not uncommon in literature. To place the phenomenon in context amongst other sinkholes, reference is made to Figure 2-1 in which White and White (1992) presented a classification scheme for sinkholes according to the predominant process of their formation. The first two categories are sinkholes

caused by bedrock dissolution and bedrock collapse. Sinkholes from subsurface erosion fits into the third category and are referred to as “cover collapse sinks” or “ravelling sinks” caused by soil piping.

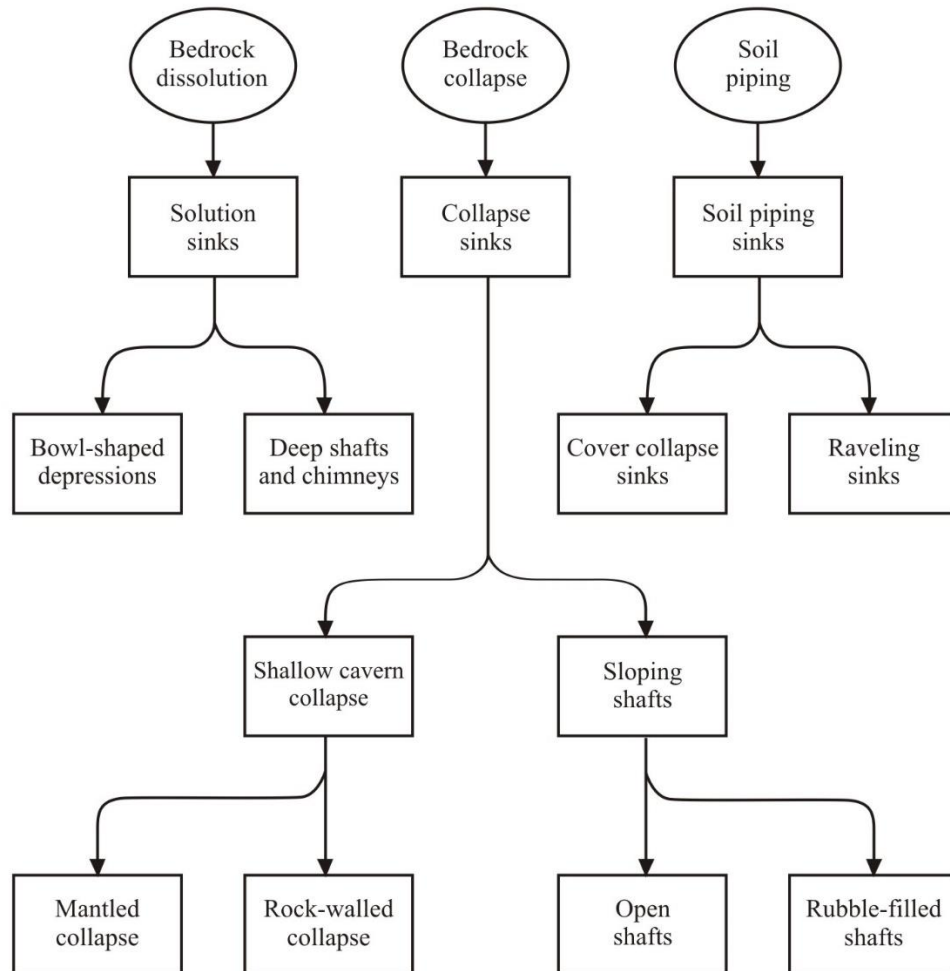


Figure 2-1: Classification scheme for sinkholes based on the predominant process of their formation (White and White, 1992).

Other authors present different sinkhole classification systems and terminology. These are not discussed in detail here and only the relevant classifications are summarised, as pertaining to sinkholes formed by subsurface erosion. Beck (1984) referred to them as “ravelling sinks” or “subsidence sinkholes”, whilst Culshaw and Waltham (1987) repeated the subsidence sinkhole reference and further differentiated between slow subsidence in areas with non-cohesive overburden and dropouts occurring in areas where a cohesive overburden cover collapses into the cavity. Waltham and Fookes (2003) and Waltham *et al.* (2005) also referred to the

phenomenon as “dropouts” while Beck (2011) and Chen and Beck (1989) also referred to cover collapse sinkholes.

Van der Merwe and Madden (2010) specifically referred to sinkholes caused by subsurface erosion as “potholes” and reserved the term “sinkhole” for sinkholes caused by crown or intersection failure of mined-out cavities. It is believed that the difference in nomenclature is to clearly distinguish between the two types of sinkholes caused by undermining activity.

For the purposes of this research project, the cavities which form on surface are referred to as sinkholes. Included in this definition is the formation of a soil bridge overlying the cavity which upon collapse results in a sinkhole.

2.3 SSE RESULTING IN SINKHOLES ABOVE UNDERMINED GROUND IN SOUTH AFRICA

2.3.1 Introduction

In this section, the current available literature on sinkhole formation due to SSE above undermined ground in South Africa is summarised. The purpose is to present a clear picture of the current understanding of the problem in South Africa. After a summary of historical occurrences of SSE sinkholes, the process is described in detail and a proposed method for the prediction of sinkhole size, presented.

The study of sinkholes due to SSE above undermined ground straddles the fields of rock and soil mechanics as mentioned by Van der Merwe (2017c) and the bulk of the South African research done on the topic has been done by rock engineers. As such, some of the terminology used in literature are not typical terms from the geotechnical engineering framework. In order to accurately reflect the literature reviewed, the original terminology is kept and only where relevant, does the author comment on and suggest alternative terminology to communicate the engineering concepts in the geotechnical context.

2.3.2 Historical occurrences of sinkholes due to SSE above undermined ground

Van der Merwe (1990) described the first recorded instance of SSE resulting in sinkhole formation related to undermining activity in South Africa. The first sinkhole was reported by a farmer in the first half of 1985 on the farm “Die Pan” in an area which had been undermined by Sigma Colliery.

Van der Merwe (1990) stated that a “sinkhole like depression was found” with dimensions of 8m x 5m in plan with a depth of 7m. Van der Merwe (2017a) referred to the same sinkhole and gives a diameter of 4m. It is possible that the earlier reference refers to the dimensions at ground level where some collapse of the sidewalls could have occurred increasing the plan dimensions and that the later reference refers to the throat of the sinkhole. In any case, based on current records, this is the largest sinkhole formed by undermining related SSE as will be shown in the remainder of the literature review.

On either side of the sinkhole, a subterranean tunnel extended outwards with a width of 1m and a height of 1,5m. Photographs of the first sinkhole and subterranean tunnel are shown in Figure 2-2.

In the immediate vicinity of the first sinkhole, another two strip like holes were found, according to Van der Merwe (1990). The holes were approximately 1,5m to 2m deep, 1m wide with a length of 5m to 7m. A subterranean tunnel, similar to the first sinkhole, was found linking the holes with a soil arch, roughly 30cm thick, bridging over the tunnel in between the holes as shown in Figure 2-3.



Figure 2-2: Photo of the first sinkhole at Sigma Colliery (left) and subterranean tunnel (right) (Van der Merwe, 1990)



Figure 2-3: Strip like sinkholes with the soil arch above the subterranean tunnel (Van der Merwe, 1990).

When the position of the first sinkholes was compared to the geometry of the underground mine workings, it was noted that the sinkholes appeared near the edges of a longwall panel, in the zone where tensile cracks were formed by subsidence due to the undermining. No mining had taken place in that area since 1978, meaning almost 8 years had passed before the sinkholes appeared (Van der Merwe, 1990).

Subsequent to the finding of the first sinkholes, an additional investigation was launched to determine if there were any other areas on Sigma Colliery where sinkholes had formed. A total of 42 additional holes were found in an area above three longwall panels, also located on “Die Pan”. The holes were smaller than the first ones, but were also strip like with dimensions 1m to 5m long, 0,5m to 1m wide and 1m deep. Some were roughly circular with diameters of 0,5m to 1m and 1m deep. Comparison with the undermining layout showed that most of these holes formed along the perimeter of the longwall panels in 3-seam as shown in Figure 2-4. The sinkholes noted in the centre of the panel are along the perimeter of another panel mined on the 2B-seam (Scheppel, 2017b), which underlies 3-seam.

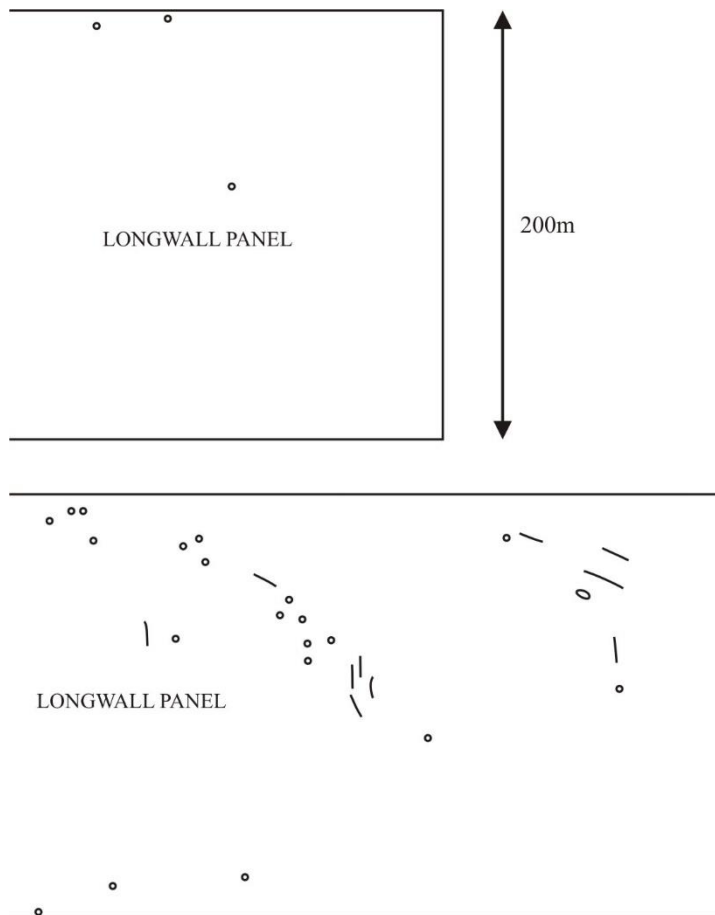


Figure 2-4: Positions of sinkhole features relative to longwall panels at Sigma Colliery (Adapted from Van der Merwe, 1990).

Van der Merwe (2017a) showed the positions of additional sinkholes found in 2006 located above undermined areas on “Donkerhoek” farm. No details on the dimensions of the sinkholes were given.

The most recent record of sinkholes at Sigma Colliery is the 38 sinkholes which appeared in November 2016. According to Van der Merwe (2017a) the diameter of the sinkholes ranged from a few centimetres to more than a metre and the depth from a few centimetres to 1,6m. The largest hole had a diameter of 1,5m and depth of 1,6m, and is depicted in Figure 1-1 (above).

Other than Sigma Colliery near Sasolburg, the only other area in South Africa with SSE related sinkholes due to undermining found in available literature is above two undermined areas near Secunda: Middelbult Mine and Brandspruit Colliery.

According to Van der Merwe (1990), the first holes were noticed towards the end of 1988 on Middelbult farm, and were approximately 0,5m in diameter and 0,5m deep. Wagener *et al.* (1990) carried out a detailed investigation of a portion of Middelbult farm and located more than 150 sinkhole features. Most of the features were smaller than 0,5m in diameter and less than 0,5m deep.

During December 1989, a study was carried out to evaluate sinkhole features above Brandspruit Colliery and 72 features were identified. However, Van der Merwe (1990) reported that following the detailed assessment, it was noticed that some of the features recorded were animal burrows and thus the data was discarded.

It is not only in South Africa where sinkholes due to SSE above undermined ground have occurred. Singh and Dhar (1997) described the formation of a sinkhole after a fault line was intersected during the advancement of the underground workings in a coal mine in India. Some of the weathered, friable sandstone in the overburden material was eroded into the underground workings along the fault line resulting in the formation of shallow cavities close to the surface leading to a sinkhole that formed within 7 days of the fault being intersected.

Culshaw and Waltham (1987) referred to the opening of existing fissures in competent rock as a result of tensile strain caused by subsidence due to longwall mining in England. These result in the formation of subsurface cavities which may have led to sinkhole formation.

Van der Merwe (2017a) referred to examples of “piping” sinkholes in the Long Beach area of California which resulted from subsidence cracks caused by oil extraction and similar sinkholes in England and Wales caused by high extraction coal mining. Bell (1988) referred to several examples of fissuring and cracking due to subsidence caused by the extraction of fluids, being either groundwater, oil, natural gas or brines. The maximum fissure width reported is 6,4cm and occasionally, several closely spaced, parallel fissures have been noticed on surface.

2.3.3 Current understanding of the SSE and sinkhole formation process

Introduction

Van der Merwe (2017a) listed three requirements for sinkhole formation through SSE:

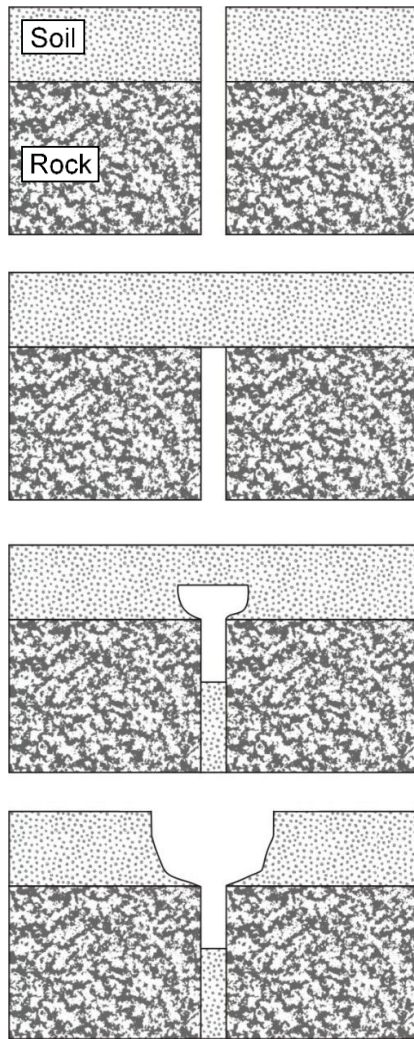
- A reservoir must exist into which the volume of soil can be transported.
- A medium must be present to erode the soil particles into the reservoir.

- The soil must be transportable and a measure of stratification is required, i.e. the upper portion of the soil profile must be less erodible than the lower profile with a capacity to sustain the formation of an arch over the cavity below.

This section reviews the factors influencing and the mechanisms present in the SSE and sinkhole formation processes. As the scope of this research project is limited to the properties of the soil within which the SSE occurs, this section places more emphasis on the second and third requirements listed above, namely the transport medium and the erodibility and arching ability of the soil. Where relevant, salient references are made to the properties of the reservoirs into which the soil is transported.

SSE and sinkhole formation process

The most recent detailed description of the SSE process causing sinkholes over undermined ground is found in Van der Merwe (2017a). The four-phase process is first summarised in Figure 2-5. The schematics in the figure were obtained from Van der Merwe and Madden (2010) while the text is mainly from Van der Merwe (2017a). Each of the four phases is then expanded on in more detail.

**Phase 1**

- Subsidence of the ground surface occurs following the extraction of coal.
- Cracks develop on the surface around the perimeter of the subsidence area. The cracks extend from surface through the soil overlying the rock mass and into the rock mass itself.

Phase 2

- After one or more rainy seasons, soil washes into the cracks in the soil and they disappear. However, the cracks in the underlying rock mass remain open

Phase 3

- Over time, as the soil above the rock is saturated with water, soil particles are washed into the crack, resulting in the formation of a cavity below surface.
- If the top soil layer is less "transportable" than the underlying layer directly above the rock, a lid is formed bridging over the cavity

Phase 4

- When the cavity reaches a critical size, the lid fails and the sinkhole appears.

Figure 2-5: Process of SSE resulting in sinkholes (adapted from Van der Merwe, 2017a and Van der Merwe and Madden, 2010).

Phase 1 – Subsidence and crack formation

The first phase in the SSE and sinkhole formation process is discussed in more detail.

The extraction of coal through longwalling or pillar extraction invariably leads to subsidence and crack formation, because the roof of the mined-out cavity is left unsupported (Van der Merwe and Madden, 2010). The formation process is illustrated in Figure 2-6, showing a typical cross section through a longwall panel with the width of the panel across the page and the length of the panel into the page. Typically, the longwall panels at Sigma Colliery are 200m wide and 1000m long; the typical mining height (height of the cavity once the coal has been removed) is 4m and the mining depth 120m (Scheppel, 2017b).

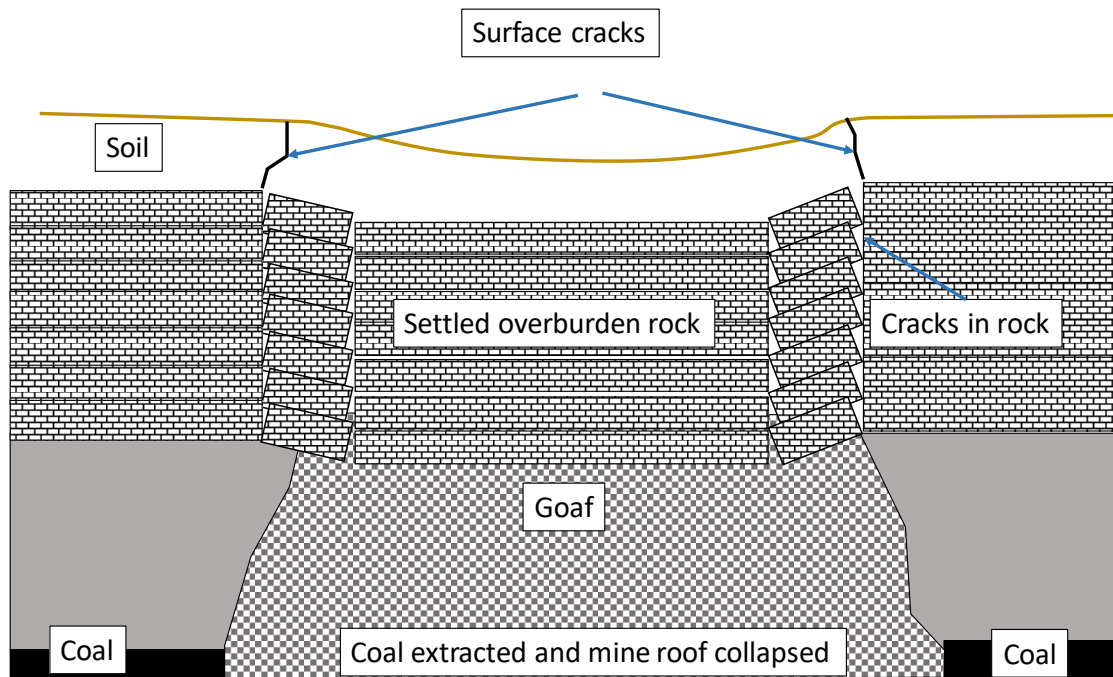


Figure 2-6: Cross section through longwall panel showing subsidence and surface cracks as adapted from Van der Merwe, 2017a.

Once the roof has collapsed, the collapsed area extends vertically upwards until the top of the collapsed material makes contact with the overlying uncollapsed rock. The collapsed material is called goaf. Bulking during the collapse process leads to void formation within the goaf. As such, the goaf always occupies a larger volume than the original rock. With time, failure of the uncollapsed overlying strata occurs leading to compression of the goaf and subsidence on surface (Van der Merwe and Madden, 2010). To give perspective, subsidence of more than 4m was recorded at Sigma Colliery where double seam longwalling was carried out (Van der Merwe, 2017a).

Although the maximum subsidence typically occurs in the centre of the panel as shown in Figure 2-6, the largest surface cracks appear along the perimeter of the panels where the tensile strain is the greatest (Van der Merwe and Madden, 2010). Examples of surface cracks are shown in Figure 2-7. Note the matchbox included in both photos for scaling purposes.



Figure 2-7: Surface cracks as a result of tensile strain shortly after mining (Van der Merwe and Madden, 2010).

It will be shown in the subsequent sections that the subsidence cracks within the rock mass are the receptacles for the eroded soil, and therefore their properties play a vital role in sinkhole formation. The location of the cracks will determine where sinkholes are likely to form and the width and depth of the crack limit the receptacle volume and thereby the size of sinkhole likely to form. The location, width and depth of the cracks are discussed in more detail below.

Regarding the location of the cracks relative to the *longwall panel* perimeter, Wagener *et al.* (1990) described crack formation on surface at an angle of 15° to the vertical from the edge of the panel at depth, which corresponds to the offset of between 20m and 30m given by Van der Merwe (2017a) – for similar mining depths. Van der Merwe (2017a) further pointed out that crack formation is not limited to the edges of the panels, with 80% of holes forming around the perimeter and 20% forming on the interior of the panel.

Above *high extraction panels* the distinction in crack location is not as clear. Van der Merwe (2017a) stated that sinkholes form randomly above high extraction panels, while Wagener *et al.* (1990) found cracks on the interior of the panels and along the perimeter.

Wagener *et al.* (1990) also found sinkholes above a fracture zone on the interior of the high extraction panels, where no clear crack could be identified. It was assumed that transportation of the material must have taken place along minute cracks or fractures.

To compound the issue of crack location even further, Van der Merwe (2017a) concluded that some of the November 2016 sinkholes on Donkerhoek farm could have formed above *bord and pillar areas* where pillar failure had occurred.

It is evident that since SSE only occurs where subsidence cracks have formed, any method developed to predict the likelihood of sinkhole formation needs to include the prediction of subsidence cracks as well.

As far as the width of the cracks are concerned, this is dependent on the tensile strain which depends on the magnitude of subsidence. Van der Merwe and Madden (2010) lists five subsidence classes with predicted crack widths ranging from barely noticeable to more than 500mm (see Figure 2-7). Wagener *et al.* (1990) recorded crack widths of 10mm to 50mm in the Secunda area and Van der Merwe (1990) reported crack widths between 100mm and 200mm at Sigma Colliery.

The cracks are seldom continuous as they tend to form where existing joints in the rock mass have opened under the tensile strain (Van der Merwe, 2017a). Typically, two or three cracks form on surface (Van der Merwe, 1990), running parallel to the edge of the panel as stated by Van der Merwe (2017a) with an offset of 1m to 2m between the cracks (Wagener *et al.*, 1990).

As far as the depth of the cracks into the underlying rock is concerned, Wagener *et al.* (1990) carried out an extensive investigation in the Secunda area and could not establish how far the surface cracks extended into the underlying rock. They mentioned that the possibility of the cracks extending all the way into the goaf could not be excluded. Van der Merwe (2018) pointed out that it is unlikely that the cracks will be continuous up to the goaf material, since horizontal displacement along the bedding planes occur, as is shown in Figure 2-8. Based on back calculations of the crack depth from observed sinkhole cavities, Van der Merwe (2018) recommended a continuous crack depth of 25m as reasonable for calculation purposes.

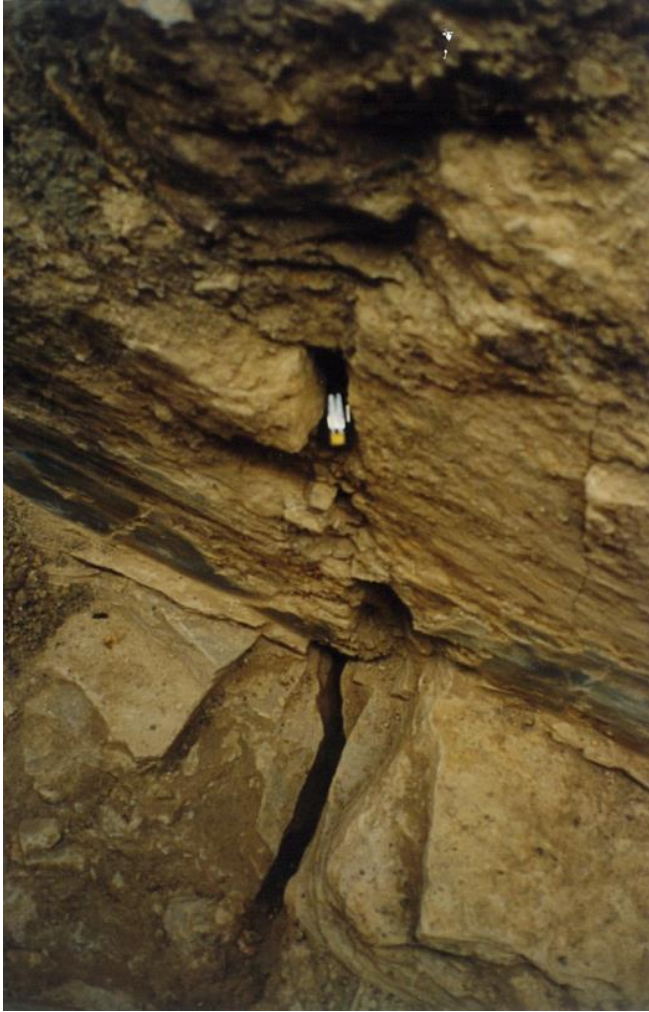


Figure 2-8: Displaced open crack in rock with no crack in soil above (Wagener *et al.*, 1990).

Regarding the duration between mining and first appearance of the cracks, Van der Merwe and Madden (2010) stated that for longwall panels, 90% of the subsidence occur within 6 weeks of mining with the remaining 10% occurring over several years.

Phase 2 – Surface cracks are filled with in-washed soil

During the second phase of the SSE process summarised above and in Figure 2-5, soil washes into the crack after one or two rainy seasons leaving a scar on surface. However, the crack in the rock remains open (Van der Merwe and Madden, 2010 and Van der Merwe, 2017a). An open crack in the rock with no crack in the soil above is shown in Figure 2-8 (above).

It is the author's opinion that there may be other factors contributing to the sealing of the cracks in the soil after one or two rainy seasons, such as swelling of the clay due to an increase in moisture content. However, no reference to this possibility was found in literature on SSE above undermined ground.

Phase 3 – SSE commences and cavity is formed below ground

The third phase of the SSE process comprises the formation and enlargement of the cavity below ground, covered by a “lid” of soil. This section describes the mechanisms and soil properties found in literature in more detail.

According to Van der Merwe (1990), *water* is seen as the *erosion agent* driving the process and has a twofold effect: firstly it “reduces the cohesion and friction of the soil” which leads to greater “transportability” and secondly “it serves as the direct mechanical transport agent of soil particles”. Van der Merwe (2017a) further added that by implication, the rate of SSE and sinkhole development will not be constant, but will fluctuate with the availability of water, with the highest rates occurring when high rainfall occurs following an extended period of drought.

But where do the soil particles get eroded to? The answer to the *reservoir location* question has developed over time. Van der Merwe (1990) viewed the void filled goaf as the reservoir into which the soil particles are eroded and the subsidence cracks as the connection between the goaf and the soil being eroded. This point of view was based on observations made at Sigma Colliery at the time. When Wagener *et al.* (1990) excavated trenches perpendicular to the subsidence cracks in the Secunda area in 1990, the observation was made that the cracks themselves could also be the reservoir as shown in Figure 2-9. Van der Merwe (2018) referred to the trenches excavated near Secunda and stated that this is where the hypothesized process was visually confirmed. To date, this phenomenon (namely that the cracks act as the reservoir) has not been visually confirmed at Sigma Colliery (Van der Merwe 2017d).

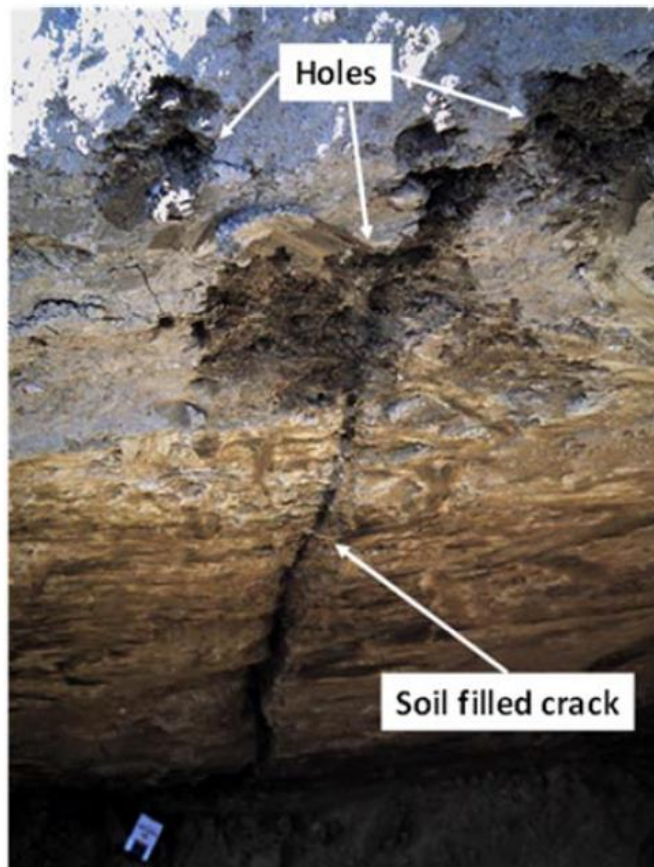


Figure 2-9: Cavities below ground surface with soil filled crack in rock below (Van der Merwe, 2018).

As the soil is eroded downwards, a cavity is formed. Different views are expressed about the *location of the cavity below ground*. If the cavity formation process is shown in Figure 2-5 is compared with Figure 2-10, two points are noted:

- Firstly, in Figure 2-10, material being eroded into the crack chokes in the crack, resulting in the entire crack not being filled up. In Figure 2-5, the material fills the crack from the bottom upwards.
- Secondly, in Figure 2-10, the cavity does not form directly above the rock, but rather at a shallower depth close to surface. By implication, no more material is eroded into the crack before the lid at the top collapses and at the time of collapse, the crack in the rock is not visible from surface. In Figure 2-5, the cavity forms directly above the rock and material is eroded into the crack in the rock until the lid collapses. Once collapsed, an open cavity is found all the way from surface to the crack in the rock.

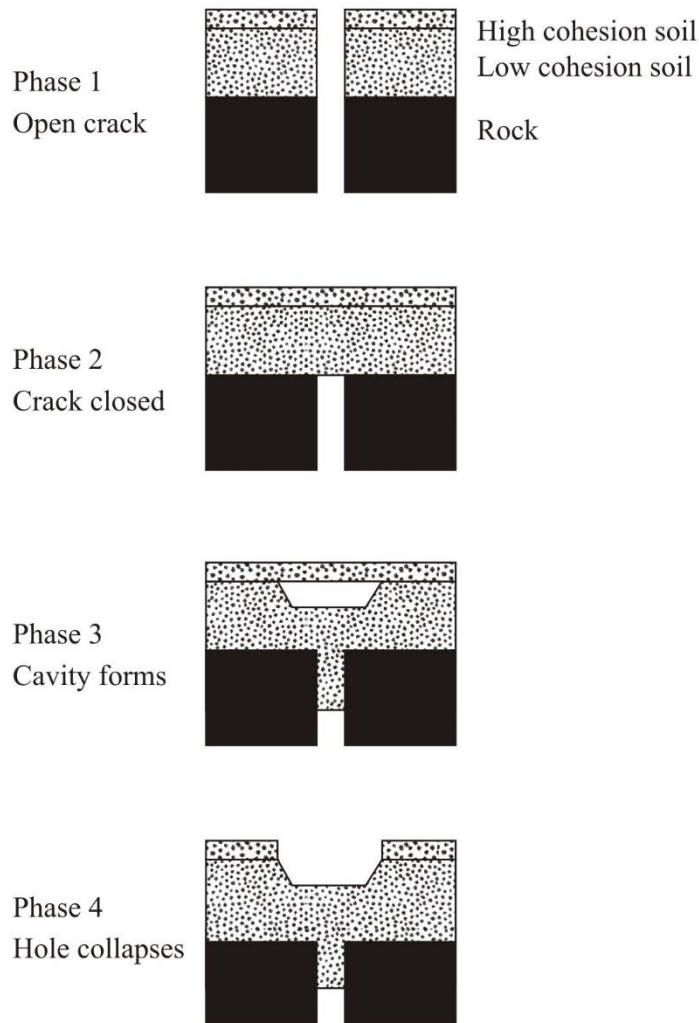


Figure 2-10: SSE schematic as found in Van der Merwe (2017a).

As shown in Figure 2-2, a *subterranean tunnel* was found on either side of the first sinkholes noticed above Sigma Colliery. Van der Merwe (2017a) noted that this feature is often found between adjacent holes and can vary in width between nearly 1 metre and only a few centimetres depending on the stage of maturity of the SSE development. He also stated the tunnel is the original crack in the soil that is in the process of being reopened. Wagener *et al.* (1990) made no mention of subterranean tunnels found during the investigation in the Secunda area.

Other than the SSE mechanism itself, the characteristics of the soil overburden play an important role in the SSE process.

On the *overburden soil thickness*, Van der Merwe (2017a) stated that sinkholes have both been found in the thick, sandy soils at Sigma Colliery (sinkholes up to 4m diameter) and in the

Secunda area where the soil cover is thinner and comprises a tough, black clay (with smaller sinkholes up to 0,5m in diameter). Van der Merwe and Madden (2010) reported sinkhole formation in predominantly sandy soil profiles with a thickness of about 6m.

As mentioned in the list of requirements at the beginning of this section, a critical requirement in the process is *stratification* in the soil profile, i.e. the upper portion of the soil profile must be less erodible than the underlying portion. Van der Merwe (1990 and 2017a) pointed out that if the soil profile is not stratified, i.e. if the soil profile is homogeneous, a sinkhole will not form and the soil will merely slump and be washed into the crack resulting in immediate subsidence on surface. The stronger the upper layer is, the wider the cavity underneath can grow before collapse (Van der Merwe and Madden, 2010). Wagener *et al.* (1990) agreed with the statements above and illustrated it as shown in Figure 2-11 and Figure 2-12.

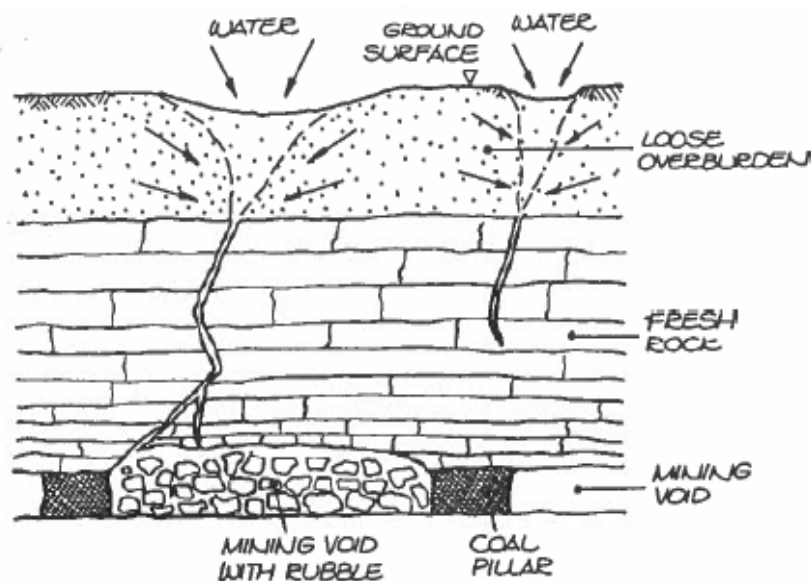


Figure 2-11: Development of local depression in homogenous profile (Wagener *et al.*, 1990).

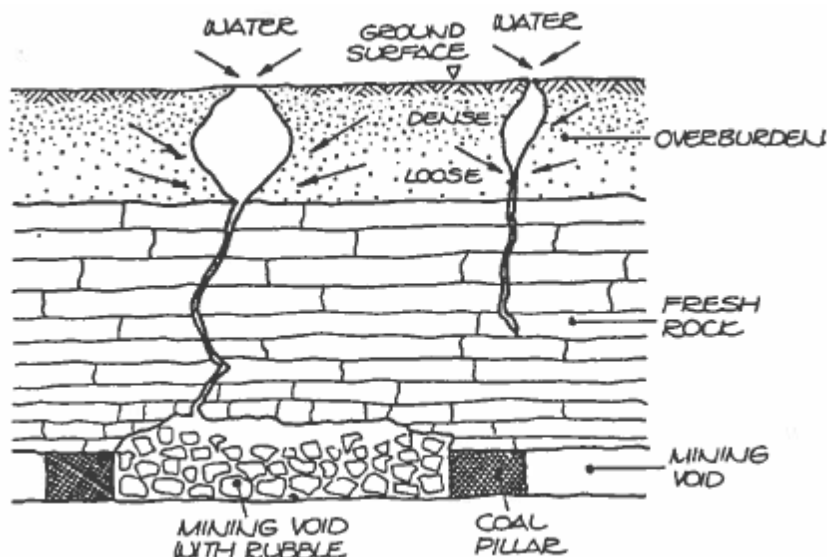


Figure 2-12: Development of sinkhole in stratified profile (Wagener *et al.*, 1990).

The stratification can be provided through various means including the presence of a ferricrete layer or a denser soil layer (Wagener *et al.*, 1990), road or paved surfaces (Van der Merwe and Madden, 2010 and Van der Merwe, 2017a) and plant roots (Van der Merwe, 1990 and Van der Merwe and Madden, 2010).

As far as the mechanism of lid formation is concerned, Wagener *et al.* (1990) points out that a condition of arching is required to develop within the overburden, where the self-weight of the lid is “carried by arching thrusts into abutments”.

As far as the *soil properties* of the overburden are concerned, very little information is available on the properties in the Sigma Colliery area, apart from the references stating that the soil is predominantly more sandy than in the Secunda area (Van der Merwe, 2017a). However, as part of their detailed SSE assessment in the Secunda area, Wagener *et al.* (1990) carried out geotechnical laboratory tests yielding the following results:

- The transported material was a black and grey sandy clay with a high to very high potential expansiveness. The clay content ranged between 27% and 52% (average 33%), the plasticity index (PI) between 31% and 47% with an average of 36% and the linear shrinkage ranged from 15% to 20% (average 18%).
- Consolidated undrained triaxial tests indicated an average cohesion of 12kPa and friction angle of 27°.

- It was concluded that the soil was non-dispersive based on double hydrometer tests, crumb tests and determination of the exchangeable sodium percentage (ESP). (A detailed discussion on dispersivity is given in section 2.5.)
- However, even though the clay was non-dispersive, it was observed that drying of the clay caused a crumb structure to develop with distinct grains rather than an intact structure. In this crumbed state, the clay would become erodible and susceptible to being transported by the mechanical action of water.

Wagener *et al.* (1990) recorded wide surface cracks in the clay caused by shrinkage during the dry months. These would be ideal location where the above-mentioned crumb structure could develop. However, Wagener *et al.* (1990) also pointed out that at thicker clay deposits, the entire layer will not dry out. The lower portions will retain the high moisture content and remain erosion resistant, limiting the erosion to the upper portions only.

Phase 4 – Lid collapses and sinkhole forms

In Figure 2-13 the final phase of the SSE and sinkhole formation process is shown, namely the collapse of the soil cover over the subterranean cavity resulting in sinkholes on surface. The photos were taken a few months apart and show the initial circular collapses on the left and the progressive failure on the right (Van der Merwe, 2018).



Figure 2-13: Progressive failure of the cover to the subterranean cavity (Van der Merwe, 2018).

This section describes the time to failure, the factors influencing the size of the cavities and the mechanisms involved in the collapse.

Van der Merwe and Madden (2010) gives a typical *time to failure* range of between 6 and 8 years after mining. The November 2016 sinkholes on Donkerhoek farm formed 24 years after mining and Van der Merwe (2017a) mentioned instances where sinkholes have formed more than 100 years after mining had ceased.

As will be shown in this section, the time to failure is a complex process involving many factors. One of the factors is the availability of water to act as the erosion medium. As mentioned above, Van der Merwe (2017a) stated that the highest rate of sinkhole development will occur when a prolonged drought is followed by high rainfall. This was the case with the formation of the November 2016 sinkholes. Van der Merwe (2017a) recommended that rainfall records be analysed to determine if any of the earlier occurrences were also preceded by a dry period followed by high rainfall.

Once the cover has collapsed, the sinkholes which formed have the following characteristics in their *appearance* (Van der Merwe, 2017a): In the early stages of development, the holes will have a small opening on surface, widening out to a bowl-shaped cavity underneath whilst with

mature holes, the sides are vertical. Sinkholes often appear along lines, but not necessarily straight. It has also been observed that they often appear in clusters or “hot spots” (Van der Merwe, 2018).

As with the time to failure, the *size* of the sinkholes is determined by many interdependent factors. Van der Merwe (1990) stated that the size of the cavity is related to the thickness of the soil layer, the angle of repose of the material, the transportability of the soil and degree of stratification (see comments in Phase 3 discussion above). Van der Merwe and Madden (2010) listed the soil type, thickness, size of the reservoir and strength of the upper soil layer as contributing factors. Van der Merwe (2017a) pointed to the interdependency of the factors by stating that “the stiffer the upper soil layer and thicker and more transportable the bottom layers, the larger the cavity will be prior to collapse”.

In Van der Merwe (2017b and 2018), a model was developed to calculate the expected sinkhole diameter (see section 2.3.4 for a detailed description). The model is based on a volume comparison between the size of the reservoir and the formed cavity and an evaluation of the capacity of the lid to span the cavity. Upon examination of the model, it becomes clear that the most critical factor in determining the size of the sinkhole is the capacity of the lid to span across the cavity.

As far as the *mechanism* of the cover collapse is concerned, Wagener *et al.* (1990) stated that a disturbing agency, such as water, is required to cause the roof of the arch to collapse. Van der Merwe (2017b) listed exceedance of the critical span of the cover by widening of the cavity below or an increase in the surcharge load (such as a person walking or a vehicle) on the cover as possible causes of failure. Three different failure modes are included in the model proposed by Van der Merwe (2017b and 2018). These are included with the description of the prediction method in the next section.

2.3.4 **Predictive model for undermining related SSE sinkhole size**

Introduction

The unexpected formation of the sinkholes on Donkerhoek farm in November 2016 highlights the requirement for a method to be able to assess the likelihood of sinkhole formation. For the risk to be quantified, such a method needs to include both the likelihood of the sinkholes occurring (where will the sinkholes occur?) and their predicted size.

Van der Merwe (1990) recorded that at the time, it was not yet possible to integrate the factors involved in SSE into a predictive model. However, in Van der Merwe (2017b and 2018), a method to predict the size of sinkholes was proposed. As far as the probability of occurrence is concerned, Van der Merwe (2018) suggested that this be done based on the mining parameters, meaning that the probability of subsidence and crack formation be calculated based on undermining stability assessments.

As the scope of this research project is focussed on the soil contribution to SSE, only the method to predict the sinkhole size is discussed further.

The Van der Merwe method to predict sinkhole size

In the discussion of the fourth phase of SSE in section 2.3.3, several factors are listed which influence sinkhole size. The method proposed by Van der Merwe (2017a and 2018) determines the maximum sinkhole size (indicated by its width and depth) by evaluating the key limiting factors in a systematic way. The reasoning is as follows: The maximum *depth* of the sinkhole is limited by the thickness of the soil layer while the *width* is determined by the reservoir size into which the soil can be eroded and the capacity of the cover to span across the cavity. If the cavity width exceeds the maximum width which the cover can span, a sinkhole will form.

A two-step process is followed as described below with reference to Figure 2-14.

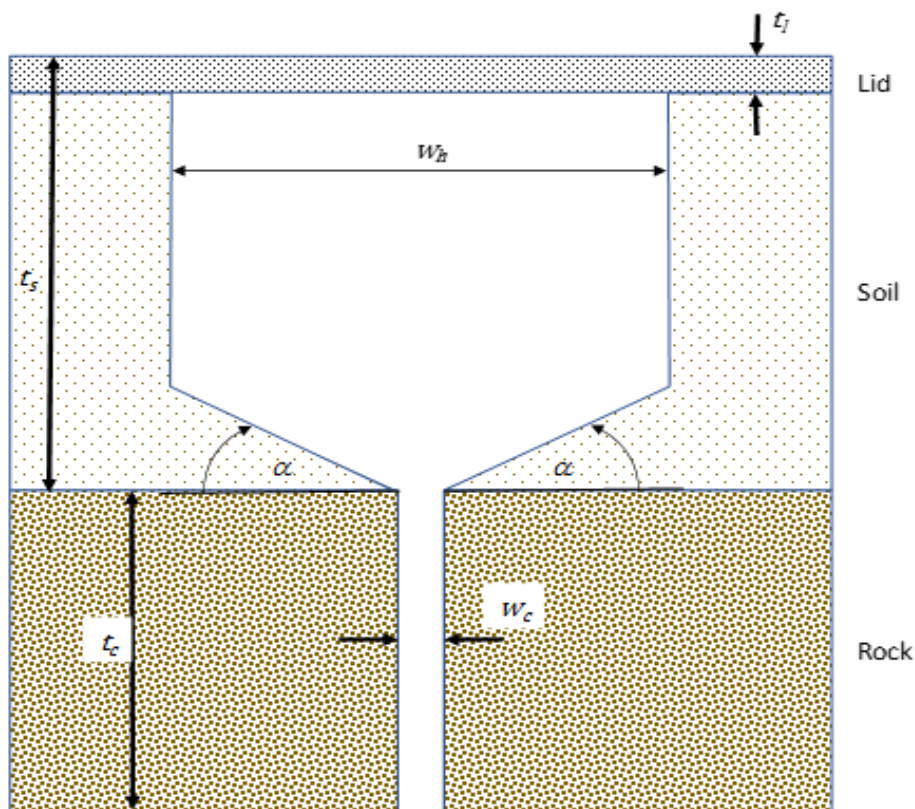


Figure 2-14: Cross section through SSE sinkhole (Van der Merwe, 2018).

First, the maximum width of the cavity is calculated on a volume comparison basis, with the volume of the cavity formed in the soil being equal to the volume of the reservoir (the width and depth of the crack in the rock). The relationship is shown in equation 2-1 (Van der Merwe, 2018) below.

$$w_h = \frac{1/2 w_c \tan \alpha + t_s - t_l - \sqrt{(-1/2 w_c \tan \alpha - t_s + t_l)^2 - \tan \alpha (1/4 w_c^2 \tan \alpha + t_c w_c)}}{1/2 \tan \alpha} \quad (\text{Equation 2-1})$$

Where:

w_h = cavity width (m)

t_s = soil depth (m)

t_l = thickness of the lid (m)

t_c = depth of crack (m)

w_c = width of crack (m)

α = angle of internal friction of the soil ($^{\circ}$).

The soil depth (t_s) can be measured on site and can be taken as the depth to the underside of the erodible layers in areas where alternating sandy and clayey layers occur. It is not necessarily the full depth to the rock contact (Van der Merwe 2017a).

Van der Merwe (2018) stated that the lid thickness (t_l) can also be measured on site and should typically be taken as the thickness of the upper clayey layer (if it exists) or the thickness of the upper layer compacted by human traffic and strength by plant roots. If little information is available, a value of 0,1m is recommended.

As mentioned in the Phase 1 discussion in section 2.3.3, the crack depth (t_c) is difficult to determine. Cracks may not be continuous, as displacement along bedding planes often occur. A value of 25m is recommended by Van der Merwe (2018).

The crack width (w_c) is a function of the horizontal tensile strain as discussed in section 2.3.3. Van der Merwe (2018) gave equation 2-2 to calculate the crack width.

$$w_c = \frac{21S_m + 8,5}{1000} \quad \text{(Equation 2-2)}$$

Where:

S_m = the maximum amount of subsidence in the centre of the mining panel (m)

Note that the units for S_m is in metres and the answer from equation 2-2 is in m. Reference can be made to Van der Merwe (2018) for the subsidence equation.

Van der Merwe (2017a) further commented that should a different typical shape to that shown in Figure 2-14 be found, equation 2-1 could be amended to suit the new geometry. In addition, Van der Merwe (2018) stated that Equation 2-1 is relatively insensitive to the value for α , and that the equation can be simplified by setting α equal to zero.

The second step is the evaluation of the capacity of the cover to span the calculated width of the cavity. Three failure modes were described by Van der Merwe (2018). These are depicted as circular tensile plate failure, simple beam failure and shear plug failure in Figure 2-15. Their respective equations are set out below.

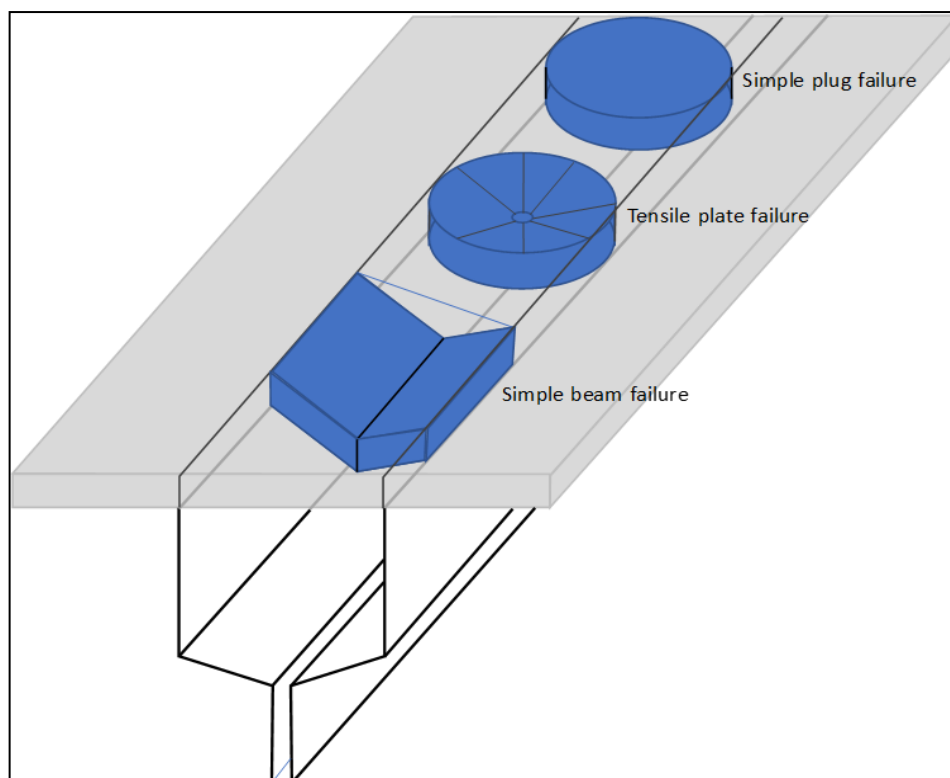


Figure 2-15: Sinkhole cover failure modes (Van der Merwe, 2018).

Circular tensile plate failure

The equation for failure of the cover as circular lid is

$$\sigma_t = \frac{F}{t_l^2} \left[(1 + \nu) \left(0.485 \ln r/t_l + .52 \right) + .48 \right] + \frac{3(3+\nu)\gamma r^2}{8t_l^2} \quad (\text{Equation 2-3})$$

Where:

σ_t = The tensile strength of the cover material (kPa)

F = Point load (kN)

ν = Poisson's ratio

r = Radius of the sinkhole (m)

γ = Unit distributed weight of the cover material ($\rho g t_l$)

Van der Merwe (2018) recommended values of between 50kPa to 80kPa for the tensile strength of the soil (σ_t) based on Li *et al.* (2004) who carried out soil tensile strength measurements on

discrete fibre reinforced soil. The premise is that the discrete fibres would have a similar effect to that of plant roots in increasing the tensile strength of the soil.

Simple beam failure

The equation for failure of the cover above the cavity as a simple beam is:

$$W_h = \frac{-\frac{1.5F}{t_l^3} + \sqrt{\left(\frac{1.5F}{t_l^3}\right)^2 + \frac{3\rho g}{t_l^2}\sigma_t}}{\frac{1.5\rho g}{t_l^2}} \quad (\text{Equation 2-4})$$

Shear plug failure

The equation for shear plug failure is

$$r = \frac{2\pi t_l C + \sqrt{(2\pi t_l C)^2 - 4F t_l \rho g \pi}}{2 t_l \rho g \pi} \quad (\text{Equation 2-5})$$

Where:

r = Radius of the cavity (m)

C = Cohesion of the upper soil layer (kPa)

ρ = Density of the material (kg/m³)

According to Van der Merwe (2018) most sinkholes form as circular failures first followed by the simple beam failure mechanism as shown in Figure 2-13. For this reason, Van der Merwe (2018) recommends first checking the cavity width (w_h) against the circular tensile plate failure followed by the simple beam failure. Only in isolated cases have the shear plug failure been observed in the field.

2.3.5 Remaining questions about the SSE process in SA

The preceding sections seek to set out the historical development and current understanding of sinkholes due to SSE above undermined ground in South Africa based on the available

literature. The bulk of the current understanding has been written up by Professor J.N. Van der Merwe and includes his method to predict the maximum sinkhole size discussed above.

Professor Van der Merwe listed several comments and questions on the current understanding of SSE and sinkhole formation in Van der Merwe (2017a) and (2017b). The most pertinent ones are summarised below and were penned as part of his work following his desk top assessment of the 38 sinkholes which formed on Donkerhoek farm in November 2016.

- Trenches must be excavated at the positions of the sinkholes, similar to the ones excavated in the Secunda area in the 1990s (see Wagener, (1990)) to determine similarities between the mechanisms at work between the Secunda areas and Sigma.
- Soil characteristics that are more prone to SSE need to be identified. How much water is required to result how large a SSE hole in a specific soil type with how wide a crack in rock?
- The long term efficiency of coarse and fine ash filters installed into soil cracks in the Sasolburg area in the 1990s to limit SSE and sinkhole formation need to be evaluated.
- Why does there appear to be “SSE hot spots”? Conceptually, the “hot spots” should be areas with sandy soil and deep subsidence (therefore wider cracks). However, it has also been seen that SSE holes develop in areas with more clayey soil and much less subsidence than at Sigma.
- Why do the holes have different sizes in the same area with the same soil, subsidence and rainfall? It has been seen that the crack reservoirs are displaced in some cases, restricting the available volume – is it possible that once a conduit for soil flow has developed in one spot the surrounding water flow will concentrate in that spot, increasing the size of the SSE hole in that locality and reducing the size in the immediate surroundings? Is the subterranean tunnel indicative of this process? Does this mean that the large hole occurs where soil is washed into a crack and that the subterranean tunnel is formed by horizontal water flow toward the draining position?
- Is there a link between topography and SSE development?
- Are there cycles in SSE development? There appears to be long periods with little or no activity followed by the discovery of several holes. Is this perception real or are there other reasons why holes are simply not reported? Is there a link between rainfall cycles and SSE development, i.e. can more holes be expected after prolonged dry

periods when the rock reservoirs dry out, followed by increased erosion when rainfall suddenly increases?

- Is Ground Penetrating Radar (GPR) suitable for use in the Sasolburg area and does it supply consistent results?

An attempt to answer all these questions is beyond the scope of this research project. They are included as part of this literature study to further describe the phenomenon and to complete the picture on the current status in South Africa.

2.4 SSE AND SINKHOLE FORMATION UNRELATED TO UNDERMINING

2.4.1 Introduction

In the preceding section the focus was limited to SSE resulting in sinkholes above undermined ground in South Africa, with the purpose to present the current understanding of the phenomenon. In this section, the net is cast wider to include other examples of sinkholes due to SSE, but not related to undermining, with the purpose to look for similar factors and mechanisms at work, identify new aspects not considered before and to see if some of the questions posed in the previous section can be answered.

To present the information on this complex process in a clear manner, emphasis is first placed on the *subsurface erosion phenomenon* with a detailed discussion of the factors influencing it and the mechanisms involved. Thereafter the *sinkhole formation process* is discussed, including the upward migration and possible widening of the cavity and the eventual collapse of the cover. Some of the factors are exclusive to either of the processes while other factors are mutual. A summary of the predictive models relating to sinkhole formation is given at the end of the section.

2.4.2 Factors influencing and mechanisms involved in SSE

Beckedahl (1998) defined subsurface erosion as the “removal of material by water below the soil surface”. By definition, this includes both the chemical removal by solution and physical removal by suspension. The scope of this review is limited to the physical removal only.

However, there are several other terms used to describe this process in literature. Jones (1981) listed several terms used e.g. “pseudo karst”, “suffusion”, “percoline drainage”, “subsurface

gullying”, and “piping” or “tunnel erosion” while Dunne (1990) described the additional terms “spring sapping”, “seepage erosion” and “tunnel scour”. A comprehensive discussion and assessment of each of these definitions does not fall within the ambit of this literature review. Rather, a description of the different factors and mechanisms involved in the process of the removal of soil to create a cavity below surface is given to address the problem at hand. The terms “piping” and “subsurface erosion”, abbreviated as SSE, are used. Two images of a soil pipes are shown in Figure 2-16.

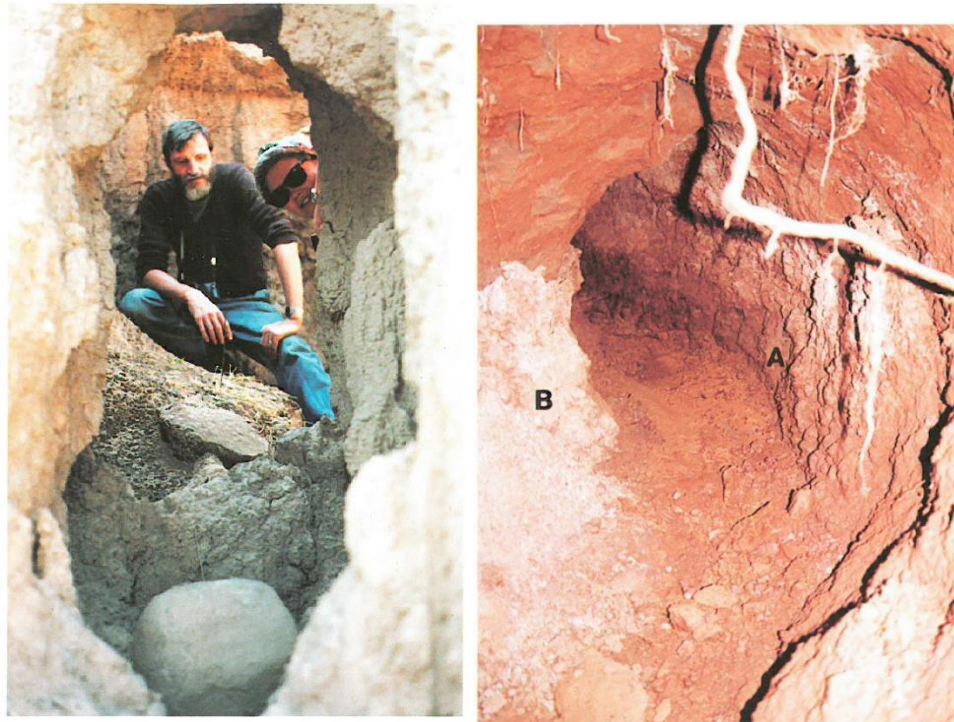


Figure 2-16: Image of soil pipes (Beckedahl, 1998).

Jones (1981) presented a comprehensive review of research on soil piping and summarised several lists of requirements to be met for piping to occur presented by different authors. The list by Fletcher *et al.* (1954) is as follows:

- a water source;
- the ground surface must have a greater infiltration capacity than the permeability of the underlying soil unless the less permeable surface layer is broken by ploughing or rodents i.e. the water must be able to penetrate the soil layers;
- within the soil body, an erodible layer must exist underlain by a retarding layer;
- there must be sufficient hydraulic gradient, and

- an outlet must exist for the material to be eroded to.

Although the list above does not describe the entire piping process comprehensively, it does provide a basic framework to start from. Each of the requirements is expounded on in more detail below. The list above is not a sequential process of pipe formation and there is significant overlap between the factors.

A source of water

The water required to effect the SSE can be due to rainfall (Jones, 1981 and Beckedahl, 1998) or irrigation of crops as mentioned by Marr (1955), García-Ruiz *et al.* (1997) and Higgins and Schoner (1997) and a clear link is established between higher volumes of water increases in SSE.

However, in the case of rainfall, the *timing* of the event can also be significant. Jones (1981) reported on several cases where an increase in piping was noted with intense rainfall after a dry period. The main reasons are desiccation cracking of the upper soil layers and the ionic imbalance between the fresh rainwater and the salts in the soil. Both of these factors are discussed in more detail later in this chapter.

Infiltration capacity of the upper soil layers

If the water cannot penetrate into the soil layer beyond the surface, no piping will take place. Apart from the animal burrowing and ploughing referred to above, *desiccation cracking* (shrinkage cracking) within the upper soil layers is one of the largest factors influencing soil piping as reported by Jones (1981), Dunne (1990), Marr (1955), Beckedahl (1998), Higgins and Schoner (1997) and García-Ruiz *et al.* (1997). An image of a shrinkage crack in a cultivated field is shown in Figure 2-17.



Figure 2-17: Shrinkage crack in cultivated field (Marr, 1955).

The phenomenon of desiccation cracking due to shrinkage is mainly found in fine grained materials. Hoffmann *et al.* (1998) identified SSE caused by desiccation cracks in predominantly silt and clay sediments as the major contributing factor to more than 1700 sinkholes in the Santa Cruz River flood plain in Arizona, USA. No sinkholes (and no cracks) were found above medium- to coarse grained paleo channels, located in between the fine grained material.

Dunne (1990) pointed out that desiccation cracks play an important role in pipe initiation as they provide the initial subsurface passageways for runoff and sediment transport and due to the low hydraulic conductivity of the fine grained material, saturation is promoted and flow in the passages enhanced.

García-Ruiz *et al.* (1997) recorded preferential pipe development at the *crossing of two desiccation cracks*. The connection of cracks leads to a concentration of water which results in more pipe formation over time.

Often, in cultivated fields, the desiccation cracks and soil pipe networks are destroyed by ploughing, as described by García-Ruiz *et al.* (1997), who found more piping and resultant sinkholes in lucerne and fruit tree fields than in cereal fields. The reason being that the latter is ploughed on a yearly basis, whilst the former is not deeply ploughed for several years, leaving the door open for a network of subsurface channels to form.

The depth of desiccation cracking is also influenced by *plant roots* extracting moisture from the soil. Marr (1955) reported roots drying the soil to depths of more than 6m and Higgins and Schoner (1997) listed several other occurrences of desiccation cracking influenced by plant roots, especially in alfalfa (lucerne) fields. Beckedahl (1998) listed both positive and negative influences from plant roots: On the one hand roots bind the soil, add strength and prevent disaggregation while on the other hand vegetation enhances infiltration by increasing surface roughness and by providing potential conduits through root channels. When the roots have decayed, the organic material increases the overall permeability.

An erodible soil layer underlain by an impeding layer

The third requirement for soil piping is that the soil must have a layered structure with an erodible layer underlain by an impeding or impervious layer. The effect of the impeding layer is that it causes lateral flow in the overlying soil leading to erosion (Dunne, 1990 and García-Ruiz *et al.*, 1997). Interestingly, Jones (1981) reported this requirement was first reported by South Africans in 1938 based on observations made in Natal (as it was called then). The mechanics of the horizontal erosion process is discussed in more detail with the fourth requirement below.

The questions as to what defines an *erodible soil* is a very complex one and lies close to the heart of this research project. As part of their research in Arizona, Hoffmann *et al.* (1998) found no difference in the field density, clay mineralogy, moisture content and Atterberg limits between soils where SSE occurred and those where no SSE had occurred.

The erodibility of the soil layer is strongly influenced by its *degree of dispersivity* as noted by Beckedahl (1998) and Jones (1981). The mechanisms of soil dispersion and identification methods are discussed in section 2.5.

Sufficient hydraulic gradient

Before any cavity is formed in the soil below surface, the energy to effect the removal of soil particles is provided by the hydraulic gradient. White and White (1992) explained the piping process as part of the formation of a soil piping sinkhole. Infiltration water soaks through the soil focusing on the opening in the rock which is the only way through the impermeable rock. Due to the flow net characteristics, there is a substantial increase in flow velocity as water is channelled into the opening, with sufficient energy to move soil particles into the crack and

initiate the cavity. Over time, as more and more particles are washed into the opening, the cavity enlarges.

Apart from the infiltration process described above, the hydraulic gradient can also be provided by the *lowering of the water table* (Arkin and Gilat, 2000; White and White, 1992 and Hoffmann *et al.*, 1998) or the *rising of the water table* as reported by Lei *et al.* (2016).

White and White (1995) provided thresholds for both the *vertical and horizontal transport* of material below ground in a karst environment. Vertical transport is determined by the bedrock fracture aperture, soil cohesion, moisture content and particle size distribution. The threshold for lateral transport is dependent on the energy available for sediment movement which depends on the maximum flow velocity and particle size.

Arkin and Gilat (2000) reported on sinkholes near the Dead Sea and found that piping only occurs once the horizontal flow changes from laminar to turbulent.

Dunne (1990) provided a detailed description of the seasonal enlargement of a shrinkage crack through *tunnel erosion* as depicted in Figure 2-18. With the first rains after a dry season, the desiccation cracks are open and surface water flowing into the crack will have sufficient energy to erode particles from the bottom of the crack. Towards the end of the rainy season, as the moisture content increase causing swelling and closure of the crack, a tunnel is formed which is enlarged by further erosion. As this process is repeated over consecutive wet and dry seasons, a network of tunnels can form, bridged by an arch of cohesive soil.

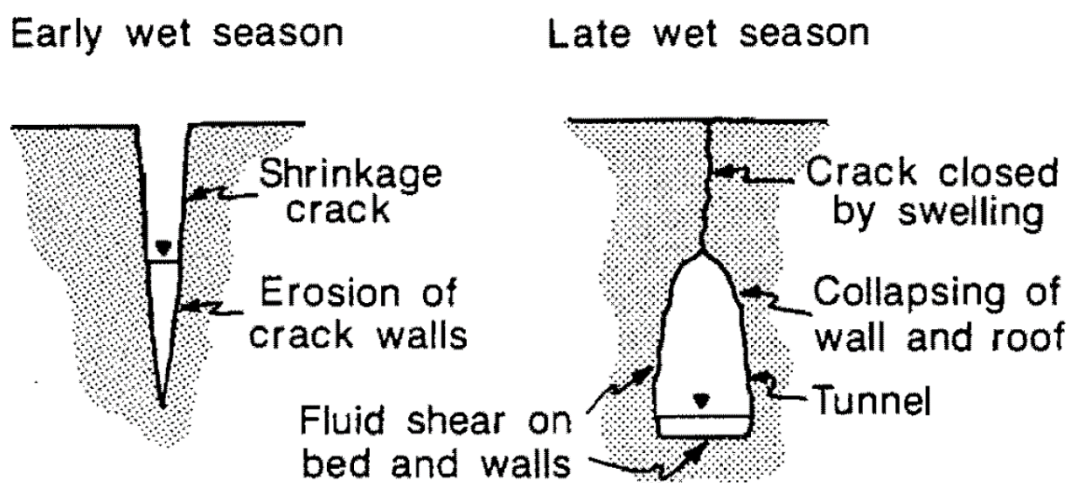


Figure 2-18: Enlargement of shrinkage crack by tunnel erosion (Dunne, 1990).

An outlet to dispose of material

In many references on piping, the “outlet” referred to is a piping opening in the side of a gully wall or runoff channel (Beckedahl, 1998) or a terrace wall (García-Ruiz *et al.*, 1997). However, a similar outlet is also provided by an opening or fracture in the karst bedrock as described by White and White (1992). It is important to note that the outlet must have sufficient capacity to dispose of (or receive) the eroded material, otherwise the erosion process will be choked (White and White, 1995).

Unsaturated soil behaviour

Since much of the subsurface erosion process takes place above the water table where the soil is unsaturated (Dunne, 1990 and Beckedahl, 1998) the process of subsurface erosion cannot be properly reviewed without consideration of unsaturated soil behaviour. The topic has sufficient significance to be reviewed on its own and is presented in section 2.5.2.

2.4.3 Factors influencing and mechanisms involved in sinkhole formation

In this section some of the physical characteristics of sinkholes are listed, followed by a discussion of the factors influencing and mechanisms of the process. The section concludes with a summary of some of the available predictive models for sinkhole formation.

Sinkhole physical characteristics

Although there are many examples of isolated sinkholes, especially on karst terrain (Beck, 2012), sinkholes are often found along underground *flow lines*. Currens (2012) referred to an extended study of sinkholes over karst terrain by Taylor (1992) where a correlation was established between sinkhole alignments and faults and major joints in the rock. Arkin and Gilat (2000) reported sinkhole formation along subterranean flow lines near the Dead Sea in Israel, while the sinkholes reported by Hoffmann *et al.* (1998) often followed the linear desiccation cracks.

Sinkholes often appear in *clusters* as reported by Zhou *et al.* (2014) and Hoffmann *et al.* (1998) as shown in Figure 2-19, which could be influenced by the connection of underground cracks and tunnels discussed in section 2.4.2.



Figure 2-19: Sinkholes due to SSE in Arizona, USA (Hoffmann *et al.*, 1998).

Some further characteristics of sinkholes are:

- The shape of the sinkholes is often *circular or linear* (Hoffman *et al.*, 1998 and Zhou *et al.*, 2014) and occur in wide range of sizes from up to 60m diameter (Beck, 2012) to diameters of about 1m (García-Ruiz *et al.*, 1997).
- Soon after formation, the sides are *vertical* and the edges sharp-rimmed (White and White, 1992).
- In many cases, the opening in the rock cannot be seen from surface, but is masked by collapsed overburden inside the hole (Beck 2011).
- In many cases, while the cavity is propagating upwards towards the surface from the opening in the rock below, and if the cavity has a larger diameter than the opening in

the rock below, the top of the cavity will have a dome shape while the lower sides will slope downwards to the rock opening at an angle greater than or equal to the friction angle of the soil (Tharp, 2001 and referenced in Tharp, 2003).

- By virtue of their nature, sinkholes due to SSE are considered to pose the highest environmental hazard amongst sinkhole types because they can form in such a short time span (White and White, 1992). In residential areas, entire houses may be at risk (Beck, 2012) while in many agricultural settings the greatest risk is posed to farming equipment being damaged (Marr, 1955).

Factors influencing sinkhole formation

Once the SSE mechanism has resulted in the formation of a small cavity below ground, the sinkhole formation process essentially comprises two phases: the *upwards migration* of the cavity and the eventual *collapse of the cover* (Drumm *et al.*, 1990). In many cases, the two phases happen continuously.

Chen and Beck (1989) described the process eloquently based on a series of laboratory experiments carried out: In sandy material, the collapse process occurs upwards from the drain in a cylindrical zone until the surface is breached where failure of the sidewalls occur until a stable angle is reached. However, if cohesive strata (such as a clay layer) is reached during the upwards propagation, the upwards migration will be stopped and lateral erosion will occur increasing the size of the cavity below ground. This will continue until the cohesive strata collapses into the void or if the erosion process ceases. The principle of lateral widening only occurring once a cohesive layer is reached was also confirmed by Beckedahl (1998), Beck (2012), White and White (1992), White and White (1995) and Oberholzer (2017).

The cohesive layer does not necessarily have to be a clay layer. The “cohesion” can also be provided by the *roots of plants* or pavement structures as mentioned by White and White (1992) who further add that the more cohesive the layer is, the more abrupt the collapse of the cover is.

Many of the factors which influence SSE also affect the formation of sinkholes. Currens (2012) found a correlation between *high rainfall* and sinkhole formation and Gertje and Jeremias (1989) as quoted by Tharp (1999) reported modest rainfall after a prolonged drought resulting in sinkholes. Marr (1955) and García-Ruiz *et al.* (1997) reported a correlation between increases in *irrigation* and sinkholes formation.

García-Ruiz *et al.* (1997) also reported a correlation between the farming method and sinkhole formation where areas with deeper and more frequent *ploughing* resulted in less sinkholes. This is equivalent to the earlier mentioned influence on piping.

The *degree of saturation* also plays a role in sinkhole formation. Chen and Beck (1989) reported that sandy sediments collapse rapidly in either a dry or saturated condition, but are more stable when partially saturated. Clayey sediments, on the other hand, will span across cavities when dry, but will erode when saturated. Oberholzer (2017) evaluated cavity propagation through fine and coarse sand in centrifuge trapdoor experiments. He found that under moist conditions and for the same trapdoor width, the cavity in coarse sand propagated vertically upwards until the surface was breached, but for the fine sand a stable arch formed, and the upward propagation stopped. He attributed the stable arch formation to the higher levels of matric suction realised in the fine sand than in the coarse sand. A more detailed discussion on soil suction is presented in section 2.5.2.

Overburden thickness is also a factor influencing the size of a sinkhole. White and White (1995) stated that thick soil develops larger diameter sinkholes than thin soils. Drumm *et al.* (1990) concluded that, based on numerical modelling of a cylindrical void in the overburden, for a given overburden thickness, small cavities are more stable than large cavities. However, if the cavity diameter is kept the same, large overburden thicknesses are more stable than thinner ones.

Mechanisms of sinkhole formation

It is clear from literature that the stability of the roof above the initial depth is provided by *soil arching* (White and White, 1992; White and White, 1995; Currens, 2012). According to White and White (1992), a combination of continued inflow of water combined with gravitational collapse and spalling causes the arch to be enlarged and *migrate upward*.

Some mechanisms involved in the upward migration of the cavity were observed through centrifuge trapdoor experiments carried out by Oberholzer (2017) on both coarse and fine sand in wet and dry conditions. The progressive formation of shear bands forming upwards from the trapdoor edges is shown in Figure 2-20. At first, the shear bands form a triangular shape. As the cavity progresses upwards, a parabolic shape is seen followed by vertical shear bands at failure. Note that no wetting fronts were introduced in the experiments and no clay layer was present.

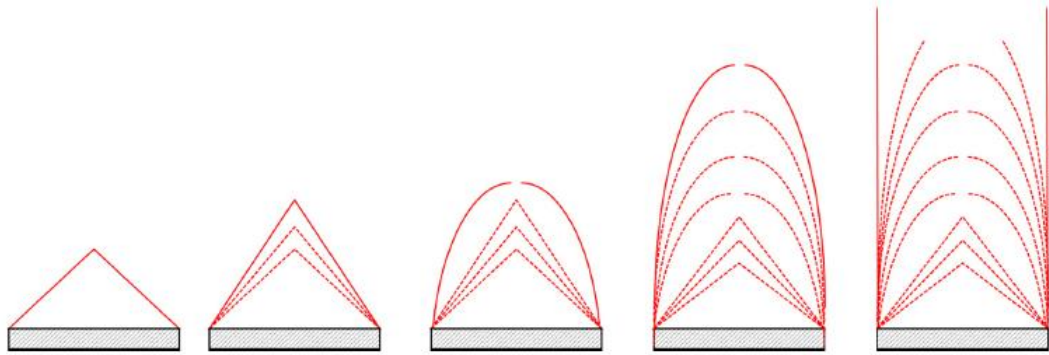


Figure 2-20: Progressive failure mechanisms (Oberholzer, 2017).

Tharp (1999) discussed the mechanical failure mechanisms involved in the upwards migration of the cavity. Essentially the cavity progresses upwards through sloughing as the soil arches fail in unconfined compression. He pointed out that at the face of the soil arch in the cavity, both the pore pressure and the radial stress is zero. As you move away from the face, both these values increase. If, at the same point, the increase in pore pressure exceeds the increase in the radial stress, a net tension perpendicular to the cavity face will exist which can lead to sloughing. In other words, sloughing will only occur if the radial pore pressure gradient exceeds the radial stress gradient. He concluded that steady state pore pressure gradients are inadequate to initiate sloughing, except in the case of extreme stress relaxation or cracking adjacent to the soil void.

However, Tharp (1999) presented three scenarios where transient pore pressure gradients can result in sloughing. These are:

- *Rapid drawdown* of the water table leading to loss of buoyant support. As the water table is lowered in soils with a low permeability relative the rate of drawdown, the increase in load is initially carried by the pore water leading to high pore pressure gradients close to the face of the cavity.
- A *wetting front* advancing through an unsaturated soil. If the soil has a low permeability and is relatively dry, the soil behind the wetting front will be at almost constant head and the entire head drop will occur across the wetting front. As the wetting front approaches the cavity face, a high pore pressure gradient can result in sloughing. Toll (2012) stated that the progress of the wetting front through the soil depends on the suction ahead of the wetting front and the unsaturated permeability.

Behind the wetting front, where the soil approaches saturation, the infiltration rate is determined by the saturated permeability.

- The *exsolution of air bubbles* as water seeps into the cavity through the unsaturated soil above. Exsolution, expansion and nucleation of the air bubbles decrease the degree of saturation and the permeability of the soil, leading to a high pore pressure gradient at the face of the cavity which can cause sloughing.

It should be pointed out that, even though the last two scenarios above given by Tharp (1999) occur in unsaturated soil, the loss of surface tension due to saturation is not considered in any of the mechanical models he presents.

The effect of the rapid drawdown of the water table was further discussed by Tharp (2003) as shown in Figure 2-21, which shows the head drop required for hydraulic fracture versus the rate of head drop. The different graphs reflect a parameter “d” which Tharp (2003) related to the soil cohesion. The modelled dome shaped cavity has an initial radius of 0,1m and the thickness of the soil overlying the cavity is 5m. From the graph it is clear that for an increased drawdown rate, a smaller head drop is required. Also, soils with more cohesion required either larger head drops or quicker head drops for hydraulic fracture and sloughing.

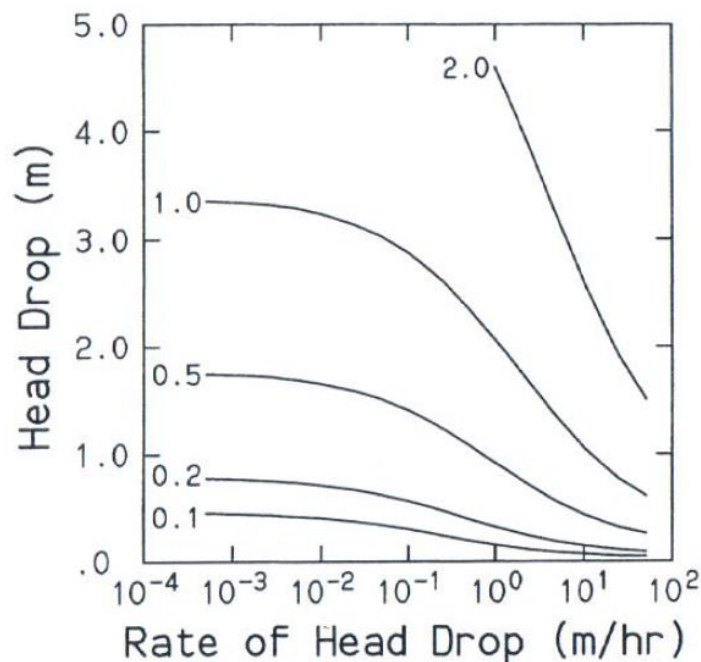


Figure 2-21: Head drop for hydraulic fracture vs rate of head drop (Tharp, 2003).

Zhou *et al.* (2014) investigated the formation of sinkholes in irrigated fields located at the top of a 26,5m high cracked loess slope in Heifangtai, China, by means of instrumented full scale field tests and a numerical study using a finite difference program to perform a mechanical-hydraulic coupled analysis in unsaturated soil.

In essence, the study explored the mechanisms at work when the cracks are filled with water and then drained again at different rates. It is important to note that the cracks were pre-existent prior to the tests and did not form as a result of the wetting.

The study identified *wetting induced loss of shear strength* and the *rapid loss of lateral support provided by the water to the sides of the crack* as the critical factors which resulted in sinkholes. During the field test, no sinkholes formed during the initial stages of water ponding on surface resulting in the cracks also being filled with water. It was only when an outlet in the hillside slope was opened at a crack intersection (i.e. the water in the crack breached face of the slope), that the sudden release of water from the crack and the rapid drawdown of the water level inside the crack, resulted in the sinkholes on surface. The location of some of the outlets in the hillside slope are shown in Figure 2-22, as obtained from Xu *et al.* (2011) which describes other aspects of the investigation than Zhou *et al.* (2014).

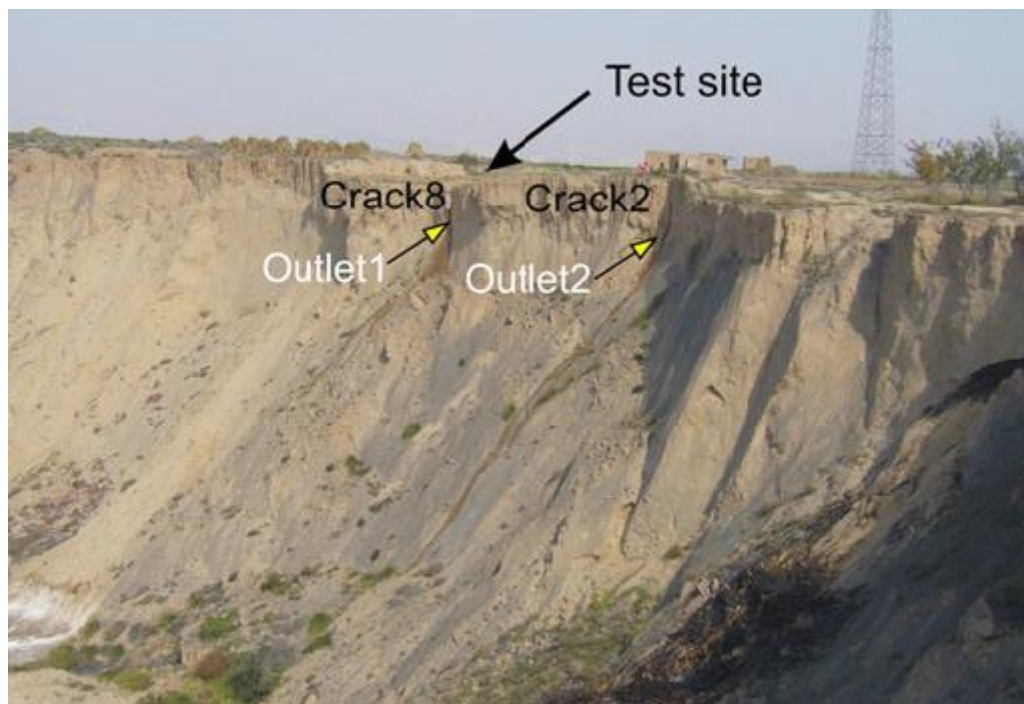


Figure 2-22: Location of some of the crack outlets in the hillside slope (Xu *et al.*, 2011)

Zhou *et al.* (2014) also noted that sinkholes formed in clusters along cracks as the “sinkholes rapidly gathered water from the connected cracks and transferred eroded soil out of the slope”.

Models to predict sinkhole size

Several methods have been published to assist in the prediction of sinkhole size and are summarised in this section. Note that the methods focus on the size of the sinkhole only and not on the likelihood of sinkhole formation. As most of the methods are based on site specific soil conditions, their applicability to other soil conditions (e.g. unsaturated soils) is limited.

Craig (1990) carried out centrifuge model tests to evaluate the collapse of soft to very soft overburden following removal of a support. An upper bound solution was found to predict the critical void size for a range of overburden depth to void diameter. The model considered a plug type failure and was based on the undrained shear strength of the material.

Drumm *et al.* (1990) presented a lower bound solution to evaluate the stability of soil adjacent to a vertical cylindrical cavity under drained conditions. The method was based on classical plasticity theory and gave equations to determine the surcharge load needed for instability and to estimate sinkhole size and extent of damage.

Abdulla and Goodings (1996) and Goodings and Abdulla (2002) considered the formation of sinkholes in loose sand underlain by a weakly cemented sand. The influences of geometry and soil properties were investigated through centrifuge experiments and design charts developed to predict failure.

Augarde *et al.* (2003) evaluated the undrained stability of cavities submerged below the water table using finite element analyses and presented upper and lower bound values of a load parameter, which is an indication of the maximum allowable difference between surcharge and cavity pressure.

Drumm *et al.* (2009) presented stability charts for both drained and undrained conditions developed using numerical modelling. They related the ratio between the soil thickness above the cavity and the cavity diameter to a stability number for different friction angles.

Jiang *et al.* (2015) proposed using the soil anti-permeability strength (defined as the minimum water pressure required to reduce soil cohesion) to evaluate a soil’s susceptibility to sinkhole formation.

2.5 FURTHER FACTORS CONTRIBUTING TO SSE AND SINKHOLE FORMATION

In the preceding sections, it was mentioned that soil erodibility and dispersivity as well as unsaturated soil behaviour influence the SSE and sinkhole formation. A discussion on these factors is presented in this section.

2.5.1 Erodibility and Dispersivity

It stands to reason that the likelihood of a cavity formation below ground is tied to how easily the soil particles can be lifted from the current location and transported elsewhere by water. While referring to erodibility in soil, Paige-Green (2009) distinguished between three aspects of soil erodibility, namely *erodibility*, *slaking* and *dispersivity*. Each of these aspects are discussed in more detail below.

Erodibility

Erodible soils are soils in which the cohesive strength when wet is insufficient to resist the tractive forces of water flowing over the surface according to Nascimento and de Castro (1974). As mentioned by Paige-Green (2009), the main factors influencing erodibility are grain size, swelling and petrification. In addition, the flow velocity must also exceed the critical velocity required for sufficient tractive forces to develop for particles to be dislodged, as also referred to by White and White (1995) on page 2-33. On slopes comprising erodible soils, the erosion is often only present towards the lower end of the slope where the flow velocity is the highest. In South Africa, the research done on erodible soils only comprises limited application of the swell test described by Nascimento and de Castro (1974), and Paige-Green (2009) recommended that further research on this topic be done.

Slaking

According to Paige-Green (2009) slaking soils are soils which, when wetted from either a dry or partially saturated state, lose all the soil suctions on soaking. When placed in non-flowing water, the soil disintegrates rapidly into smaller particles of gravel, sand and silt without any fines going into suspension. Thus, the water remains clear.

Paige-Green (2009) stated that no specialised testing is needed to identify slaking materials, and that the standard crumb test where the crumb disintegrates within one minute in a solution of NaOH, and where the solution remains clear, can be used to identify slaking materials.

Dispersivity

Properties of dispersive soils

Dispersive soils are soils where the clay component goes into suspension in non-flowing water, after Sherard *et al.* (1976a). In contrast to erodibility and slaking discussed above, according to Bell and Maud (1994), dispersivity is not caused by flow velocity and loss of suctions, but rather by the chemical factors such as the osmotic influences at the surface of the clay particles. The phenomenon is caused when the repulsive forces between the clay particles exceed the attractive forces, causing the clay particles to de-flocculate and disperse in the presence of relatively pure water (Bell and Maud, 1994). It is important to note that the water does not need to flow for dispersion to occur.

Craig (2005) provided more detail on the chemical mechanisms at work in dispersion. As the surface of the clay particles are negatively charged, they attract cations to their surface. While being attracted, the attracted cations also tend to move away from each other due to thermal energy effects. The result is a dispersed layer of cations around the clay particles, with the concentration in cations decreasing with increasing distance away from the clay particle surface until the concentration reaches the same value as in the pore water as a whole. This layer formed by the negative particle surface and the dispersed cations is called the double diffused layer. It is the properties of the double diffused layer which determine the degree to which the clay will disperse in non-flowing water.

One of the main chemical factors influencing dispersion is the presence of sodium cations on the clay particle surfaces, also referred to as exchangeable sodium (Bell and Maud, 1994). The measure of influence is expressed as the exchangeable sodium percentage (ESP), calculated as the exchangeable sodium as percentage of the cation exchange capacity (CEC) of the soil.

However, the dispersivity of a soil is also controlled by the type and concentration of ions in the pore water or eroding fluid (Bell and Maud, 1994), which is also referred to as the salts in the pore water (Bell and Walker, 2000). An increased salt concentration causes the clay to flocculate while a decrease causes the clay to be more dispersive (Craig, 2005). Gerber and

Harmse (1987) provided values for clays with different CEC values which will remain flocculated if the total dissolved salts in the pore water remain above a certain value.

The implication of the above is that if the salt content in the pore water were to decrease, the clay may become dispersive. This is evidenced in the phenomenon where clays with an ESP value of as low as 10% may be rendered dispersive if the free salts are leached by seepage of relatively pure water (Elges, 1985). One example of where the eroding fluid may be relatively pure is in the case of fresh thunderstorm rainwater seepage following a period of drought. Brown (1961), as referenced by Jones (1981), pointed to this phenomenon as the source of an ionic imbalance which led to accelerated soil erosion.

The influence of the salt content of the pore water on dispersivity can be evaluated by calculation of the sodium absorption ratio (SAR) (Beckedahl, 1998) and the concentration of dissolved sodium as percentage of the total dissolved salts (Sherard *et al.*, 1976a). In both methods, it is the concentration of sodium relative to the other salts in the pore water, which is an indication of the dispersivity.

The question can be asked as to what percentage of the soil need to comprise a dispersive clay for the soil to be classified as dispersive? Bell and Maud (1994) stated that dispersive soils have a moderate to high clay content, and should the clay content be less than 10%, there may not be sufficient colloids for piping to develop.

Testing for dispersive soils

According to Bell and Maud (1994), the standard tests for soil classification do not identify dispersive soils. At present, various methods are employed in South Africa to identify dispersive soils as described by Elges (1985), Bell and Maud (1994), Bell and Walker (2000), Paige-Green (2009) and Maharaj (2013). The tests can be divided into two groups, namely the mechanical and chemical tests.

During the mechanical tests the soil's dispersive behaviour in water is directly observed. The tests include the double hydrometer test, crumb test and pinhole test.

- Sherard *et al.* (1976a) described the double hydrometer test: Two hydrometer tests are carried out on the soil sample. In the first, a dispersion agent is added as per the standard procedure and in the second, no dispersion agent is added and the sample is not mechanically agitated. The dispersion ratio is calculated as the ratio of the <0,005mm diameter particles of the second test divided by the first test. According to

Bell and Maud (1994) a dispersion ratio more than 50% is considered dispersive, 30% - 50% moderately dispersive, 15% - 30% slightly dispersive and less than 15% non-dispersive.

- The crumb test was also described by Sherard *et al.* (1976a): A small soil sample is placed to a beaker with distilled water and a second sample in a beaker with a NaOH solution. The tendency of the clay particles to go into suspension is then graded to either no reaction, slight reaction, moderate reaction or strong reaction.
- Sherard *et al.* (1976b) described the pinhole test to evaluate dispersivity. A 1mm hole is punched through a sample and distilled water is allowed to flow through the sample, starting at a hydraulic head of 50mm. The hydraulic head is increased in steps. The degree of dispersivity is determined from the colour of the flow emerging from the specimen, the rate of through flow and the increase in hole diameter observed once the test is completed.

The chemical tests can further be sub-divided into two groups:

- Tests based primarily on the chemical properties of the surface of the clay particles, also known as bound cations. Amongst these, the most commonly used ones in South Africa are the Harmse (1980) method and the Gerber and Harmse (1987) chart. In the former the ESP, pH, conductivity, exchangeable magnesium percentage (EMgP) and SAR are used to identify dispersive soils while in the latter, the ESP values are plotted against the CEC (with units in me/100g clay) to identify dispersive behaviour as per the chart shown in Figure 2-23 from Gerber and Harmse (1987). The values of ESP and CEC are often determined using the ammonium acetate method as described by Schollenberger and Simon (1945).

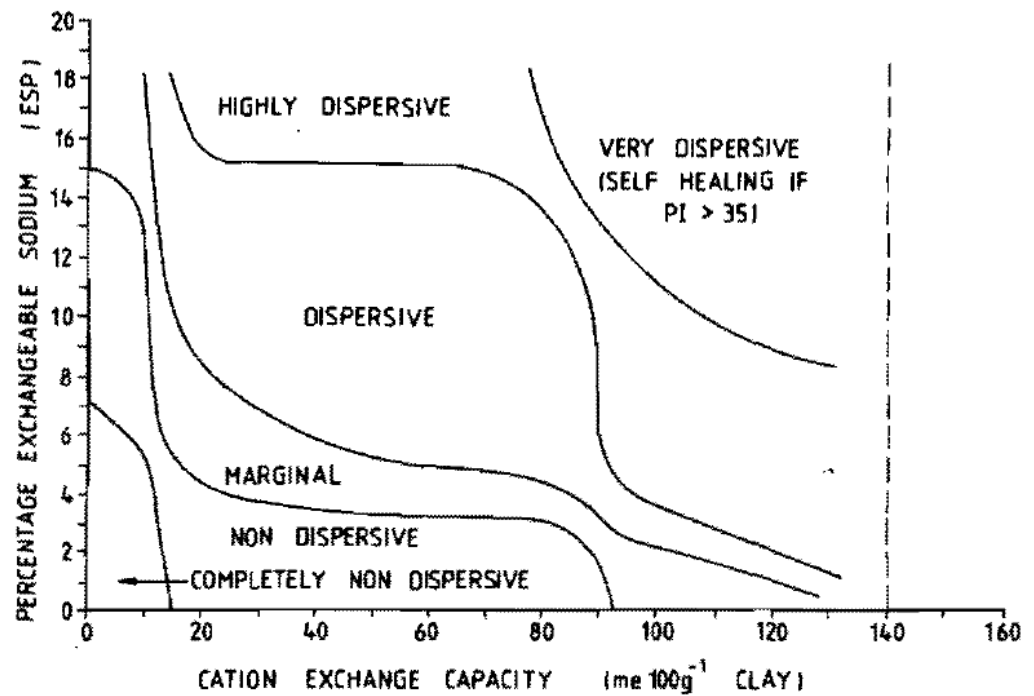


Figure 2-23: Diagram of determination of dispersion potential as a function of ESP and CEC per 100g clay (Gerber and Harmse, 1987).

- In the second group, the pore water is extracted from a soil paste saturated with distilled water and the test focusses on the unbound cations. The properties of the saturation extract are analysed to calculate the SAR, which according to Bell and Maud (1994), indicates a dispersive soil if higher than 2. A second method to evaluate the pore water is the chart developed by Sherard *et al.* (1976) in which the percentage sodium in the total dissolved salts is plotted against the total dissolved salts as per the diagram in Figure 2-24. The dispersivity is assessed either dispersive, intermediate or nondispersive.

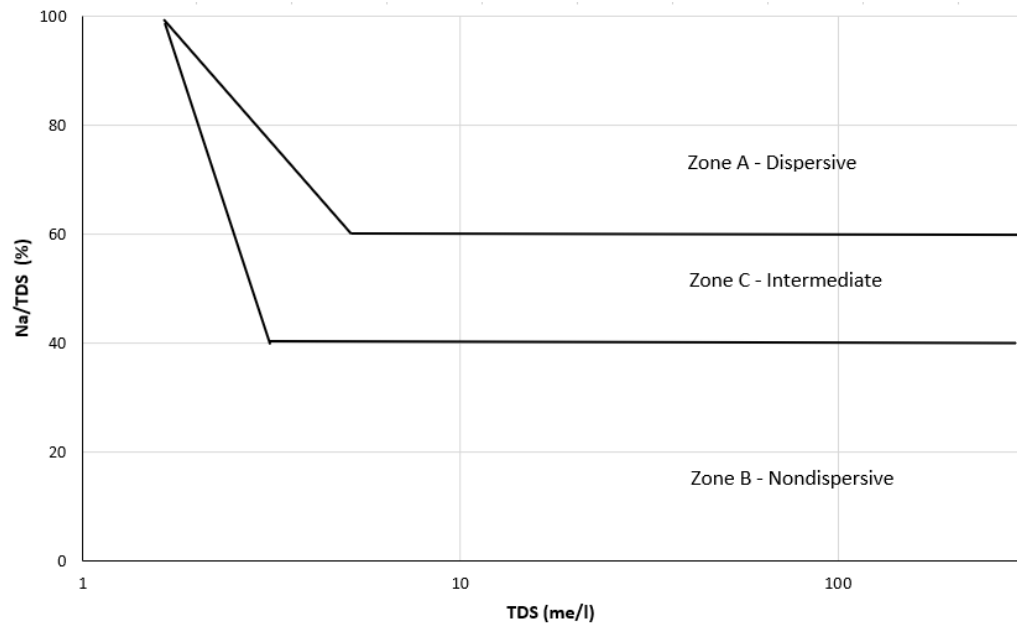


Figure 2-24: Potential dispersivity based on TDS and percentage sodium (Sherard *et al.* 1976a).

A rating system for dispersivity testing

Bell and Walker (2000) carried out an extensive testing programme on dispersive soils in KwaZulu Natal and concluded that there is no single testing method suitable for the positive identification of dispersive soils. According to Maharaj (2013), there is no clear and defined procedure for identification of dispersive soil in South Africa and various authors have published conflicting results between the methods. In light of this, Paige-Green (2009) recommended the use of a rating system based on various tests to evaluate the dispersivity of a soil.

Several rating systems have been developed over the years, but Paige-Green (2009) recommended the Bell and Walker (2000) rating system summarised in Table 2-1.

Table 2-1: Bell and Walker (2000) dispersivity rating system

Pinhole Test	Class Rating	Dispersive 5	Moderate 3	Slightly 1	Nondispersive 0
CEC vs ESP	Class Rating	Highly dispersive 4	Dispersive 3	Marginal 1	Nondispersive 0
Crumb test	Class Rating	Strong reaction 3	Moderate 2	Slight 1	No reaction 0
SAR	Class Rating	Over 2 2	1.5 to 2 1	1.5 to 2 1	Less than 1.5 0
TDS vs. %Na	Class Rating	Dispersive 2	Intermediate 1	Intermediate 1	Nondispersive 0
TOTAL	Class Rating	Highly dispersive 12 or above	Moderately dispersive 8 to 11	Slightly dispersive 5 to 7	Nondispersive 4 or less

In addition to the above three aspects (i.e. erosion, slaking and dispersion), Wagener *et al.* (1990) found that the clay in which SSE related sinkholes formed in the Secunda area was non-dispersive. However, it was observed that drying of the clay caused a desiccated crumb-like structure to develop with distinct grains rather than an intact structure. In this crumbed state, the clay would become erodible and susceptible to being transported by the mechanical action of water.

2.5.2 Unsaturated nature of soils and suction measurement

As mentioned towards the end of section 2.4.2, subsurface erosion often takes place above the water table and therefore in unsaturated soil conditions (Dunne, 1990 and Beckedahl, 1998). As such, any study of the phenomenon will be incomplete if unsaturated soil mechanics are not considered.

However, within the scope of this study, the influence of unsaturated soils is not limited to SSE only, but it also affects the strength of the lid spanning the below ground cavity as the suctions in the unsaturated soil increase the tensile strength of the soil (Gaspar, 2017). This further underlines the relevancy of unsaturated soil mechanics to the problem at hand.

There are three categories of soil suction as described by Al Haj and Standing (2016), namely *matric suction* (which is related to the mechanical effect of the water menisci between the soil particles), *osmotic suction* (which is influenced by the salt concentration in the pore water) and *total suction* (which is the combination of the matric and osmotic suction).

Jacobsz (2018) mentioned that pore water or matric suction is a crucial aspect controlling the behaviour of unsaturated soils. As the soil dries out or wets up, the suction changes and this relationship between suction and moisture content is known as the Soil Water Retention Curve (SWRC) (Toll, 2012). Al Haj and Standing (2016), further stated that SWRCs are frequently used to investigate the coupled hydromechanical behaviour of unsaturated soils. Fredlund *et al.* (2012), stated that the curves express the relationship between the logarithm of soil suction and either the degree of saturation, void ratio, volumetric water content or gravimetric water content. In other words, it describes the relation between soil suction and the changes in volume and / or moisture content.

The theoretical framework for SWRCs and the related terminology is depicted schematically in Figure 2-25 taken from Al Haj and Standing (2016). As indicated, the solid line is the primary drying curve (PDC) and the bold dashed line the primary wetting curve (PWC). As a fully saturated sample starts to dry out, the suctions will gradually increase without a change in the degree of saturation. The relationship will follow the PDC until the air entry value is reached. At this point the degree of saturation starts to decrease and the relationship follows the PDC until the residual degree of saturation is reached, where there is no further change in the degree of saturation while suction increases. Under an ambient laboratory temperature of 20°C, a zero value for the degree of saturation is seldom reached. It is only when oven dried that the sample reaches a state of zero water content (Toll, 2012).

Upon wetting a sample from the residual state, the relationship follows the PWC until the fully saturated state is reached, often at a lower degree of saturation than on the PDC due to hysteresis.

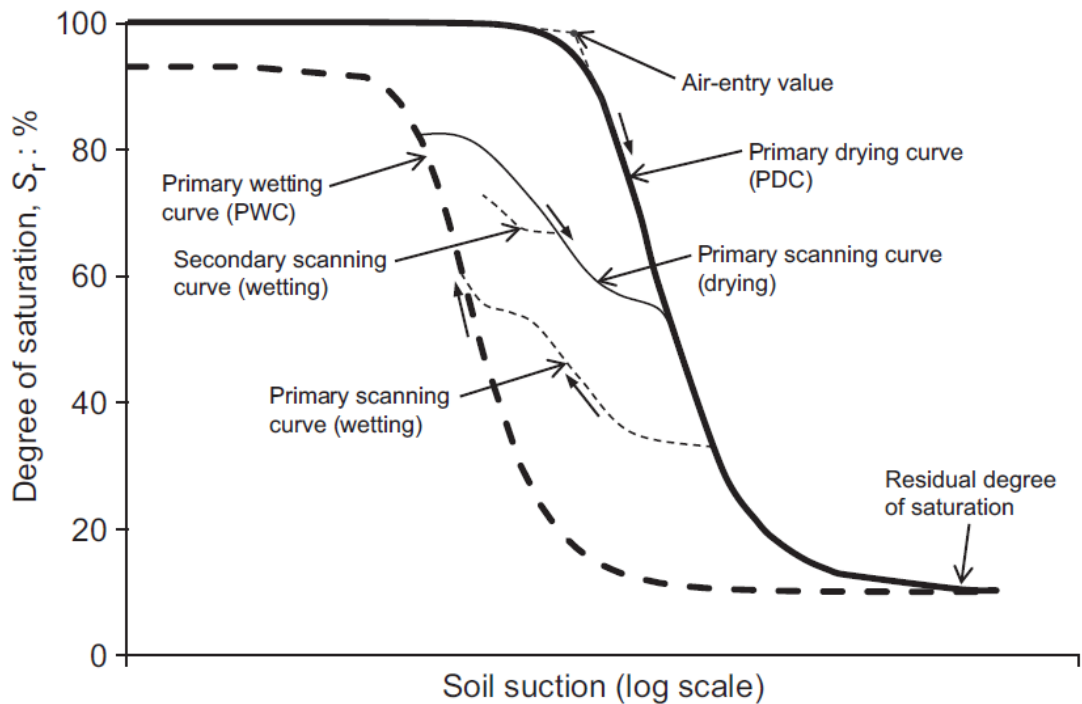


Figure 2-25: The SWRC framework and terminology from Al Haj and Standing (2016).

According to Toll (2012) the PDC and PWC define an envelope of possible states within which the soil can exist. It is important to note, as mentioned by Al Haj and Standing (2016) and Toll (2012), that the PDC and PWC can only be determined by drying the sample from a saturated state or wetting it from the residual state. Wetting or drying from any other condition or intermediate point will follow what are called scanning curves, which are not unique to the sample being tested.

As stated by Toll (2012) and Al Haj and Standing (2016), SWRC are void ratio dependent, meaning that a different SWRC can be obtained if the sample is dried from different void ratios.

Toll (2012) cautioned against determining the SWRC based on suction and gravimetric moisture content measurements, without volume change measurements, and then expressing the results in terms of degree of saturation or volumetric water content based on the initial void ratio. This practice can lead to errors for soil that swell or shrink significantly during wetting or drying.

There are several methods or techniques to measure soil suction listed by Toll (2012), including conventional and high capacity tensiometers, filter paper test, psychrometers, porous block sensors, pressure plates, vapour control techniques and osmotic control technique. For the

purposes of this study, only the tensiometer and filter paper technique will be used and are discussed in further detail.

Jacobsz (2018) described the construction and use of tensiometers in the geotechnical laboratory at the University of Pretoria for the measurement of matric suction. The tensiometers are similar to the original design by Ridley and Burland (1993) in that they also comprise a porous ceramic with a high air-entry value fixed to a pressure transducer with a small water reservoir in between. Rather than using a steel housing, the tensiometer is sealed with an epoxy resin. The completed tensiometers are oven dried for at least 4 hours at 60°C (to ensure that any moisture in the porous disk and water reservoir is removed) and then saturated in a triaxial cell at a positive cell pressure of 700kPa.

To verify that saturation was achieved, the cell pressure is cycled up and down and the response time of the tensiometer observed. A sluggish response indicates incomplete saturation and the tensiometers are then left at a pressure of 700kPa and the process repeated until the result is satisfactory. Once saturated, the tensiometers are calibrated and ready for use.

While the tensiometer only measures matric suction, the filter paper technique can be used to measure both matric and osmotic suction. According to Toll (2012), pieces of filter paper are wrapped with the soil sample, sealed and left to equilibrate for at least 7 days. The filter paper is a highly controlled material with a closely defined suction to water content relationship, i.e. based on the moisture content of the filter paper at the end of the test, the suction of the sample can be estimated. Hamblin (1981) produced a calibration curve to be used for Whatman® No.42 filter paper. Toll (2012) further stated that if the filter paper is wrapped in direct contact with the soil, equilibration takes place through liquid water flow and matric suction is measured. To measure osmotic suction, the soil and filter paper are separated by mesh, to allow equilibration to occur only through vapour transfer.

2.6 SUMMARY

The unexpected formation of 38 sinkholes due to subsurface erosion on Donkerhoek farm more than 24 years after mining in the area ceased, brings the need for a method to predict the likelihood of sinkhole formation to the fore. At present, no such a method is available.

Having reviewed the available literature on sinkholes caused by SSE above undermined ground in South Africa, the phenomenon of subsurface erosion and the mechanisms, soil properties

and predictive models related to sinkhole formation, the scene is set for the fieldwork and experimental programme.

It is hypothesised that a method can be developed to predict the likelihood of sinkhole formation due to subsurface erosion above undermined ground. It is believed that by investigation of the 38 sinkholes that formed on Donkerhoek farm through fieldwork and laboratory testing, the key mechanisms and critical soil properties can be identified. These results, when viewed against the available information in the literature review, are anticipated to be sufficient to form the crux of the prediction method.

3 FIELDWORK

3.1 INTRODUCTION

In this chapter, the fieldwork investigation and results are presented. The site location and regional geology are briefly described followed by the fieldwork methodology and results. Although the main discussion of the fieldwork relating to the evaluation of the hypothesis is contained in Chapter 5, limited discussion of the fieldwork results is given in this chapter. This is regarded as necessary to provide perspective on the laboratory testing programme in Chapter 4.

The purpose of the fieldwork was twofold: to understand the mechanism at work in SSE leading to sinkhole formation and to collect samples for laboratory testing to identify the critical soil properties influencing the phenomenon. Both are critical components of any attempt to develop a method to predict the likelihood of sinkhole formation.

Some of the observations made during the fieldwork are not directly relevant to the evaluation of the hypothesis. As these observations are still relevant to the topic of SSE above undermined ground, they are briefly mentioned in this chapter but not discussed further in detail.

3.2 SITE LOCATION AND REGIONAL GEOLOGY

The 38 sinkholes noticed in November 2016 are all located on the farm Donkerhoek. This farm, and the neighbouring farm to the south called De Pan¹, have a history of sinkholes due to SSE as described in section 2.3.2. As such they provide the ideal location to investigate the mechanisms and soil parameters involved in the SSE and sinkhole formation process.

The farms are located to the south-west of Sasolburg in the northern Free State as shown in Figure 3-1. The portions of the farms investigated are indicated in red and discussed in detail in section 3.3.1.

¹ Although Van der Merwe (1990) refers to the farm as Die Pan, the current farm owner refers to it as De Pan.

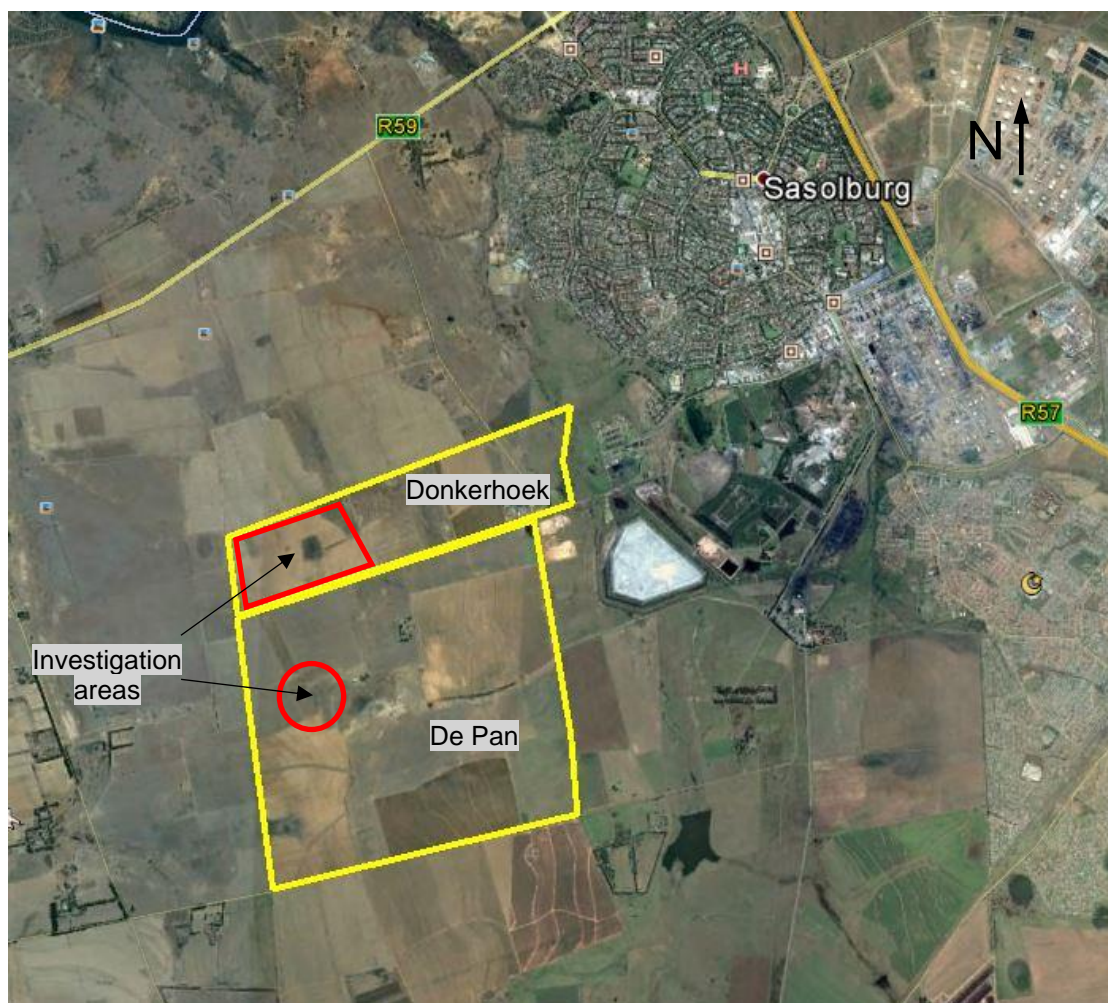


Figure 3-1: Location of Donkerhoek and De Pan farms near Sasolburg with investigation portions indicated.

As mentioned in Chapter 2, Donkerhoek and De Pan farms have been undermined by Sigma Colliery. Since active mining has ceased, the mine is now known as Sigma Defunct Mine. According to Antrobus (2016) Sigma Defunct Mine is located in the Sasolburg-Vereeniging Coalfield. In terms of its regional geology, the coal bearing horizon is known as the Vryheid formation which forms part of the Ecca Group of Sediments, which comprises mainly sandstone, shale, interbedded siltstone and coal of varying thickness. The Ecca Group forms part of the Karoo Supergroup.

Antrobus (2016) further states that there are four mineable coal seams found within the Sasolburg-Vereeniging coalfield. They are numbered from the base upwards as Seams 1, 2A, 2B and 3. Two dolerite sills are present over the entire coal field.

3.3 METHODOLOGY

3.3.1 Selection of investigation areas

To ensure that sufficient data is gathered in the fieldwork phase to evaluate the hypothesis, it was essential that the investigation areas be chosen with care – especially with the limited time and budget available. The location of the historical and 2016 sinkholes, in combination with the undermining subsidence records were used to select the investigation areas.

The starting point in selection was the location of historical and current sinkholes on Donkerhoek and De Pan farms. The sinkholes were current at the time of the investigation in that the November 2016 sinkholes were still visible during the investigation in June 2017, since the fields had not been ploughed in between.

The location of all the sinkholes which have formed due to SSE on Donkerhoek farm, as gleaned from the available records in the literature review, are shown in Figure 3-2 and detailed below. These are all located within the study area indicated in Figure 3-1.

- Sinkholes found in 2006 (indicated by blue dots) and a subsidence crack investigated in 1992 (indicated by a red line) as reported by Van der Merwe (2017a).
- The 38 sinkholes noticed in November 2018 are indicated by the orange markers (Scheppel, 2017a).

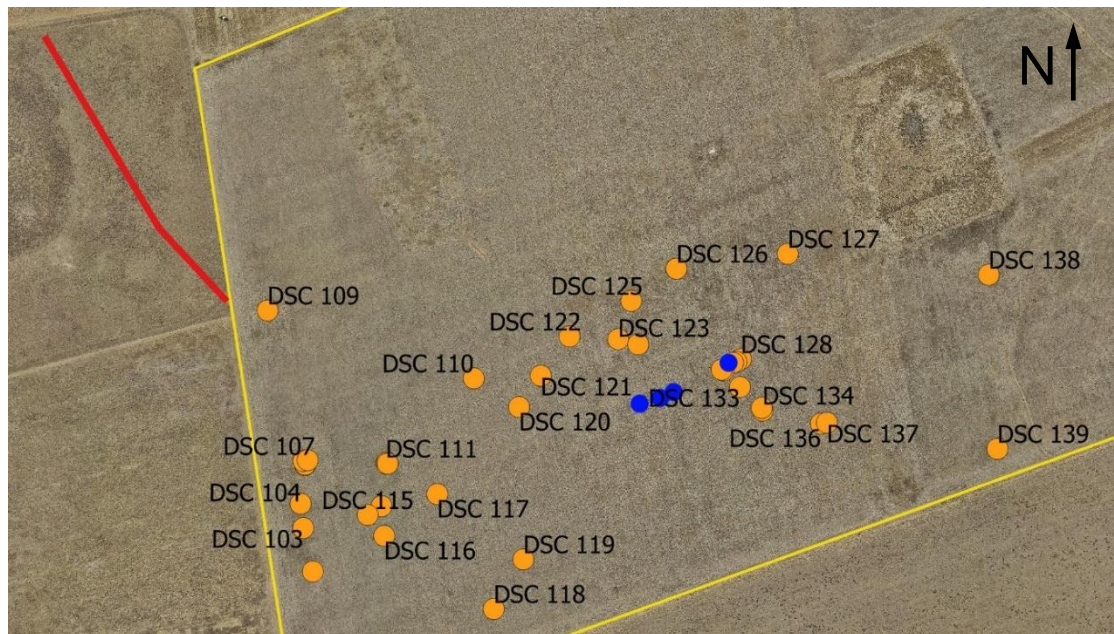


Figure 3-2: Location of sinkholes on Donkerhoek farm.

On De Pan farm, the only sinkhole records found in literature are those shown in Figure 3-3. Included, and re-orientated, are the sinkholes shown in Figure 2-4 (recorded before 1990 and shown by the red dots) and sinkholes found in 2006 within the green circled zone as scaled from Van der Merwe (2017a). Refer to Figure 3-1 for the general location on De Pan farm.

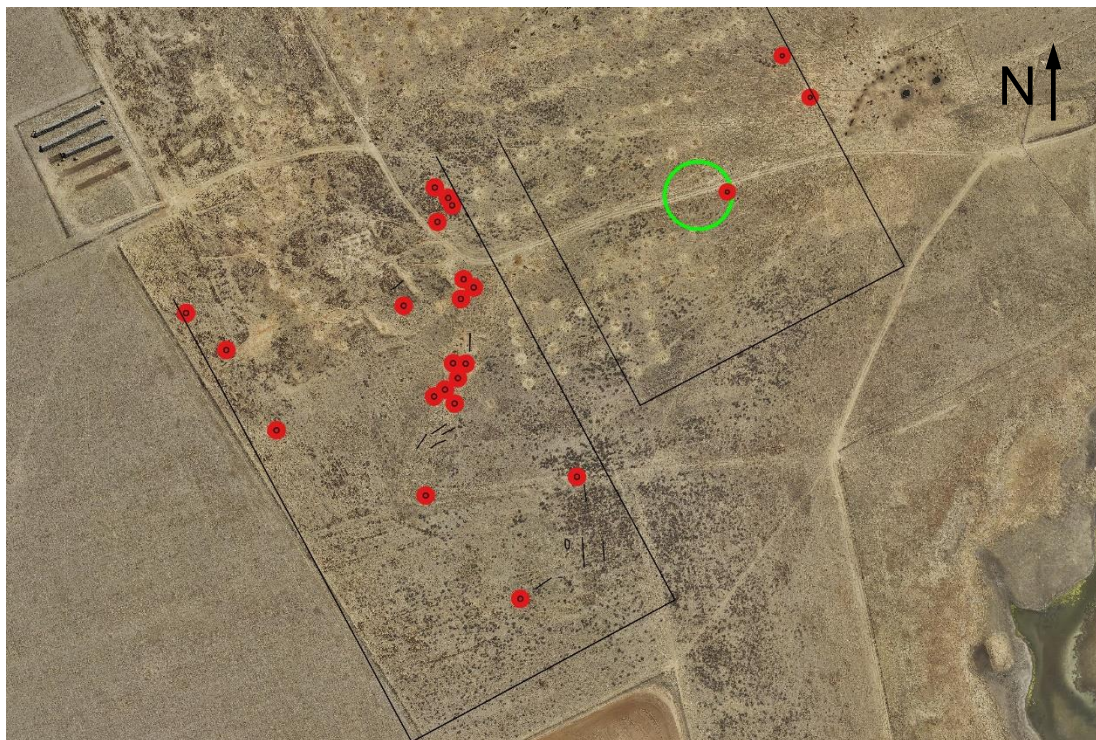


Figure 3-3: Location of sinkholes on De Pan farm.

As mentioned in the literature review, it was confirmed through test pit excavation in the Secunda area that SSE occurs when overlying soil is eroded into cracks in the rock mass caused by subsidence due to undermining.

In order to isolate the critical soil properties and factors involved in SSE and sinkhole formation in the current study, it was essential to not only investigate areas where sinkholes had formed, but also areas where they had not. The objective, therefore, was to find and investigate an area where subsidence (and presumably cracking of the rock mass) had occurred, but no records of sinkholes were available.

Such an area was located to the north of the November 2016 sinkholes on Donkerhoek farm as shown by the green circle in Figure 3-4. The proof that subsidence has occurred in the area was obtained from the limit of subsidence lines recorded at the time of mining as reported by Van der Merwe (2017a). The subsidence lines are the turquoise lines in Figure 3-4. Apart from

the subsidence lines, the area was also chosen as double longwall mining was carried out, which would lead to subsidence of approximately 3m (Coetser, 2014) and the cracking of the rock mass and the possibility for SSE to occur.

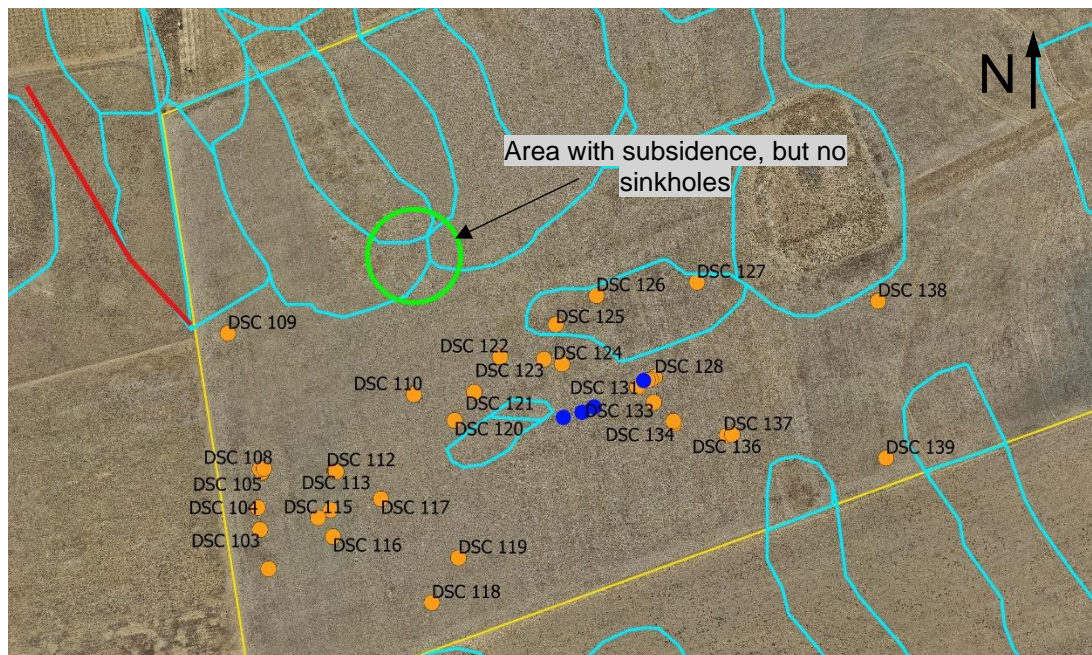


Figure 3-4: Location of area with subsidence cracks, but no record of sinkholes.

3.3.2 Investigation methods and positions

The initial investigation positions were chosen based on the desk-top data described above. Based on the investigation area selection criteria mentioned above, three categories of test pits were excavated.

- In places where existing sinkholes were visible, test pits were excavated at the sinkhole positions. Where large diameter sinkholes were present (>1m in diameter), an attempt was made to only excavate half the sinkhole and keep the remainder intact so that the mechanism could be observed. In most cases, once the excavation is made, all evidence of the sinkhole at ground surface is destroyed.
- To investigate the location of historical sinkholes, trenches were excavated at the approximated positions, perpendicular to the subsidence lines, to locate any evidence of the historical sinkholes.
- Thirdly, in areas where no records of sinkholes exist, trenches were excavated perpendicular to subsidence lines to look for evidence of the original subsidence cracks.

As the position of the trenches in the second and third categories were scaled from small figures in Van der Merwe (2017a), a limited level of confidence could be placed on the accuracy of the coordinates. Thus, the trenches were excavated approximately 20m long (10m on either side of the coordinate) and then both sides of the trench were inspected with a geological pick to identify any signs of subsidence cracking or sinkholes.

A summary of all the investigation positions is given in Table 3-1 and the locations shown by the yellow markers in Figure 3-5 and Figure 3-6 for each of the farms.

Table 3-1: Summary of all investigation positions

Test Pit / Borehole	Coordinates (Cape Datum Lo27)		Method	Comment
	X	Y		
TP01	2970448	-077268	Excavator	West of DSC109A
TP02	2970452	-077269	Excavator	At sinkhole DSC109A
TP03	2970453	-077275	Excavator	At sinkhole DSC109
TP04	2970513	-077812	Excavator	Between DSC129 and DSC130
TP05	2970510	-077814	Excavator	Through DSC128, east of TP04
TP06	2970568	-077844	Excavator	Through DSC134
TP07	2970576	-077836	Excavator	No sinkhole
TP08	2970342	-077497	Excavator	Profiled in trench 33A - 33B
TP09	2970320	-077515	Excavator	Profiled in trench 32A1 - 32B1
TP10	2970381	-077518	Excavator	Profiled in trench 30A1 - 30B1
TP11	2971615	-077998	Excavator	Profiled in trench 13A - 13B
TP12	2971654	-078012	Excavator	Profiled in trench 15A1 - 15B1
TP13	2971632	-077880	Excavator	Profiled in trench 26A1 - 26B1
TP14	2971644	-077870	Excavator	Profiled in trench 25A1 - 25B1
TP15	2971660	-077845	Excavator	Through existing unnamed sinkhole
TP16	2971498	-077879	Excavator	Near borehole D225028
TP17	2970625	-077322	Excavator	Through DSC106
TP18	2970458	-077277	TLB	East of TP03
TP19	2970381	-077523	TLB	Near TP10
TP20	2970515	-077807	TLB	West of DSC130 and TP04
TP21	2971547	-078003	TLB	Found buried animal carcass, closed again
TP22	2971538	-077991	TLB	Near TP21
BH01	2970342	-077494	Drilled	Drilled near TP08
BH02	2970388	-077522	Drilled	Drilled near TP10 and TP19

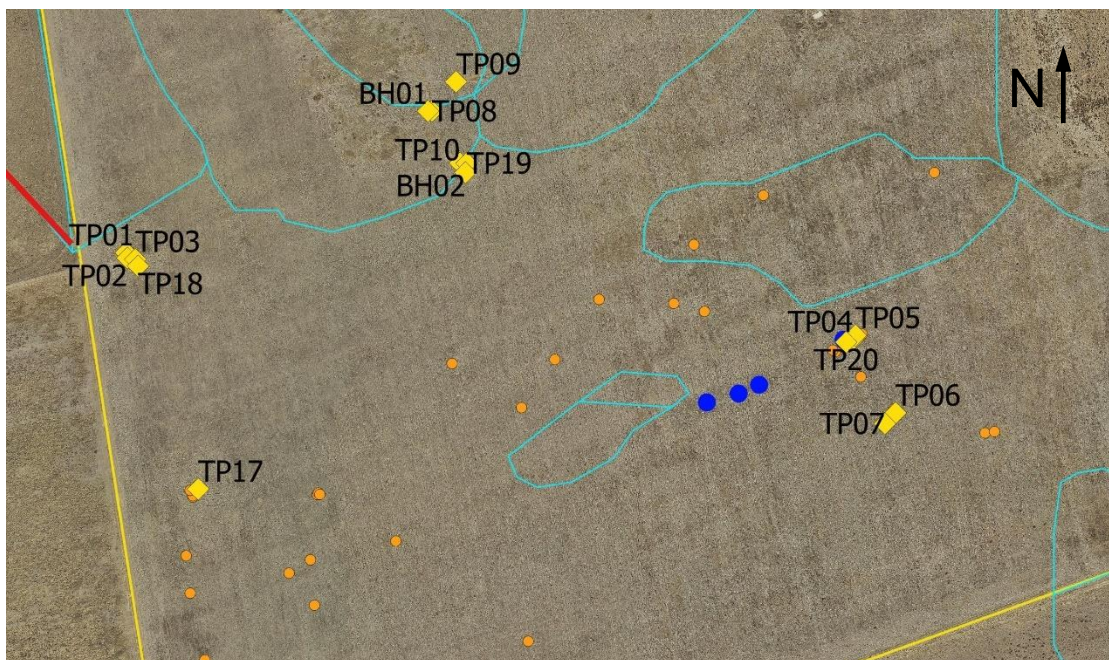


Figure 3-5: Location of all investigation positions on Donkerhoek farm.

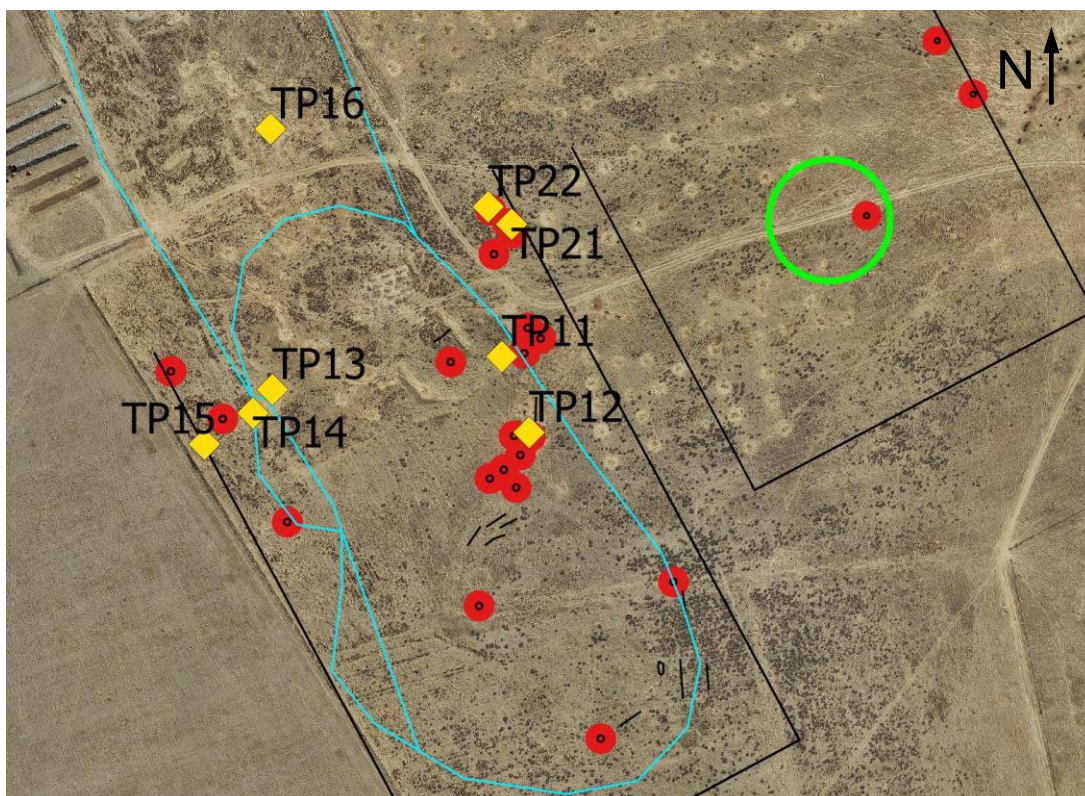


Figure 3-6: Location of all investigation positions on De Pan farm.

During the test pit excavation, the main soil horizons were separated on either side of the trench / test pit. In this way, the horizons could be sampled easier and the top soil could be placed on top during backfilling as these were cultivated fields. Both disturbed and undisturbed soil samples were collected from the spoil: Disturbed samples were bagged and sealed while the undisturbed samples were wrapped in layers of cling wrap and aluminium foil. It should be noted that in many cases a sample comprised a few sample bags or undisturbed blocks – in these cases the same sample name was used, but a unique number was assigned to each sample bag or block sample.

The fieldwork was carried out in two phases: In the first phase, test pits TP01 up to TP17 were excavated and profiled between 26 June 2017 and 1 July 2017. A 20 ton excavator was used as is shown in Figure 3-7. The purpose was to cover all three categories mentioned above to collect as much information as possible.



Figure 3-7: 20 ton excavator excavating at TP06.

After a review of the results of the first phase (mainly regarding the diameters of the sinkholes encountered while walking on site), three study areas were identified to focus on in the second phase, as described below and shown in Figure 3-8.

- *Area 1 – Large sinkholes:* The largest sinkhole formed in November 2016 with a diameter of 1,5m is located in this area (see Figure 1-1).

- *Area 2 – No sinkholes:* This area was selected as the area shown in Figure 3-4, where no sinkholes were recorded, but where subsidence cracks were previously recorded.
- *Area 3 – Small sinkholes:* Smaller sinkholes formed in November 2016, with diameters less than 0,3m.

All three study areas are located on Donkerhoek farm.

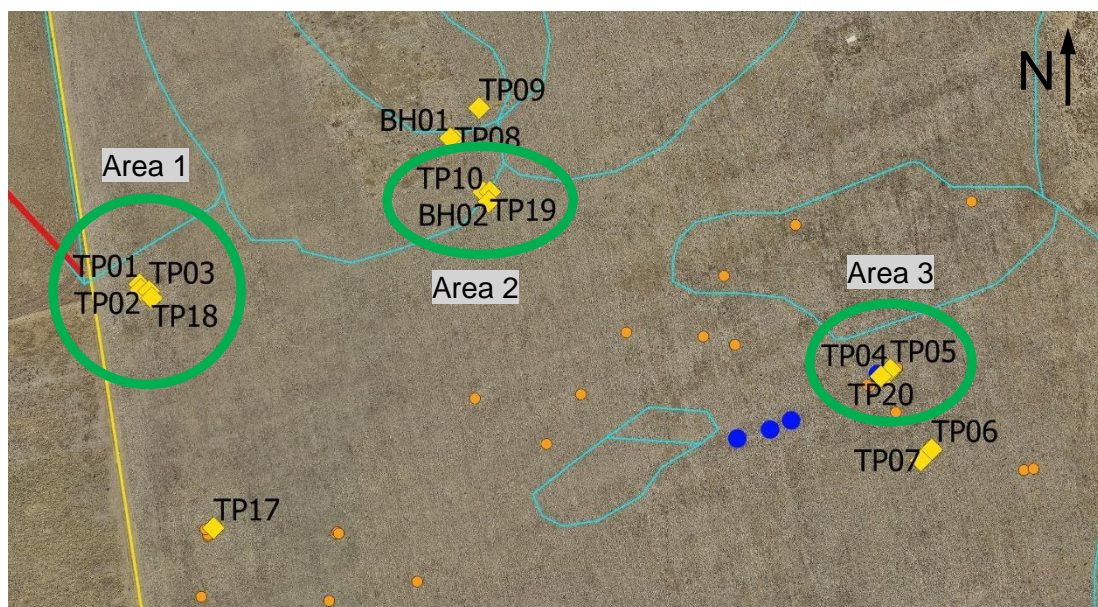


Figure 3-8: Location of three selected study areas on Donkerhoek farm.

The study areas were chosen to identify the critical parameters involved in the SSE and sinkhole formation process to be able to evaluate the hypothesis. As will be seen in Chapter 5, the comparison of the results from the study areas form the backbone of the result analysis.

In the second phase, test pits TP18 to TP22 were excavated with a TLB and profiled on 8 August 2018. As the depth to rock could not be found in the area where TP08, TP09, TP10 and TP19 were excavated (Area 2), two percussion boreholes were drilled on 21 March 2018 to determine the depth of the rockhead. A photo of the percussion drill rig is shown in Figure 3-9.



Figure 3-9: Percussion borehole rig drilling BH01.

During the second phase of the fieldwork, an attempt was made to excavate in the area on De Pan farm where the first largest sinkholes were noticed in 1986 (see Figure 2-2 and Figure 2-3). Although the exact locations could not be determined from records, the area was pointed out by Mr Douw Crous (Crous, 2017). TP21 was positioned on a local depression area (approximately 1,8m diameter). After the first few buckets were excavated, an animal carcass was exposed and the excavation stopped. Abundant coarse ash was also found. TP22 was positioned close to TP21 to obtain an idea of the soil profile, but the TLB had a hydraulic failure when a depth of 2m was reached and the excavation was stopped. Unfortunately, a detailed assessment of the soil in this specific area could not be carried out and the results are not discussed further.

3.4 RESULTS

The results of the fieldwork are presented in this section. The soil profile results are given, followed by descriptions of observations made during the test pit excavation on the mechanisms involved in SSE and sinkhole formation.

3.4.1 Soil profiles

In broad terms, a similar soil profile was encountered in each of the test pits, with the depth to rock being one of the main variables. The typical soil profile comprised a transported horizon in the upper 0,4m, underlain by residual sandstone to a depth of 3,0m with soft rock sandstone below. A detailed description of the typical profile is given below, described according to Jennings *et al.* (1973).

- 0 – 0,4m: Slightly moist, light brown, loose, pinhole voided, silty fine sand with abundant ferricrete nodules and fine roots. Hillwash
- 0,4m – 3,0m: Slightly moist, grey mottled light orange brown and black, very stiff, fine sandy clay with scattered calcrete nodules. Reworked residual sandstone.
- +3,0m: Yellow brown speckled black, completely weathered, medium fine grained, soft rock probably becoming medium hard rock with depth. Sandstone.

Detailed soil profiles are included in Appendix A.

3.4.2 Observations

The observations made during the test pit excavations are listed in this section. Rather than discussing the test pits one by one, the main observations in each study area are presented first, followed by some of the additional observations in other areas. All the observations made during the fieldwork phase are recorded in Appendix A, in the following sections:

- Some observations are included in the soil profiles.
- Fieldwork photographs.
- A summary of all the key observations in table format for comparison purposes.
- Additional fieldwork notes not included in the soil profiles.

Area 1 – Largest sinkhole from November 2016

During the planning for Area 1, only one test pit was envisaged at the largest sinkhole referred to as DSC109 and shown in Figure 1-1. However, upon arrival at the location, another partially collapsed sinkhole was noticed to the north west of DSC109. (The partially collapsed sinkhole must have formed between November 2016 and June 2017 as it was not recorded with the November 2016 sinkholes.) Consequently, four test pits were excavated in Area 1 with layout shown in Figure 3-10. The photograph was taken long after the test pits were backfilled. The findings of each test pit are presented below and combined cross sections to show the mechanism are given in Figure 3-15. The depth to sandstone rock in all 4 test pits in Area 1 was 3m.

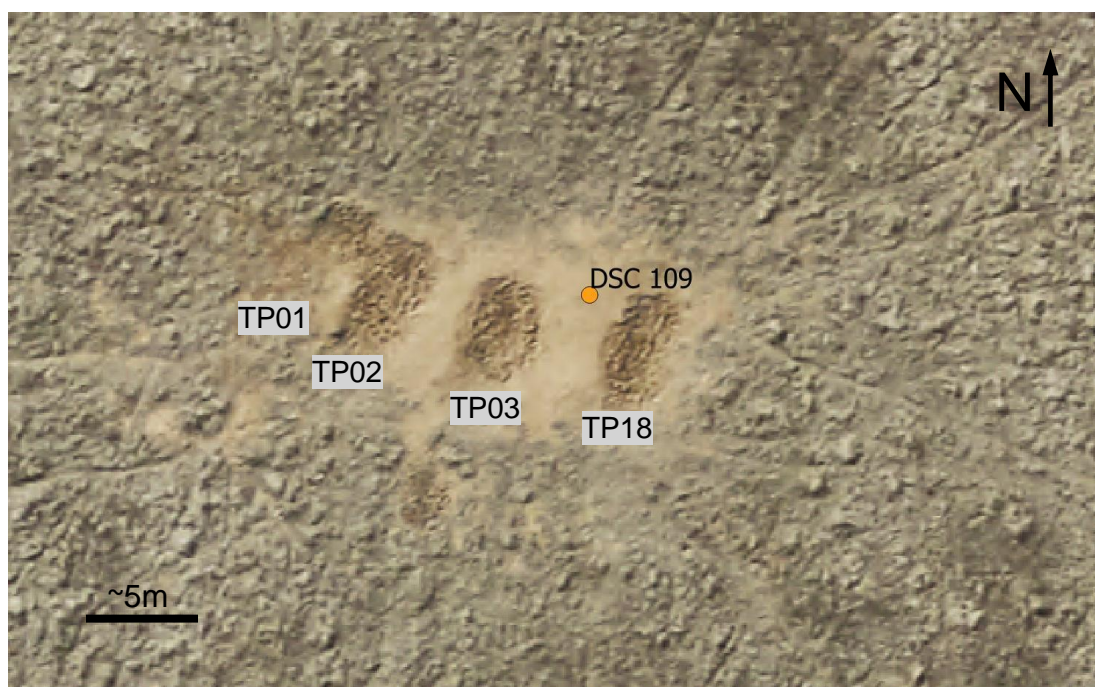


Figure 3-10: Test pit layout in Area 1.

TP01 – no sinkhole

TP01 was excavated to the north west of the partially collapsed sinkhole. It revealed a 50mm wide infilled crack in the sandstone rock at 3m depth. Between the rock head and the bottom of the hillwash layer above, a crack infilled with hillwash was noticed running through the residual sandstone. Figure 3-11 shows both the infilled cracks through the residual sandstone and in the rock at the bottom of the test pit. In the photo, the infill has been scraped out with a

geological pick. The upper portion of the residual sandstone layer had a micro-shattered appearance with a dense network of fissures.

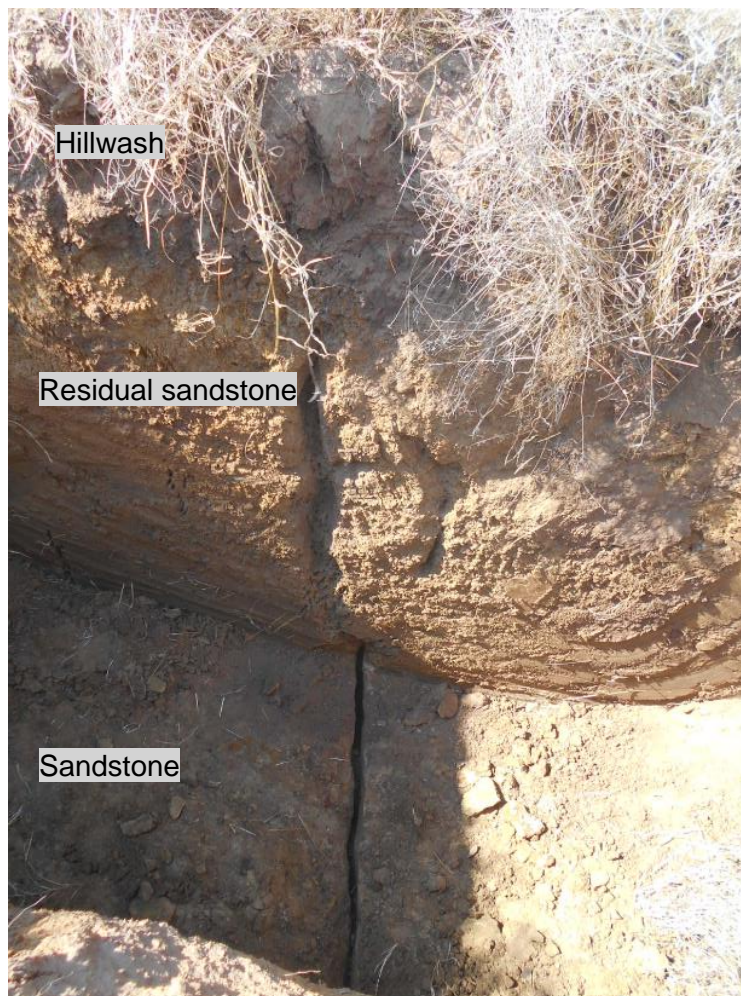


Figure 3-11: Looking downwards into TP01 showing the infilled cracks in the residual sandstone and rock below.

TP02 – Partially collapsed sinkhole

TP02 was excavated through the partially collapsed sinkhole. The photos in Figure 3-12 were taken prior to excavation and show the collapsed lid opening of approximately 700mm diameter, the lid thickness of 350mm and how the sinkhole widens to approximately 1500mm diameter below surface. The underside of the lid was not horizontal between the perimeter of the opening and the full sinkhole width, but shaped in the form of a dome (arched) with the lid thickness increasing with diameter.



Figure 3-12: The partially collapsed sinkhole at TP02.

Once the excavation through half of the sinkhole down to refusal on rock was completed, a V-shaped zone infilled with hillwash extending through the residual sandstone to the crack in the rock, was noticed. The top of the V-shape had the same width as the original diameter of the sinkhole.

TP03 – Largest November 2016 sinkhole

At TP03, excavated through sinkhole DSC109, a similar V-shaped zone of infilled hillwash was noticed below the sinkhole bottom as in TP02. A marked-up image of the V-shape zone is given in Figure 3-13 with the crack in the rock below (the crack infill had been excavated by hand). It was noticed that the residual sandstone between the bottom of the V-shape and the crack in the rock had an almost leached appearance with a softer consistency than the residual sandstone to either side. It appears that this soft zone was in fact the collapsed subterranean tunnel which has formed above the crack in the rock. The V-shape extended from the collapsed tunnel to the perimeter of the sinkhole above at an angle of 57° above the horizontal.



Figure 3-13: V-shaped zone in TP03 above the collapsed tunnel and crack in the rock below.

TP18 – No sinkhole

TP18 was excavated to the south east of TP03 to collect more samples for laboratory testing. No sinkhole was found on surface and there were no dominant infilled cracks within the residual sandstone as in TP01. However, at the bottom of TP18, a subterranean tunnel was found as shown in Figure 3-14. When TP18 was widened towards TP03, it was noticed that the tunnel invert decreased towards TP03 as shown in Figure 3-15. Below the tunnel, an infilled crack was found in the sandstone rock.



Figure 3-14: View downwards into TP18 showing the subterranean tunnel running from right to left.

The findings of the four test pits in Area 1 are summarised through the cross sections in Figure 3-15.

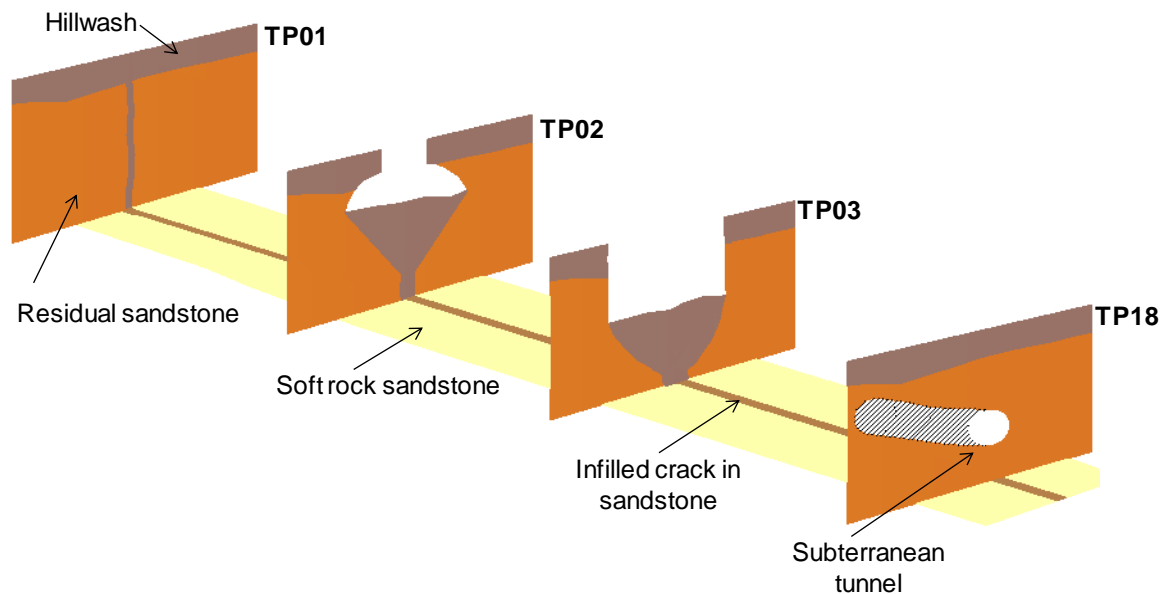


Figure 3-15: Cross section through each test pit in Area 1.

The main observations made from Figure 3-15 are:

- As shown by the partially collapsed sinkhole at TP02, the residual sandstone provides a significant contribution to the support of the lid.
- The probability of lateral flow (flow in a horizontal direction instead of only vertical flow) occurring during the subsurface erosion process cannot be excluded. Although the crack in the rock below the tunnel in TP18 was filled in, the downwards sloping of the tunnel towards TP03 (where the largest sinkhole was) points to possible flow towards TP03.
- In Area 1, over a length of 25m and above a 50mm wide infilled crack in the rock, half the area had two large sinkholes and the other half no sinkholes.
- In all four test pits in Area 1, the upper portion of the residual sandstone layer had micro-shattered appearance.

Area 2 – No records of sinkholes.

In Area 2, as there were no records of sinkholes in the area, three 20m long trenches were excavated perpendicular to the subsidence lines in Figure 3-4, as shown in Figure 3-16. The objective was to find similar hillwash-infilled cracks within the residual sandstone as found in Area 1. During the fieldwork, the steep slopes around the perimeter of the subsided area above the longwall panel was clearly visible. No crops were planted within the panel perimeter as they do not survive the surface run-off accumulating in the subsided area.

The first two trenches (at TP08 and TP09) yielded no evidence of infilled cracks and it was only in the third trench near TP10 that an infilled crack was found. Photos of one of the trenches and of the infilled crack are shown in Figure 3-17. The infilled crack was found on both sides of the trench and had a width of up to 150mm at the top on the eastern side, decreasing in width and terminating in the residual sandstone at a depth of 1,2m.

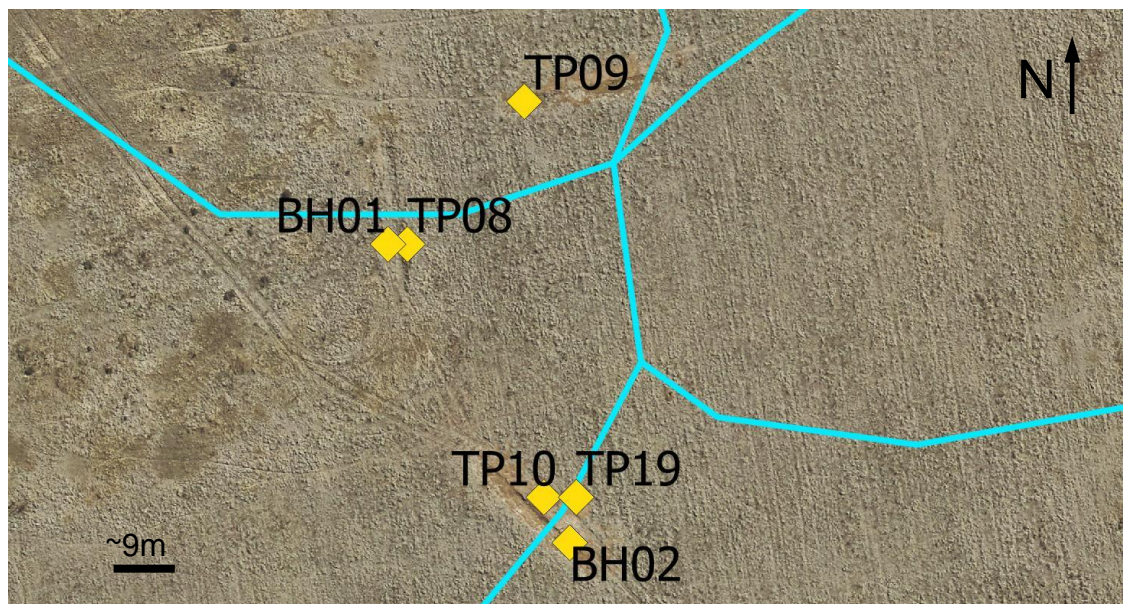


Figure 3-16: Layout of test pits and boreholes in Area 2.



Figure 3-17: Trench in Area 2 at TP10 and hillwash infilled crack in the residual sandstone.

As no rock was found in TP10 (nor in any of the other trenches and test pits in Area 2), the infilled crack could not be linked to a subsidence crack in the rock as was done in Area 1. As such, the possibility exists that the crack found was merely a desiccation crack infilled with hillwash. However, since the crack was continuous on either side of the trench; as it was the only crack found over a length of 20m and since its location ties up with the subsidence cracks in Figure 3-4, it was concluded that this was a subsidence crack.

TP19 was also excavated with a TLB in Area 2, very close to TP10 as shown in Figure 3-16, to obtain additional samples for laboratory testing. At both TP10 and TP19, the upper portion of the residual sandstone layer did not have the same densely fissured appearance as in Area 1.

The undermining plans (Scheffel, 2017b) indicated an overburden thickness of 18m in Area 2, implying that the rock depth is at 18m. To be able to compare the mechanisms observed and soil properties obtained in Area 2 with the other study areas to evaluate the hypothesis, it was essential that the depth to rock be confirmed. Two percussion boreholes were drilled in Area 2 at the locations shown in Table 3-1. Very soft rock sandstone was found at 6,5m in BH01 and at 5,7m in BH02.

Area 3 – Small sinkholes

Area 3 was chosen due to the appearance of small diameter sinkholes, typically less than 0,3m in diameter. The test pits excavated and profiled in Area 3 are TP04, TP05 and TP20 as shown in Figure 3-18, together with the locations of some of the November 2016 sinkholes as recorded by Scheppel (2017a). At the location of the test pits, several small sinkholes were found in an east-west alignment, parallel to the edge of the high extraction panels. The broken arch at the top of the sinkholes was formed mostly within the hillwash horizon, with little widening below into the residual sandstone horizon. A subterranean tunnel, located in the upper soil layers with a width of approximately 50mm and depth of 450mm, linked some of the sinkholes. It is postulated that the vertical sides of the tunnel are the edges of the original subsidence crack. One of the sinkholes and the corresponding tunnel are shown in Figure 3-19.

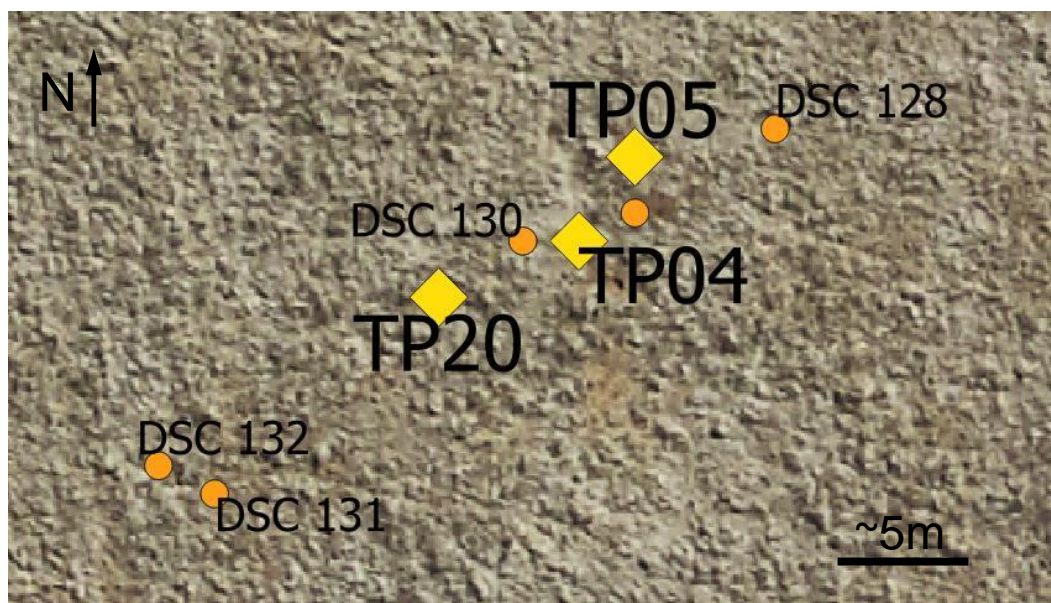


Figure 3-18: Layout of test pits in Area 3.



Figure 3-19: Typical sinkhole (0,3m diameter) in Area 3 and subterranean tunnel (0,45m deep).

In Area 3, an infilled crack in the sandstone rock at a depth of 3m was found, similar to Area 1, with similar infilled V-shaped zones linking the sinkhole at the top to the crack in the rock. However, the sides of the V-shape were much steeper as shown in Figure 3-20. The coarse material visible at the bottom of the V-shape in Figure 3-20 is coarse ash used in the past to backfill the subsidence cracks in an attempt to limit sinkhole formation.

The upper portion of the residual sandstone layer in Area 3 was not highly fissured as noticed in Area 1.



Figure 3-20: V-shape infilled with coarse ash above crack in sandstone rock in Area 3.

Observations from other test pits

Apart from the observations listed above for each of the study areas, there were several other relevant observations made in the other test pits which provide further understanding of the mechanism involved in SSE above undermined ground. These observations are presented below.

Crack in rock capped with sandstone and open below

TP06 was excavated through an existing sinkhole. The sinkhole cover had collapsed completely, and the open V-shape could be observed from surface prior to the excavation as shown in Figure 3-21. The excavator refused at 3m depth and the subsidence crack was found directly below the bottom of the open V-shape. However, the crack in the rock was not infilled with hillwash, but rather capped with intact pieces of soft rock sandstone clamped at the top of the crack as shown in Figure 3-22. Below the sandstone cover, the crack was open with the sides of the crack stained with hillwash washed in from above. The air inside the crack was

warm to the hand. Further photos from TP06 are presented in Appendix A and a possible explanation for the clamping of the rock at the top of the crack is presented in section 5.6.5.



Figure 3-21: Looking down into the empty V-shape of the sinkhole at TP06.



Figure 3-22: Crack in the rock at TP06 covered with sandstone and open below.

It was not possible to measure the depth of the crack with a measuring tape. A measuring attempt was made by dropping pebbles (15mm – 20mm in diameter) into the crack and

recording the time taken until no further noise from the pebble hitting the sides of the crack could be heard. The fall durations of the pebbles are summarised in Table 3-2.

Table 3-2: Fall duration for pebbles in to crack at TP06

Gravel drop	Time (s)
Drop #1	3,15
Drop #2	Nothing heard
Drop #3	4
Drop #4	4,19
Drop #5	4,2
Drop #6	4,3

Using a typical value of 4 seconds, the displacement of a falling object can be calculated as approximately 80m using the equations of motion. If the displacement is halved to allow for the collisions with the crack sides on the way down, a depth of 40m is calculated. Although this is a highly theoretical and unproven calculation, the value is of a similar order of magnitude as the 25m crack depth suggested by Van der Merwe (2018) in section 2.3.3.

TP07 was excavated approximately 20m west of TP06, in line with the crack found in TP06 but at a location where no sinkholes had formed. A similar crack, capped with clamped sandstone rock pieces at the top and open below, was found at a depth of 3,6m. However, the main difference was that the sides of the crack was not stained with hillwash as at TP06.

Termite activity within infilled subsidence cracks

In many of the sinkholes and infilled subsidence cracks within the residual sandstone, evidence of termite activity was found. Two of the instances are shown in Figure 3-23. Prior to excavating TP03, abundant termite activity was noticed in the sides of the collapsed sinkhole DSC109. At TP10, a termite nest was found within the hillwash infilled crack within the residual sandstone. Some further discussion of the termite activity is given in section 5.6.6.



Figure 3-23: Termite activity in the side of sinkhole DSC109 (left) and TP10 (right).

Appearance of collapsed subterranean tunnel

As mentioned in the results from Area 1 above, a zone with a leached appearance and a softer consistency than the residual sandstone on either side, was noticed between the base of the V-shape and the crack in the rock in test pits TP02 and TP03. Following the excavation of TP18, it was realised that the zone is in fact the collapsed subterranean tunnel. Similar zones were recorded in TP07 and TP14.

Cluster appearance of sinkholes

A visual inspection of the sinkholes which formed in November 2016, showed that many of them appeared in clusters. At TP17 a circular, 0,3m deep depression with a diameter of 2,5m was noticed with many small diameter (50mm to 100mm) sinkholes around the perimeter.

Fractured zone rather than crack

At all the test pits excavated through sinkholes in Areas 1 and 3, a clearly defined crack was observed in the rock. However, at TP11 (excavated near sinkholes in Van der Merwe (1990)) and at TP15 and TP17 (excavated through existing sinkholes), a single defined crack in the rock was not found. Rather, a fractured rock zone was encountered directly below the position of the sinkholes. Further discussion on this fractured zone is presented in section 5.6.3.

3.4.3 Discussion with farmers

Mr Douw Crous has intimate knowledge of the history of Donkerhoek and De Pan farms. The following information was obtained from Mr Crous during the fieldwork and through a telephone conversation.

- In the area on Donkerhoek farm where the 38 sinkholes were noticed in November 2016, the ploughing direction was changed by 90° around 2014 or 2015. The area was ripped to a depth of 350mm in April 2016. (Crous, 2017 and Crous, 2018).
- Prior to November 2016, a period of prolonged drought was experienced and the sinkholes formed after rainfall occurred ending the dry period (Crous, 2017).
- In his experience, based on observations of other sinkholes on the farms, termite nests are often found within or close by the sinkholes (Crous, 2017).

3.4.4 Coarse Ash backfilling as remedial method

Van der Merwe (2017a) describes the use of a coarse and fine ash filter to remediate sinkholes which had formed on Sigma Colliery in the 1990's. When a subsidence crack or sinkhole appeared, coarse ash was first pushed into the crack followed by fine ash and topsoil on top. The idea was for the fine and coarse ash to act as a filter by allowing water to flow through into the crack in the rock, but limiting the transport of finer soil particles.

During fieldwork, several ash-backfilled sinkholes were exposed in the test pits, as shown in Figure 3-20 and Figure 3-24.



Figure 3-24: Historical sinkhole backfilled with ash (TP15).

It appears that the use of the ash filters is reasonably successful in mitigating the risk of future sinkhole formation.

3.5 SUMMARY OF FIELDWORK RESULTS

As mentioned above, the fieldwork carried out had a dual purpose, namely to observe the mechanisms at work in SSE and sinkhole formation and to obtain samples for laboratory testing.

During the fieldwork, three study areas were identified for investigation: Area 1 with large sinkholes, Area 2 with no sinkholes and Area 3 with small sinkholes. The results of the fieldwork observations are summarised in Table 3-3.

Table 3-3: Summary of fieldwork results from three study areas

Characteristic	Area 1	Area 2	Area 3
Typical sinkhole diameter	1,5m	No sinkholes	<0,3m
Hillwash infilled V-Shape found in residual sandstone	Slopes at 57° above horizontal	Steep slopes, no sinkhole found	Sloped at >75° above horizontal
Depth to rock	3m (Test pit)	5,7m (Borehole)	3m (Test pit)
Crack width in rock at bottom of test pit	50mm	Not exposed, too deep	50mm
Densely fissured horizon in residual sandstone	Yes	No	No

The main result of the fieldwork is the identification of the mechanism responsible for sinkhole formation: the erosion of soil from below the ground surface into underlying subsidence cracks in the rock resulting in the formation of a below-ground cavity. The collapse of the cover or lid over the cavity results in a sinkhole on surface. This mechanism is similar to the mechanism described in the literature study (see section 2.3.3 and Figure 2-5). However, the literature is largely based on observations and investigations in the Secunda area. The fieldwork presented above is the first occasion in which the same mechanism is confirmed at Sigma Colliery in the Sasolburg area.

Although the main mechanism of formation is identified, insufficient information is available to identify the reasons for the difference in sinkhole diameter between Area 1 and Area 3 and the reason for no sinkhole formation in Area 2. These reasons will be influenced by the laboratory test results presented in chapter 4 and are expanded upon in the discussion of all the relevant results in chapter 5.

4 EXPERIMENTAL PROGRAMME

4.1 INTRODUCTION

The purpose of the laboratory testing programme was to determine which soil properties have the most influence on SSE and sinkhole formation. As such, a wide range of laboratory tests were carried out on the soil samples including grading and indicator, dispersion tests, mineralogy, consolidated undrained triaxial and permeability tests and the determination of soil water retention curves.

During the first phase of the fieldwork carried out in June and July 2018, it was thought that the properties of the hillwash layer overlying the residual sandstone was the main contributing factor influencing the size and formation of sinkholes due to SSE. As such, the samples collected during the first fieldwork phase and the first round of foundation indicator and dispersion tests were focussed on determining the properties of the hillwash layer for comparison purposes.

However, following a careful examination of the soil profiles and the mechanisms observed during the fieldwork against the mechanisms in the literature review, it became apparent that the residual sandstone layer underlying the hillwash was the horizon to focus on in the laboratory testing. After the three study areas were identified (i.e. Area 1, Area 2 and Area 3) the laboratory tests focussed on comparing the soil properties of these areas with each other.

The laboratory test results are presented in this chapter. Emphasis is placed on the test done on the residual sandstone samples obtained from the three study areas. The comparison of the results from the three study areas forms a central part of the evaluation of the hypothesis in the next chapter. The test results from all the samples are included in Appendix B.

4.2 LABORATORY TESTS AND RESULTS

The laboratory tests carried out are mentioned in this section and a summary of the results presented. Detailed descriptions of standard geotechnical laboratory tests are not given - discussions are reserved for non-standard tests such as the determination of the soil water retention curves.

A summary of all the samples submitted for laboratory testing and the test carried out on each sample is presented in Table 4-1. In addition to these the study area, sample depth, sample type and soil description are also listed.

Table 4-1: Samples submitted for laboratory testing and tests carried out

Study Area	Sample	Depth (m)	Sample type	Soil description	Grading (UP)	Grading & Indicator	Dispersivity	Mineralogy	Bulk density	CU Triaxial	Triaxial permeability	SWRC	Specific gravity
1	TP01/1	3	Disturbed	Hillwash infill in crack (in rock)	x	x		x					x
1	TP02-DSC109A/2	0-0,35	Disturbed	Hillwash	x	x		x					
1	TP02-DSC109A/3	0-0,35	Block	Hillwash			x		x				x
1	TP02-DSC109A/4/1	>3	Disturbed	Crack infill, granular east (in rock)	x	x		x					x
1	TP02-DSC109A/4/2	>3	Disturbed	Crack infill, sandy east (in rock)	x	x		x					x
1	TP02-DSC109A/4/3	>3	Disturbed	Crack infill, clayey west (in rock)	x	x		x					x
1	TP03-DSC109/1	2,5	Disturbed	RW Residual sandstone, above crack	x	x		x					x
1	TP03-DSC109/2	2,5	Disturbed	RW Residual sandstone, north of crack	x	x	x	x	x				x
1	TP03-DSC109/3	0,6	Disturbed	Shattered Reworked residual sandstone.	x	x		x					x
1	TP03-DSC109/4	3	Disturbed	Eastern crack infill (in rock)				x					
3	TP05/1	1,2-3,0	Disturbed	RW Residual sandstone	x	x	x		x				x
3	TP05/3	0,2-0,4	Disturbed	Hillwash	x	x							
3	TP05/4	0,2-0,4	Block	Hillwash			x	x	x				x
3	TP05/5	1,2-3,0	Block	Residual Sandstone				x					x
N/A	TP08/1	2,6-4,1	Disturbed	Residual siltstone / sandstone	x	x							
N/A	TP09/2	0-0,4	Block	Hillwash			x	x	x				
N/A	TP09/3	0-0,4	Disturbed	Hillwash	x	x							x
N/A	TP09/4	0,8-1,8	Block	Residual sandstone				x					x
N/A	TP09/5	0,8-1,8	Disturbed	RW Residual sandstone	x	x	x		x				x

Table 4-1: Samples submitted for laboratory testing and tests carried out (continued)

Study Area	Sample	Depth	Sample type	Soil description	Grading (UP)	Grading & Indicator	Dispersivity	Mineralogy	Bulk density	CU Triaxial	Triaxial permeability	SWRC	Specific gravity
2	TP10/1	0-0,4	Disturbed	Hillwash	x	x							
2	TP10/2	0,45-1,3	Disturbed	Residual sandstone	x	x							x
2	TP10/4	0-0,4	Block	Hillwash			x	x	x				x
2	TP10/5	0,45-1,3	Block	Residual sandstone			x	x	x				
N/A	TP12/1	0,35-0,8	Disturbed	Hillwash	x	x							x
N/A	TP12/2	0,8-1,3	Disturbed	Reworked residual sandstone	x	x	x						x
N/A	TP12/3	0,35-0,8	Block	Hillwash					x				
N/A	TP14/1	0-0,5	Disturbed	Hillwash	x	x							x
N/A	TP14/2	1,7-2,4	Disturbed	RW Residual siltstone	x	x							x
1	TP18/2	2	Disturbed	Reworked residual sandstone		x	x						
1	TP18/4	0,5-2,0	Block	Reworked residual sandstone		x	x	x		x	x	x	
1	TP18/5	1,9	Disturbed	Reworked residual sandstone				x					
1	TP18/6	2,55	Disturbed	Reworked residual sandstone		x	x						
2	TP19/1	0,5-1,3	Block	Reworked residual sandstone (reddish)		x	x	x		x	x	x	
2	TP19/2	1,3-2,0	Block	Reworked residual sandstone (grey)				x					
2	TP19/3	2-3,6	Block	Reworked residual sandstone (grey)				x					
2	TP19/5	3	Disturbed	Reworked residual sandstone (grey)		x	x						
3	TP20/1	1,3-3,0	Block	Reworked residual sandstone		x	x	x		x	x	x	

To assist in the interpretation of the results, a distinction is made between the results from the hillwash and residual sandstone. A comparison of the tests done on these two horizons is given in Table 4-2, which clearly shows that the main focus in the testing was on the residual sandstone as described above.

Table 4-2: Distribution of tests between hillwash and residual sandstone

Laboratory test	Hillwash	Residual Sandstone
Grading analysis	x	x
Atterberg limits	x	x
Mineralogy (XRD)	x	x
Element composition (XRF)	x	x
Dispersion tests: Pinhole test, Crumb test, Double Hydrometer test and Chemical Analysis	x	x
Consolidated Undrained Triaxial		x
Triaxial permeability		x
Soil water retention curves (SWRC) using tensiometers and the filter paper method		x

4.2.1 Grading and foundation indicator results

Grading curves for the soil samples were determined through sieve and hydrometer analyses done by a commercial laboratory. The grading curves for the hillwash samples taken from the three study areas (DSC109A/2, TP05/3 and TP10/1) and two samples from De Pan (TP12/1 and TP14/1) are shown in Figure 4-1.

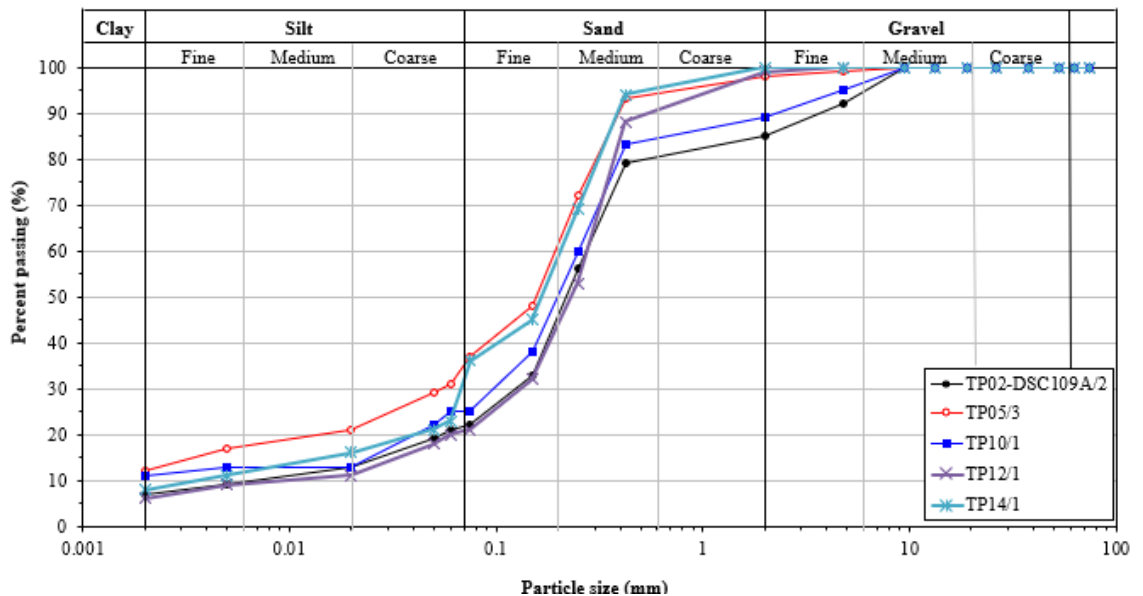


Figure 4-1: Grading curves for hillwash in Area 1, 2 and 3 and two test pits on De Pan.

The grading properties, foundation indicator and soil classification results for the hillwash samples are summarised in Table 4-3.

Table 4-3: Foundation indicators and soil classification for hillwash samples

Sample	TP02-DSC109A/2	TP10/1	TP05/2	TP12/1	TP14/1
Study Area	1	2	3	N/A	N/A
Grading properties					
Gravel (%)	15	2	11	1	0
Sand (%)	64	67	64	79	77
Silt (%)	14	19	14	14	15
Clay (%)	7	12	11	6	8
Atterberg limits					
Liquid limit (%)		16			
Plastic limit (%)		10			
Plasticity Index (%)	NP	6	NP	NP	NP
PI whole sample (%)	NP	6	NP	NP	NP
Linear Shrinkage (%)		3			
Clay Activity		Inactive			
Van der Merwe Swell	Low	Low	Low	Low	Low
Classification					
Matrix Description	Silty SAND	Silty SAND	Silty SAND	Silty SAND	Silty SAND
British	SML	MLS	SML	SML	MLS
AASHTO	A-2-4[0]	A-4[0,4]	A-2-4[0]	A-2-4[0]	A-4[0,2]
Unified	SM	SC-SM	SM	SM	SM

It is evident that all the hillwash grading curves follow a narrow band with a similar particle size distribution. The clay content is very low, and this is also reflected in the Atterberg limits where the samples are mostly non-plastic. The observation that the grading and indicator properties of the hillwash across the three study areas and from two test pits on De Pan are very similar, was one of the main reasons why the residual sandstone horizon was identified as the probable source of the differentiation between the study areas.

Grading curves for the residual sandstone samples from Areas 1, 2 and 3 are shown in Figure 4-2. The grading properties and foundation indicators are summarised in Table 4-4 and the soil classification in Table 4-5.

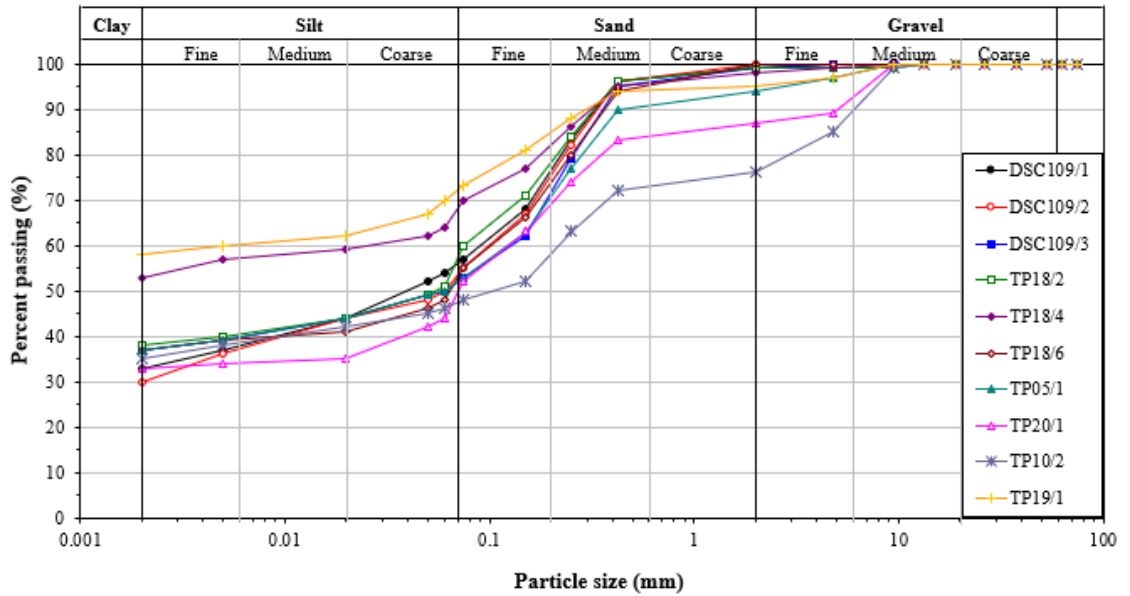


Figure 4-2: Grading curves for residual sandstone in Area 1, 2 and 3.

Table 4-4: Foundation indicators and soil classification for residual sandstone samples

Sample	TP03-DSC109/1	TP03-DSC109/2	TP03-DSC109/3	TP18/2	TP18/4	TP18/6	TP05/1	TP20/1	TP10/2	TP19/1
Study Area	1	1	1	1	1	1	3	3	2	2
Grading properties										
Gravel (%)	1	0	1	1	2	0	6	13	24	5
Sand (%)	45	50	49	48	34	52	44	43	30	25
Silt (%)	21	20	13	13	11	11	13	11	11	12
Clay (%)	33	30	37	38	53	37	37	33	35	58
Atterberg limits										
Liquid limit (%)	42	46	46	45	58	44	39	43	45	62
Plastic limit (%)	19	20	20	25	31	23	19	20	22	31
Plasticity Index (%)	23	26	26	20	27	21	20	23	23	31
PI whole sample (%)	22	25	25	19	26	20	18	19	17	29
Linear Shrinkage (%)	11,5	13,0	12,5	8,5	13,0	8,0	10,0	10,0	11,5	12,0
Clay Activity	0,7	0,87	0,7	0,53	0,51	0,57	0,54	0,7	0,66	0,53
Van der Merwe Swell	Med	High	High	Med	Low	Med	Low	Med	Low	High

Table 4-5: Classification of residual sandstone samples

Sample	Study Area	Matrix Description	British	AASHTO	Unified
TP03-DSC109/1	1	Sandy CLAY	CIS	A-7-6[9,82]	CL
TP03-DSC109/2	1	Sandy CLAY	CIS	A-7-6[11]	CL
TP03-DSC109/3	1	Sandy CLAY	CIS	A-7-6[10,22]	CL
TP18/2	1	Sandy CLAY	CIS	A-7-6[9,63]	CL
TP18/4	1	CLAY	MH	A-7-5[16,95]	MH/OH
TP18/6	1	Sandy CLAY	CIS	A-7-6[8,8]	CL
TP05/1	3	Sandy CLAY	CIS	A-6[7,4]	CL
TP20/1	3	Sandy CLAY	CIS	A-7-6[8,47]	CL
TP10/2	2	Sandy CLAY	CIS	A-7-6[7,22]	SC
TP19/1	2	CLAY	CH	A-7-5[19,4]	CH

From the grading curves, some differentiation between the three study areas is evident, with sample TP18/4 (Area 1) and sample TP19/1 (Area2) showing a 50% higher clay content than the samples from Area 3. The higher clay content is also reflected by the generally higher PI values.

In assessing the potential for volume change with changes in moisture content, the “Van der Merwe Swell” classification is preferred over the “Clay Activity” value as the former takes the PI of the whole sample into account while the latter only considers the PI based on the particles smaller than 0,425mm. Higher swell potentials are observed for Areas 1 and 2 than for Area 3. An increase in moisture will lead to swelling and a decrease in moisture will cause shrinkage, possibly resulting in desiccation cracking. It follows that during a dry season, more desiccation cracks are likely to appear in Areas 1 and 2 than in Area 3. The difference in swell potential was also visually confirmed during the filter paper tests done to determine the SWRCs: Area 2 showed the greatest reduction in volume upon drying, followed by Area 1 and then Area 3 (see Figure 4-10 on page 4-19).

4.2.2 Dispersivity tests

As listed in Table 4-2, the suite of tests carried out to evaluate the dispersive characteristics of the samples included mechanical tests (crumb test, pinhole test and double hydrometer) and chemical analysis. All the tests were carried out by commercial soil laboratories.

Each of the tests and the dispersivity evaluation criteria (based on the discussion in section 2.5.1) are briefly described below.

The *dispersion ratio* was calculated from the double hydrometer results using the 0,005mm particle size criteria as stipulated by Sherard *et al.* (1976a). From the dispersion ratio, the degree of dispersivity was determined according to Bell and Maud (1994) as described in section 2.5.1.

The *crumb tests* were analysed according to the four grades of dispersion given by Sherard *et al.* (1976a) as described in section 2.5.1.

Pinhole tests were also carried out. However, the results were not included in the analysis as potable tap water, rather than distilled water as specified by Sherard *et al.* (1976b), was used. As the salt content of the potable water was unknown, the influence on soil dispersion could not be quantified.

Chemical analysis of the samples was done to evaluate both the bound and unbound cations in the soil (see section 2.5.1). From these results, the ESP vs CEC /100g clay, SAR and %Na vs TDS were evaluated.

The results of the tests done on the hillwash samples are summarised in Table 4-6, followed by graphs of the chemical test results and observations. The complete results are included in Appendix B.

Table 4-6: Summary of dispersion test results on hillwash samples

Sample	Study Area	Mechanical				Chemical				
		Double hydrometer (%)		Crumb		ESP	Conductivity (mS/m)	ESP vs CEC/ 100g clay	%NA vs TDS	SAR (%)
TP05/4	3	25	SD	1	ND	1.3	10,65	ND	ND	0,10
TP09/2	N/A	12	ND	3	D	1.4	5,05	ND	ND	0,10
TP10/4	2	22	SD	2	ND	0.8	4,74	ND	ND	0,15
TP02-DSC109A/	1	46	MD	3	D	1.8	7,27	ND	ND	0,13

ND = Non-dispersive ; D = Dispersive

The results of the ESP vs CEC charts by Gerber and Harmse (1987) in Table 4-6 are based on Figure 4-3 and the %Na vs TDS based on Figure 4-4.

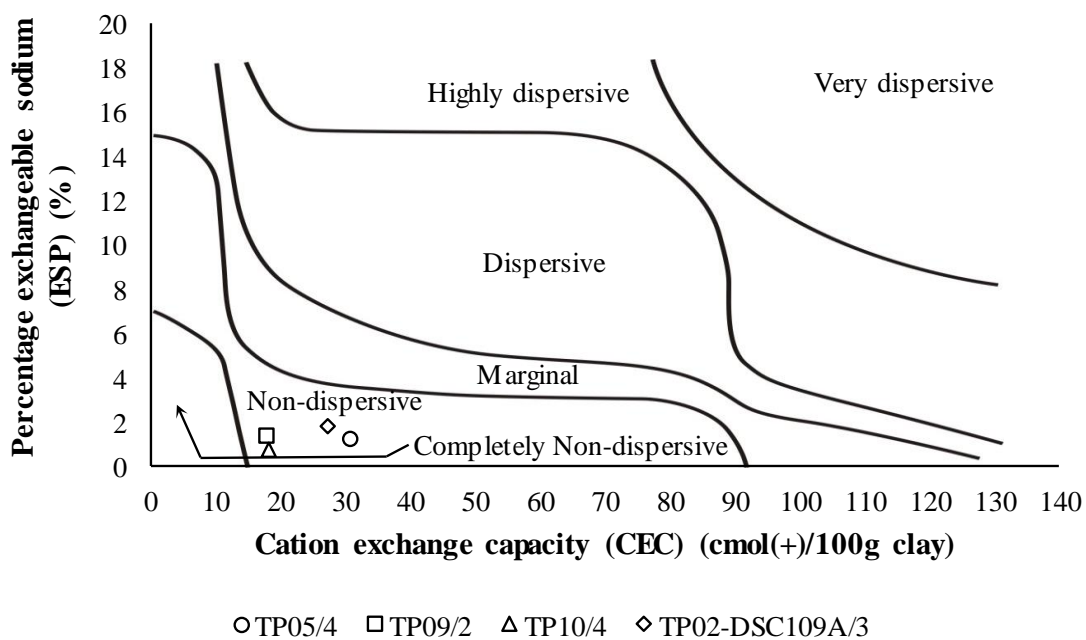


Figure 4-3: ESP versus CEC per 100g clay for hillwash samples.

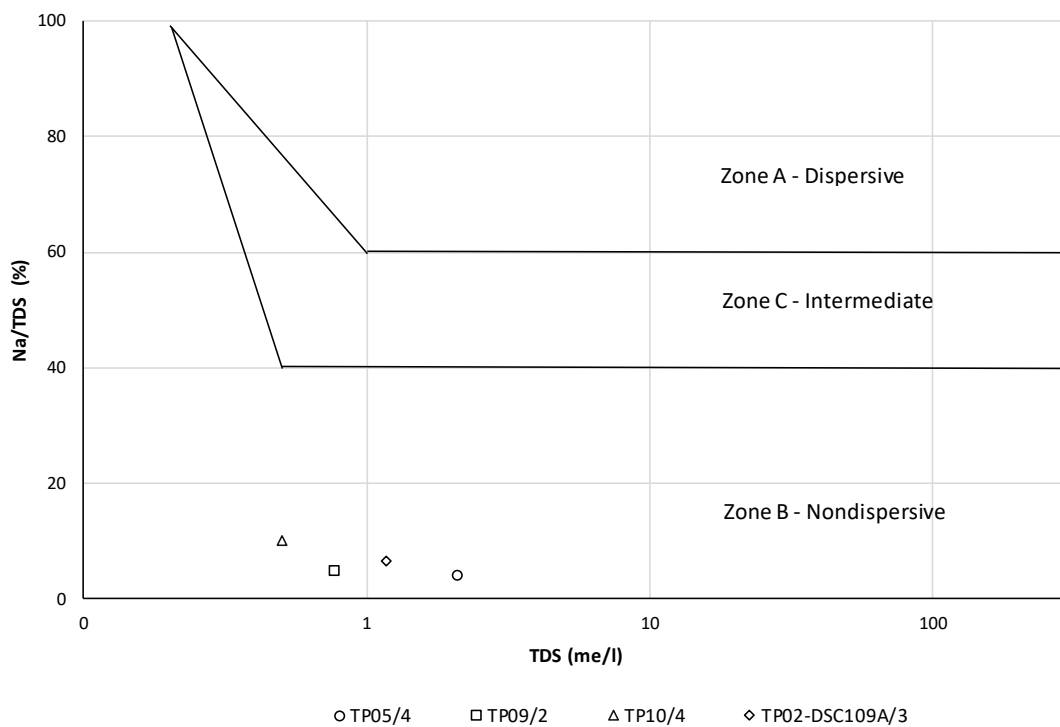


Figure 4-4: %Na versus TDS for hillwash samples.

As mentioned in section 2.5.1, it is recommended that the Bell and Walker (2000) rating system be used to evaluate dispersivity. As shown in Table 2-1, the test with the highest rating in the Bell and Walker (2000) rating system is the pinhole test. For reasons discussed above, the pinhole test results in the current study cannot be relied upon. As such, the Bell and Walker (2000) rating system is applied with caution.

The results are summarised in Table 4-7, which shows all the samples to be nondispersive. Even if all the pinhole tests had indicated dispersive soils, and all the ratings were increased by 5 points, the sample from Area 1 would have been slightly dispersive at most.

Table 4-7: Hillwash results according to the Bell and Walker (2000) rating system

Sample	Study Area	ESP vs CEC/ 100g clay	Crumb test	SAR	%NA vs TDS	Total	Rating
TP05/4	3	0	0	0	0	0	Nondispersive
TP09/2	N/A	0	2	0	0	2	Nondispersive
TP10/4	2	0	1	0	0	1	Nondispersive
TP02-DSC109A/	1	0	2	0	0	2	Nondispersive

Bell and Walker (2000) did not include the double hydrometer results in their rating system as they could not find a strong correlation between this and the other tests. If the double hydrometer results from the hillwash samples are considered (see Table 4-6), it is noticed that two of the four samples classify as slightly dispersive with one moderately dispersive, which is in contrast with the results from the rating system above. It should be kept in mind, however, that based on the definition of the dispersion ratio, one could find very high values even if the clay content in the sample is very low. The question is whether a small percentage of highly dispersive clay will render the entire sample as dispersive. As discussed in section 2.5.1, Bell and Maud (1994) question whether a dispersive clay fraction of 10% or less will be sufficient for piping to develop. As the clay content of the hillwash samples tested above is 12% at most, it is concluded that the medium dispersivity indicated by the double hydrometer results will not result in dispersive behaviour of the soil.

As such, it is concluded that the hillwash sampled from all three study areas is nondispersive, with no difference between the study areas. This conclusion corresponds to the observations on site, as no areas of surface erosion were noticed, apart from the areas immediately surrounding the sinkholes along the ploughed furrows.

The results from the residual sandstone samples are summarised in Table 4-8. As with the hillwash samples above, the charts for the ESP vs CEC and %Na vs TDS are shown in Figure 4-5 and Figure 4-6.

Table 4-8: Summary of dispersion test results on residual sandstone samples

Sample	Study Area	Mechanical				Chemical				
		Double hydrometer (%)		Crumb		ESP	Conductivity (mS/m)	ESP vs CEC/ 100g clay	%NA vs TDS	SAR (%)
TP05/1	3	31,0	MD	4	HD	2.2	17,13	ND	ND	0.42
TP10/5	2	3,0	ND	4	HD	10.0	4,94	D	ND	0.25
TP12/2	N/A	4,0	ND	4	HD	4.1	18,22	ND	ND	0.43
TP03-DSC109/2	1	79,0	D	4	HD	38.1	1,62	HD	ND	0.18
TP09/5	N/A	30,0	MD	4	HD	4.1	10,92	CND	ND	0.44
TP18/2	1	38,4	MD	4	HD	14.1	8,05	D	ND	0.60
TP18/4	1	39,3	MD	4	HD	4.2	7,67	ND	MD	0.77
TP18/6	1	95,1	D	4	HD	25.1	8,46	HD	ND	0.60
TP19/1	2	41,7	MD	4	HD	2.9	11,49	ND	MD	0.84
TP19/5	2	61,5	D	4	HD	6.5	9,13	D	MD	1.15
TP20/1	3	31,6	MD	4	HD	1.6	17,69	ND	ND	0.21

CND = Completely non-dispersive ; ND = Nondispersive ; MD = Medium dispersive ; D = Dispersive ; HD = Highly dispersive

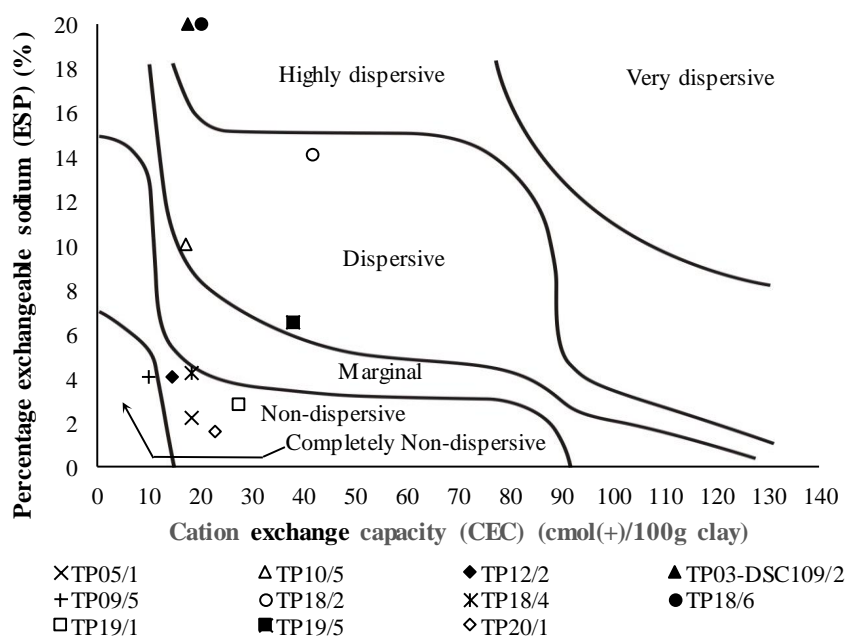


Figure 4-5: ESP versus CEC per 100g clay for residual sandstone samples.

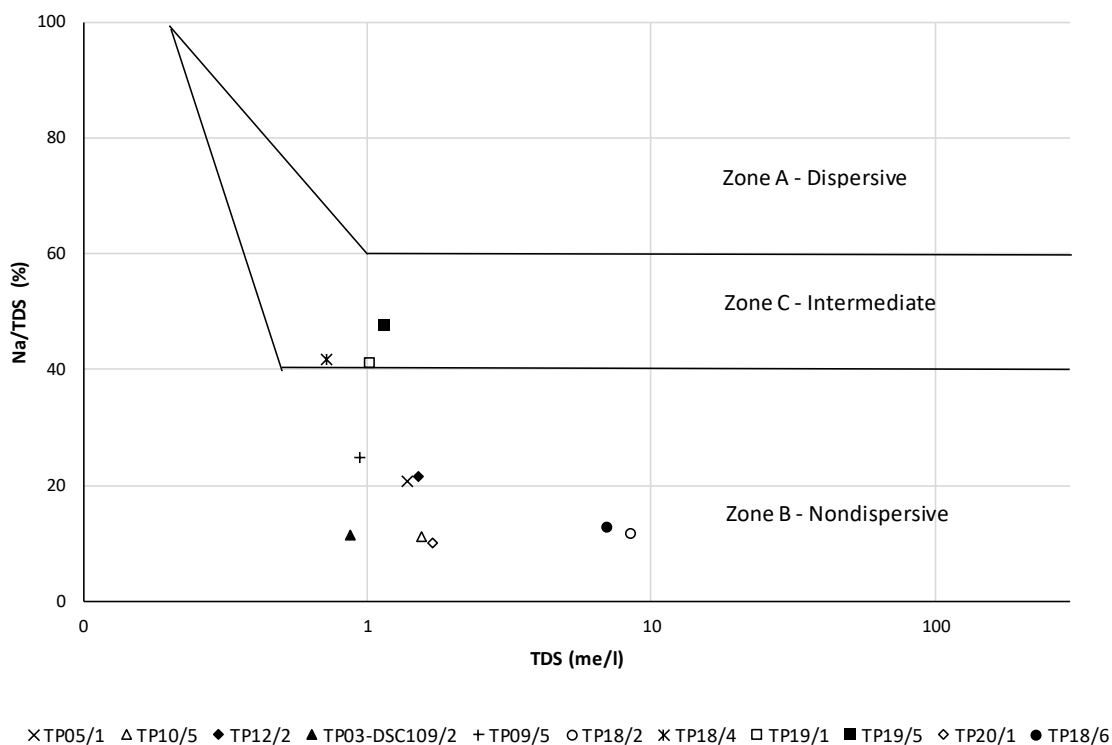


Figure 4-6: %Na versus TDS for residual sandstone samples.

Before applying the Bell and Walker (2000) rating system, it is worth pointing out that there is a reasonable correlation between the double hydrometer results and ESP vs CEC /100g clay results. In both tests, the samples from Area 1 are the most dispersive, with Area 2 slightly less dispersive. The samples from Area 3 are nondispersive. In contrast with the hillwash samples, the clay content of the samples in the double hydrometer is above 30%.

The results of the application of the Bell and Walker (2000) rating system to the residual sandstone samples are given in Table 4-9.

Table 4-9: Residual sandstone results according to the Bell and Walker (2000) rating system

Sample	Study Area	ESP vs CEC/ 100g clay	Crumb test	SAR	%NA vs TDS	Total	Rating
TP05/1	3	0	3	0	0	3	Nondispersive
TP10/5	2	3	3	0	0	6	Slightly dispersive
TP12/2	N/A	0	3	0	0	3	Nondispersive
TP03-DSC109/2	1	4	3	0	0	7	Slightly dispersive
TP09/5	N/A	0	3	0	0	3	Nondispersive
TP18/2	1	3	3	0	0	6	Slightly dispersive
TP18/4	1	0	3	0	1	4	Nondispersive
TP18/6	1	4	3	0	0	7	Slightly dispersive
TP19/1	2	0	3	0	1	4	Nondispersive
TP19/5	2	3	3	0	1	7	Slightly dispersive
TP20/1	3	0	3	0	0	3	Nondispersive

The results in Table 4-9 show that residual sandstone from Area 1 and Area 2 is more dispersive than Area 3, with Area 1 slightly more dispersive than Area 2.

As with the hillwash samples, it must be kept in mind that the pinhole tests are not included in the above rating system. If the maximum value of 5 points were to be added to all the samples for a theoretical dispersive pinhole test result, the samples from Areas 1 and 2 would have been regarded as highly dispersive (>12) and the samples from Area 3 moderately dispersive at most.

It is concluded that the residual sandstone from Area 1 and Area 2 is more dispersive than the residual sandstone from Area 3.

4.2.3 XRD and XRF tests

X-Ray diffraction (XRD) and X-Ray fluorescence (XRF) tests were carried out by the Department of Geology at the University of Pretoria.

XRD tests are done to identify the mineralogical composition of the sample based on the crystallographic parameters measured. The data was then interpreted by the Department and the Rietveld method used to estimate the quantities of each mineral (Grote, 2017).

The XRD results are summarised in Table 4-10. More detailed descriptions of the sample locations are given in Table 4-1.

Table 4-10: XRD – Estimated mineralogical percentage by weight

Sample	Study Area	Microcline	Quartz	Kaolinite	Goethite	Ankerite	Muscovite	Rutile
TP01/1	1	3,43	69,11	22,7	4,76			
TP02-DSC109A/2	1	1,9	98,1					
TP02-DSC109A/4/1	1	2,54	90,33	7,13				
TP02-DSC109A/4/2	1	4,77	90,22	5,01				
TP02-DSC109A/4/3	1	3,59	83,94	12,46				
TP03-DSC109/1	1	4,69	79,6	15,71				
TP03-DSC109/2	1	4,12	82,86	13,02				
TP03-DSC109/3	1	4,28	73,81	16,69	4,95			
TP03-DSC109/4	1	3,39	79,92	7,14		9,56		
TP05/4	3	2,29	93,69	4,02				
TP05/5	3	4,83	79,51	15,66				
TP09/2	N/A	3,14	92,89	3,97				
TP09/4	N/A	4,66	43,38	43,52	8,44			
TP10/4	2	1,11	89,19	2,19	7,51			
TP10/5	2	9,98	59,98	15,93	2,17		11,94	
TP18/4	1	4,9	70,07	19,17	4,2			1,66
TP18/5	1	4,62	77,11	17,06				1,21
TP19/1	2	7,61	58,66	28,3	5,43			
TP19/2	2	2,46	62,7	19,1	4,36		11,38	
TP19/3	2	3,65	76,96	11,47	8,14		7,92	
TP20/1	3	4,53	69,48	17,85	4,76			

Jones (1981) and Gerber and Harmse (1987) and Hoffmann *et al.* (1998) all listed a range of minerals found in dispersive soils. Although the most examples are from the montmorillonite group, other clays minerals such as kaolinite have also been shown to be dispersive. Hoffmann *et al.* (1998) also found no correlation between mineralogy and the formation of sinkholes in the Santa Cruz river valley.

A review of the minerals found in the three study areas shown above does not point to a clear correlation between any of the minerals and any of the study areas. The most abundant mineral is quartz, followed by kaolinite. It is thus concluded that the mineralogy on its own is not a critical factor influencing the formation of sinkholes.

X-ray fluorescence tests were also done on the samples listed in Table 4-10 to determine the distribution of elements within the soils. The results, which are included in Appendix B, show no clear correlation between an element and the study areas.

4.2.4 Consolidated undrained triaxial and triaxial permeability tests

Consolidated undrained (CU) triaxial tests and triaxial permeability tests were done on undisturbed samples from the residual sandstone from each of the study areas. No triaxial tests were done on the hillwash samples as, based on the fieldwork observations and preceding test results, the hillwash layer was not deemed to be the cause of the difference in sinkhole formation between the study areas. For each of the CU triaxial tests, two specimens were prepared and consolidated to effective stresses of 50kPa and 100kPa, respectively. These were deemed to be realistic effective stresses as the sinkhole features were found very close to surface. The permeability tests were also done at an effective stress of 100kPa.

For study area 2 (sample TP19/1) and study area 3 (sample TP20/1), all the specimens were cut and trimmed from the same undisturbed block sample. For study area 1 (sample TP18/4) each specimen was cut from a different block.

The results are summarised in Table 4-11 and the complete results included in Appendix B.

Table 4-11: Consolidated undrained triaxial and triaxial permeability results

Sample	Study Area	Friction angle (°)	Cohesion (kPa)	Permeability (cm/s)
TP18/4	Area 1	28	0kPa	1,1E-08
TP19/1	Area 2	24	2kPa	1,2E-08
TP20/1	Area 3	32	0kPa	7,9E-06

The highest friction angle was found in Area 3 (small sinkholes), with the smallest friction angle in Area 2 where no sinkholes were recorded. The cohesion values are either zero or very low. Thus, no correlation was found between an increase in the shear strength parameter and an increased sinkhole diameter. It is noteworthy to point out that the friction angles obtained for the residual sandstone are completely different to the values for α (being the slope of the sides of the V-shape) measured during the fieldwork (see sections 2.3.4. and 3.4.2). It should be kept in mind that the cohesion values are based on saturated soil conditions and do not reflect the tensile strength due to suction in the unsaturated state.

The permeability values for Areas 1 and 2 are almost 700 times lower than for Area 3. The permeability results concur with the particle size distributions in that Areas 1 and 2 had a higher clay content than Area 3. It should be borne in mind that the above permeability values are for the saturated condition. Comments on the unsaturated hydraulic conductivity are given at the end of the section 4.2.5 on page 4-30.

4.2.5 Soil water retention curves

Soil water retention curves (SWRCs) were determined for intact residual sandstone samples from the three study areas. The purpose was to evaluate the suction response to changes in moisture content, as the suction influences the tensile strength of the soil which, in turn, plays a critical role in the ability of the lid to span across the sinkhole (see sections 2.3.4 and 2.5.2).

The objective of the testing was to determine the primary wetting and drying curves for each of the samples, for reasons set out in section 2.5.2. The lower range of matric suction values (typically between 0kPa and 700kPa) were measured with a tensiometer embedded into the specimen (for the drying curve only) while higher matric suctions (typically 700kPa to 30MPa) were determined using Whatman[®] No. 42 filter paper and the calibration curve proposed by Hamblin (1981). The test methods and results are presented in this section.

Filter paper method

In their use of the filter paper method, Al Haj and Standing (2016) prepared a range of specimens, and then applied the filter paper method to the same specimen and different moisture contents. The testing took several weeks as the same specimens were used.

In the case of this SSE research project, due to time constraints, the same specimen was not used at different moisture contents. Rather, individual specimens were prepared for each moisture content targeted in the test for each of the study areas.

Specimens were cut from an intact block of residual sandstone by gradually advancing an oedometer ring into the block sample while carving out material from around the outer perimeter with a spatula. Snapshots from the process are shown in Figure 4-7. By containing the specimens in the oedometer ring, it was easier to handle the specimens during the repeated wrapping and unwrapping and ensure they were kept contained through significant volume changes. As many specimens as possible were carved out of the same block sample and only

once there was insufficient sample left, was another block used. A summary of the specimens and the blocks they were carved from is included in Table 4-12 (see page 4-20).



Figure 4-7: Specimen carved out from clock sample into oedometer ring.

For each of the block samples used to cut the specimens from, wax density tests were done on lumps to determine the in-situ bulk density for use in calculating the degree of saturation. Every effort was made to make the lumps as large as possible, as the influence of ferricrete nodules on the lump mass was more pronounced in small lumps than larger lumps.

At least six specimens were prepared for each of the study areas and tested at moisture contents targeted based on earlier trials. For the primary drying curve, the specimens were first dried out in the oven, then saturated with de-aired water and then placed into the oven again. The moisture contents were monitored during drying and once the targeted moisture content was reached, the filter paper was applied and the samples wrapped. After 1 week, the samples were unwrapped and the filter paper weighed and moisture content calculated. The matric suction at each specimen's moisture content was then determined using the calibration curve provided by Hamblin (1981).

Once the drying curve tests were done, the same specimens were used to determine the primary wetting curve. The specimens were first oven dried and then de-aired water was added until the targeted moisture content was reached as shown in Figure 4-8. The same moisture contents were targeted as for the drying curves. At this point, the same filter paper procedure was repeated and the matric suctions measured.



Figure 4-8: Wetting of specimens to target moisture content.

As the matric suction values were determined relative to moisture content, and not the degree of saturation, no volume change measurements were required. It is worth pointing out that during the wetting and drying of the specimens, significant volume changes were observed as shown in Figure 4-9. At the completion of the tests, it was noted that specimens from Area 2 had undergone the greatest volume change, followed by Area 1 and then Area 3. This can be seen by comparing the final sample diameter with the oedometer rings in Figure 4-10. Also, the specimens from Area 3 saturated and dried out much quicker than those from the other two areas.



Figure 4-9: Swelling of the specimen upon wetting.



Figure 4-10: Specimens after the completion of the wetting curve tests.

The results of all the tests are summarised in Table 4-12. Although specimens A9, A10, C7, C8, B7 and B8 were not used in the filter paper method, but with the tensiometer measurements, their details are included in the table for ease of comparison with the other specimens.

Table 4-12: Summary of suction measurement specimens and results of filter paper tests

Specimen	Sample and block		Study Area	In-situ properties		Drying curve		Wetting curve	
				Bulk density (g/cm ³)	Degree of saturation (%)	Moisture content (%)	Matric suction (mPa)	Moisture content (%)	Matric suction (mPa)
A1	TP18/4	12/14	1	1.851	71.22	14.80	2974	15	867
A2	TP18/4	12/14	1	1.851	72.04	18.84	911	19	577
A3	TP18/4	3/14	1	1.882	70.09	13.01	7112	13	3982
A4	TP18/4	3/14	1	1.882	69.09	13.97	4700	14	3419
A5	TP18/4	3/14	1	1.882	69.91	16.09	907	16.5	914
A6	TP18/4	5/14	1	1.850	68.99	19.02	663	19	571
A7	TP18/4	5/14	1	1.850	67.63	21.59	351	22	529
A8	TP18/4	13/14	1	1.815	65.47	24.88	105	25	82
<i>A9</i>	<i>TP18/4</i>	<i>13/14</i>	<i>1</i>	<i>1.815</i>	<i>66.49</i>	<i>N/A</i>	<i>N/A</i>	<i>N/A</i>	<i>N/A</i>
<i>A10</i>	<i>TP18/4</i>	<i>13/14</i>	<i>1</i>	<i>1.815</i>	<i>65.08</i>	<i>N/A</i>	<i>N/A</i>	<i>N/A</i>	<i>N/A</i>
C1	TP19/1	4/6	2	1.806	77.48	14.58	19719	14.6	14188
C2	TP19/1	4/6	2	1.806	76.19	16.00	14161	16	10645
C3	TP19/1	4/6	2	1.806	73.83	17.45	13800	17.5	16140
C4	TP19/1	4/6	2	1.806	74.96	19.03	3013	19	5552
C5	TP19/1	2/6	2	1.670	65.65	21.95	399	22	1055
C6	TP19/1	2/6	2	1.670	64.91	24.72	176	25	447
<i>C7</i>	<i>TP19/1</i>	<i>2/6</i>	<i>2</i>	<i>1.670</i>	<i>63.90</i>	<i>N/A</i>	<i>N/A</i>	<i>N/A</i>	<i>N/A</i>
<i>C8</i>	<i>TP19/1</i>	<i>3/6</i>	<i>2</i>	<i>1.784</i>	<i>75.18</i>	<i>N/A</i>	<i>N/A</i>	<i>N/A</i>	<i>N/A</i>
B1	TP20	14/14	3	1.808	57.44	25.00	3	25	4
B2	TP20	14/14	3	1.808	57.00	22.00	19	22	16
B3	TP20	6/14	3	1.831	67.63	18.84	87	19	60
B4	TP20	6/14	3	1.831	67.39	16.37	242	16.5	261
B5	TP20	6/14	3	1.831	67.78	14.00	758	14	523
B6	TP20	10/14	3	1.959	68.35	13.11	1126	13	1822
<i>B7</i>	<i>TP20</i>	<i>10/14</i>	<i>3</i>	<i>1.959</i>	<i>67.85</i>	<i>N/A</i>	<i>N/A</i>	<i>N/A</i>	<i>N/A</i>
<i>B8</i>	<i>TP20</i>	<i>10/14</i>	<i>3</i>	<i>1.959</i>	<i>67.52</i>	<i>N/A</i>	<i>N/A</i>	<i>N/A</i>	<i>N/A</i>

Note: Tensiometer specimens shown in italics.

The matric suction versus moisture content results in Table 4-12 are shown graphically as SWRCs in the figures below, with matric suction on the vertical scale and gravimetric moisture content on the horizontal scale. This is different to the presentation in Figure 2-25, where the axes are reversed. The reason for the difference is that in the current study, the moisture content is varied (independent variable) and the matric suction measured (dependant variable). In many other studies, the suction is varied and the volumetric response measured.

For each case, the graph on the left shows matric suction on a log scale, while the right hand graph shows matric suction on a normal scale. The drying and wetting curves for all areas are compared first, followed by the graphs for each area individually.

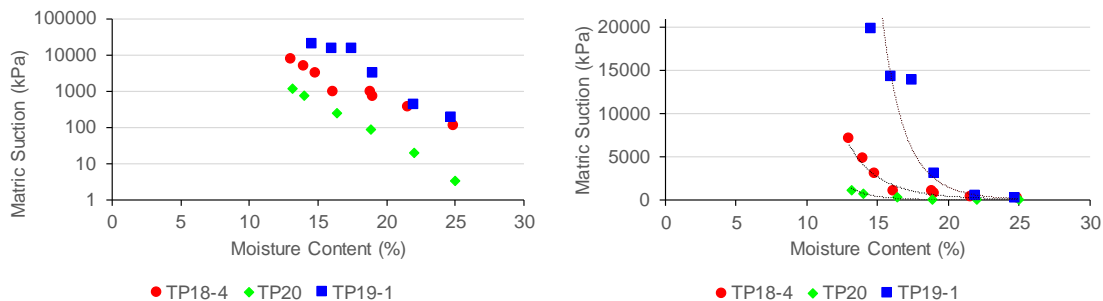


Figure 4-11: Primary drying curves for residual sandstone specimens.

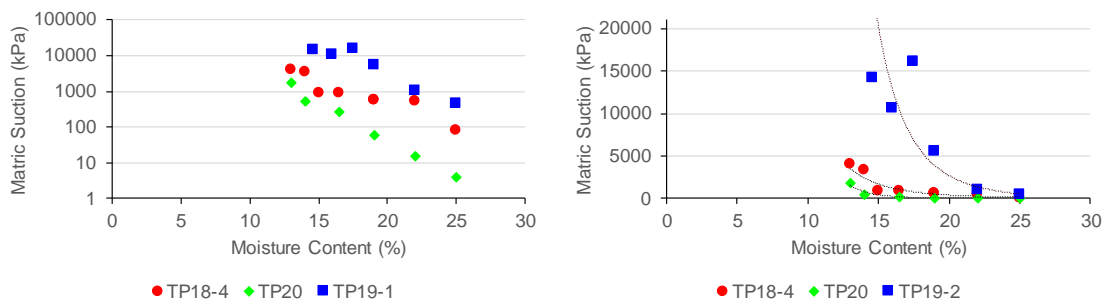


Figure 4-12: Primary wetting curves for residual sandstone specimens.

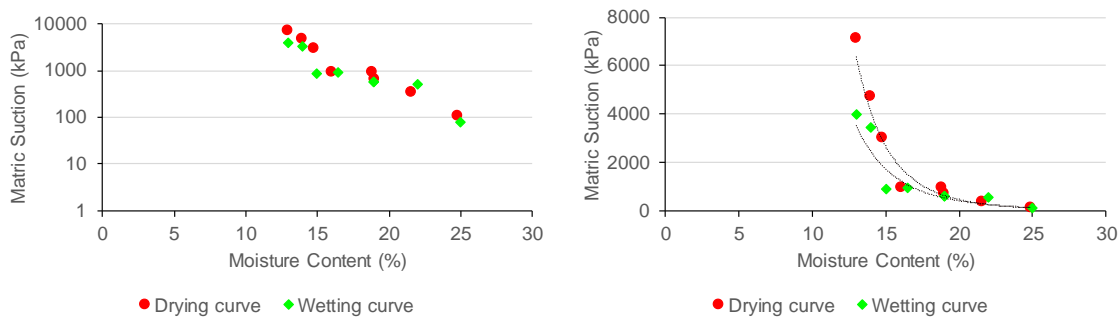


Figure 4-13: Primary drying and wetting curves for Area 1.

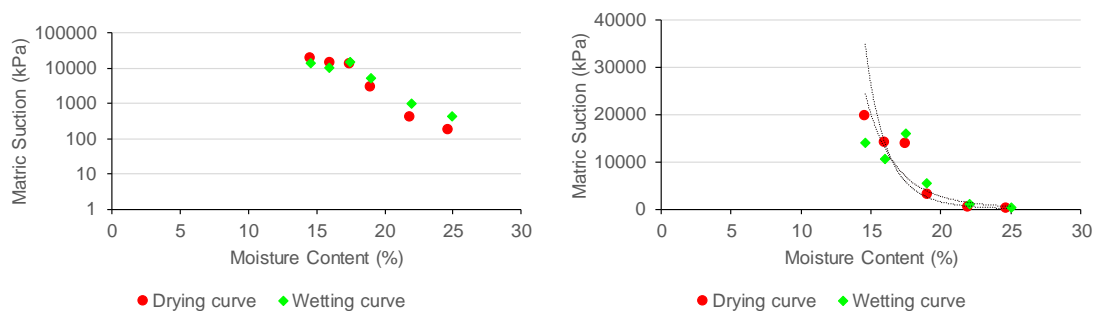


Figure 4-14: Primary drying and wetting curves for Area 2.

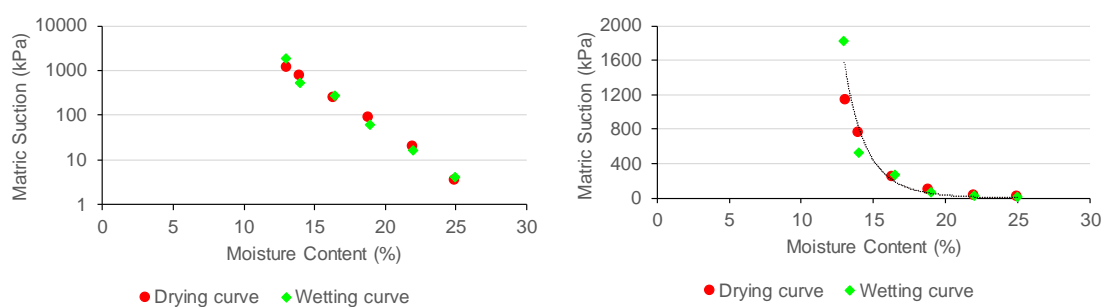


Figure 4-15: Primary drying and wetting curves for Area 3.

It was pointed out in section 2.5.2 that SWRCs are void ratio dependant. Thus, an evaluation of the change in the SWRC with change in original void ratio should form part of any study in which SWRCs from different soils are compared. However, as the specimens in this study were cut from undisturbed block samples representing the in-situ condition, and not reconstituted, it is considered that a comparison of the results has merit. The main observations drawn from the primary wetting and drying curves shown above, are as follows:

- Even though the same specimens were not tested over a range of moisture contents, but rather different specimens cut from the same sample, the results do indicate a distinctive suction response for each of the study areas.
- Area 2 has significantly higher suction values for the same moisture content range than the other two areas.
- As can be seen from Figure 4-11 and Figure 4-12 the rate of change in suction is higher for Area 2 than for the other areas, i.e. as the moisture content decreases, the rate of increase in suction is higher.

- A relatively small amount of hysteresis is noted between the wetting and drying curves for each area as seen from Figure 4-13, Figure 4-14 and Figure 4-15. For the specimens from Area 3, there is almost no hysteresis.
- The residual state (as described in section 2.5.2) was not reached in any of the tests as it probably falls beyond the 30MPa limit of the Hamblin (1981) calibration curve.

Suction measurement with tensiometers

Six specimens were instrumented with tensiometers to obtain continuous measurement of the matric suction response to changes in moisture content. The tests were only done to determine the primary drying curves, starting in a fully saturated state and continued until the tensiometer cavitated. For the testing to be repeated for the wetting curve, the specimen would need to be wetted from the completely dry state, and the tensiometer inserted at a stage when the suctions are estimated to be lower than the cavitation pressure of the tensiometer.

Two specimens from each study area were prepared in the same manner as the specimens for the filter paper testing. The details of specimens A9, A10, B7, B8, C7 and C8 are given in Table 4-12 on page 4-20.

The tensiometers were constructed, saturated and calibrated in a similar manner as described in Jacobsz (2018). In this case, porous ceramic disks with an air entry value of 500kPa and pressure sensors capable of measuring up to 700kPa, were used. Once the specimens were saturated, a hole was drilled into the specimen and the tensiometer carefully inserted and sealed with a slurry paste made from the same block sample (see Figure 4-16). Thus, the installation differed from the method used by Jacobsz (2018) where the tensiometers were installed from below the specimen.



Figure 4-16: Slurry paste used to seal tensiometer into drilled hole.

The change in moisture content was determined by continuously weighing each specimen on instrumented cantilever scales. As the samples were left undisturbed while drying, the only change in mass was a change in the moisture content.

The complete experimental set-up for suction measurement using tensiometers is shown in Figure 4-17.

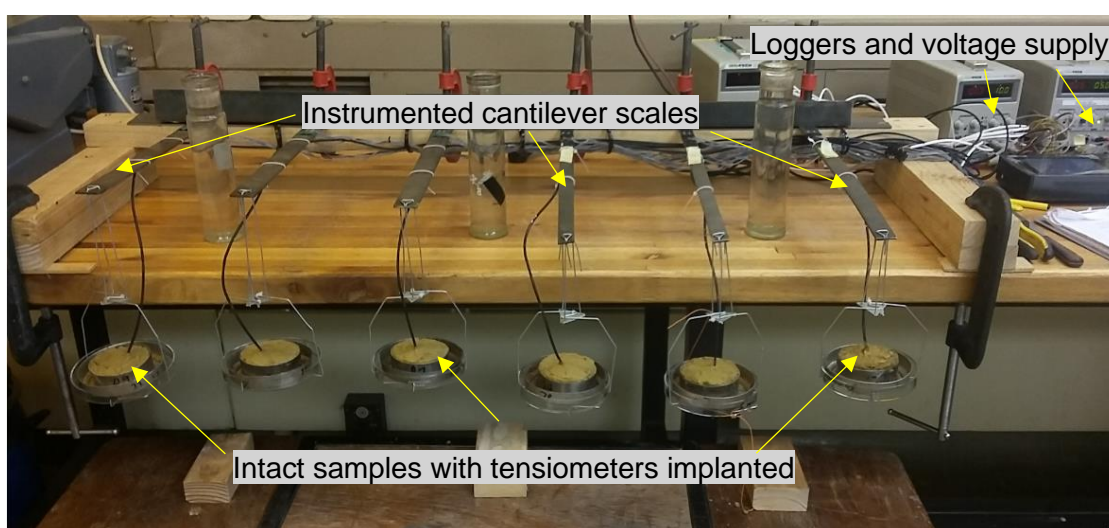


Figure 4-17: Experimental set-up to measure primary drying curves with tensiometers.

All the filter paper specimens were kept in the same room as the tensiometer specimens during the testing. The temperature and relative humidity in the room was logged continuously. Over the 3,5 days duration of the tensiometer tests, the temperature varied between 13,5°C and 16,6°C and the relative humidity between 31% and 70%. The cause of the variations was beyond the control of this research project. Although these variations are significant, all the specimens were exposed to the same conditions and as such the results are still comparable.

The change in total mass and matric suction over time for specimen C6 (Area 2) is shown in Figure 4-18. The matric suction increased from near zero to a maximum value of -377kPa, while the total mass reduced by approximately 35g as the specimen dried out.

As is evident from Figure 4-18, considerable variance was picked up in the total mass measurements of the cantilever scales. A detailed data analysis was done to identify the cause of the variance, but no correlation to the temperature, relative humidity, slight variation in the excitation voltage and possible disturbance when data was downloaded from the datalogger, could be found. The variance between the specimens was also not similar. Despite the variance, the overall trend in the mass reduction could still be identified and thus the data was used.

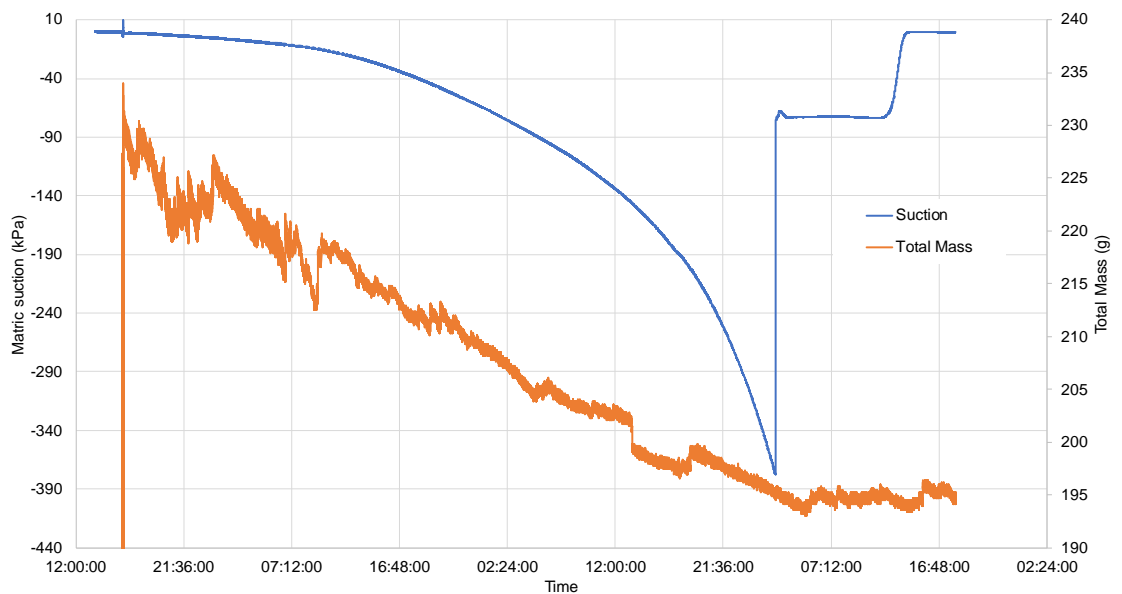


Figure 4-18: Matric suction and total mass change for specimen C6 (Area 2).

The change in matric suction was plotted against the change in moisture content to obtain the initial stages of the primary drying curve. To simplify the further analysis, curves were fitted by hand to remove the variation in the data.

The primary drying curves from the tensiometers are plotted with the wetting and drying curves from the filter paper tests as shown in Figure 4-19, Figure 4-20 and Figure 4-21. The graphs show that the tensiometer results tie in reasonably well with the filter paper results.

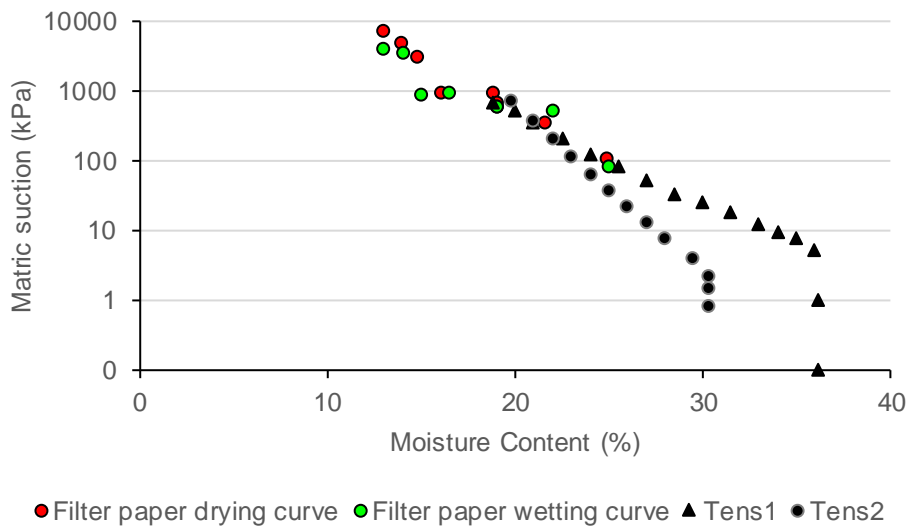


Figure 4-19: Primary drying curve from tensiometer data with filter paper results for Area 1.

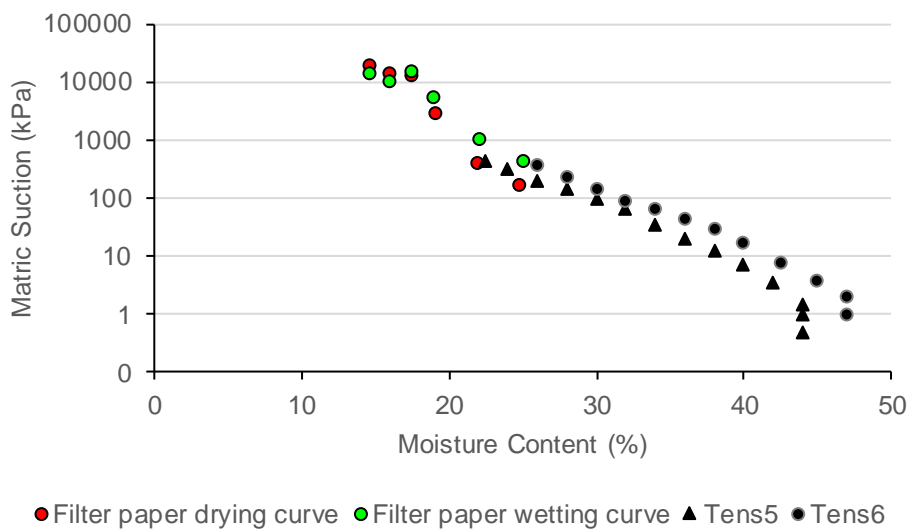


Figure 4-20: Primary drying curve from tensiometer data with filter paper results for Area 2.

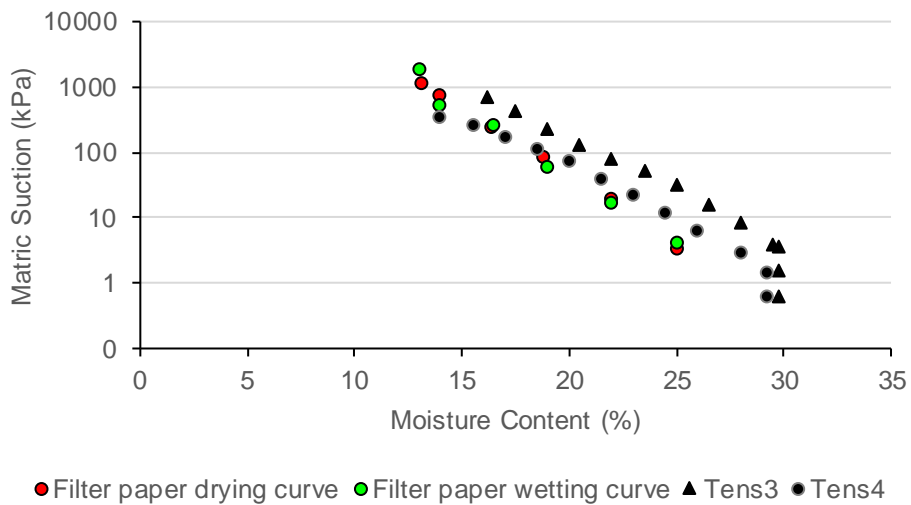


Figure 4-21: Primary drying curve from tensiometer data with filter paper results for Area 3.

In Figure 4-22 the primary drying curves from all three study areas are plotted together. As with the filter paper tests results, it is once again shown that the residual sandstone from Area 2 retains higher suctions for the same moisture content, followed by Area 1 and then Area 3.

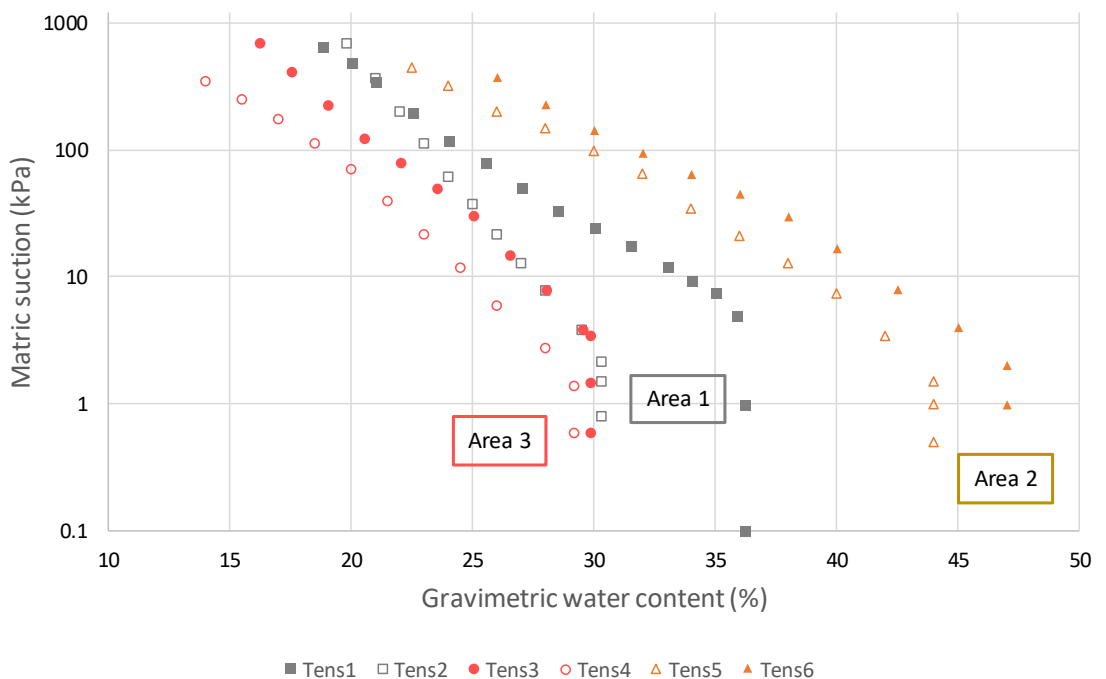


Figure 4-22: All primary drying curves from tensiometer tests combined.

In Figure 4-23, the same graphs as in Figure 4-22 are repeated, but with the primary wetting curves from the filter paper tests added. Furthermore, an attempt is made to evaluate the range of decrease in matric suction as the soil is wetted from the in-situ moisture content to saturation. (The values from the tensiometer tests cannot be used as these reflect the drying curve.) As no volume change measurements were taken during the tests, any calculation of the degree of saturation will be inaccurate as mentioned in section 2.5.2. Thus, the degree of saturation parameter cannot be used to evaluate the results.

The value of the in-situ moisture content was taken as the average moisture content of all the filter paper test samples for each study area in their in-situ state. To estimate the suction at saturation, the wetting curves for Areas 1 and 2 (from the filter paper tests) are extrapolated up to points approximating the air-entry value on the tensiometer drying curves, based on the presumption that at suctions lower than the air-entry value on the PDC, the sample will be saturated. These approximations are shown in the coloured lines in Figure 4-23. The observation that the approximated saturation points are at a lower moisture content than the PDC is in line with the theory that the PWC reaches saturation at a lower moisture content than the start of the PDC (see section 2.5.2). For Area 3, the lowest suction value measured on the filter paper wetting curve is near the air-entry value of the drying curve and therefore no extrapolation was required.

For ease of reference, the decrease in matric suction for each area is summarised in Table 4-13 together with the percentage increase in moisture content (calculated as the percentage moisture required to reach saturation from the *in-situ* moisture content).

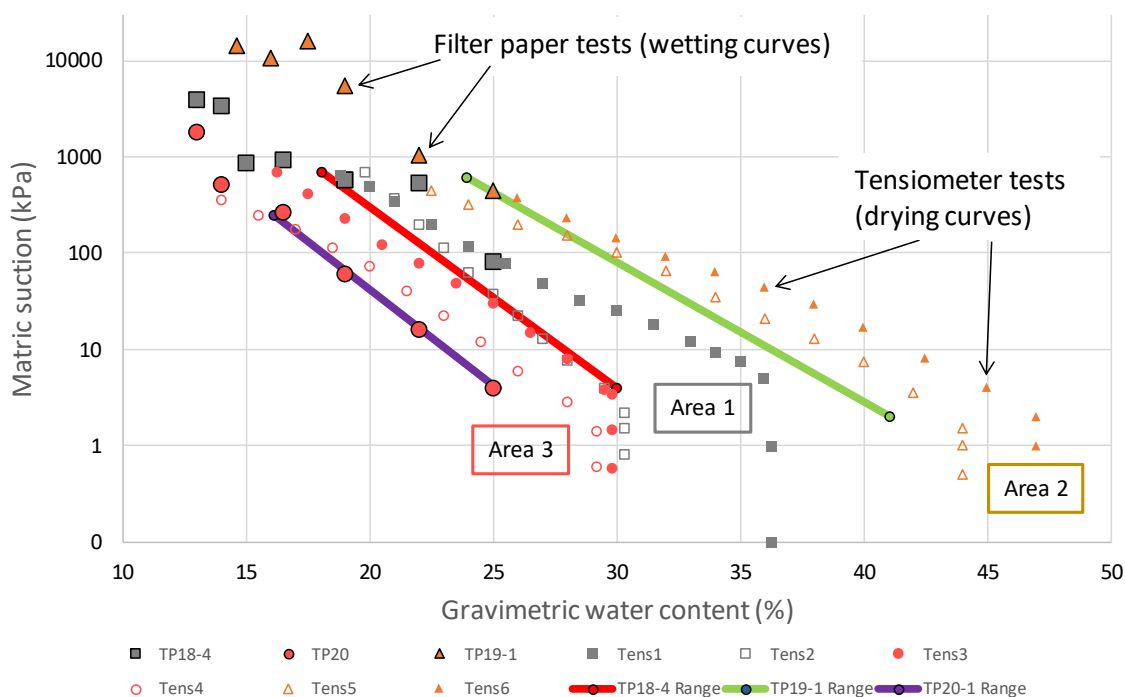


Figure 4-23: Tensiometer PDCs with filter paper PWC and moisture content variation added.

Table 4-13: Decrease in matric suction from in-situ moisture content to saturation

Condition	Variable	Area 1	Area 2	Area 3
<i>In-situ</i>	Moisture content	18,0%	23,9%	16,1%
	Matric suction	700kPa	620kPa	250kPa
Saturation	Moisture content	30%	41%	25%
	Matric suction	4kPa	2kPa	4kPa
Percentage increase in moisture content		67%	72%	55%

The results show that since the *in-situ* matric suction for Areas 1 and 2 are higher than Area 3, a greater percentage increase in moisture content is required to reach saturation. This conclusion is confirmed by the observation mentioned above that during the filter paper specimen preparation, the samples from Area 3 took less time to saturate and dry out than the samples from Area 1 and 2. For the same percentage increase in moisture content from the *in-situ* state, it can be deduced that the matric suction for Area 3 will reduce more than Areas 1 and 2, i.e. Areas 1 and 2 will retain higher suctions when wetted from the *in-situ* state.

The loss of matric suction during wetting gives an indication of the loss of strength that the soil will experience when wetted from a dryer condition. Higher suction values in the soil increases the soil's tensile strength which increases the lid's capacity to span across an open cavity and restrains erodibility. When the soil is wetted, the loss of strength can result in increased erodibility of the soil and collapse of the lid.

Upon wetting, the rate at which the wetting front will advance through the soil is a function of the hydraulic conductivity of the soil. As demonstrated by Ng *et al.* (2016), it cannot be assumed that if soil A has a higher permeability in the saturated condition than soil B, the permeability of soil A across the unsaturated spectrum will also be higher. To evaluate the unsaturated hydraulic conductivity of samples from Area 1, 2 and 3, the Van Genuchten (1980) formula was used.

The results are shown in Figure 4-24. For each study area, two drying curves are plotted (based on the data from the tensiometer tests in Figure 4-22) and one wetting curve based on the filter paper test results. Added on to Figure 4-24 are the possible ranges of *in-situ* hydraulic conductivity based on the calculated matric suction from either the primary drying or primary wetting curves.

From Figure 4-24 it is evident that in general, the hydraulic conductivity of Area 3 remains higher than that of Areas 1 and 2 over the unsaturated soil spectrum. This is similar to the saturated condition. This result further underlines the conclusion that suctions in the residual sandstone in Area 3 will be reduced upon wetting at a higher rate than the suctions in Areas 1 and 2, leading to a decreased lid strength in Area 3.

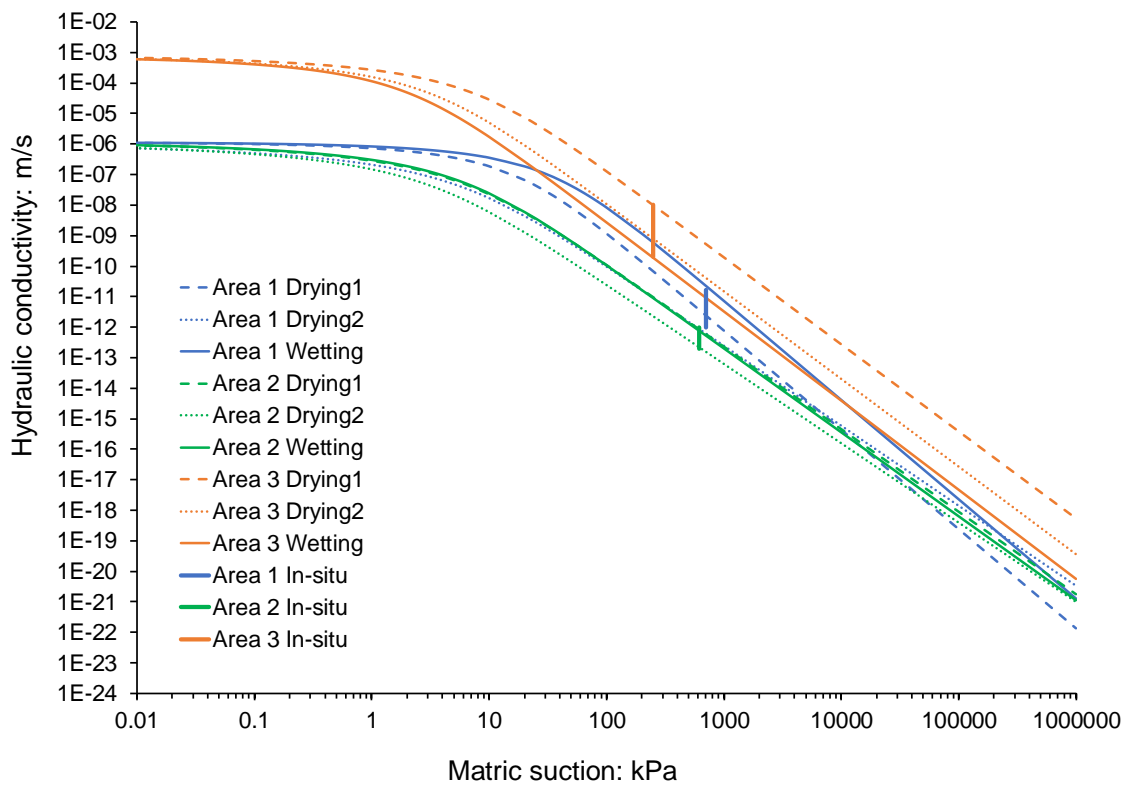


Figure 4-24: Hydraulic conductivity for change in matric suction for the three study areas.

4.3 SUMMARY OF LABORATORY TEST RESULTS

In line with the fieldwork result summary given at the end of chapter 3, the laboratory test results are summarised in Table 4-14 with respect to the three study areas.

Table 4-14: Summary of laboratory test results from the three study areas.

Soil property	Area 1	Area2	Area 3
Grading analysis	50% - 60% clay	50% - 60% clay	30% - 40% clay
Swell potential	Low to high	Low to high	Low to medium
Mineralogy and elemental composition	No clear distinction	No clear distinction	No clear distinction
Dispersivity	Medium-High	Medium	None
Shear strength parameters	$c' = 0 \text{ kPa}$ $\phi' = 28^\circ$	$c' = 2 \text{ kPa}$ $\phi' = 24^\circ$	$c' = 0 \text{ kPa}$ $\phi' = 32^\circ$
Permeability	1,1 E-08 cm/s	1,2 E-08 cm/s	7,9 E-06 cm/s
Matric suction	Retains higher suction when wetted from <i>in-situ</i> moisture content	Retains higher suction when wetted from <i>in-situ</i> moisture content	Loses more suction when wetted from <i>in-situ</i> moisture content

5 DISCUSSION

5.1 INTRODUCTION

In the previous two chapters, the fieldwork results and laboratory test results were presented, and the discussion thereof limited to their respective spheres. In this chapter, a more comprehensive discussion of the results is given taking the integration of the literature survey, fieldwork results and laboratory test results into account.

The results from the three study areas are compared to identify the critical soil parameters influencing SSE leading to sinkhole formation. This is followed by a discussion of the mechanisms at work and an attempt is made to answer some of the questions raised on the phenomenon in South Africa as summarised in section 2.3.4.

As the objectives of this research project and the hypothesis include the development of a method to predict the likelihood of SSE resulting in sinkhole formation, the second half of this chapter is devoted to developing a method. The Van der Merwe method to predict the maximum sinkhole size is reviewed in light of the discussion. This is followed by the development and presentation of a new method to predict the likelihood of sinkhole formation.

The chapter ends with further comments on the mechanisms involved which demonstrate the complexities involved in this phenomenon and places the proposed method in perspective.

5.2 IDENTIFICATION OF CRITICAL SOIL PARAMETERS

In chapter 2, the current understanding of the SSE above undermined ground was presented both in terms of the mechanism at work in the phenomenon and the influencing factors. The mechanism was described as soil from the overburden material being washed into cracks in the underlying rock mass caused by subsidence due to undermining, resulting in cavities which, when the lid covering them collapses, result in sinkholes on surface.

The factors which influence SSE and sinkhole formation in general (and thus not limited to undermined ground only) presented in Chapter 2 include the following:

- Overburden thickness – it was said that a thicker overburden results in larger sinkholes;
- Stratification of the overburden whereby a less erodible layer, or a layer with a higher tensile strength, overlies a more erodible or weaker layer. If the entire overburden is

homogenous, the soil will merely slump into the cavity with no sinkhole on surface, or the hole on surface will have a similar width to the width of the receptacle, if the receptacle volume is large enough. Stratification can either be provided by man-made layers such as road surfaces, plant roots or a change in the soil profile.

- A source of water to initiate the piping / erosion;
- The infiltration capacity of the upper layers must exceed that of the lower layers. Desiccation cracks in clayey layers increases the infiltration capacity;
- The presence of an erodible layer above an impeding layer. The erodibility is influenced by the dispersivity, propensity to slaking and clayey layers obtaining an erodible crumb-like structure upon drying out;
- A water outlet, such as the crack into the rock mass below;
- Geometrical considerations – the size of the cavity below the surface is limited by the size of the reservoir into which the soil is eroded;
- Rainfall cycles, especially heavy rain after a prolonged period of drought; and
- The strength of the lid covering the sinkhole, which although linked to the stratification in profile mentioned above, is also influenced by soil suctions increasing its tensile strength.

But which of these factors are the most critical in the formation of the 38 sinkholes on Donkerhoek farm? The answer can be found by comparing the results from the different study areas, as summarised in Table 5-1, which is a combination of Table 3-3 and Table 4-14.

Table 5-1: Summary of fieldwork and laboratory test results for study areas.

Characteristic / Soil property	Area 1	Area 2	Area 3
Fieldwork			
Typical sinkhole diameter	1,5m	No sinkholes	<0,3m
Hillwash infilled V-Shape found in residual sandstone	Slopes at 57° above horizontal	Steep slopes, no sinkhole found	Sloped at >75° above horizontal
Depth to rock	3m (Test pit)	5,7m (Borehole)	3m (Test pit)
Crack width in rock at bottom of test pit	50mm	Not exposed, too deep	50mm
Densely fissured horizon in residual sandstone	Yes	No	No
Laboratory testing			
Grading analysis	50% - 60% clay	50% - 60% clay	30% - 40% clay
Swell potential	Low to high	Low to high	Low to medium
Mineralogy and elemental composition	No clear distinction	No clear distinction	No clear distinction
Dispersivity	Medium-High	Medium	None
Shear strength parameters	$c' = 0 \text{ kPa}$ $\phi' = 28^\circ$	$c' = 2 \text{ kPa}$ $\phi' = 24^\circ$	$c' = 0 \text{ kPa}$ $\phi' = 32^\circ$
Permeability	1,1 E-08 cm/s	1,2 E-08 cm/s	7,9 E-06 cm/s
Matric suction	Retains higher suction when wetted from <i>in-situ</i> moisture content	Retains higher suction when wetted from <i>in-situ</i> moisture content	Loses more suction when wetted from <i>in-situ</i> moisture content

In the discussion below, Area 1 is first compared with Area 3 and then Area 1 is compared with Area 2. The observations made from Table 5-1 are stated and discussed.

5.2.1 Area 1 vs Area 3

Apart from the difference in sinkhole diameter (and the angle of the V-shapes) the fieldwork observations of Area 1 and Area 3 are similar; in both areas rock was found at 3m depth with an infilled, 50mm wide subsidence crack in the rock underlying the sinkholes. As the grading

and foundation indicator results for the hillwash in both areas are also similar, the difference in sinkhole diameter can be attributed to the properties of the residual sandstone layer.

With reference to Table 5-1 it can be seen that large sinkholes (Area 1) tend to form in soils with a high clay content, high swell potential, high dispersivity and with capacity to retain more suctions when wetted from the natural moisture content. These properties are found in Area 1 and are different to those from Area 3 (small sinkholes).

As shown in Figure 3-12 and Figure 3-15, the lid observed at TP02 during the fieldwork did not consist of the hillwash horizon alone, but it was supported along the perimeter by the residual sandstone layer underneath. It was the contribution of the residual sandstone to the lid support which enabled the lid to span across a greater diameter resulting in a larger sinkhole. For Area 3, the properties of the residual sandstone are different which resulted in less lid support and the formation of smaller sinkholes. In fact, as mentioned in section 3.4.2, in Area 3, the sinkhole arches were formed mainly in the hillwash horizon, with very little widening into the residual sandstone layer below.

An important point to note is that for all cases where a sinkhole will form at the surface, the final sinkhole diameter is determined by the strength of the lid, i.e. the ability of the lid to span over the underlying cavity. All the other factors such as desiccation cracking, dispersivity and erodibility will only influence the rate at which the sinkhole forms and whether the critical span will be exceeded. These factors do not determine the final sinkhole diameter at failure. To illustrate the statement: even if the residual sandstone in Area 3 had been highly dispersive and erodible, the final sinkhole diameter would still have been small as the lids would still have collapsed once the critical diameter was exceeded.

It is believed that the main property which increased the lid strength in Area 1 is the higher suctions developed and maintained in Area 1, with respect to Area 3 (see Table 4-13). These higher suctions increased the tensile strength of the soil, resulting in the ability of the lid to span. Upon wetting, the suctions in Area 3 reduced more rapidly, resulting in a loss of tensile strength and collapse of the lid. The higher permeability and lower clay content of Area 3 are also related to the quicker loss in suctions, as the wetting front will move quicker through the residual sandstone in Area 3 than in Area 1 (see Figure 4-24).

As mentioned in section 4.2.4, the strength parameters determined from saturated triaxial testing on undisturbed samples showed zero cohesion, indicating the absence of cementation in the ground. The absence of cementation implies that any tensile strength that the lid material would have possessed was the result of matric suction (and a contribution from plant roots).

Regarding dispersivity, it is not necessary for the entire overburden layer to be dispersive for it to be a factor in sinkhole formation. In Area 1, the samples which were the most dispersive based on the ESP vs CEC chart from Gerber and Harmse (1987) (samples TP18/6 and TP03-DSC109/2 as shown in see Figure 4-5) were both located at a depth of around 2,5m where the subterranean tunnel formed. Sample TP18/4, taken at a shallower depth from the layer which supported the lid in the hillwash and on which the triaxial tests and SWRCs were done, was less dispersive.

Apart from dispersivity, the densely fissured horizon with the apparent crumb structure found towards the top of the residual sandstone in Area 1 may cause the horizon to be erodible, in a similar fashion as the clay found in the Secunda area by Wagener *et al.* (1990) as discussed in section 2.3.3.

It is concluded that larger sinkholes form in areas with highly dispersive soils, higher clay content and swell potential, but that the final diameter of the sinkhole is determined by the strength of the lid. Stronger lids lead to larger sinkholes.

5.2.2 Area 1 vs Area 2

A comparison of the residual sandstone properties for Area 1 and Area 2 in Table 5-1 shows significant similarity, especially in terms of grading, swell potential, suction retention capacity upon wetting and permeability. The properties of the hillwash horizons are also similar as shown earlier.

Since the rock depth in Area 2 was at 5,7m deep and beyond the reach of the excavator, a subsidence crack in the rock could not be exposed and measured. However, using equation 2-2 in section 2.3.4 and a maximum subsidence of 2,8m (Coetser *et al.*, 2014), the crack width was calculated as 67mm. The fact that the crack width is larger than the 50mm measured in Area 1, means that the crack width can be regarded as insignificant in terms of identifying causes for no sinkholes in Area 2. If the calculated crack width had been smaller than Area 1, it could have been a contributing factor to no sinkholes forming. Thus, with all the above properties being similar to Area 1, the question remains as to why no sinkholes were recorded in Area 2?

It is postulated that the answer lies in the difference in the thickness of the soil profile, which is 3m for Area 1 and 5,7m for Area 2. When the logic in equation 2-1 is applied, it can be seen that for two receptacles of the same volume (equal crack width and crack depth) a smaller sinkhole diameter is required to fill the receptacle below a thick overburden layer, whilst a large sinkhole is required to fill a receptacle below a thin layer. It follows that if the overburden layer

is thick enough, the crack in the rock will be filled before the upwards migrating cavity reaches the surface. It is also possible in the case of thicker soil layers with a cohesive layer found near the middle of the profile, that the upwards migrating cavity can increase in diameter below the cohesive layer, and the receptacle be filled before the cavity has reached the surface, resulting in no sinkhole forming.

The above observation may appear to be contrary to the statement by White and White (1995) that thicker soil layers lead to larger sinkholes as recorded in section 2.4.3. It must be realised that the statement is made in the context of dolomite related sinkholes, where the size of the receptacle is often very large compared to the sinkhole volume. In the case of subsurface erosion above undermined ground, the size of the receptacle is limited by the width and depth of the subsidence crack.

There are several of the other factors influencing sinkhole formation mentioned in Chapter 2 (and summarised above on page 5-1) which will have a greater effect in thinner soil layers (i.e. Area 1) than thicker soil layers like Area 2. These factors and their influence are discussed below:

- In a thinner overburden layer there is a higher probability that the desiccation crack will reach the top of the rock, and be connected to the crack in the rock. (The desiccation crack referred to is separate from the subsidence crack which can also open up as the material dries out.) With the thicker profile, it is less likely for the cracks to reach the rock head due to the higher lateral stress in the soil and the thicker profile providing resistance to being dried out as higher suctions develop.
- The desiccation cracks increase the infiltration capacity of the soil, which leads to higher volumes of water at the interface of the erodible layer above the impeding layer, causing piping and subsurface erosion. As noted by García-Ruiz *et al.* (1997) in section 2.4.2., the likelihood of piping is increased where two or more desiccation cracks connect. For the thicker layer, although the infiltration capacity will be similar, the higher water volumes will not reach the impeding layer.
- In section 3.4.2. it was mentioned that the air rising from the open subsidence crack in the rock at TP06, was warm. The warm air will contribute to the soil above the crack drying out, possibly leading to an erodible crumb structure. This will increase the likelihood of a cavity above the crack in the rock to be enlarged though subsurface erosion. For thicker profiles, although the soil may also dry out, water from surface is less likely to reach it.

In light of the above, it is concluded that the thicker soil layer in Area 2 contributed to the absence of sinkholes in this area, either by filling of the crack in the rock before the cavity reached the surface or due to the desiccation cracks not extending deep enough to effect subsurface erosion. In terms of future work, it is recommended that the full depth of the soil profile to 5,7m deep be exposed through an excavation and that the crack in the rock be investigated to confirm the above conclusion.

As a side note, in close proximity to Area 2, the undermining plans (Scheppel, 2017a) show an overburden thickness of 18m. The fact that very soft rock sandstone was found at a depth of 5,7m, indicates that care must be taken in assuming the soil thickness to be equal to the overburden thickness shown on the mine plans. It appears that the core from 5,7m down to 18m was classified during exploration as a very soft rock and subsequently classed as part of the overburden, but it will behave as competent rock in terms of the SSE process.

5.2.3 Summary

Through the comparison of the fieldwork and laboratory test results from the three study areas, the critical parameters involved have been isolated:

- The strength of the lid, which is highly influenced by the unsaturated behaviour of the lid material;
- The erodibility of the material which is influenced by dispersivity and the material contributing to a crumb structure due to desiccation;
- The activity of the soil, which influences the volume changes during drying and thereby the width and depth of desiccation cracks; and
- The thickness of the soil layer overlying the rock head.

5.3 MECHANISMS INVOLVED IN SSE AND SINKHOLE FORMATION

With the critical soil parameters identified, some further discussion of the mechanisms involved in SSE and sinkhole formation, based on the observations made during the fieldwork, is warranted. The observations in the following discussion do not necessarily distinguish between the study areas as the soil properties discussed above do, but are present in both Area 1 and 3 where sinkholes formed. They are presented in an effort to further develop the understanding of the SSE and sinkhole formation process.

One of the factors influencing sinkhole formation listed on page 5-1 is the presence of a water outlet (or receptacle), to which the eroded soil is transported away from the below ground cavity. If the subsidence crack in the rock provides the outlet, why do the sinkholes only occur in certain areas and not all along the cracks? An example of this is in Area 1, where, as described in section 3.4.2, four test pits were excavated over a length of 25m above an infilled crack in the rock. In two test pits, sinkholes with infilled V-shapes were found, and in the other two test pits no sinkholes and no infilled V-shapes were found. The scenario is depicted in Figure 5-1 (a replica of Figure 3-15 included here for ease of reference).

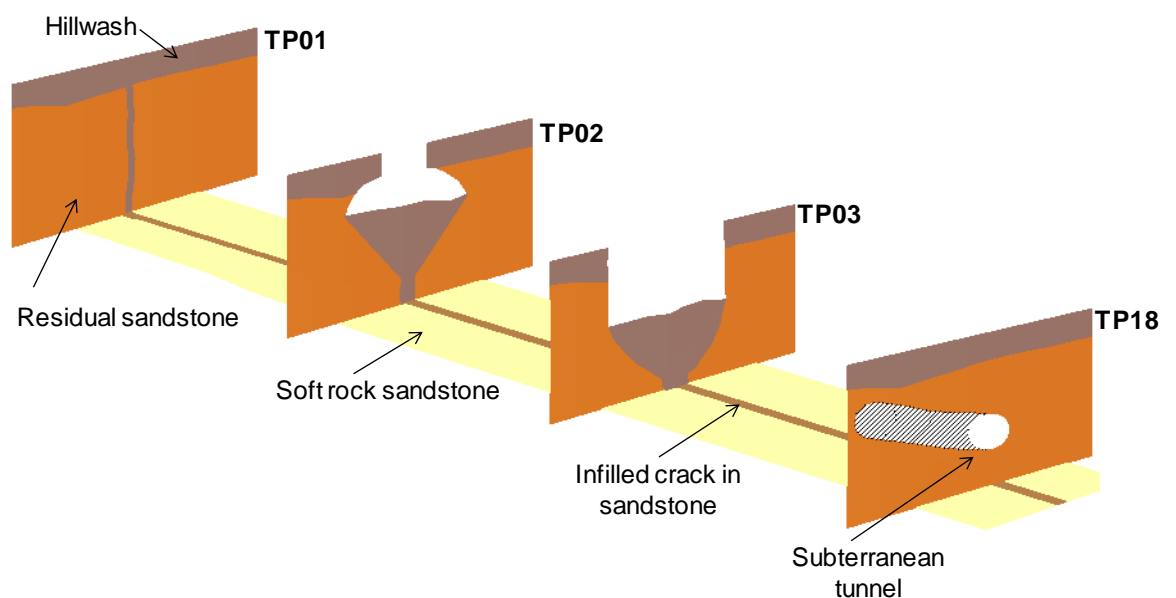


Figure 5-1: Cross sections through each test pit in Area 1.

A possible explanation is that the size of the outlets (or receptacles) along the length of the crack is not the same, with the sinkholes occurring where the receptacles are larger (Van der Merwe 2017c). Although the crack width along the length of the crack in the rock may be similar over a short distance due to the same horizontal strain, the depth of the crack will not necessarily be the same due to horizontal displacements along the bedding planes and joints within the rock mass (Van der Merwe, 2018 – see section 2.3.3). As such, the receptacle volume varies along the length of the crack.

The proposed process of formation is as follows, which is in strong agreement with some of the comments by Van der Merwe (2017a and 2017b) presented in section 2.3.4: As soil is washed vertically downwards into the crack in the rock, the smallest receptacles will close first as the

crack in the rock fills up. The larger receptacles will remain open and will attract water flow towards them, leading to increased seepage gradients with piping and subsurface erosion in a lateral direction. It is suggested that this lateral flow is the cause of the subterranean tunnel, with the tunnel originating at the larger receptacles and growing in length away from the receptacles due to backward erosion. The subterranean tunnel will form along the original infilled subsidence crack through the soil.

As the length and diameter of the subterranean tunnel increases, higher water flow volumes will be attached and mobilised towards the larger receptacles. At certain locations along the tunnel, where the material in the tunnel roof has a higher tensile strength, the tunnel diameter will increase to be more than the width of the original crack (see Figure 3-14). The roof of the tunnel then migrates upwards as more and more material is eroded towards the outlet. The width of the migrating tunnel will only increase further if a more competent layer is encountered during the upwards migration, in line with the comments from Chen and Beck (1989) and others on page 2-36, resulting in the infilled V-shapes following collapse of the lid.

At the same time as the subterranean tunnel grows sideways from the large receptacles, the cavity above the receptacles may also migrate upwards in a similar fashion.

The above process offers an explanation for the conditions found in Area 1, as shown in Figure 5-1. It is postulated that the largest receptacle was located beneath the sinkhole at TP03.

- At TP01, soil was washed downwards filling the crack in the rock. No subterranean tunnel and no V-shape formed.
- At TP02, the crack in the rock below was filled, but a collapsed subterranean tunnel was found at the bottom of the V-shape, possibly draining towards the TP03.
- At TP03, the largest sinkhole formed with the collapsed tunnel below the V-shape.
- At TP18, the tunnel was exposed and found to be inclined downwards towards TP03. There was no V-shape above the tunnel, as the tunnel was still intact.

As discussed above, the presence of desiccation cracks linked to the outlet will only increase the volume of water draining towards the outlet, thereby increasing the available energy for further erosion and sediment transport as described by Dunne (1990) and White and White (1995) on page 2-33. Furthermore, as soon as a sinkhole forms during a rain event, the hole left on ground surface will attract more surface water towards the outlet, thereby increasing the available energy even more. It is suggested that this is the main reason why sinkholes due to

subsurface erosion appear in clusters, which is in agreement with the suggestion by Van der Merwe (2017a and 2017b) in section 2.3.4.

The entire process described above will be augmented by rainfall after a prolonged period of drought as described by Gertje and Jeremias (1989) (see page 2-36) and due to the ionic imbalance between the fresh rain water and the clay particles as described in section 2.5.1. It is suggested that this was also the case with the November 2016 sinkholes on Donkerhoek farm, as they formed during a rain event following a prolonged drought.

One of the factors causing sinkhole formation discussed in section 2.4.3 (see page 2-40) is the rapid drawdown of the water table as discussed by Zhou *et al.* (2014) who studied the formation of sinkholes in irrigation fields above a loess hillslopes in China. They found that the sudden opening of a plug in the hillslope provided an outlet for the water, causing the rapid drawdown of the water table within cracks in the soil above resulting in sinkholes.

At first glance, the scenario described by Zhou *et al.* (2014) appears to be highly relevant to the present study as it also involves the formation of sinkholes above a crack through the soil. However, the observations made during the fieldwork on Donkerhoek and De Pan farms do not provide sufficient evidence to confirm that rapid drawdown is a critical factor in the present study. By way of speculation, the rapid drawdown can possibly occur if the outlet into the crack in to the rock is suddenly opened through either the dislodging of a piece of rock blocking the outlet or the failure of a soil plug with low permeability which had arched in the crack.

5.4 EVALUATION OF THE VAN DER MERWE METHOD

In the preceding sections, the critical soil parameters and mechanisms involved in SSE leading to sinkholes were identified, thereby confirming the first portion of the hypothesis. The second part of the hypothesis deals with the development of a method to predict the likelihood of sinkhole formation based on the critical soil parameters and mechanisms identified.

The logical starting point in developing such a method is the evaluation of the existing method by Van der Merwe (2018) against the results obtained earlier. The Van der Merwe method is described in detail in section 2.3.4. To evaluate the method, the equations are first applied to conditions in Area 1 followed by general comments on the applicability of the method.

The discussion in the earlier sections have all pointed to the high degree of complexity involved in the SSE and sinkhole formation process. The purpose of the comments made in this section is not to criticise the method, but rather to highlight the important aspects to keep in mind if the

method is applied. Some revisions to the method are recommended based on the results of the current study.

5.4.1 Application of method to the sinkhole at TP02

As discussed in section 2.3.4, the Van der Merwe method essentially determines the maximum sinkhole width (w_h) based on geometrical and conservation of volume considerations using equation 2-1, and then evaluates the lid's capacity to span across the width using equations 2-3, 2-4 and 2-5.

During the fieldwork, the only sinkhole found with a partially intact lid was at TP02. If the geometrical properties as determined from the field work are applied to equation 2-1, a sinkhole width of 0,48m is calculated. The measured properties are soil thickness (t_s) of 3m, lid thickness (t_l) of 0,35m, crack width (w_c) of 50mm and friction angle of the soil (α) of 28° as determined from the triaxial tests. For the crack depth in the rock (t_c) a value of 25m is used as recommended by Van der Merwe (2018).

The calculated w_h of 0,48m is significantly less than the width of 1,5m measured on site for the sinkhole at TP02. Even if the crack depth is increased to 40m, the sinkhole width only increases to 0,78m. Thus, in the case of the sinkhole at TP02, the Van der Merwe method under-predicts the width of the sinkhole.

The opening in the partially collapsed lid at TP02 had a diameter of 0,7m (see Figure 3-12). Using equations 2-3, 2-4 and 2-5, the tensile strength of the lid material at failure can be back calculated for each of the failure modes, as summarised in Table 5-2. In all cases, it is assumed that no external force (F) is applied to the lid prior to failure and that the lid collapsed under its own weight.

Table 5-2: Back calculated tensile strengths from TP02

Failure mode	Equation	Diameter (m)	Tensile strength (kPa)
Circular plate	Equation 2-3	0,7	8
		1,5	36
Simple beam	Equation 2-4	0,7	18,9
		1,5	86,6
Plug failure	Equation 2-5	0,7	3,2
		1,5	6,8

In general, the back calculated tensile strength values are lower than the range of 50kPa to 80kPa given by Li *et al.* (2004) as referred to by Van der Merwe (2018) in section 2.3.4.

Thus, for the case of the partially collapsed sinkhole at TP02, the Van der Merwe method under-predicts the sinkhole width based on the geometrical considerations and over predicts the sinkhole width based on the recommended tensile strength. It is interesting to note that apart from the lid thickness, the geometry in Area 3 (i.e. soil thickness, crack width and crack depth) is very similar to Area 1 and thus, application of the method would have over-predicted the sinkhole size for Area 3 as well.

It should be borne in mind that the results above are based on limited data and does not constitute a fair and comprehensive application of the Van der Merwe method.

The above comparison illustrates the need for further research into the tensile strength of the lids at failure. The issue is further complicated by the fact that, during wetting of the soil, the tensile strength reduces as the suctions decrease. This point is further discussed in section 5.6.4.

A last comment is that, in the author's opinion, the parameter determining the shear plug failure strength (see equation 2-5) should be the shear strength of the soil around the perimeter of the plug, rather than the tensile strength of the soil.

5.4.2 **General comments on the Van der Merwe method**

If the Van der Merwe method is evaluated against the observations and results of the fieldwork and laboratory testing discussed above, the observations listed below can be made.

No pronouncement on likelihood based on soil properties

The Van der Merwe method does not make any pronouncement on the likelihood of sinkhole formation based on soil properties. The outcome from the method is a value of the maximum sinkhole diameter where a subsidence crack due to undermining has formed, with no pronouncement on the probability of sinkhole formation above the subsidence crack. Therefore, the Van der Merwe method in isolation cannot be used to achieve the objectives of the current study.

Assumption of a rectangular lid (in section)

The geometrical volume comparison (see Equation 2-1) used to calculate the maximum sinkhole width and equations used to evaluate the lid capacity to span the cavity are based on the assumption that the lid is rectangular in section, as shown in Figure 2-14, Figure 2-15 and Figure 5-2.

As discussed above, the lid observed in the partially collapsed sinkhole in Area 1 at TP02 (see Figure 3-12) was not rectangular, but in the form of an arch. The residual sandstone provided additional support along the perimeter of the lid as shown by the red wedges in Figure 5-2.

The implication of this additional support is that a larger sinkhole can form than the maximum size predicted by the capacity evaluation equations using the tensile strength (equations 2-3, 2-4 and 2-5).

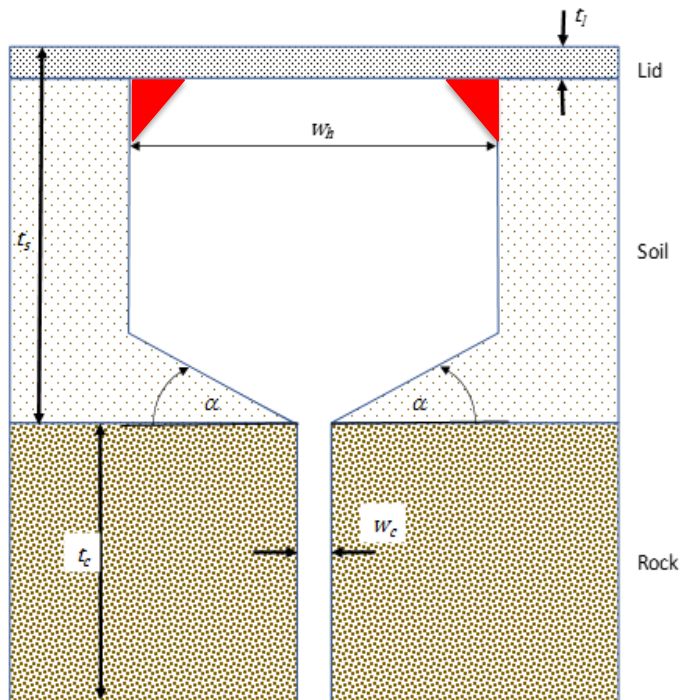


Figure 5-2: Arching support along the perimeter of the lid.

Assumption of vertical erosion only

A fundamental assumption in the geometrical volume calculation described in section 2.3.4 and above, is that erosion only takes place in a vertical direction, implying that soil is eroded downwards into the crack below and that no lateral transfer of soil particles occurs.

The observations in the fieldwork in Area 1 and the discussion in section 5.3 show that lateral flow of water does occur in the subterranean tunnel, and that the vertical erosion assumption does not always hold. However, it does appear to be a reasonable starting point in assessing the size of the sinkhole which can form.

Angle α not equal to friction angle

In Equation 2-1, the value for α is proposed to be equal to the friction angle of the soil and it was also applied in this manner in the comparison in section 5.4.1. However, as mentioned above in section 3.4.2 where the fieldwork observations are presented, the slope of the V-shapes found in Area 1 and 3 are significantly steeper than the friction angles in the material in which they form. Admittedly, Van der Merwe (2018) does comment that Equation 2-1 is not sensitive to the value for α and recommends that α be set equal to zero in the calculations. Nevertheless, it is concluded from the fieldwork that the actual value of angle α is a function of the lid strength and not the friction angle. As mentioned previously, the cavity migrates upwards through the soil from the crack in the rock below and widening of the cavity only occurs when a layer of increased strength is encountered. Thus, the angle α starts off at 90° and then decreases as the lid increases in diameter, reaching a final value when the lid collapses.

Assumption of a rectangular sinkhole (in plan view)

As described in section 2.3.3 and with reference to Figure 2-13, the initial shape of the sinkholes is circular and with time, they may connect resulting in a trench of similar width as the individual sinkholes. During the fieldwork on this project, only the initial circular shape of the sinkholes was observed.

In the Van der Merwe method, the equation used to predict the maximum width of a sinkhole based on volume considerations (as shown in Equation 2-1 and Figure 2-14) assumes that the sinkhole is rectangular in plan view. The method essentially compares the volume of a shallow cavity to the volume of the receptacle (crack in the rock) per metre of crack going into the third dimension. As such, for $w_h < 1\text{m}$, the sinkhole is less than 1m wide, but still 1m wide into the third dimension, and for $w_h > 1\text{m}$, the sinkhole is wider than 1m but still 1m wide into the third dimension. Although the method may accurately predict the final width of the collapsed trench, it may under-predict the initial diameter or width of the sinkhole, as was seen in the case of TP02 described above.

As mentioned in section 2.3.4, Van der Merwe (2017a) recommended that should a different geometry of sinkhole formation be encountered, Equation 2-1 be amended. It is thus suggested that a circular geometry be considered for the sinkhole formation to better approximate the initial condition. A comparison of sinkhole width (w_h) between the rectangular and circular shapes is given in Figure 5-3. The values are calculated for different crack widths in the rock (w_c) ranging from 0,05m to 0,5m and two crack depths in the rock (t_c), namely 25m and 5m. A soil thickness of 3m is assumed and the lid thickness is taken as zero. For all graphs, the value of α is assumed to be zero. The relevant parameters are illustrated in Figure 5-4..

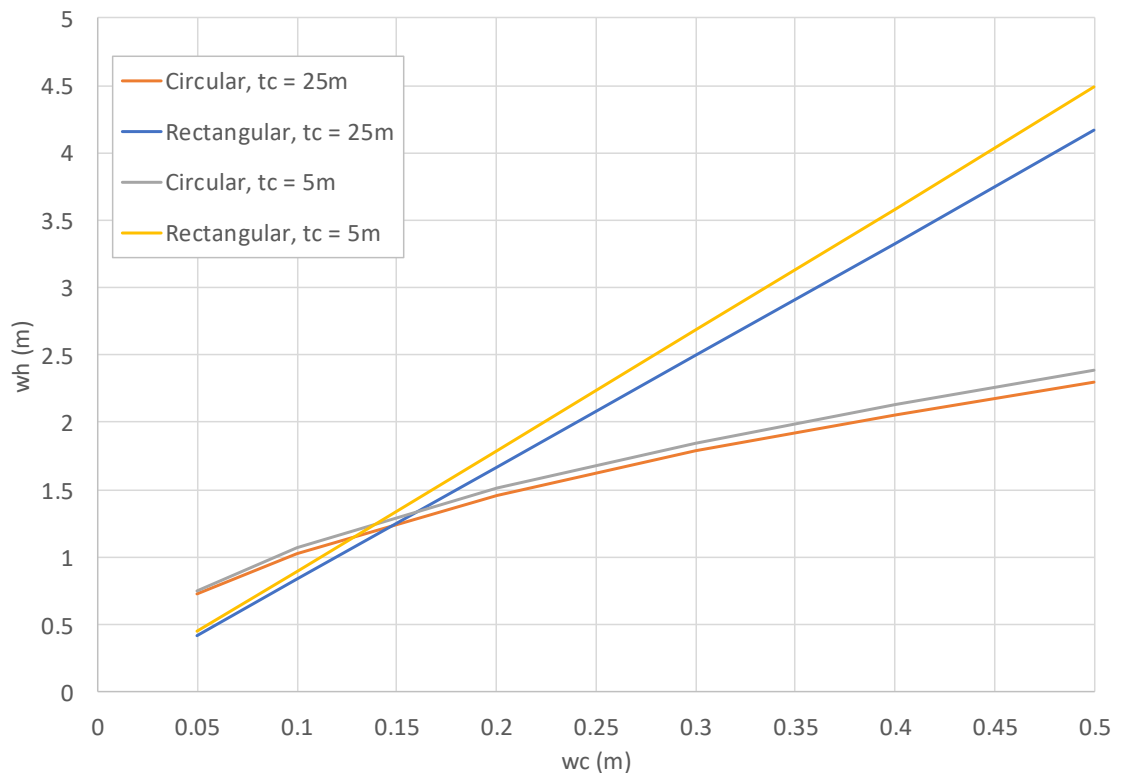


Figure 5-3: Sinkhole width for circular and rectangular shapes for varying crack width

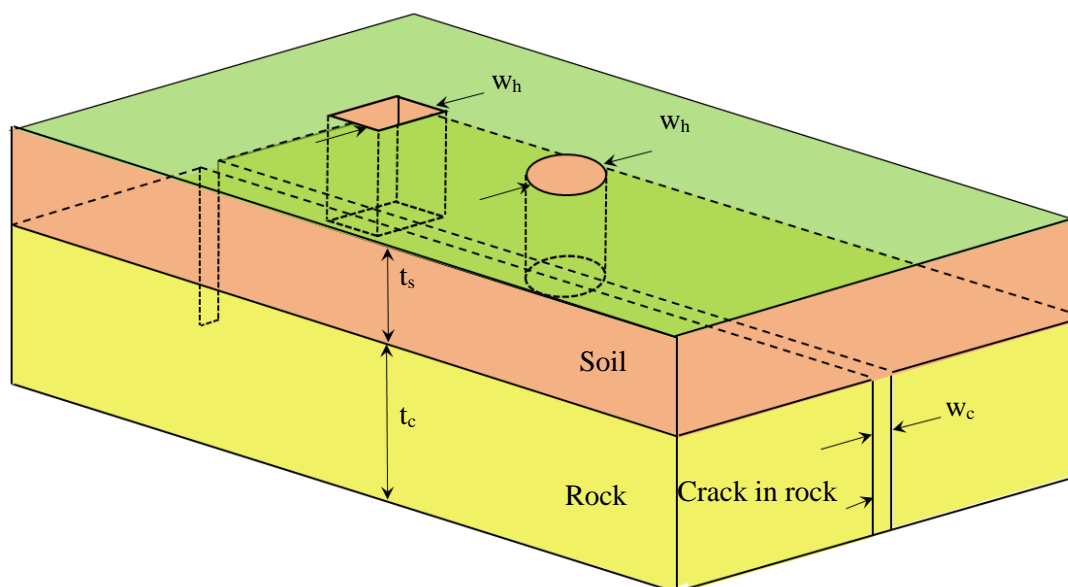


Figure 5-4: Rectangular and circular shape of sinkhole formation.

As expected, the sinkhole widths for the 5m deep crack are smaller since the volume of the receptacle is also smaller. For the smaller sinkholes, the rectangular shape underestimates the width as the sinkhole width into the page is still 1m. For the larger receptacles ($t_c = 25\text{m}$), the rectangular shape estimates a wider sinkhole width than the circular shape since the sinkholes are effectively at a 1m spacing into the third dimension and can only increase their width perpendicular to the crack to supply enough material to fill the receptacle.

All factors considered, the question is whether one wishes to predict the initial width of a circular sinkhole or the final width of the trench. From a point of view of being able to predict the sinkhole diameter for safety reasons, the initial width is more appropriate. It is therefore recommended that a circular geometry also be evaluated in addition to the rectangular geometry.

Limiting the sinkhole width by the geometrical considerations only

As mentioned above, the procedure followed in the Van der Merwe method is to first calculate the maximum sinkhole width based on the geometrical considerations and then evaluate the capacity of the lid to span across the maximum width. As illustrated in the case of TP02 above, the geometrical approach under-predicted the sinkhole width, and therefore the Van der Merwe method would have under-predicted the maximum sinkhole size.

It is recommended that, rather than limiting the evaluation of the capacity to span to the geometrical width, the two evaluations be done independently to avoid necessarily limiting the one by the other.

5.5 PROPOSED NEW METHOD TO PREDICT LIKELIHOOD

The last objective of this research project, and also part of the hypothesis, is the development of a method to predict the likelihood of sinkhole formation using the results of the fieldwork and laboratory tests. In this section, an index-based method to predict the likelihood of SSE resulting in sinkholes above undermined ground is developed, using some aspects of the Van der Merwe method. The proposed method is applied to both the study areas on Donkerhoek farm and the areas where sinkholes were recorded in the Secunda area.

5.5.1 The revised method to predict the likelihood of sinkhole formation

The main soil parameters and properties influencing the process, summarised in section 5.2.3 above, can be divided into three groups as described and expounded upon below. The first and third group have their origin in the Van der Merwe method.

1. The *strength of the lid*, as this will determine the size of the sinkhole forming.
2. The *capacity for cavity formation (CCF)* of the overburden material (soil) above the crack in the rock. Included in this group are erodibility (for sands), dispersivity (for clays), clays which can develop a shattered, desiccated and erodible crumb-like structure upon drying and the influence of high swell potential manifesting as desiccation cracks. Overall, the thickness of the soil layer also affects this group of factors, as discussed in section 5.2.2, in that if the soil layer is too thick, the desiccation cracks will not extend deep enough to allow surface water to enter and effect the subsurface erosion.
3. The *geometrical factor*. This is the relationship between the size of the receptacle (crack width and crack depth) and the available soil thickness above to fill the receptacle.

With limited data available from only three study areas in close proximity, it is unrealistic to attempt to develop a calculation-based (quantitative) method which will take all three factor groups into account. Rather, an index type (qualitative) method is proposed. For each factor group, the range of possible states or occurrences are divided into two sub-groups based on their influence on the likelihood of sinkhole formation. Thereafter, the likelihood of sinkhole formation is assessed for each of the possible sub-group combinations.

The criteria proposed to divide each of the groups into a sub-group is described below.

1. The *strength of the lid*. Strong lids with soil properties similar to Area 1 will result in large sinkholes and weak lids with properties similar to Area 3 will result in small sinkholes. In the context of SSE related sinkholes observed as described in this study, it is recommended that large sinkholes be taken as those with a diameter > 0,5m and small sinkholes a diameter < 0,5m.
2. The *CCF*. The evaluation of this factor group is the most subjective. Soils that are either highly dispersive, highly erodible, prone to desiccation shattering (intensely fissured) upon drying or which exhibit a high swell potential are regarded to have a high CCF. If none of the above properties are present, the CCF is considered to be low. However, it must be borne in mind that even if all these properties are present, the soil layer may be of sufficient thickness to limit the depth of the desiccation cracks and thereby reduce the likelihood of subsurface erosion. At the moment, there is simply insufficient information available to enable a more clear evaluation criterion for this factor group.
3. To be able to evaluate the geometrical factors in an index type environment, the following simplification of Equation 2-1 (repeated below) is proposed:

$$w_h = \frac{1/2w_c \tan\alpha + t_s - t_l - \sqrt{(-1/2w_c \tan\alpha - t_s + t_l)^2 - \tan\alpha(1/4w_c^2 \tan\alpha + t_c w_c)}}{1/2 \tan\alpha}$$

The sinkhole width (w_h) is a function of the rock crack width (w_c), crack depth (t_c), overburden soil thickness (t_s), lid thickness (t_l) and V-shape angle α . In essence, the proposed simplification considers the sinkhole width (w_h) as a function of the ratio between the crack width/soil thickness (w_c/t_s) for a certain lid thickness, depth of crack in the rock and angle α , as depicted in Equation 5-1. The simplification can also be applied to circular shaped sinkholes.

$$w_h = f\left(\frac{w_c}{t_s}\right) \quad (\text{Equation 5-1})$$

Since the continuous crack depth in the rock is the most difficult parameter to determine, a value of 25m is recommended by Van der Merwe (2018), as stated in section 2.3.3. In the author's opinion, if it is known that the rock in a particular area contains prominent medium or closely spaced horizontal joints or bedding planes making a continuous vertical crack depth of 25m unlikely, the value of t_c may be reduced with caution.

The results of the above relationship between w_h and w_c/t_s for rectangular and circular cavities are shown in Figure 5-5 for a continuous crack depth of 25m, and in Figure 5-6 for a crack depth of 5m. In all cases, a lid thickness of 0,2m is assumed. For the rectangular

cavities, the value for α is taken as very small ($<1^\circ$) and for circular cavities, α is taken as zero.

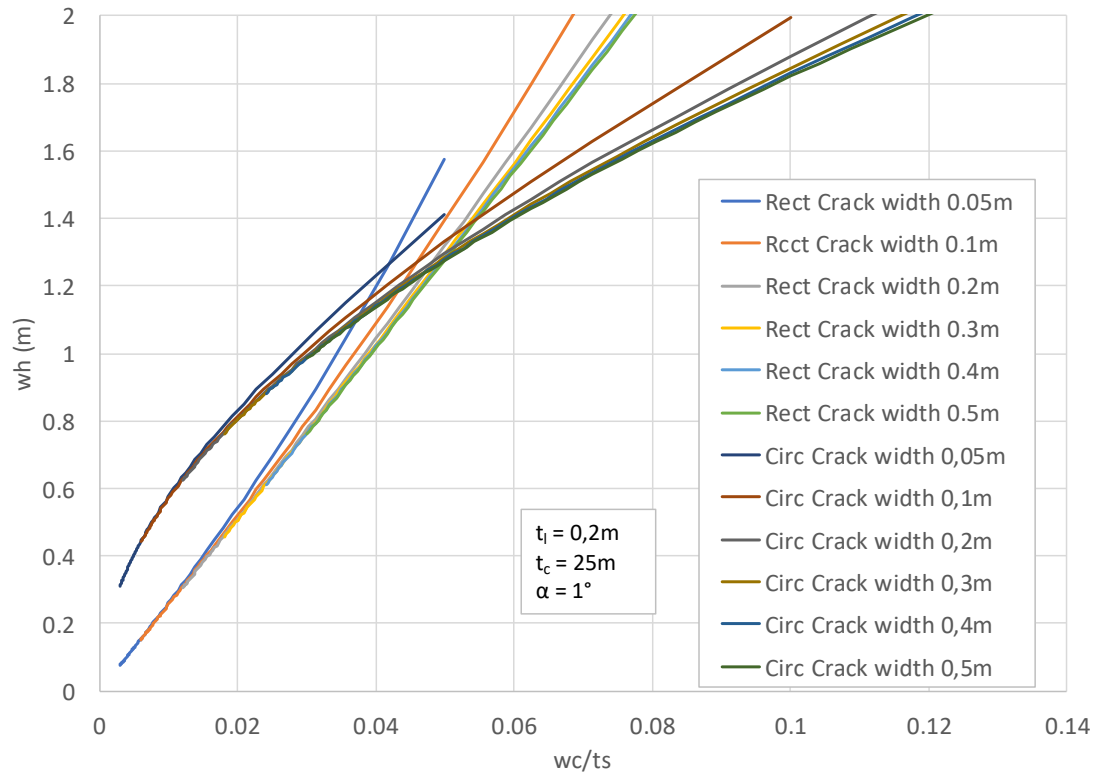


Figure 5-5: Relationship between w_h and w_c/t_s for rectangular and circular cavities for a crack depth of 25m.

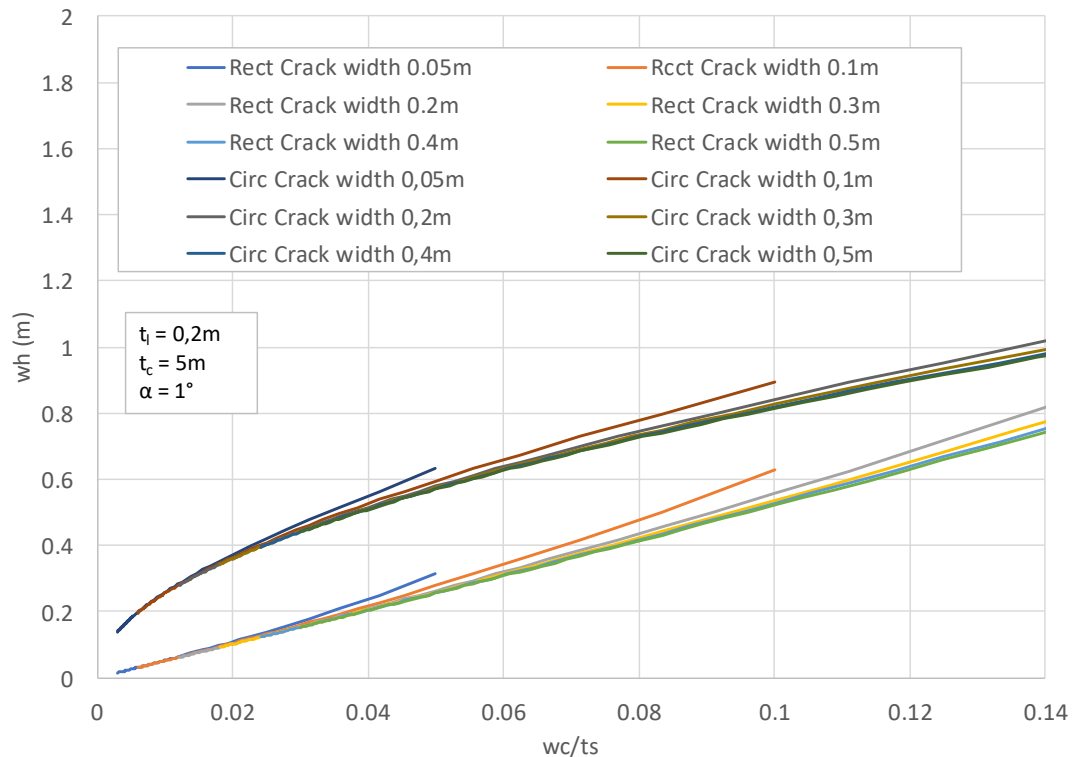


Figure 5-6: Relationship between w_h and w_c/t_s for rectangular and circular cavities for a crack depth of 5m.

The results in Figure 5-5 and Figure 5-6 indicate the effect of the parameter w_c/t_s . For a particular geometry of lid thickness and crack depth in the rock, if the thickness of the soil layer increases or the width of the crack decreases, the value of w_c/t_s decreases and the resulting sinkhole width decreases.

It is also evident that the value of w_h is very sensitive to the depth of the crack in the rock. In the absence of reliable information, the recommended value of 25m must be used.

It is proposed that for a particular location, the ratio w_c/t_s be calculated and the value of w_h be read off the above charts for both the rectangular and circular sinkholes. If the value for $w_h < 0,2\text{m}$, the likelihood of sinkhole formation (for this factor only) is considered low and if $w_h > 0,2\text{m}$, the likelihood is considered high.

It is interesting to note that for a lid thickness (t_l) equal to zero, the relationship between w_h and w_c/t_s plots as single lines for a range of crack widths for both the circular and rectangular sinkhole shapes as shown in Figure 5-7. The intersection point of the graphs is where the volume of rectangular sinkhole equals the volume of the circular sinkhole.

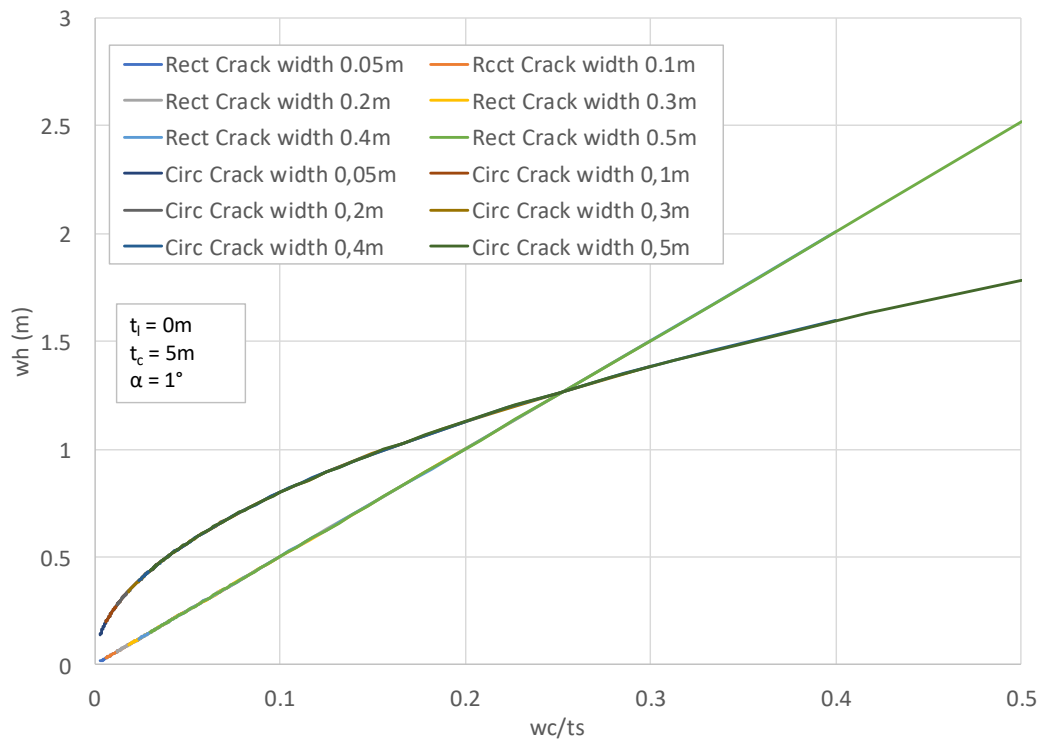










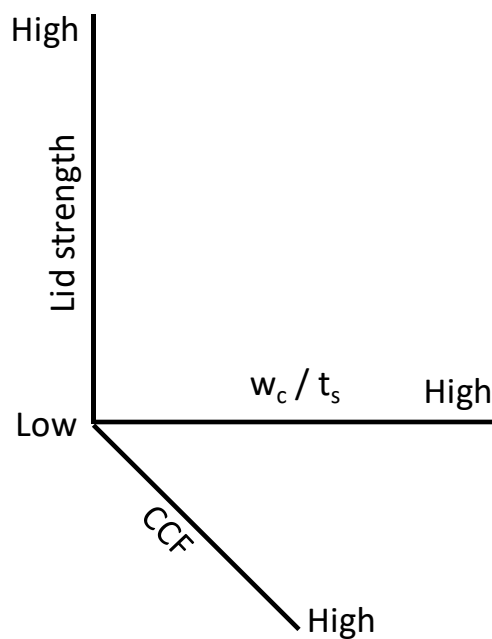
Figure 5-7: Relationship between w_h and w_c/t_s for rectangular and circular cavities for a crack depth of 5m and lid thickness equal to zero.

With the evaluation criteria for each of the factors defined, all the possible combinations of each of the factors and the likelihood of the outcomes can be considered. A summary of all the possible combinations is given in Table 5-3. The colour codes are expounded upon in the subsequent figures.

Table 5-3: Likelihood of sinkhole formation based on factor combinations

Factor and influence on likelihood			Likelihood of sinkhole formation	Combination and colour code
Lid strength	CCF	w_c/t_s		
High	High	High	High likelihood of large sinkholes	
High	High	Low	Low likelihood of large sinkholes	
High	Low	High	Low likelihood of large sinkholes	
High	Low	Low	Large sinkholes unlikely	
Low	High	High	High likelihood of small sinkholes	
Low	High	Low	Low likelihood of small sinkholes	
Low	Low	High	Low likelihood of small sinkholes	
Low	Low	Low	Small sinkholes unlikely	

The contribution of the various factor combinations can be presented graphically using a three-dimensional system as shown in Figure 5-8. The axes define a cube and by splitting each of the axes into a “high” and a “low” zone, all the possible outcomes can be grouped into 8 sub-groups reflecting the combinations in Table 5-3.

**Figure 5-8:** Axis system for graphical representation of factor combinations.

The figures below illustrate the location of the different combinations in Table 5-3 on the axis system.

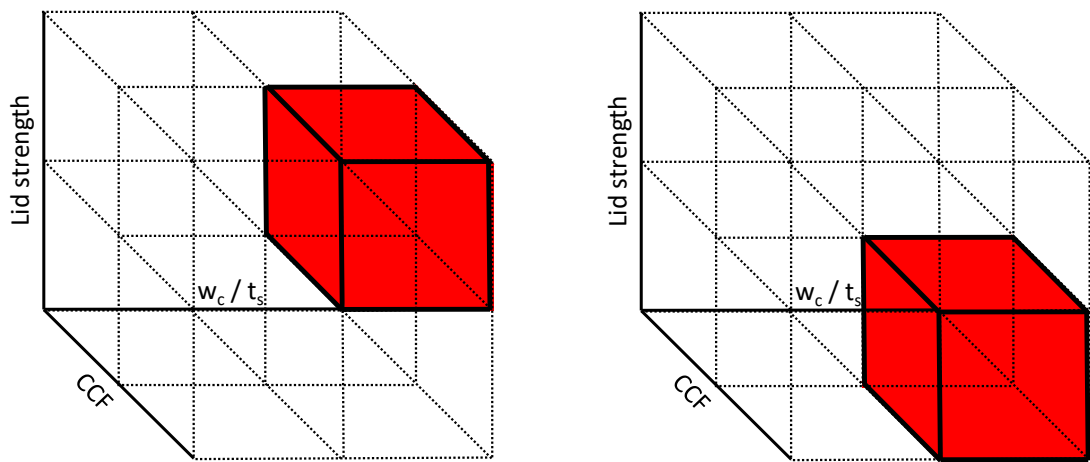


Figure 5-9: Combinations 1 and 5 showing a high likelihood of large sinkholes (left) and a high likelihood of small sinkholes (right).

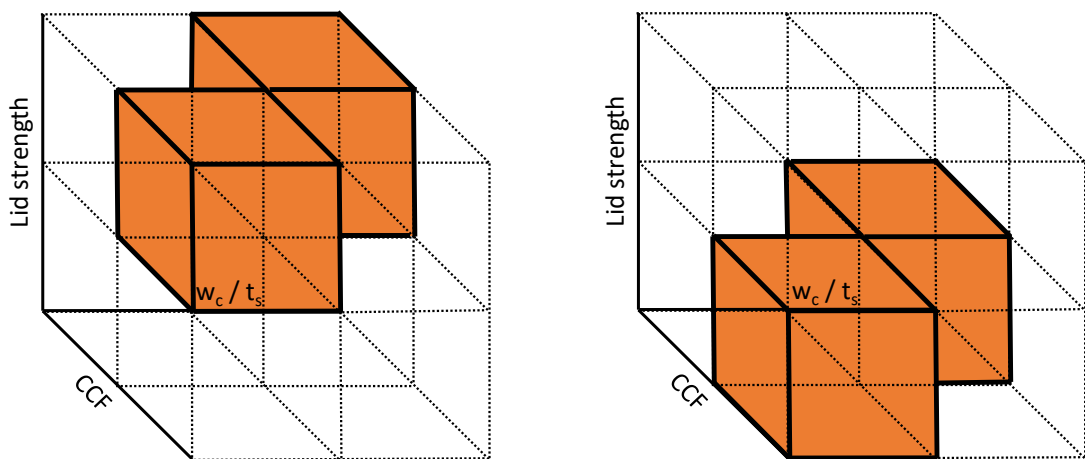


Figure 5-10: Combinations 2, 3, 6 and 7 showing a low likelihood for large sinkholes (left) and a low likelihood for small sinkholes (right).

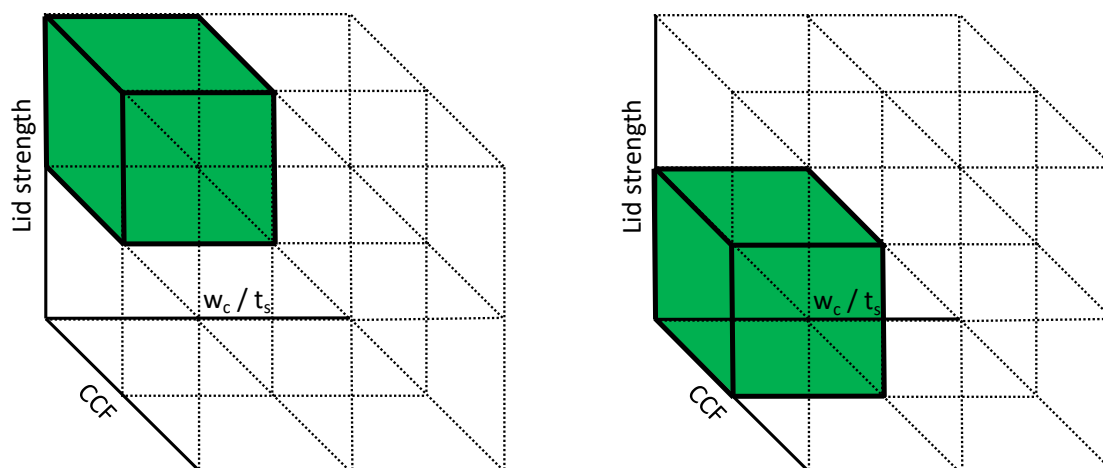


Figure 5-11: Combinations 4 and 8 showing both large (left) and small (right) sinkholes are unlikely.

For a given study area, the value (high or low) for each of the factors above can be determined and the likelihood of formation and size of the potential sinkhole assessed. In assessing the impact of each of the above scenarios, further subdivision is possible as the impact of a small sinkhole will be less than that of a large sinkhole.

It should be kept in mind that the method does not assess the likelihood that subsidence and the resultant crack formation occurred in a particular area. Rather, the method assumes that within the area being looked at, subsidence has already occurred and that the cracks have formed. It then assesses the likelihood that sinkholes will form.

Furthermore, it should be kept in mind that the method is based on limited data and due consideration must be taken if the method is applied to other areas. The criteria applied to distinguish between large and small sinkholes and high and low likelihood of formation are based on the observations in this study and must be re-evaluated before application in another area is considered.

5.5.2 Application to the three study areas

The application of the above method to the three study areas yield the following results with reference to the combinations in Table 5-3:

- For Area 1, the evaluation results in combination 1 with a high likelihood of large sinkholes. The lid strength and CCF are high and the w_c / t_s ratio results in a sinkhole

width greater than 0,2m which classifies as high. This situation is represented on the left in Figure 5-9.

- For Area 3, a high likelihood of small sinkholes (combination 5) is identified. Although the CCF is high and the w_c/t_s ratio indicates a width greater than 0,2m, the lid strength is low. This situation is represented on the right in Figure 5-9.
- In Area 2, combination 3 is identified namely a low likelihood of large sinkholes. The lid strength is high and although the soil thickness is more than in Area 1 and 3, the w_c/t_s ratio still points to a width greater than 0,2m. However, the CCF is considered to be low due to the greater thickness of the soil layer and high matric suction in the residual sandstone retarding the loss of moisture and thereby limiting volume change and desiccation cracking. This situation is represented on the left in Figure 5-10.

As mentioned above, the evaluation of the CCF factor is subjective, and in the application to Area 2 above, a degree of uncertainty remains as it was not possible to inspect the crack in the rock during the fieldwork. The uncertainty can only be addressed through the recommended excavation in Area 2 to confirm the postulated causes of no sinkhole formation.

5.5.3 Application to the sinkholes in the Secunda area

- As mentioned in section 2.3.3, the sinkholes found in the Secunda area are generally smaller than in the Sasolburg area, with a maximum diameter of 0,5m recorded. In applying the above method to the areas where sinkholes were recorded in the Secunda area, the first observation is that the lid strength in the areas where sinkholes were recorded is lower, resulting in smaller sinkholes. Another observation is that, as recorded by Wagener *et al.* (1990) and as shown in Figure 2-8, horizontal displacements across the crack in the rock decreases the continuous depth of the crack and thereby the volume of the receptacle. Therefore the calculation of the w_c/t_s ratio can be done using $t_c = 5\text{m}$ rather than $t_c = 25\text{m}$, also resulting in a smaller value for w_h . In keeping with the reasoning above that the final sinkhole diameter is determined by the strength of the lid, it can be postulated that even if the lid strength in the Secunda area were stronger, the likelihood that larger sinkholes will form is reduced by the smaller receptacle volume. This situation is represented on the right in Figure 5-9.

5.6 ADDITIONAL COMMENTS ON OBSERVATIONS

During the fieldwork and subsequent data analysis, many physical and deductive observations were made on the mechanisms involved in the formation of sinkholes due to subsurface erosion above undermined ground. Those observations directly relevant to the identification of the critical soil parameters and the development of the prediction method were discussed in the preceding sections. In this section, some additional observations are presented and discussed. The intention is to highlight the complexities involved in the formation process and to demonstrate the limitations of the index based prediction method presented above.

5.6.1 Subsidence is necessary for SSE to occur

Although it is implied in the literature survey and in the above discussion, it is worth stating that subsurface erosion above undermined ground can only occur if subsidence of the ground surface due to undermining related instability has taken place. This condition was confirmed by Scheppel (2017a). It is only as a result of subsidence that there can be sufficient deformation of the upper layer of the rock mass to undergo the horizontal and vertical deformations that will cause the receptacles in the rock mass to be formed. If no subsidence has been recorded, or is predicted in a certain area, the likelihood of sinkhole formation due to subsurface erosion can be regarded as negligible. The preceding statement excludes the possibility of improperly sealed boreholes that can provide a receptacle for subsurface erosion to occur.

5.6.2 Formation of V-shapes necessary for larger sinkhole formation

Based on the observations in study Areas 1 and 3, all the sinkholes that formed were underlain by an infilled V-shape, with the width at the top of the V-shape the same as the diameter of the sinkhole. It is postulated that without the formation of the V-shape, the formation of sinkholes wider than the crack width in the rock below is not possible.

5.6.3 Crack vs fracture zone

At all the sinkholes investigated in study Areas 1 and 3, a clearly defined subsidence crack was observed at the top of the rock mass below the sinkhole. At two of the test pits excavated outside the study areas (TP11 and TP15), a zone of fractured rock was found at the top of the rock mass, rather than a clearly defined crack. At TP15, a clearly defined V-shape below a

historical sinkhole was found and the fracture zone at the bottom of the test pit was 2,1m wide, extending approximately 1m on either side of the bottom of the V-shape as can be seen in Figure 5-12. It is noteworthy to point out that, as stated in section 2.3.3, Wagener *et al.* (1990) also found sinkholes above fractured zones in the Secunda area.



Figure 5-12: The fracture zone at the bottom of TP15.

The reason as to why some areas develop a clearly defined crack and others develop a fracture zone is beyond the scope of this study. At most, it can be ventured that a widely jointed, hard rock mass will tend to develop clearly defined cracks and that a closely jointed, more weathered rock mass will tend to develop fracture zones.

In the development of the prediction method above, the width of the crack in the rock (w_c) is an important parameter in the formation of sinkholes. The question arises as to whether the same method will be applicable if the subsidence results in a fracture zone and not a clearly defined crack. It is postulated that, since the horizontal strain around the perimeter of the undermining panel will be similar in both cases, the infiltration capacity of the fractured zone cannot be greater than for the case of a single crack. Therefore, the method can still be applied in the case of a fractured zone.

5.6.4 Possibility of saturated soil below an unsaturated lid

The discussion in section 5.2 identified the tensile strength of the lid material as one of the main factors influencing the formation of sinkholes due to subsurface erosion. It was concluded that soils that retain higher suctions when wetted will lead to larger sinkholes forming as the tensile strength remains higher.

The quantification of the tensile strength, and the reduction thereof upon wetting, is beyond the scope of this research project. However, a few comments on the tensile strength reduction upon wetting are included below as they can be of value in the further development of the method.

Assuming that the tensile strength reduction from the dry to saturated state can be quantified, for example by assigning a representative cohesion (ignoring the contribution of frictional strength) for a particular soil, the question is what value is the most realistic and appropriate to use in the calculation of the maximum sinkhole diameter using Equations 2-3, 2-4 and 2-5.

- On the one hand, using the saturated tensile strength will result in the smallest sinkhole diameter, but this does not reflect the actual conditions where the lid is in an unsaturated state most of the time while the cavity develops below ground. The calculated sinkhole diameter will be too small and the risk underestimated.
- On the other hand, a possible consideration is that using the maximum tensile strength will overestimate the sinkhole diameter, as the lid is more likely to fail during a rain event when the tensile strength is reduced, resulting in a smaller sinkhole diameter than predicted.

When the mechanism of the subterranean tunnel and lateral flow below ground is taken into account, the development of the following scenario cannot be excluded: In the event of a rain storm after a prolonged drought, the lateral flow below ground in the subterranean tunnel (as a result of water entering from surface at another location) can result in saturated soil conditions below an unsaturated lid. In this case, using the maximum tensile strength to determine the maximum sinkhole diameter is not unrealistic, and it is recommended that this approach be taken going forward.

5.6.5 Clamped rock at top of crack at TP06 and TP07

As mentioned in section 3.4.2 in the presentation of the additional observations made during the fieldwork, clamped pieces of soft rock sandstone were found at the top of the crack in the rock at TP06 and TP07. Below the clamped rock, the crack was open.

When subsidence occurs, cracks form around the perimeter of the subsided areas due to horizontal and vertical tensile strain. Generally, one would expect the cracks to be widest at the top of the rock head, becoming gradually narrower with depth. As the two rock interfaces move apart during the cracking event, one would not expect pieces of rock to be clamped near the top of the crack, unless they fell in from above and got stuck. In the case of the TP06 and TP07, the top of the rock fragments clamped in the crack was flush with the surrounding rock head, thereby rendering the possibility that the pieces could have fallen in from above as highly unlikely.

A possible mechanism leading to the clamping of the rock fragments is put forward as shown in Figure 5-13. As mentioned in section 2.3.3, during subsidence, two or three associated cracks form around the perimeter of the subsidence trough spaced at 1m to 2m apart. It is postulated that during subsidence, a block of rock between the cracks could rotate. On the exterior side of the panel, the rotation will result in a crack which tapers, becoming narrower with depth. On the interior, the crack will widen with depth, and the possibility exists that the original rock fragments could remain clamped at the top of the crack.

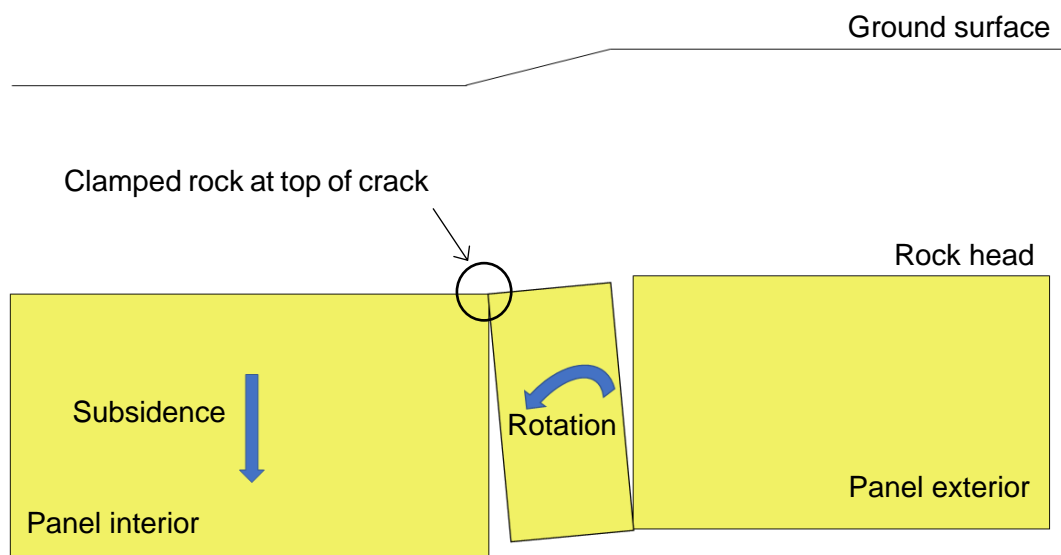


Figure 5-13: Possible mechanism for clamping of rock fragment in top of crack.

It must be pointed out that no evidence of associated cracks were found at TP06 and TP07, neither at the bottom of the test pits nor on ground surface. It is possible that the no sinkholes formed above the exterior crack (the crack on the right in Figure 5-13) as the receptacle volume is reduced due to the narrowing of the crack with depth.

5.6.6 Termite activity at sinkhole positions

During the fieldwork, evidence of termite activity was noticed within the test pit sidewalls at TP03, TP07, TP10 and TP12. A photo of the termite activity within the hillwash infilled crack in the residual sandstone at TP10 is shown in Figure 5-14. According to a local farmer (Crous, 2017), termite activity on surface has often been observed at the sinkhole positions in the corn fields.



Figure 5-14: Termite activity within hillwash infilled crack in residual sandstone at TP10.

Due to its lower clay content and lower suctions at low moisture content, the hillwash is more workable than the residual sandstone. It is suspected that the termites prefer the hillwash above the residual sandstone for nest development.

Although termite activity has been observed at many of the sinkholes, their activity is not believed to be the cause or a significant contributing factor to sinkhole formation. The mechanisms described in section 5.3 explain the formation of the sinkholes and are not dependant on termite activity.

6 CONCLUSIONS AND RECOMMENDATIONS

6.1 CONCLUSIONS

In November 2016, 38 sinkholes formed due to subsurface erosion above undermined ground on Donkerhoek farm near Sasolburg. The fact that the sinkholes formed more than 24 years after mining in the area had ceased, has brought the need for a method to predict the likelihood of sinkhole formation due to subsurface erosion, to the fore. The need for such a method is especially relevant for mining houses who need to quantify mine closure risks.

The 38 sinkholes on Donkerhoek farm presented the ideal opportunity to investigate the mechanisms and soil properties involved in the sinkhole formation, to be able to formulate a method to predict the likelihood of sinkhole formation. This study has set out to develop such a method based on the results of a fieldwork and laboratory testing programme.

Three areas were selected for test pit excavation: an area with large sinkholes, one with small sinkholes and a third with no sinkholes, but all with a history of subsidence crack formation. The same mechanism of sinkhole formation was observed in both the large and small sinkhole areas. At the soil-rock interface, soil was being eroded into a subsidence crack in the rock, resulting in an upwards migrating cavity and the eventual formation of a sinkhole on surface when the cover over the cavity collapsed. This was the first time that this mechanism was observed in the Sasolburg area, having previously only been identified in the Secunda area.

In terms of the mechanism, it was also found that between the crack in the rock and the sinkhole on surface, an upwards widening V-shape had formed which was infilled with the material from the upper soil layers. The width of each V-shape was the same as the width of the sinkhole on surface. It was concluded, as was found in the literature study, that the width of the upwards migrating cavity only increased if there is stratification in the soil profile, where the upper soil layers have a higher tensile strength than the underlying layers. This stratification led to the formation of the V-shape. Based on the mechanisms observed, it was concluded that the final width of the sinkhole is determined by the capacity of the upper soil layers to span across the underlying cavity, i.e. the strength of the lid.

Soil samples were obtained during the fieldwork and submitted to a range of laboratory tests to understand and identify the critical soil parameters involved in subsurface erosion and sinkhole formation. The laboratory tests included foundation indicator tests, dispersivity tests, XRF and XRD tests, soil water retention curves, consolidated undrained triaxial tests and permeability tests. By comparison of the results from the different study areas, it was concluded that the

larger sinkholes form in areas with highly dispersive soils, higher clay content and higher swell potential. It was found, in agreement with the mechanisms discussed above, that larger sinkholes formed in soils with a higher capacity to retain suctions when wetted, thereby retaining the tensile strength of the soil and providing capacity for the lid to span across the underlying widening cavity.

When the mechanisms observed in the fieldwork and the critical soil properties were combined, the following critical soil properties and factors were identified as the main contributors to sinkhole formation:

- The strength of the lid, which is highly influenced by the unsaturated behaviour of the lid material;
- The erodibility of the material which is influenced by dispersivity and the material obtaining a crumb structure due to desiccation;
- The activity of the soil, which influences the volume changes during drying and thereby the width and depth of desiccation cracks; and
- The thickness of the soil layer overlying the rockhead.

With these critical factors identified, the existing method for sinkhole size prediction by Van der Merwe (2018) was evaluated against the conclusions of this study and built upon to develop an index method to predict the likelihood of sinkhole formation due to subsurface erosion above undermined ground. The method considers all combinations of the following factor groups to express a high or low likelihood of the formation of large or small sinkholes in a particular area:

- The strength of the lid material, mainly influenced by the unsaturated behaviour of the soil;
- The capacity for cavity formation (CCF), which combines the dispersivity and erodibility of the material and the activity of the soil which influences the depth and width of desiccation cracks during a time of drought; and
- The influence of the thickness of the soil layer overlying the rock, which is evaluated by calculating the ratio between crack width in the rock and the soil layer thickness (w_c/t_s).

In conclusion, through the fieldwork and laboratory testing, the key mechanisms and critical soil parameters were identified and used to develop a method to predict the likelihood of

sinkhole formation due to subsurface erosion above undermined ground, validating the hypothesis.

6.2 RECOMMENDATIONS

To build on the research presented in this study, the following recommendations are made:

- The current study must be extended to include more areas on Donkerhoek and De Pan farms where sinkholes are known to have formed, with the focus to determine if the conclusions reached in this study can be confirmed.
- In Area 2 of the present study (where subsidence cracks formed, but no sinkholes were recorded), a 6m deep excavation must be made and the top of the rock be exposed to investigate the properties of the subsidence crack in the rock and mechanisms at work which negated the formation of sinkholes. The purpose is to confirm the reasons put forward in this study as to why no sinkholes formed in Area 2.

It is recommended that the study also include further investigation of other areas where subsidence cracks are known to have formed but no sinkholes were recorded.

- The study should also be extended to other mining districts with different soil types, which must include further detailed work in the Secunda area.
- As the method proposed in this study is index based and only distinguishes between large and small sinkholes, there is significant scope for the refinement of the method. Possible areas of refinement include the following topics:
 - How does the erodibility of the soil change with an increase in moisture content when wetted from a dry state? To what degree do suctions in the soil limit erodibility?
 - Quantification of the influence of the roots of typical crops and veld grass on increasing the tensile strength of the soil and hence its capacity to span cavities.

7 REFERENCES

- Abdulla, W.A., and Goodings, D.J. 1996. Modelling of sinkholes in weakly cemented sand. *Journal of Geotechnical Engineering*, Vol. 122, No 12, pp 998 – 1005.
- Al Haj, K.M.A and Standing, J.R. 2016. Soil water retention curves representing two tropical clay soils from Sudan. *Geotechnique*, 66, No. 1, pp 71 – 84.
- Antrobus, B.A. Rampersad, R. and Breyll, J. 2016. *Sigma Defunct Mine: Undermining investigation for backfill material – Factual Report*. Jones & Wagener (Pty) Ltd. Report No JW189/16/F538. Johannesburg.
- Augarde, C.E., Lyamin A.V. and Sloan S.W. 2003. Prediction of Undrained Sinkhole Collapse. *Journal of Geotechnical and Environmental Engineering*, Vol. 129, No. 3, pp 197 – 205.
- Arkin, Y. and Gilat, A. 2000. Dead Sea sinkholes – an ever-developing hazard. *Environmental Geology*, 39 (7), pp 711 – 722.
- Beck, B.F. 1984. Sinkhole Terminology. Proceedings of the *First Multidisciplinary Conference on Sinkholes*. Orlando, Florida, October 1984, pp ix – x.
- Beck, B. 2011. Soil piping and sinkhole failures. *Encyclopedia of caves*. Ed White, W.B. and Culver, D.C. Elsevier Science, pp 718 – 723.
- Beckedahl, H.R. *Subsurface Soil Erosion Phenomena in South Africa*. 1998. Justus Perthes Verlag Gotha, Gotha.
- Bell, F.G. 1988. Subsidence associated with the abstraction of fluids. *Engineering Geology of Underground Movements*. Ed Bell, F.G., Culshaw, M.G. Cripps, J.C. and Lovell M. A.. Geological Society Engineering Geology Special Publication No. 5, pp 363 – 376.
- Bell, F.G. and Maud, R.R. 1994. Dispersive soils: a review from a South African perspective. *Quarterly Journal of Engineering Geology*, 27, pp 195 – 210.
- Bell, F.G. and Walker D.J.H. 2000. A further examination of the nature of dispersive soils in Natal, South Africa. *Quarterly Journal of Engineering Geology and Hydrogeology*, 33, pp 187 – 199.
- Brown, G.W. 1961. *Some physical and chemical soil properties associated with piping erosion in Colorado*. Unpub. MSc Thesis, Colorado State University.

- Chen, J.C. and Beck, B.F. 1989. Qualitative Modelling of the cover-collapse process. Proceedings of the *3rd Multidisciplinary Conference on Sinkholes and the Engineering and Environmental Impacts of Karst*. St Petersburg Beach, Florida, pp 89 – 95.
- Coetser, K. Wardle, G.R. and Oosthuizen, A. 2014. Sasol Sigma Mine Closure – Phase 1 Underground Stability Analysis. Jones & Wagener (Pty) Ltd. Report No JW113/14/D992 Revision 01. Johannesburg.
- Craig, W.H. 1990. Collapse of cohesive overburden following removal of support. *Can. Geotech. J.* 27, pp 355 – 364.
- Craig, R.F. 2005. *Craig's Soil Mechanics*, 7th ed. E & FN Spon, Oxon.
- Crous, D. 2017, *Personal communication to author*.
- Crous, D. 2018, *Personal communication to author*.
- Culshaw, M.G. and Waltham, A.C. 1987. Natural and artificial cavities as ground engineering hazards. *Quarterly Journal of Engineering Geology*, Vol. 20, pp 139– 150.
- Currens, J.C. 2012. Cover-collapse sinkhole in Kentucky, USA: geographic and temporal distribution. *Carbonates Evaporates*, 27:137, pp 137 – 142.
- Drumm, E.C., Kane W.F. and Yoon, C.J. 1990. Application of limit plasticity to the stability of sinkholes. *Engineering Geology*, 29, pp 213-225.
- Drumm, E.C., Aktürk, O., Akgün, H. and Tutluoğlu, L. 2009. Stability charts for the collapse of residual soil in karst. *Journal of Geotechnical and Geoenvironmental Engineering*, Vol. 135, No. 7, pp 925-931.
- Dunne, T. 1990. Hydrology, mechanics, and geomorphic implications of erosion by subsurface flow. *Groundwater geomorphology; The role of subsurface water in earth-surface processes and landforms*. Ed Higgins, C.G. and Coates, D.R. Geological Society of America Special Publication 252, Boulder, Colorado, pp 1 – 28.
- Elges, H.F.W.K. 1985. Dispersive soils. *The Civil Engineer in South Africa*, 27, pp347-355.
- Fletcher, J.E., Harris, E., Petersen, H.B. and Chandler, V.N. 1954. Piping. *Trans. American Geophysical Union*, 35(2), pp 258-262.

- Fredlund, D.G. Rahardjo, H. and Fredlund, M.D. 2012. Unsaturated soil mechanics in engineering practice. John Wiley & Sons, Hoboken, NJ, USA.
- García-Ruiz, J.M. Lasanta, T. and Alberto, F. 1997. Soil erosion by piping in irrigated fields. *Geomorphology*, 20 (1997), pp 269-278.
- Gaspar, T.A.V. 2017. *Investigating the tensile behaviour of unsaturated soil using the Brazilian disk test*. MEng thesis. University of Pretoria.
- Gerber, F.A. and Harmse, H.J. von M. 1987. Proposed procedure for identification of dispersive soil by chemical testing. *Die Siviele Ingenieur in Suid-Afrika*, October 1987, pp 397-399.
- Gertje, H. and Jeremias, A.E. 1989. Building construction over an erosive sinkhole site: A case study in Lancaster County, Pennsylvania, USA. In: *Proc. 3rd Multidisciplinary Conf. on Sinkholes and the Engineering and Environmental Impacts of Karst*. Balkema, Rotterdam, pp 311 – 318.
- Goodings, D.J. and Abdulla, W.A. 2002. Stability charts for predicting sinkholes in weakly cemented sand over karst limestone. *Engineering Geology*, 65 (2002), pp 179-184.
- Grote, W. 2017. Personal communication to author.
- Hamblin, A.P. 1981. Filter-paper method for routine measurement of field water potential. *Journal of Hydrology*, 53 (1981), pp 355 – 360.
- Harmse, H.J. von M. 1980. Dispersiewe grond, hul ontstaan, identifikasie en stabilisasie. *Ground Profile*, No 22, pp 10-31.
- Higgins, C.G. and Schoner, C. 1997. Sinkholes formed by piping into buried channels. *Geomorphology*, 20 (1997), pp 307 – 312.
- Hoffmann, J.P. Donald R.P. Konieczki, A.D. and Carpenter, C.C. 1998. Causes of sinks near Tuscon, Arizona, USA. *Hydrogeology Journal*, (1998) 6, pp 349 – 364.
- Jacobsz, S.W. 2018. Low cost tensiometers for geotechnical applications. *Proc of 9th International Conference on Physical modelling in Geotechnics*, CRC Press, pp 305-310.
- Jennings J.E., Brink A.B.A. and Williams A.A.B. 1973. Revised Guide to Soil Profiling for Civil Engineering Purposes in South Africa. *The Civil Engineer in South Africa*, January 1973.

- Jiang, F., Dai, J., Lei, M., Qin, Y., Jiang, X. and Meng, Y. 2015. Experimental study on the critical triggering condition of soil failure in subsidence sinkholes. *Environ Earth Sci*, 2015, 74, pp 693 – 701.
- Jones, J.A.A. 1981. The nature of soil piping – a review of research. B.G.R.G. Research Monograph Series No. 3, Geo Books, Regency House, Norwich.
- Lei, M., Gao, Y., Jiang, X. and Guan, Z. 2016. Mechanism analysis of sinkhole formation at Maohe village. Liuzhou city, Guangxi province, China. *Environ Earth Sci*, 2016, pp 542.
- Li, J., Tang, C., Wang, D., Pei, X and Shi, B. 2014. Effect of discrete fibre reinforcement on soil strength. *Journal of Rock Mechanics and Geotechnical Engineering*, 6 (2014), pp 133 – 137.
- Maharaj, A. 2013. *The evaluation of test protocols for dispersive soil identification in Southern Africa*. MSc thesis. University of Pretoria.
- Marr, J.C. 1955. Sinkholes in Irrigated Fields. *California Agriculture*, 9 (11), pp 6-7.
- Nascimento, V. and de Castro, E. 1974. Preventative measures against slope erosion. Criteria for soil selection. *Proc 2nd Int Congr Int Assoc Engng Geol*, Sao Paulo, V-IS.I – V-IS.II.
- Ng, C.W.W., Coo, J.L., Chen, Z.K. and Chen, R. 2016. Water infiltration into a new three-layer landfill cover system. *Journal of Environmental Engineering*, 142(5): 04016007.
- Oberholzer, B.M.B. 2017. *Investigating cavity propagation to the surface through centrifuge trapdoor experiments*. MEng Thesis. University of Pretoria.
- Paige-Green, P. 2009. Dispersive and Erodible Soils – Fundamental Differences. *South African Institution of Civil Engineering: A Short Course on Problem Soils*. August 2009.
- Ridley, A.M. and Burland, J.B. 1993. A new instrument for the measurement of soil moisture suction. *Geotechnique* 43(2):321-324.
- Scheffel 2017a. *Personal communication to author, 2017*.
- Scheffel 2017b – Undermining plans J0082A U/G, J0082B U/G, J00803 U/G, K0082A U/G, K0082B U/G, K00803 U/G, J0072A U/G, J0072B U/G, J00703 U/G, K0072A U/G, K0072B U/G and K00703 U/G received via personal communication to author, 2017.

- Schollenberger, C.J. and Simon, R.H. 1945. Determination of exchange capacity and exchangeable bases in soil – Ammonium acetate method. *Soil Science*, January 1945, Vol. 59, Issue 1, pp 13-24.
- Sherard, J.L. Dunnigan, L.P. and Decker, R.S. 1976a. Identification and Nature of Dispersive Soils. *J Geotech Engng Div*, ASCE, 102 (GT4), pp 287–301.
- Sherard, J.L. Dunnigan, L.P. and Decker, R.S. 1976b. Pinhole test for identifying dispersive soils. *J Geotech Engng Div*, ASCE, 102 (GT1), pp 69–85.
- Singh, K.B. and Dhar, B.B. 1997. Sinkhole subsidence due to mining. *Geotechnical and Geological Engineering*. 15, pp 327 – 341.
- Taylor, C.J. 1992. *Ground-water occurrence and movement associated with sinkhole alignments in the Inner Bluegrass karst region of Central Kentucky*. Master's Thesis. University of Kentucky.
- Tharp, M.T. 1999. Mechanics of upwards propagation of cover-collapse sinkholes. *Engineering Geology*, 52, (1999), pp 23 – 33.
- Tharp, M.T. 2001. Cover-collapse sinkhole formation and piezometric surface drawdown. *Geotechnical and Environmental Applications of Karst Geology and Hydrology*, Eds Beck, F.G and Herring, J.G. pp 53 – 58.
- Tharp, M.T. 2003. Cover-collapse sinkhole formation and soil plasticity. *Sinkholes and the Engineering and Environmental Impacts of Karst*. Ed Beck, B.F. pp 110 – 123.
- Toll, D.G. 2012. The behaviour of unsaturated soils. *Handbook of Tropical Residual Soils Engineering*. Ed. by B.B K. Huat, D.G. Toll & A. Prasad. London: Taylor & Francis
- Van der Merwe, J.N. 1990. *Report on the current position with regards to sub surface erosion*. Strata Control. 5 March 1990.
- Van der Merwe, J.N. 2017a. *Investigation into suspected sub surface erosion on farm Donkerhoek, undermined by Sigma Colliery*. Stable Strata Consulting. Report Final 01.. Munster.
- Van der Merwe, J.N. 2017b. *Personal communication to Sasol Mining (Pty) Ltd on 8 January 2017*.
- Van der Merwe, J.N. 2017c. *Personal communication to the author 24 May 2017*.

- Van der Merwe, J.N. 2017d. *Personal communication to the author on 10 July 2017.*
- Van der Merwe, J.N. 2018. Effects of coal mining on surface topography in South Africa – updates and extensions. *Journal of the South African Institute of Mining and Metallurgy*. Vol 118, No. 7, pp 1 – 12.
- Van der Merwe, J.N. and Madden, B.J. 2010. *Rock Engineering for Underground Coal Mining*. 2nd edition. The South African Institute of Mining and Metallurgy - Special Publications Series 8, Johannesburg.
- Van Genuchten, M. T. 1980. A closed form equation for predicting the hydraulic conductivity of unsaturated soils. *Soil Sci. Soc. Am. J.* 44:892-898.
- Wagener, F. Matthews, G.B. Macfarlane, G. 1990. *Geotechnical report on subsurface erosion at proposed township extensions to eMbalenhle township over Middelbult Colliery*. Jones & Wagener Inc. Report No G44/90/3569. Johannesburg.
- Waltham, T., Bell, F. and Culshaw, M. 2005. *Sinkholes and Subsidence – Karst and Cavernous Rocks in Engineering Construction*. Praxis Publishing, Chichester, UK.
- Waltham, A.C. and Fookes, P.G. 2003. Engineering classification of karst ground conditions. *Quarterly Journal of Engineering Geology and Hydrogeology*. Vol. 36, pp 101 – 118.
- White, W.B. and White, E.L. 1992. Sinkholes and Sinkhole Collapses. *Natural and Technological Disasters: Causes, Effects and Preventative Measures*. Ed Majumdar, S.K. Forbes G.S. Miller, E.W. and Schmalz, R.F. The Pennsylvania Academy of Science, pp 280 – 293.
- White, W.B. and White, E.L. 1995. Thresholds for soil transport and the long term stability of sinkholes. *Karst GeoHazards – Engineering and environmental problems in karst terrane*. Ed Beck, B.F. Balkema, Rotterdam.
- Xu, L., Dai, F.C., Tham, L.G., Tu, X.B., Min, H., Zhou, Y.F., Wu, C.X. and Xu, K. 2011. Field testing of irrigation effects on the stability of a cliff edge in loess, North-west China. *Engineering Geology*, 120 (2011), pp 10 – 17.
- Zhou, Y.F. Tham, L.G., Yan, R.W.M. and Xu, L. 2014. The mechanism of soil failures along cracks subjected to water infiltration. *Computers and Geotechnics*. 55 (2014), pp 330 – 341.

APPENDIX A

FIELDWORK RESULTS

A.1 INTRODUCTION

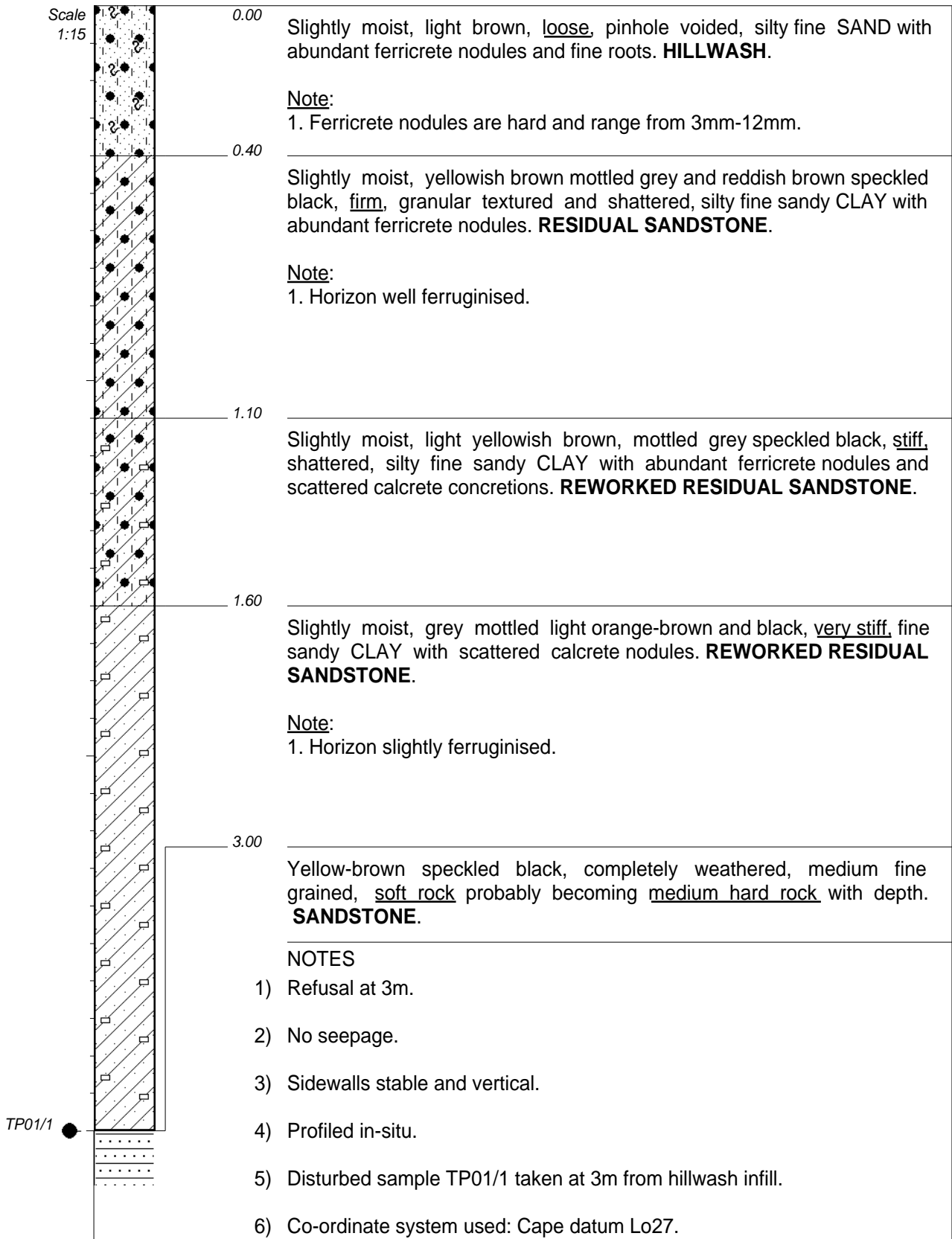
Additional information obtained from the fieldwork is included in this appendix. The purpose is to substantiate the discussion presented and conclusions reached in the main body of the dissertation. As a secondary purpose, the intention is to place some of the fringe observations on record as they may of use in future

A.2 CONTENTS OF APPENDIX A

The following sets of fieldwork results are contained in Appendix A:

- a) Test pit profiles
- b) Photographs from test pits
- c) Test pit observation summary
- d) Additional notes taken during test pit excavation

A.2a) TEST PIT PROFILES



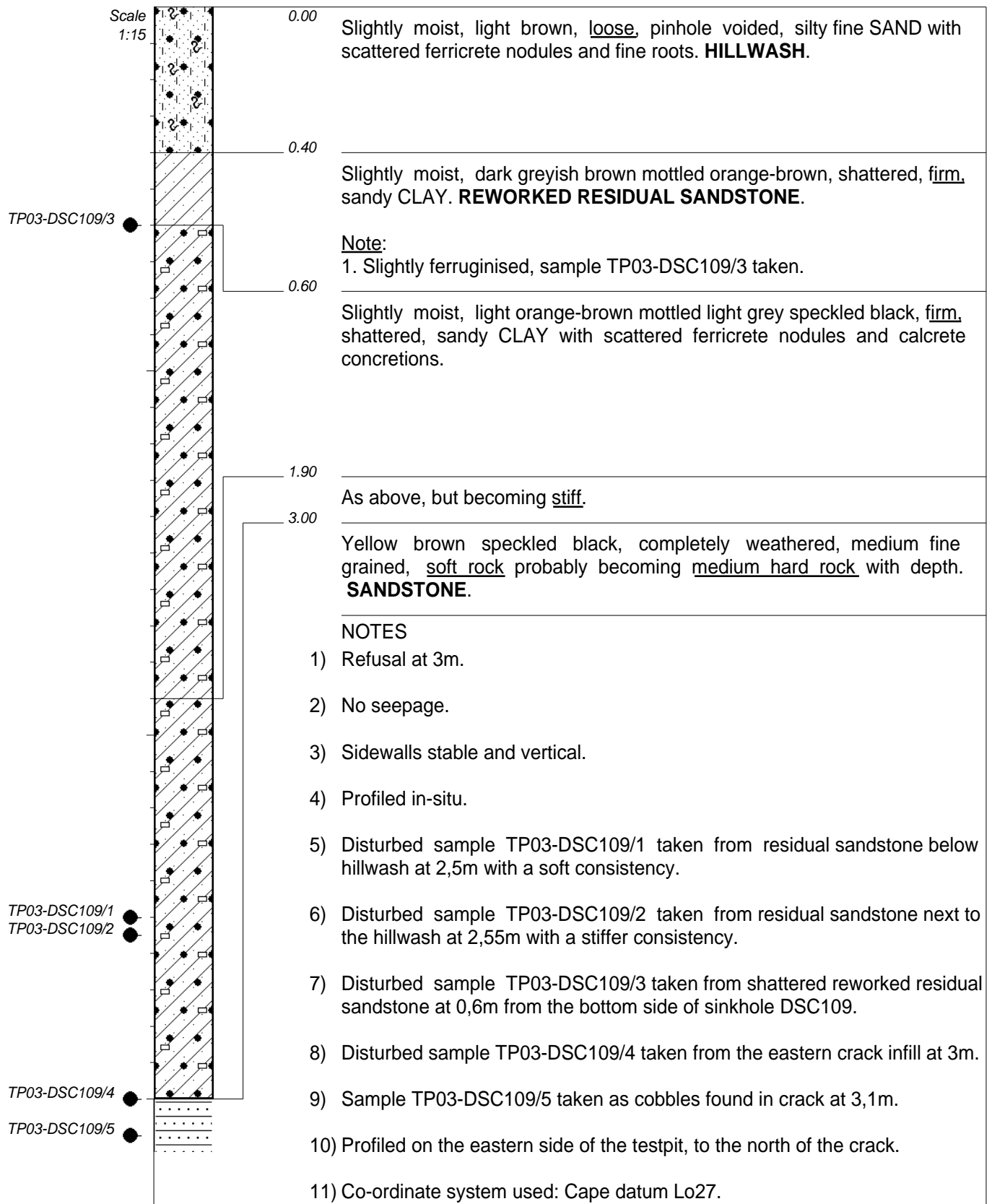
CONTRACTOR : CJ Terblanche Beleggings
MACHINE : Volvo 360 Excavator
DRILLED BY : Frans Matli
PROFILED BY : M Dlamini

INCLINATION : Vertical
DIAM : 1,66m tined bucket
DATE : 27 June 2017
DATE : 27 June 2017

ELEVATION :
X-COORD : 2970448
Y-COORD : -077268

TYPE SET BY : Beth
SETUP FILE : STANDARD.SET

DATE : 03/01/2018 16:40
TEXT : ..\G34100PRO\JOB20170714.DOC



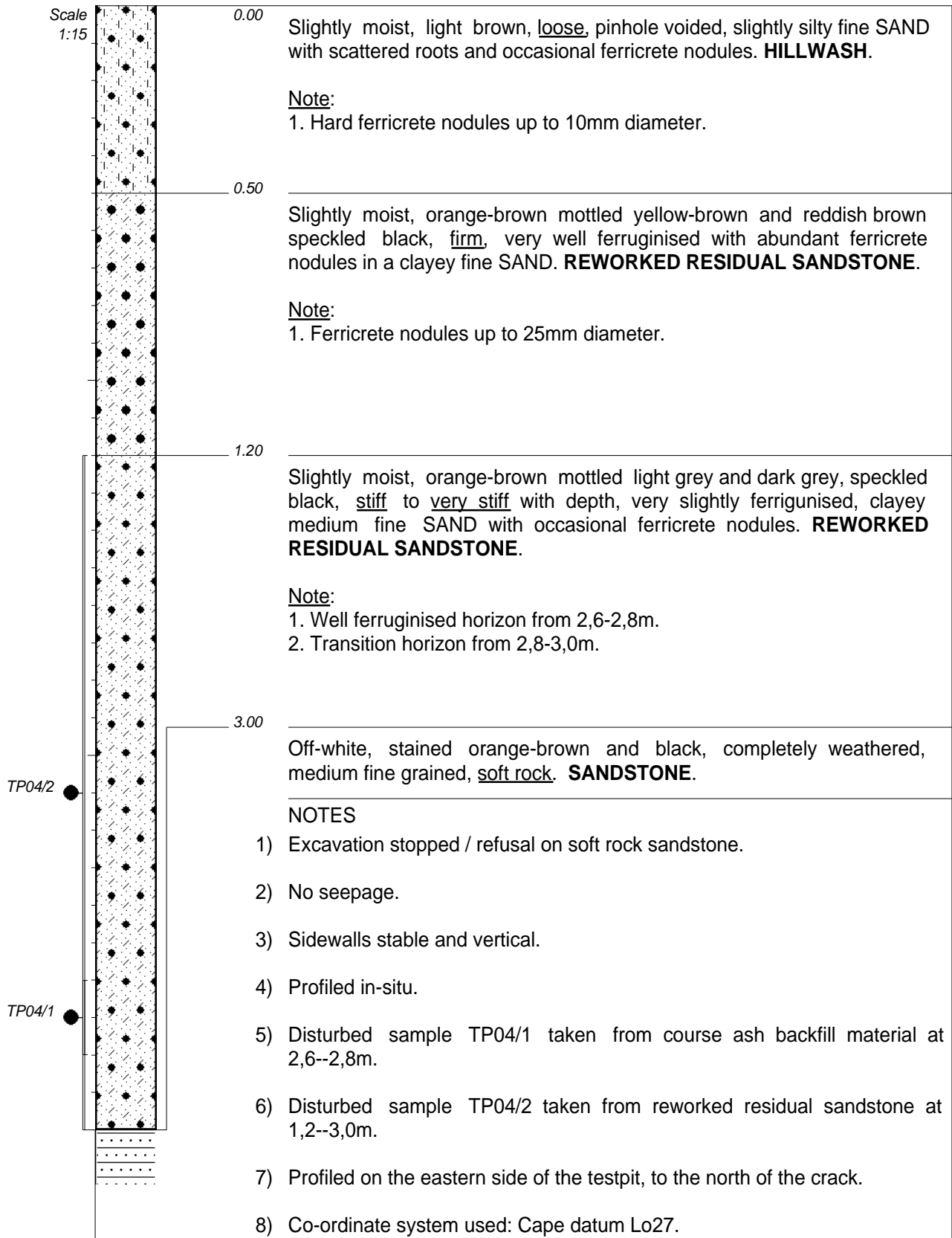
CONTRACTOR : CJ Terblanche Beleggings
MACHINE : Volvo 360 Excavator
DRILLED BY : Frans Matli
PROFILED BY : M Dlamini

INCLINATION : Vertical
DIAM : 1,66m tined bucket
DATE : 27 June 2017
DATE : 27 June 2017

ELEVATION :
X-COORD : 2970453
Y-COORD : -077275

TYPE SET BY : Beth
SETUP FILE : STANDARD.SET

DATE : 03/01/2018 16:40
TEXT : ..\G34100PRO\JOB20170714.DOC



CONTRACTOR : CJ Terblanche Beleggings
MACHINE : Volvo 360 Excavator
DRILLED BY : Frans Matli
PROFILED BY : J Breyl

INCLINATION : Vertical
DIAM : 1,66m tined bucket
DATE : 28 June 2017
DATE : 28 June 2017

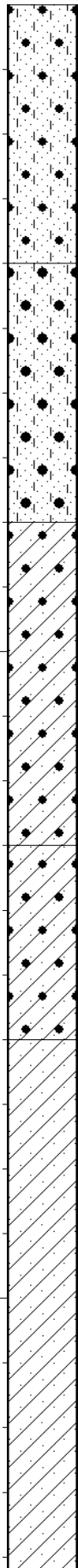
ELEVATION :
X-COORD : 2970513
Y-COORD : -077812

TYPE SET BY : Beth
SETUP FILE : STANDARD.SET

DATE : 03/01/2018 16:40
TEXT : ..\G34100PRO\JB20170714.DOC



Scale
1:10



0.00

Slightly moist, light brown, loose, pinhole voided, silty fine SAND with scattered ferricrete nodules and fine roots. **HILLWASH.**

Note:

1. Subrounded hard ferricrete nodules up to 10mm diameter.

0.40

Relatively closely packed, subrounded, medium hard ferricrete nodules up to 30mm in diameter in a matrix of as above but ferruginised. **HILLWASH.** Overall consistency medium dense.

Note:

1. From 0,8-0,9m, west side, coarse ash backfill found below hillwash.

0.80

Slightly moist, orange-brown mottled reddish brown and grey speckled black, firm, shattered, sandy CLAY with scattered ferricrete nodules. **REWORKED RESIDUAL SANDSTONE.**

Note:

1. Horizon ferruginised.

1.30

Slightly moist, grey mottled orange-brown speckled black, firm, shattered, sandy CLAY with scattered ferricrete nodules. **REWORKED RESIDUAL SANDSTONE.**

Note:

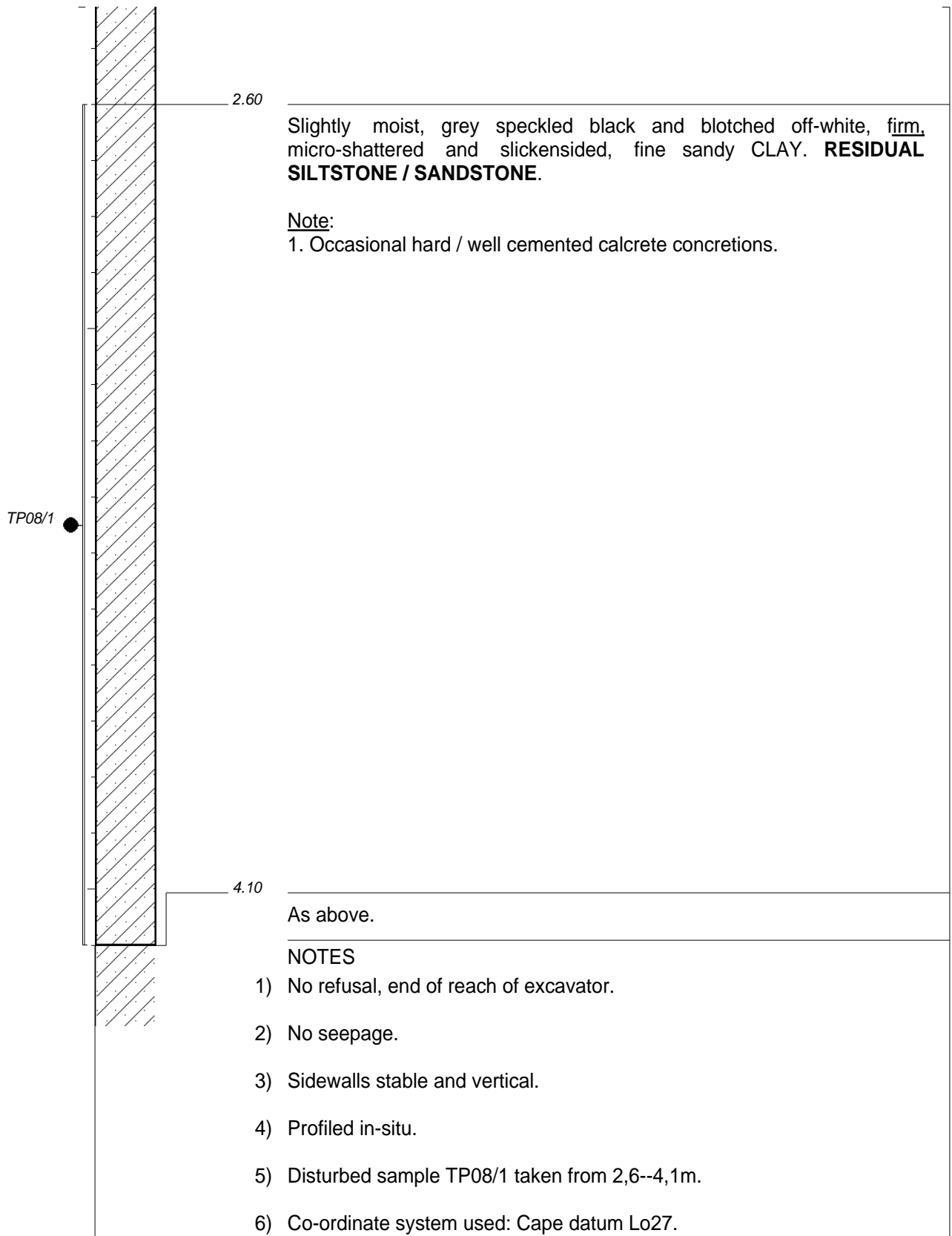
1. Horizon slightly ferruginised.

1.60

Slightly moist, grey speckled black and mottled light orange-brown, stiff, shattered, sandy CLAY. **REWORKED RESIDUAL SANDSTONE.**

Note:

1. Evidence of hillwash present within the shattered vertical planes.



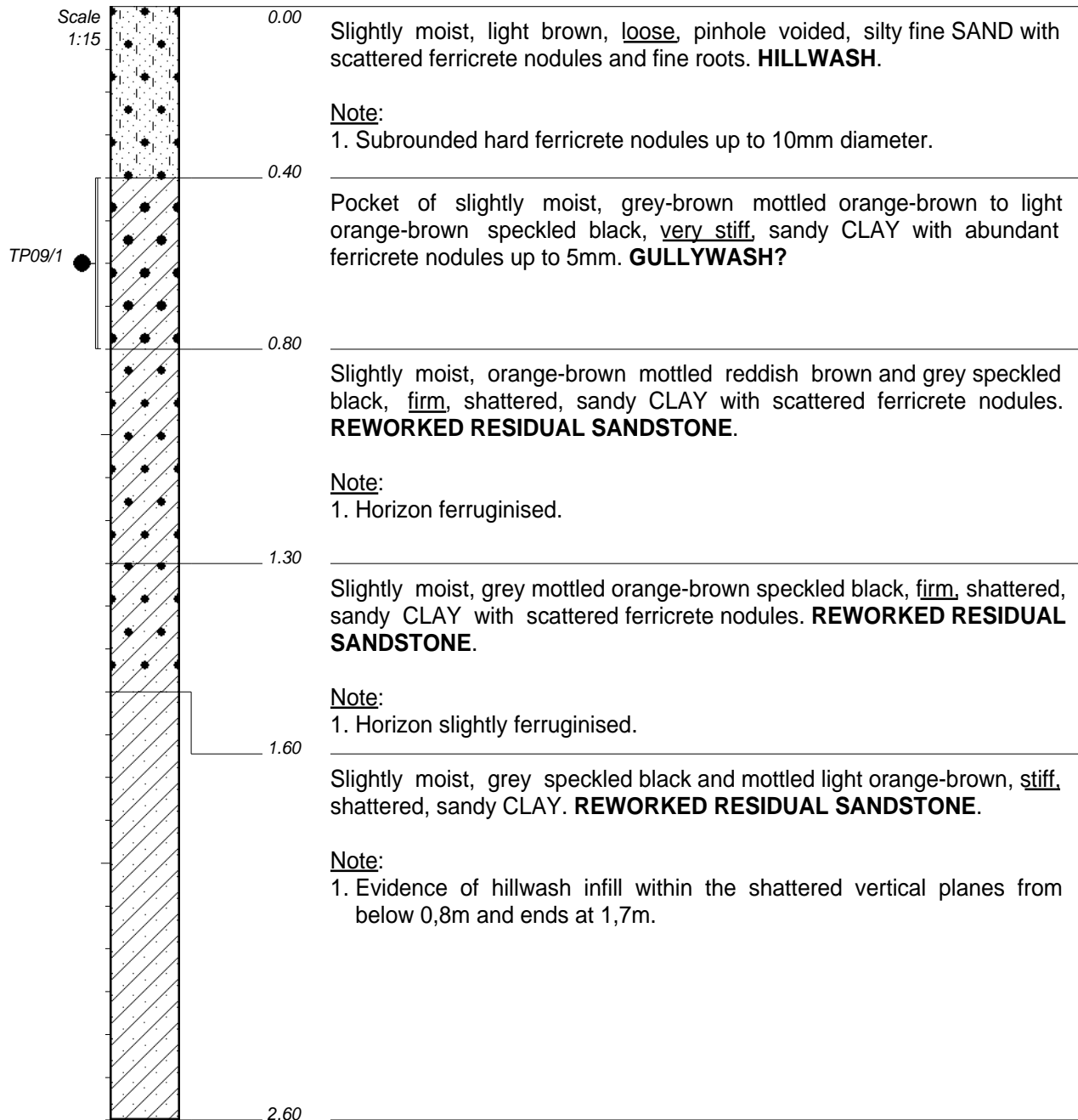
CONTRACTOR : CJ Terblanche Beleggings
MACHINE : Volvo 360 Excavator
DRILLED BY : Frans Matli
PROFILED BY : M Dlamini

INCLINATION : Vertical
DIAM : 1,66m tined bucket
DATE : 29 June 2017
DATE : 29 June 2017

ELEVATION :
X-COORD : 2970342
Y-COORD : -077497

TYPE SET BY : Beth
SETUP FILE : STANDARD.SET

DATE : 03/01/2018 16:40
TEXT : ..\G34100PRO\JOB20170714.DOC



NOTES

- 1) TP09a profiled on southern face.
- 2) Disturbed sample TP09/1 taken from 0,4--0,8m.

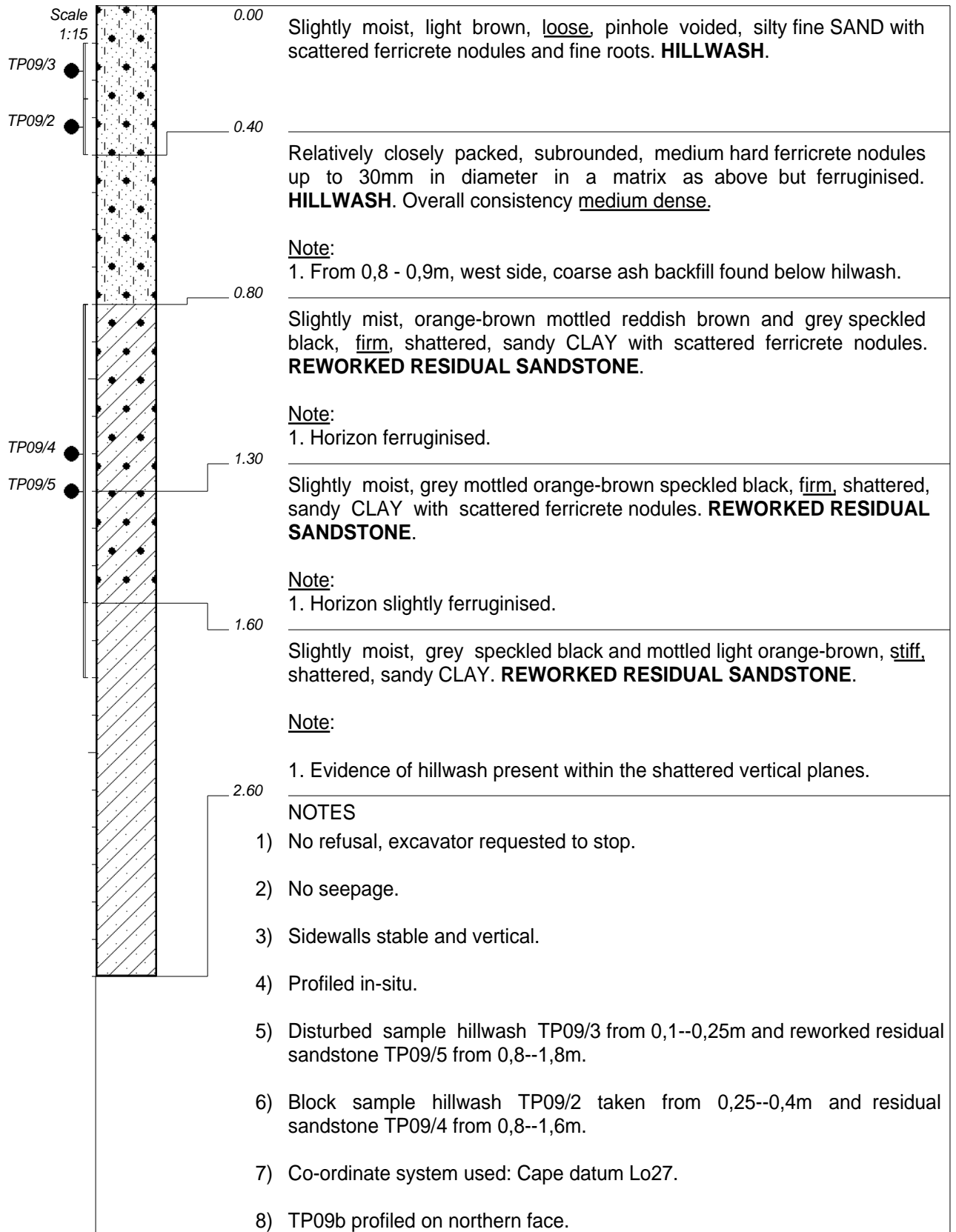
CONTRACTOR : CJ Terblanche Beleggings
MACHINE : Volvo 360 Excavator
DRILLED BY : Frans Matli
PROFILED BY : M Dlamini

TYPE SET BY : Beth
SETUP FILE : STANDARD.SET

INCLINATION : Vertical
DIAM : 1,66m tined bucket
DATE : 29 June 2017
DATE : 29 June 2017

DATE : 03/01/2018 16:40
TEXT : ..\G34100PRO\JOB20170714.DOC

ELEVATION :
X-COORD : 2970320
Y-COORD : -077515



CONTRACTOR : CJ Terblanche Beleggings
MACHINE : Volvo 360 Excavator
DRILLED BY : Frans Matli
PROFILED BY : M Dlamini

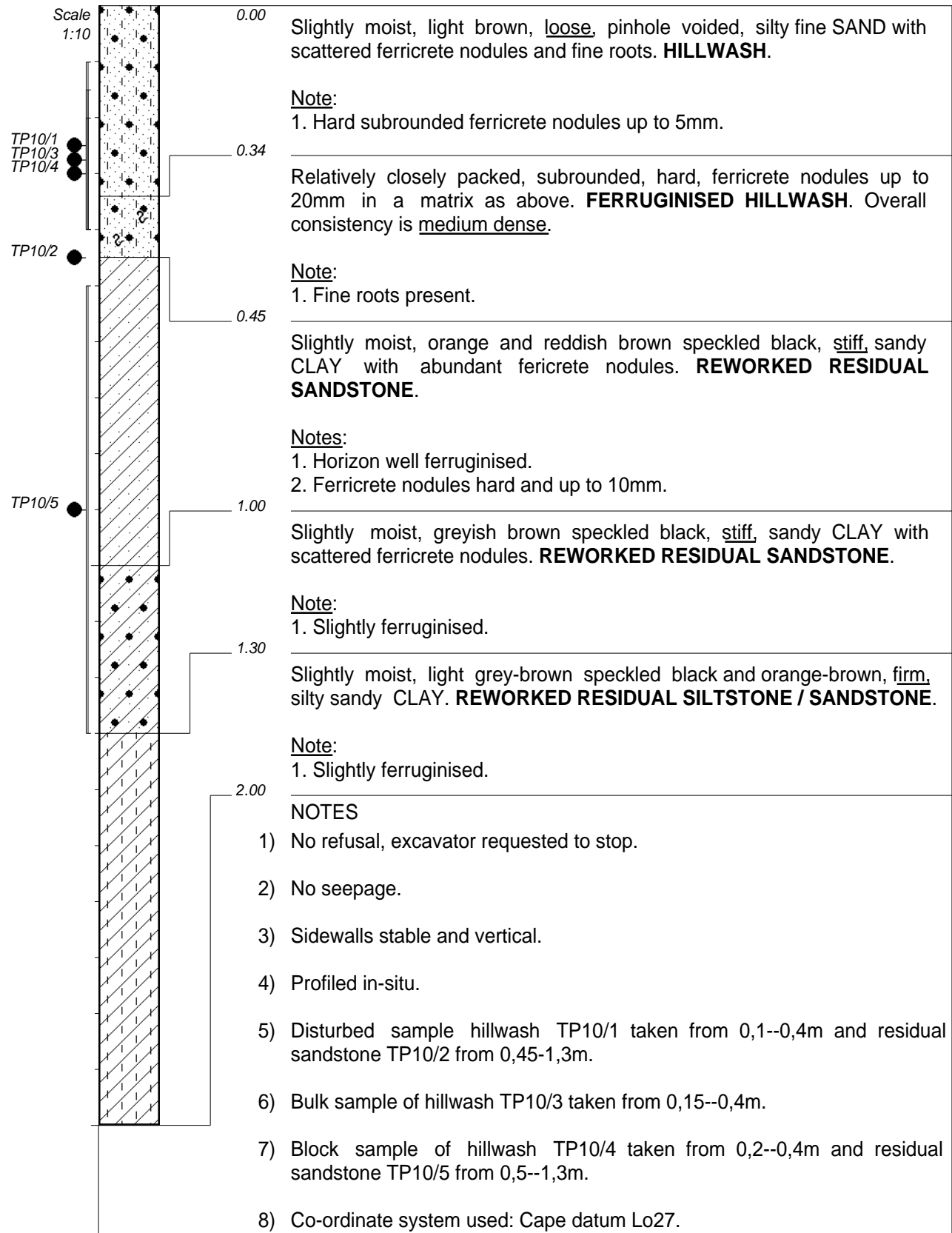
INCLINATION : Vertical
DIAM : 1,66m tined bucket
DATE : 29 June 2017
DATE : 29 June 2017

ELEVATION :
X-COORD : 2970320
Y-COORD : -077515

TYPE SET BY : Beth
SETUP FILE : STANDARD.SET

DATE : 03/01/2018 16:40
TEXT : ..\G34100PRO\JOB20170714.DOC

HOLE No: TP09b
North face



CONTRACTOR : CJ Terblanche Beleggings
MACHINE : Volvo 360 Excavator
DRILLED BY : Frans Matli
PROFILED BY : M Dlamini

INCLINATION : Vertical
DIAM : 1,66m tined bucket
DATE : 29 June 2017
DATE : 29 June 2017

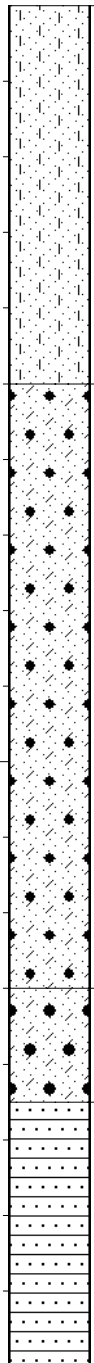
ELEVATION :
X-COORD : 2970381
Y-COORD : -077518

TYPE SET BY : Beth
SETUP FILE : STANDARD.SET

DATE : 03/01/2018 16:40
TEXT : ..\G34100PRO\JOB20170714.DOC



Scale
1:10



0.00

Slightly moist, light orange-brown, loose, occasionally pinhole voided, slightly silty fine SAND with scattered roots. **HILLWASH.**

0.50

Slightly moist, orange-brown speckled reddish brown, firm, slightly clayey fine SAND with scattered ferricrete nodules up to 8mm in diameter and scattered roots. **REWORKED RESIDUAL SANDSTONE.**

Notes:

- 1. Ferricrete nodules break easily with soft blow of pick.
- 2. Zone from 1,0m to 1,2m more ferruginised than above.

1.30

Relatively closely packed, black, very soft ferricrete nodules up to 30mm diameter in a matrix as above. Overall consistency medium dense. **FERRUGINISED REWORKED RESIDUAL SANDSTONE.**

1.45

Light yellow-brown streaked orange-brown and black, completely weathered, medium grained, soft rock. **SANDSTONE.**

1.80

NOTES

- 1) Excavator refused on sandstone.
- 2) No seepage.
- 3) Sidewalls stable and vertical.
- 4) Profiled in-situ.
- 5) No samples taken.
- 6) Co-ordinate system used: Cape datum Lo27.
- 7) Profiled to the west of the fractured sandstone zone.

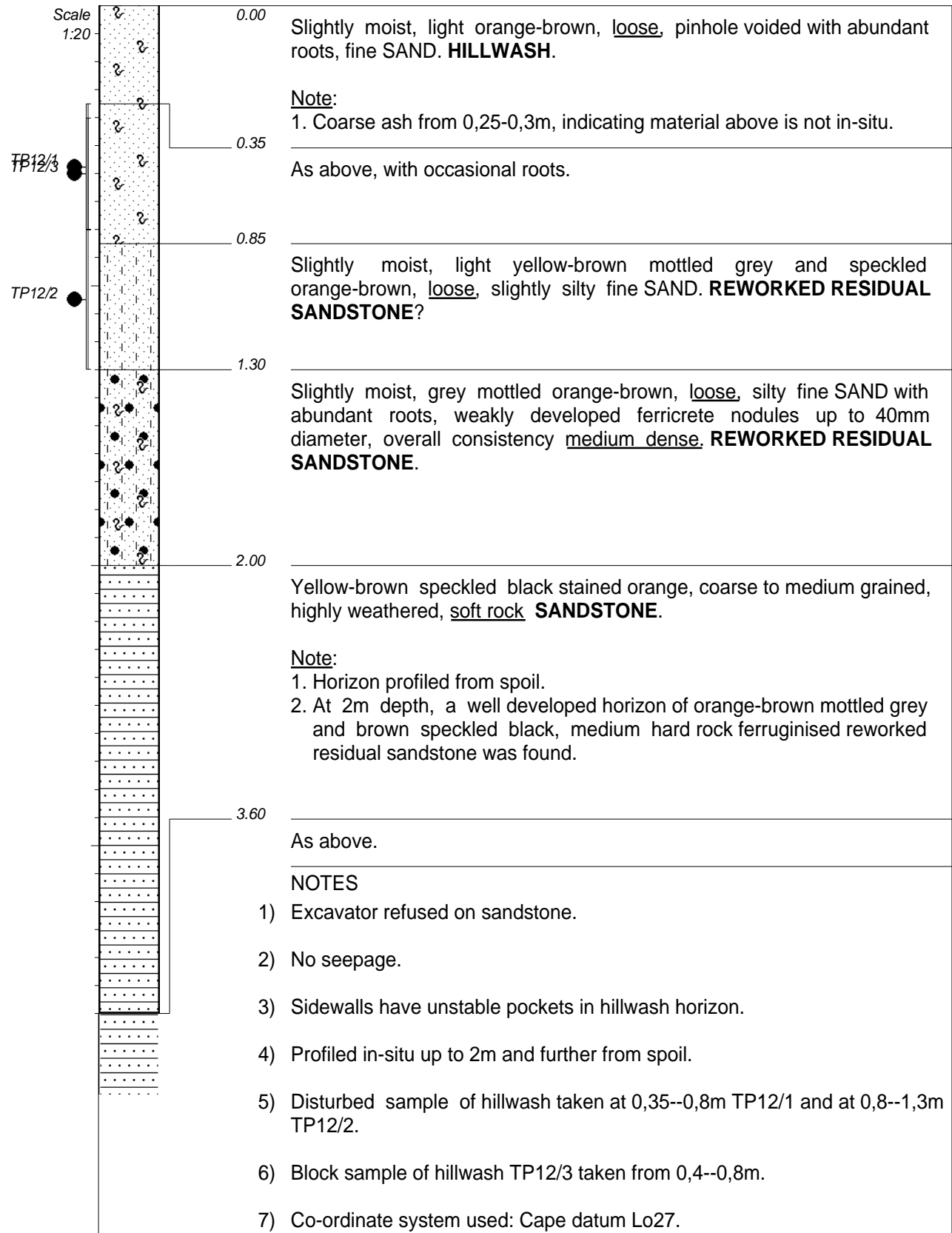
CONTRACTOR : CJ Terblanche Beleggings
MACHINE : Volvo 360 Excavator
DRILLED BY : Frans Matli
PROFILED BY : J Breyl

INCLINATION : Vertical
DIAM : 1,66m tined bucket
DATE : 30 June 2017
DATE : 30 June 2017

ELEVATION :
X-COORD : 2971615
Y-COORD : -077998

TYPE SET BY : Beth
SETUP FILE : STANDARD.SET

DATE : 03/01/2018 16:40
TEXT : ..\G34100PRO\JOB20170714.DOC



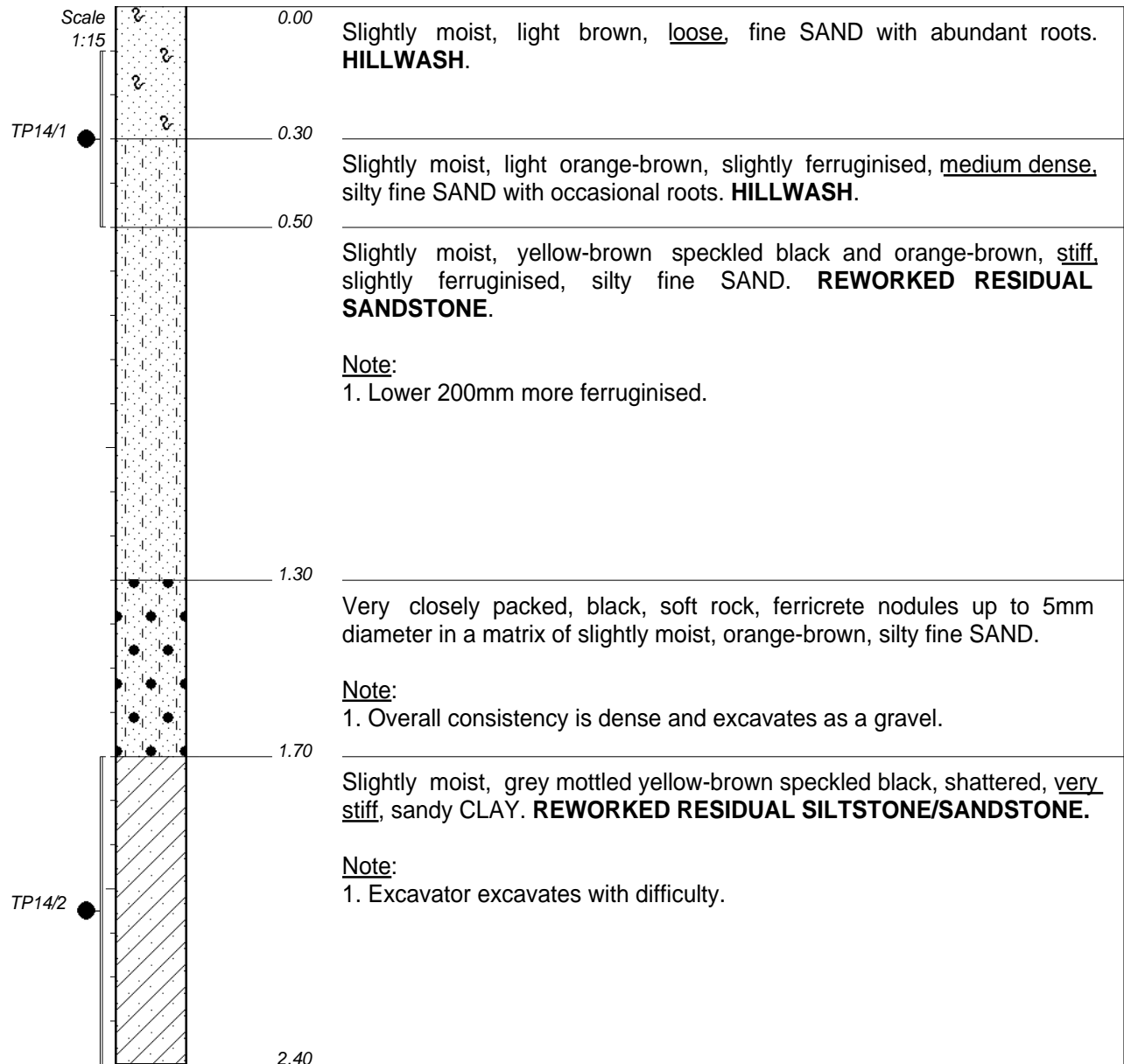
CONTRACTOR : CJ Terblanche Beleggings
MACHINE : Volvo 360 Excavator
DRILLED BY : Frans Matli
PROFILED BY : J Breyl

INCLINATION : Vertical
DIAM : 1,66m tined bucket
DATE : 30 June 2017
DATE : 30 June 2017

ELEVATION :
X-COORD : 2971654
Y-COORD : -078012

TYPE SET BY : Beth
SETUP FILE : STANDARD.SET

DATE : 03/01/2018 16:40
TEXT : ..\G34100PRO\JOB20170714.DOC



NOTES

- 1) Excavator requested to stop, excavated with difficulty.
- 2) No seepage.
- 3) Sidewalls stable and vertical.
- 4) Profiled in-situ.
- 5) Disturbed sample of hillwash taken at 0,1--0,5m TP14/1 and of reworked residual siltstone/sandstone at 1,7--2,4m TP14/2.
- 6) Co-ordinate system used: Cape datum Lo27.

CONTRACTOR : CJ Terblanche Beleggings
MACHINE : Volvo 360 Excavator
DRILLED BY : Frans Matli
PROFILED BY : J Breyl

INCLINATION : Vertical
DIAM : 1,66m tined bucket
DATE : 30 June 2017
DATE : 30 June 2017

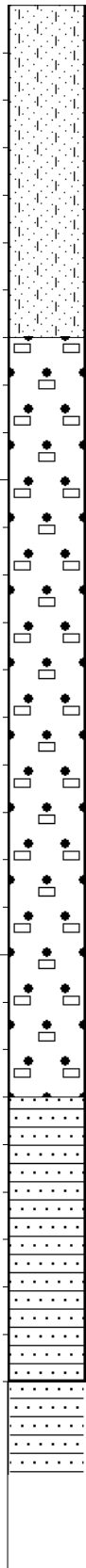
ELEVATION :
X-COORD : 2971644
Y-COORD : -077870

TYPE SET BY : Beth
SETUP FILE : STANDARD.SET

DATE : 03/01/2018 16:40
TEXT : ..\G34100PRO\JB20170714.DOC



Scale
1:15



0.00

Slightly moist, light brown, loose becoming medium dense with depth, pinhole voided, slightly silty fine SAND with occasional roots. **HILLWASH.**

0.70

Slightly moist, orange-brown blotched reddish brown and olive-brown speckled black, with scattered, very soft, black and red-brown ferricrete nodules up to 10mm in diameter and calcrete nodules, firm, **REWORKED RESIDUAL SANDSTONE.**

Note:

1. Horizon slightly ferruginised.

2.30

Off-white stained black streaked orange-brown, medium weathered, medium grained, medium hard rock **SANDSTONE.**

2.90

As above.

NOTES

- 1) Excavator refusal.
- 2) No seepage.
- 3) Sidewalls stable and vertical.
- 4) Profiled in-situ.
- 5) No samples taken.
- 6) Co-ordinate system used: Cape datum Lo27.

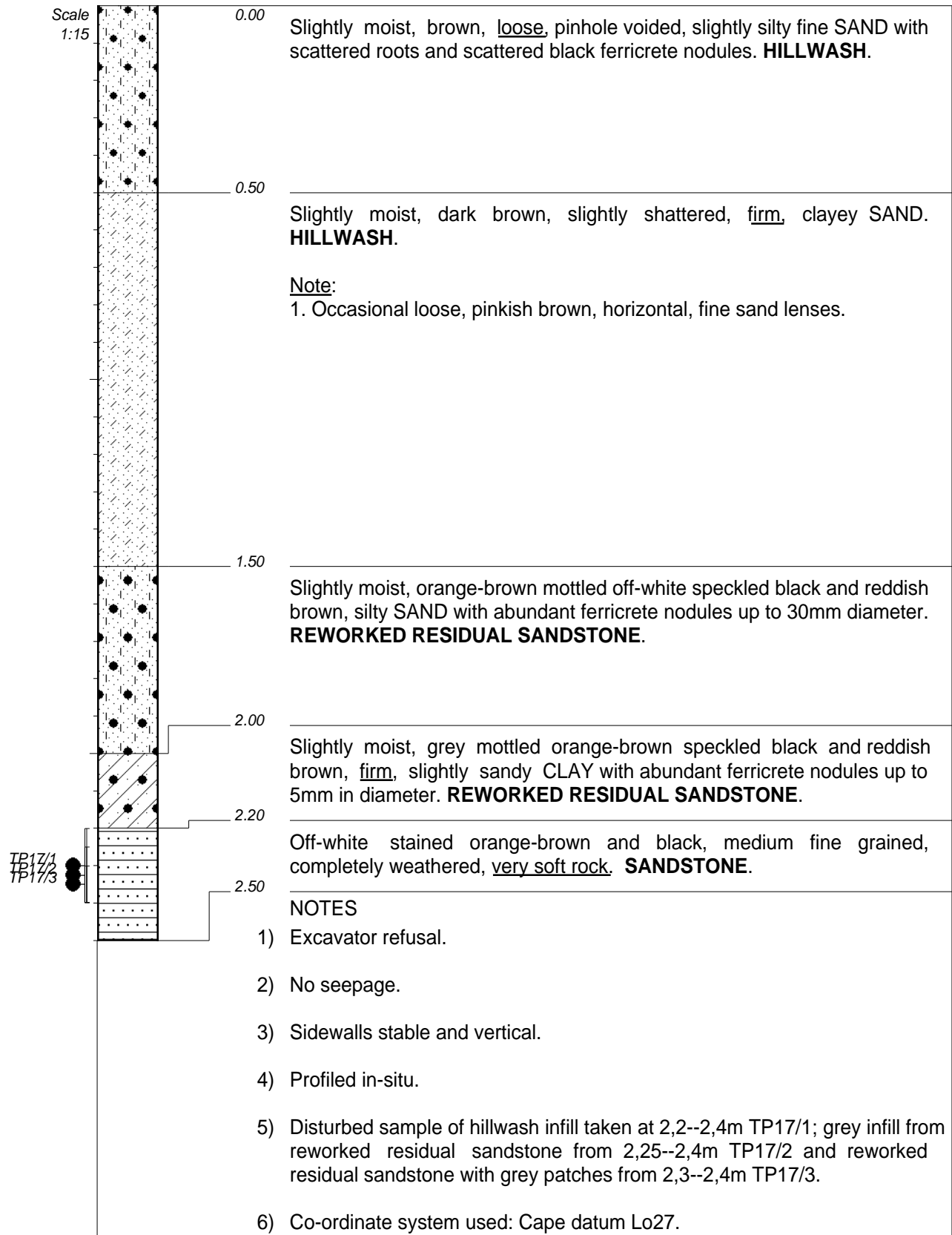
CONTRACTOR : CJ Terblanche Beleggings
 MACHINE : Volvo 360 Excavator
 DRILLED BY : Frans Matli
 PROFILED BY : J Breyl

INCLINATION : Vertical
 DIAM : 1,66m tined bucket
 DATE : 1 July 2017
 DATE : 1 July 2017

ELEVATION :
 X-COORD : 2971660
 Y-COORD : -077845

TYPE SET BY : Beth
 SETUP FILE : STANDARD.SET

DATE : 03/01/2018 16:40
 TEXT : ..\G34100PRO\JOB20170714.DOC



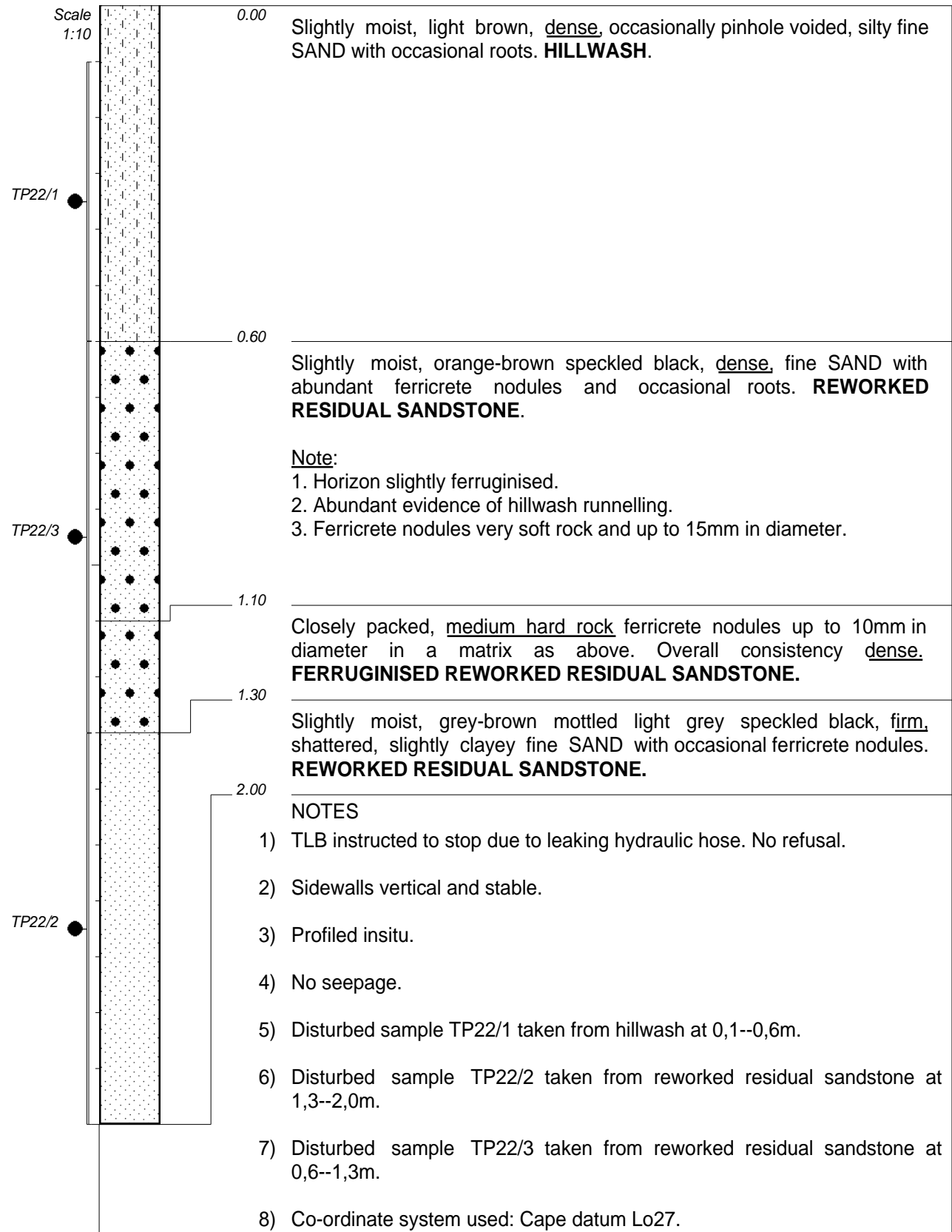
CONTRACTOR : CJ Terblanche Beleggings
MACHINE : Volvo 360 Excavator
DRILLED BY : Frans Matli
PROFILED BY : J Breyl

INCLINATION : Vertical
DIAM : 1,66m tined bucket
DATE : 1 July 2017
DATE : 1 July 2017

ELEVATION :
X-COORD : 2970625
Y-COORD : -077322

TYPE SET BY : Beth
SETUP FILE : STANDARD.SET

DATE : 03/01/2018 16:40
TEXT : ..\G34100PRO\JOB20170714.DOC



CONTRACTOR : CJ Terblanche Beleggings
MACHINE : Case TLB
DRILLED BY : Frans Matli
PROFILED BY : J. Breyl
TYPE SET BY : Beth
SETUP FILE : STANDARD.SET

INCLINATION :
DIAM : 600mm tined bucket
DATE : 1 July 2017
DATE : 8 August 2017
DATE : 03/01/2018 16:40
TEXT : ..\G34100PRO\JB20170714.DOC

ELEVATION :
X-COORD : 2972538
Y-COORD : -077991

A.2b) TEST PIT PHOTOGRAPHS

TP01 – TP03



Looking east at TP01, with sinkholes at TP02 and TP03 in the background.

TP04 and TP05



Looking east across TP04 and TP05, showing the excavated crack in the rock, infilled V-shape and small sinkhole on surface in the foreground.

TP06



Start of the excavation at TP06, showing the sinkhole on surface and the intersected subterranean tunnel below.

TP06



Looking down into crack in the rock at TP06. Note the staining on the rock surface.

TP11



Vertical displacement across fracture zone at edge of subsided area exposed in TP11.

TP14



Clockwise from top left: Infilled V-shape at TP14, excavated V-shape and apparent “leached zone” at bottom of V-shape which is the presumed collapsed subterranean tunnel.

TP18



Loose material of collapsed sub-terranean tunnel excavated at bottom of TP18 above infilled crack in rock.

A.2c)

TEST PIT OBSERVATION SUMMARY

TEST PIT SUMMARY

Rev 01

Test pit	Rock depth	Sinkholes?	Crack infill in residuum	Infill link	V-shape	Crack infill in rock	Ferruginisation	Shattering	Roots	Comments
TP01	3m	Excavated west of DSC109A	<ul style="list-style-type: none"> Only exposed on east, where sinkhole is present 30mm to 50mm thick 	Yes	No	Crack 50mm wide and infilled with hillwash and 20mm FC nodules	<ul style="list-style-type: none"> 0-0.4m: Abundant FC nodules 0.4-1.1m: Abundant FC nodules, well ferruginised 1.1-1.6m: Abundant FC nod 1.6-3.0m: Slightly ferruginised 	<ul style="list-style-type: none"> 0.4-1.1m: Shattered, granular textured 1.1-1.6m: Shattered 1.6-3.0m: Slightly ferruginised 	Abundant in HW	<ul style="list-style-type: none"> Crack filled with HW. Further sinkholes unlikely
TP02	3m	Through DSC109A	<ul style="list-style-type: none"> V-shaped infill below sinkhole. 	Not clear, possible	Yes	<ul style="list-style-type: none"> Variable: Clayey in west Sandy / Gravel in east 70mm quartz cobble 	Similar to TP01	Similar to TP01	Similar to TP01	<ul style="list-style-type: none"> Crack filled with HW. Further sinkholes unlikely
TP03	3m	Through west of DSC109	<ul style="list-style-type: none"> V-shaped infill below sinkhole 	No	Yes	<ul style="list-style-type: none"> More clayey in west, not below sinkhole. More sandy in east. Large cobbles 	<ul style="list-style-type: none"> 0-0.4m: Scattered FC nodules 0.4-0.6m: Slightly ferruginised 0.6-3.0m: Scattered FC nod 	<ul style="list-style-type: none"> 0.4-0.6m: Shattered 0.6-3.0m: Scattered, but becoming stiff below 1,9m 	Fine roots in HW	<ul style="list-style-type: none"> Maybe clayey infill caused crack to seal? Green lichen / moss on sinkhole floor. Link to crack in bottom may have been excavated??
TP04	3m	Between sinkholes	<ul style="list-style-type: none"> Coarse ash backfilling on both sides to 2.3m. HW infill as well 	Yes, only on west	Some in west with ash backfilling	<ul style="list-style-type: none"> West: capped with sandstone rock, empty below. East: filled with ash, hillwash and sandstone. 	<ul style="list-style-type: none"> 0-0.5m: Occasional FC nod 0.5-1.2m: Very well ferruginised with abundant FC nodules 1.2-3.0m: Very slightly ferruginised, well ferruginised 2.6-2.8m 	Not noted. To be checked during second test pit excavation.	Scattered in HW	<ul style="list-style-type: none"> East: soil below HW appears looser than on sides. Tunnels in hillwash
TP05	3m	Through DSC128	<ul style="list-style-type: none"> Crack infilled with hillwash and coarse ash. 	Yes, on east	Yes, only on east	<ul style="list-style-type: none"> West: infilled with clayey res sandstone East: infilled with ash 	<ul style="list-style-type: none"> Next to TP04, similar 	As TP04	As TP04	<ul style="list-style-type: none"> Tunnels in hillwash
TP06	3m	Through DSC134	<ul style="list-style-type: none"> Hillwash infilled crack 	No	Empty V-shaped cavity from surface	<ul style="list-style-type: none"> Capped with sandstone rock, empty below. Crack sides stained with hillwash. 	Not profiled	Not profiled	Not profiled	<ul style="list-style-type: none"> Empty V-shaped cavity below sinkhole, possibly of similar origin as other filled V-shapes observed. Material transported past sandstone capping in crack.

Test pit	Rock depth	Sinkholes?	Crack infill in residuum	Infill link	V-shape	Crack infill in rock	Ferruginisation	Shattering	Roots	Comments
TP07	3.6m	No	<ul style="list-style-type: none"> Hillwash infilled crack on east to 2.6. Looser material below above crack in rock 	No	No	<ul style="list-style-type: none"> Capped with sandstone rock, empty below. No hillwash infill in crack. No staining recorded. 	Not profiled	Not profiled	Not profiled	<ul style="list-style-type: none"> Due to no hillwash in crack, further penetration of hillwash into crack unlikely and therefore sinkhole development is unlikely.
TP08	>4,1m	No	<ul style="list-style-type: none"> No 	N/A	N/A	<ul style="list-style-type: none"> N/A 	<ul style="list-style-type: none"> 0-0.4m: Scattered FC nod 0.4-0.8m: Relatively closely packed FC nod 0.8-1.3m: Scattered FC nod 1.3-1.6m: Scattered FC nod 	<ul style="list-style-type: none"> 1.3-1.6m: Shattered 1.6-2.6m: Shattered 2.6-4.1m: Microshattered and slickensided 	0-0.4m: Fine roots	<ul style="list-style-type: none"> No evidence of hillwash infilled crack in residuum. No rock found.
TP09a (South)	>2.6m	No	<ul style="list-style-type: none"> Only minor crack noticed on surface which penetrated 300mm into hillwash. Not due to subsidence. Hillwash infill in vertical planes. Not due to subsidence. No further hillwash infill. 	N/A	N/A	<ul style="list-style-type: none"> N/A 	<ul style="list-style-type: none"> 0-0.4m: Scattered FC nod 0.4-0.8m: Abundant FC nod 0.8-1.3m: Scattered FC nod 1.3-1.6m: Scattered FC nod 	<ul style="list-style-type: none"> 0.8-1.3m: Shattered 1.3-1.6m: Shattered 1.6-2.6m: Shattered 	0-0.4m: Fine roots	<ul style="list-style-type: none"> Profile a shattered pocket on south face, not representative. Calcretised dome present below shattered pocket.
TP09b (North)	>2.6m	No	<ul style="list-style-type: none"> Hillwash infill in vertical planes. Not due to subsidence. No further hillwash infill. 	N/A	N/A	<ul style="list-style-type: none"> N/A 	<ul style="list-style-type: none"> 0-0.4m: Scattered FC nod 0.4-0.8m: Relatively closely packed FC nod 0.8-1.3m: Scattered FC nod 1.3-1.6m: Scattered FC nod 	<ul style="list-style-type: none"> 0.8-1.3m: Shattered 1.3-1.6m: Shattered 1.6-2.6m: Shattered 	0-0.45m: Fine roots	<ul style="list-style-type: none">
TP10	>2.0m	No	<ul style="list-style-type: none"> Yes. Crack infilled with hillwash 	No.	Yes	Rock not exposed, too deep.	<ul style="list-style-type: none"> 0-0.34m: Scattered FC nod 0.34-0.45m: Relatively closely packed FC nod 0.45-1.0m: Abundant FC nodules, well ferruginised. 1.0-1.3m: Scattered FC nod, slightly ferruginised 1.3-2.0m: Slightly ferruginised. 	<ul style="list-style-type: none"> No 	0-0.4m: Fine roots	<ul style="list-style-type: none"> Termite nest in infilled hillwash on west. V-shape only to 1.2m

Test pit	Rock depth	Sinkholes?	Crack infill in residuum	Infill link	V-shape	Crack infill in rock	Ferruginisation	Shattering	Roots	Comments
TP11	0.8m to 1.8m Varies due to step	Yes, historically	<ul style="list-style-type: none"> Not noticed. Fracture zone 	N/A	N/A	<ul style="list-style-type: none"> Hillwash infill in fractured zone 	<ul style="list-style-type: none"> 0.5-1.3m: Scattered FC nod 1.3-1.45m: Relatively closely packed FC nod 	<ul style="list-style-type: none"> Not noticed 	Scattered roots 0-1.3m	<ul style="list-style-type: none"> 1m vertical step in rock head with fracture zone
TP12	2.0m	Yes, historically	<ul style="list-style-type: none"> Yes, below coarse ash 	No link to rock seen	Yes	No crack in rock observed	<ul style="list-style-type: none"> 1.3-2.0m: Slightly ferruginised 	<ul style="list-style-type: none"> No 	Abundant roots to 2m	<ul style="list-style-type: none"> Roots go deeper than in previous testpits.
TP13	Not found	Yes, historically	<ul style="list-style-type: none"> No 	No	No	<ul style="list-style-type: none"> No 	<ul style="list-style-type: none"> Yes 	<ul style="list-style-type: none"> No 	Not profiled in detail	<ul style="list-style-type: none"> Deeper hillwash pocket, with no infill below. Trench probably missed crack position
TP14	>2.4m	Yes, historically	<ul style="list-style-type: none"> Yes 	No, crack stops in residual siltstone	Yes	<ul style="list-style-type: none"> No rock found 	<ul style="list-style-type: none"> 0.3-0.5m: Occasional FC nod, slightly ferruginised 0.5-1.3m: Slightly ferruginised, lower 200mm more ferruginised 1.3-1.7m: Very closely packed FC nod 	<ul style="list-style-type: none"> Residual siltstone at bottom of infilled crack in reworked residual sandstone 	Abundant roots in hillwash infill	<ul style="list-style-type: none"> No
TP15	2.3m	Yes, at position of existing backfilled sinkhole. New sinkhole to the south	<ul style="list-style-type: none"> Yes 	Yes	Yes	<ul style="list-style-type: none"> Yes, crack infilled with hillwash, reworked residual sandstone, and soft rock sandstone. Crack not singularly defined but within fractured zone. 	<ul style="list-style-type: none"> 0.7-2.3m: Scattered FC nod, Slightly ferruginised 	<ul style="list-style-type: none"> Not noticed 	Occasional roots in hillwash	<ul style="list-style-type: none"> V-shapes very well developed
TP17	2.2m	Yes, DSC106	<ul style="list-style-type: none"> Noted in upper horizon, but not found when excavation deepened. 	No	No	<ul style="list-style-type: none"> No crack found in rock 	<ul style="list-style-type: none"> 0-0.5m: Scattered FC nod 1.5-2.2m: Abundant FC nod. 	<ul style="list-style-type: none"> 0.7- 1.5m: Slightly shattered 	0-0.5m: Scattered	<ul style="list-style-type: none"> Testpit could have missed crack entirely. May have found crack if excavation was re-oriented by 90°.

Test pit	Rock depth	Sinkholes?	Crack infill in residuum	Infill link	V-shape	Crack infill in rock	Ferruginisation	Shattering	Roots	Comments
TP18	2.9m	No, east of TP03	<ul style="list-style-type: none"> Many small infilled cracks up to 5mm thick. Two prominent infilled cracks up to 15mm wide. 	Yes	No	Yes	<ul style="list-style-type: none"> Not profiled, appeared similar to TP03 	<ul style="list-style-type: none"> Yes, similar to TP03 	Abundant in HW	<ul style="list-style-type: none"> Open tunnel found at bottom sloping downwards towards TP03
TP19	>3.6m	No	<ul style="list-style-type: none"> No. 	No	No	Rock not found	<ul style="list-style-type: none"> Not profiled, appeared similar to TP10 	See TP10	See TP10	<ul style="list-style-type: none"> Profile from 2m to 3.6m less firm than above.
TP20	3m	West of DSC130, very close to TP04.	<ul style="list-style-type: none"> Yes 	Yes	Yes	Yes	<ul style="list-style-type: none"> Not profiled, similar to TP04 and TP05 	<ul style="list-style-type: none"> See TP04 and TP05 	See TP04 and TP05	<ul style="list-style-type: none"> Ash backfill in V-shape on east.
TP21	N/A	Yes, visible depression from old sinkhole	N/A	N/A	N/A	N/A	N/A	N/A	N/A	<ul style="list-style-type: none"> Excavation aborted after animal skeleton found
TP22	>2m	Near old sinkholes	<ul style="list-style-type: none"> Not found 	N/A	N/A	Rock not found	<ul style="list-style-type: none"> 0.6-1.1m: Abundant soft nodules 1.1-1.3: Closely packed nodules. 1.3-2.0m: Occasional nodules. 	<ul style="list-style-type: none"> Yes, 1.3-2.0m 	Occasional	<ul style="list-style-type: none"> Significant hillwash runnelling. Purpose to evaluate soil properties where large historical sinkholes formed.

A.2d) ADDITIONAL NOTES TAKEN DURING TEST PIT EXCAVATION

(These notes are supplementary to the test pit profiles)

TP01

Supplementary notes:

- Hillwash infill noted in the sidewall below hillwash horizon. Infill 30mm to 50mm thick
- Rock at bottom was exposed and a 50mm wide crack found in the sandstone infilled with hillwash.
- Hillwash infill in crack was very moist, light brown, loose (can push finger in), soft, clayey silty sand.
- Ferricrete nodules up to 20mm found in hillwash in crack.
- 750mm long peg was pushed vertically into the infilled crack.

TP02

Sinkhole DSC109A

New sinkhole noticed to the west of DSC109, called DSC109A.

See dimensions in site notes.

TP02 excavated through DSC109A

Supplementary notes:

- Crack in rock at bottom 50mm wide
- On eastern side, bottom of sinkhole is visible on side @ 0,7m with large pockets of hillwash infill below. Different to TP01.
- Pockets of hillwash more moist than above (see photos). Filled tunnel?
- Crack infill very moist
- Infill in crack is more clayey than in TP01.
- Infill in west, different from east. In east, infill more granular with depth.
- See samples of infill taken.
- Large quartz cobble found in crack at depth in west, 70mm in diameter.

TP03

Supplementary notes:

- Excavated through throat of sinkhole DSC109
- See dimensions and sketch of sinkhole and areas around hillwash infill in site notes.
- Hillwash infill in centre to depth of 2,4m. Shattered, reworked, residual sandstone on sides of hillwash with looser reworked residual sandstone below.
- No clear link between the hillwash pocket and the crack in the bottom.
- No evidence of hillwash infill in the west of the testpit (where there was no sinkhole, except for DCS109A).
- No clear link between hillwash pocket and crack in rock in bottom.
- Crack in rock 60mm in east and 70mm in west.
- West infill is more clayey, not below sinkhole
- East infill is more sandy – see sample

- Large rounded and sub-rounded cobbles found in crack, not sandstone, either quartzite or dolerite?
- Green moss or lichen growth on bottom of sinkhole floor evidence of water ponding in the past (see photo)

Sinkhole DSC131/DSC132 - Collapsed sinkholes with ash backfill visible as excavated by animals.

DSC132 – 1m in diameter and 0,5m deep with surrounding inlets.

DSC131 – 0,5m diameter and 0,25m deep.

DSC130 – collapsed, 0,6m deep at throat with tunnel going east, ash backfill removed by animals.

DSC129 – collapsed, 1m deep, see cross section in site notes, vertical sides with tunnel going east

DSC128 – tunnel going west and east linked to two more holes to the east, cracks in sides of sinkholes.

See site notes for cross sections and positions of test pits TP04 and TP05.

.....

TP04

Supplementary notes:

- Excavated between DSC130 (west) and DSC129 (east)
- On the western side, found ash backfilled hole with new sinkhole on side and a backfilled / open crack below new sinkhole. Exposed hole linked to tunnel at bottom of DSC130. At bottom of test pit (2m deep), very wide crack infilled with ash and hillwash. Crack width 270mm in west and 360mm to 650mm in east. (Excavation then deepened to 3m).
- On the eastern side, crack / tunnel exposed with infill, soil below hillwash in east appears looser than to the sides of the hillwash as noted in TP03 on 27/06.
- Evidence of coarse ash backfilling on both sides down to 2,3m (west and east).
- Backfilled area is ± 600mm x 400mm.
- Open crack in sandstone rock at bottom of testpit in sandstone rock below 3m.
- Open crack in west, width 40mm, cracks extend forward to the west (bends southwards). Crack in west was choked by sandstone with evidence of clayey fine sand infill present on top.
- Evidence of backfill material (sandstone, ash and hillwash) on eastern side.
- No clear link between ash backfill / hillwash and crack in east. (TP04 between sinkholes).

.....

TP05

Excavated immediately to the east of TP04, through DC128, with same crack exposed in bottom.

Supplementary notes:

- Crack in western end overlaps crack in TP04 (crack at bottom).
- West infilled with clayey residual sandstone and east infilled with ash. See sketch in site notes.
- Crack width 50mm

- Ash backfill in sidewalls above crack widens going upwards, to wider width seen at higher level in TP04.

DSC134

See site notes for sinkhole sketch. Opening on surface 0,5m x 0,6m.

Open crack visible through residual material to a depth of 3m (which is up to where the end of the measuring tape crack could be seen.)

Furrows to north and south of sinkhole

New sinkhole had formed to the west of the DSC134.

TP06

Excavated immediately to the west of DSC134 to depth of 1,5m and exposed sinkhole in side of testpit. See photos

Then moved test pit 0,8m east to excavate through sinkhole.

Supplementary notes:

- Crack exposed at bottom of testpit at 3m
- Top of crack filled with soft rock sandstone, but empty below sandstone.
- Sides of crack below rock stained with hillwash, indicating material transported from above.
- Dropped pebbles into crack and measured time until no sound heard anymore. Pebbles could be heard rebounding from the sides while falling. Time duration for 7 drops:
 - 1. 3,15s, and 2,2s
 - 2. Nothing heard
 - 3. 4s
 - 4. Wrong measurement
 - 5. 4,19s
 - 6. 4,2s
 - 7. 4,3s
- Crack filled with hillwash and residual sandstone.
- Air in crack feels warm on hand when pushed in.
- Crack is undulating and dips to the north.
- Horizontal delamination (delaminated piece is vertical) in western of crack – See photos. Further evidence of delamination also present. Stress relief? Cracks can widen?

TP07

Excavated in line of crack with TP06, but in virgin soil with no sinkhole. Interested to see what crack looks like where there is no sinkhole above.

Supplementary notes:

- Rock encountered at 3,6m with crack in rock found.

- Crack filled with soft rock sandstone which could be easily removed and empty below.
- Crack 50mm wide with soft rock infill to 110mm deep. See sketch in notes.
- No hillwash found in crack
- Hillwash on east face of testpit clearly visible to 2,6m as a moist, light brown, loose, fine grained slightly silty sand.
- From 2,6 – 3,6m, a moist, olive grey, very stiff, silty sandy clay was found.
- No hillwash link to the crack below
- Zone on eastern side above crack is moist and stiff as opposed to very stiff on sides.
- Some delamination in sandstone on sides of crack, as at TP06.
- Termite nest in crack on western end going downwards – see photo
- Crack is curved to the north, meaning the eastern and western end are further north than the centre. Would have expected crack to be curved to the south based on longwall mining plans?

.....

TRENCH 33A – 33B (AT TP08)

Excavated above double long wall area on Donkerhoek.

No recorded sinkholes, but settlement cracks recorded following mining.

Excavate trench 20m long to 1,5m depth and look for infilled cracks in sidewalls.

No clear signs of crack infilled with hillwash found. Some scattered small cracks infilled with hillwash were found.

Portions of trench has hillwash to 0,6m, with the lower 0,3m ferruginised to a nodular ferricrete (almost honeycomb).

Towards the south of the trench, on the western side, ash backfill was noticed accompanied by a loose, more moist area on the east of the trench. TP08 was excavated at this location.

.....

TRENCH 32A1 – 32B1 (AT TP09)

Found crack in soil north west of original point 32A – see photos. Moved trench further west to excavate below crack noted on surface.

Excavated to 2,6m, profile similar to TP08.

Supplementary notes:

- Crack observed on surface only visible in upper 300mm of hillwash on south. Crack may be caused by sandy clay layer?
- Difference between north and south face of trench
- No clear evidence of crack filled with hillwash, only infill into vertical planes.
- Hillwash infill in planes contain ferricrete nodules up to 5mm in diameter
- A cone shaped calcretised horizon was noted below the shattered pockets. See sketch in site notes and photos.
- No evidence infilled crack in remained of trench. Plotting of points afterwards shows trench may be too far west to intersect crack.

Trench 30A1 – 30B1

Excavated near position of proposed trench 30A – 30B.

Excavated 1,8 to 2m deep

Profiled TP10 within trench

Supplementary notes:

- Crack infilled with hillwash found in trench at position of TP10. The crack ran diagonally across the trench and was noticed on both sides.
- Crack decreases in thickness towards bottom, ranging from 150mm at the top to 50mm at the bottom on eastern side. See sketch in site notes.
- Cracks disappeared at depth of 1,2m.
- Hillwash on top appears looser than in TP01. Significant amounts of hillwash was blown into the trench.
- Tension cracks were noted in hillwash above area where crack was exposed.
- Termites nest / tunnel noted on west. No tunnel in the feruginised hillwash as too hard. See photos.
- A second infilled crack was noted only on the eastern side. See photos

Trench 13A – 13B

TP11

Supplementary notes:

- TP11 profiled in trench 13A-13B to the west a crack found on the western end of the fractured zone exposed in the trench.
- A 1m deep vertical displacement was noted within the trench, with the west being 1m lower than the east. The fracture zone is 3,5m wide and at the top of the step, the rock is 0,8m below natural ground level. See photos
- Open cavities between the rock fragments at the crack position.
- Evidence of hillwash infill between cracked sandstone.

Trench 15A1 – 15B1

TP12

Supplementary notes:

- TP12 profiled in trench 15A1-15B1.
- Backfilled ash pockets noticed in sidewall with hillwash filled crack below. See photos
- Soil appears much looser and less clayey than in Donkerhoek TP01, thus sidewalls less stable and similar to TP10. Sinkholes lids will not span large distances. Abundant fine roots were noted to 2m depth in looser profile.
- Termite nest found. See photo.
- Lots of porcupine holes in this area, also confirming looser profile.
- See photos of excavator track marks in undisturbed topsoil.

Trench 26A1 – 26B1

TP13

Supplementary notes:

- TP13 logged in trench 26A1-26B1.
- Trench sidewall inspected and no evidence of hillwash infilled crack found.
- At western end, hillwash profile to 0,9m underlain by orange brown speckled black residual sandstone.
- Centre of trench, local deeper pocket of hillwash down to 1,2m in the northern face with no evidence of infilled crack below the pocket. See photo. On southern face, some evidence of hillwash infill in the vertical planes.
- Eastern end, hillwash layer 0,6m deep, underlain by a ferruginised sandstone layer to 1,6m with a completely reworked residual siltstone below.
- No samples taken.

Trench 25A1 – 25B1

TP14

Supplementary notes:

- TP14 profiled in trench 25A1-25B1.
- Hillwash infilled crack found in south and north face from below hillwash horizon.
- Crack width ranges from 100mm – 140mm
- Abundant roots in hillwash infill.
- Crack terminates at residual siltstone layer, but evidence of further hillwash ingress in the siltstone below.
- Residual siltstone next to bottom of crack highly shattered with an apparent leached texture.

TP15

Supplementary notes:

- TP15 excavated at position of existing backfilled sinkhole.
 - On northern side below sinkhole, evidence of two ash backfillings with a fractured rock zone below. See photos. Hillwash in between ash.
 - Sinkhole diameter 2,8m and depth 350mm.
 - On southern face, hillwash infill into residual sandstone in fractured zone.
 - Crack at bottom of testpit through fractured zone. Length of fractured zone 2,1m, i.e. 1m on either side of crack.
 - Crack not as well defined as in TP01 as rock is fractured.
 - Crack infilled with ash, hillwash, reworked residual sandstone, soft rock sandstone.
-

TP16

Not profiled

Excavated near existing borehole to evaluate depth to bedrock.

At 3,8 to 4,1m, completely weathered very soft rock sandstone.

Would crack if under tensile strain.

TP17

Excavated at sinkhole DSC106

Supplementary notes:

- TP17 excavated through throat of sinkhole DSC106. See sketch on notes.
- TP17 excavated perpendicular to original planned position of trench 04A – 04B based on other sinkholes found.
- Dimensions of DSC106 are 2,6m x 2,4m x 0,3m deep with small inlets along perimeter. See photos.
- Apparent throat of hillwash infilled crack found during initial stages of excavation, but could not be located lower down once excavation was deepened.
- No clear sign of fracturing in sandstone rock along sides of testpit at bottom.
- Testpit floor appears fractured in centre, could also have been due to excavation.
- Field mouse nest exposed at 1m depth.

TP18

Excavated immediately to the east of TP03

Profile is similar to TP03.

Supplementary notes:

- TP18 excavated immediately east of TP03.
- Tunnel exposed at the depth of 2m (crown of tunnel). Tunnel ran parallel to crack observed in TP01 – TP03 with a width of 50cm and height of 40cm (approximated). Dimensions are estimated since crown of tunnel was destroyed during excavation.
- Tunnel appeared to be dipping to the west – subsequently the test pit was widened to the west.
- Excavated to 2,9m and found crack in sandstone as with TP03.
- Crack was infilled with hillwash and reworked residual sandstone.
- East of test pit, tunnel depth 1,9m (crown)
 - Material below tunnel has a looser (softer) texture than to the sides. (Also noted at TP03). Possible collapsed tunnel debris
 - Hillwash link found to crack, although thin (5mm wide).
- Centre of test pit
 - Hillwash link to crack

- West of test pit
 - Tunnel crown at 2,55m below ngl (lower than on east)
- No V-shapes encountered.
- 2 prominent hillwash infilled cracks (15mm width) noticed on the east and south face. The northern set was linked to the crown of the tunnel.
- Tunnel was positioned above crack with tunnel debris present immediately above rockhead.

.....

TP19

Excavated immediately east of TP10

Supplementary notes:

- Excavated to 3,6m and profiled from 2m to 3,6m. Profile similar to above, but less firm.

.....

TP20

Excavated immediately west of DSC130, very close to TP04.

Profile is similar to TP04 and TP05.

Samples:

Supplementary notes:

- Excavated to 3m and found crack in rock.
- Crack infilled with hillwash and reworked residual sandstone.
- Hillwash link between infill in residual sandstone and crack in rock.
- Significant ash backfill in east face with near vertical sides (limited V-shape.)
Ash backfill approx. 0,45m wide and found from 0,5m to 2m deep.

.....

TP21

Excavated TP21 on local depression found.

Excavation found significant ash backfilling in upper horizon and a what appears to be a cow skeleton.

Excavation terminated at 0,3m and hole filled.

.....

TP22

Supplementary notes:

- No crack or infilled crack found in residual sandstone

APPENDIX B

LABORATORY TEST RESULTS

B.1 INTRODUCTION

The detailed laboratory test results are included in Appendix B.

B.2 CONTENTS OF APPENDX B

The following sets of laboratory test results are contained in Appendix B:

- a) Grading and foundation indicator test results
- b) Dispersion tests: Double hydrometer, crumb test and chemical analysis
- c) XRF and XRD
- d) Consolidated undrained triaxial tests
- e) Triaxial permeability tests

B.2a) GRADING AND FOUNDATION INDICATOR TEST RESULTS



Jones & Wagener

Consulting Civil Engineers

59 Bevan Road PO Box 1434 Rivonia 2128 South Africa
Tel: (011) 519-0200 Fax: (011) 803-1456 email: post@jaws.co.za

Client: SSE Research Project

Job:

Lab:

Tests:

Our Ref:

Set no.:

Made by:

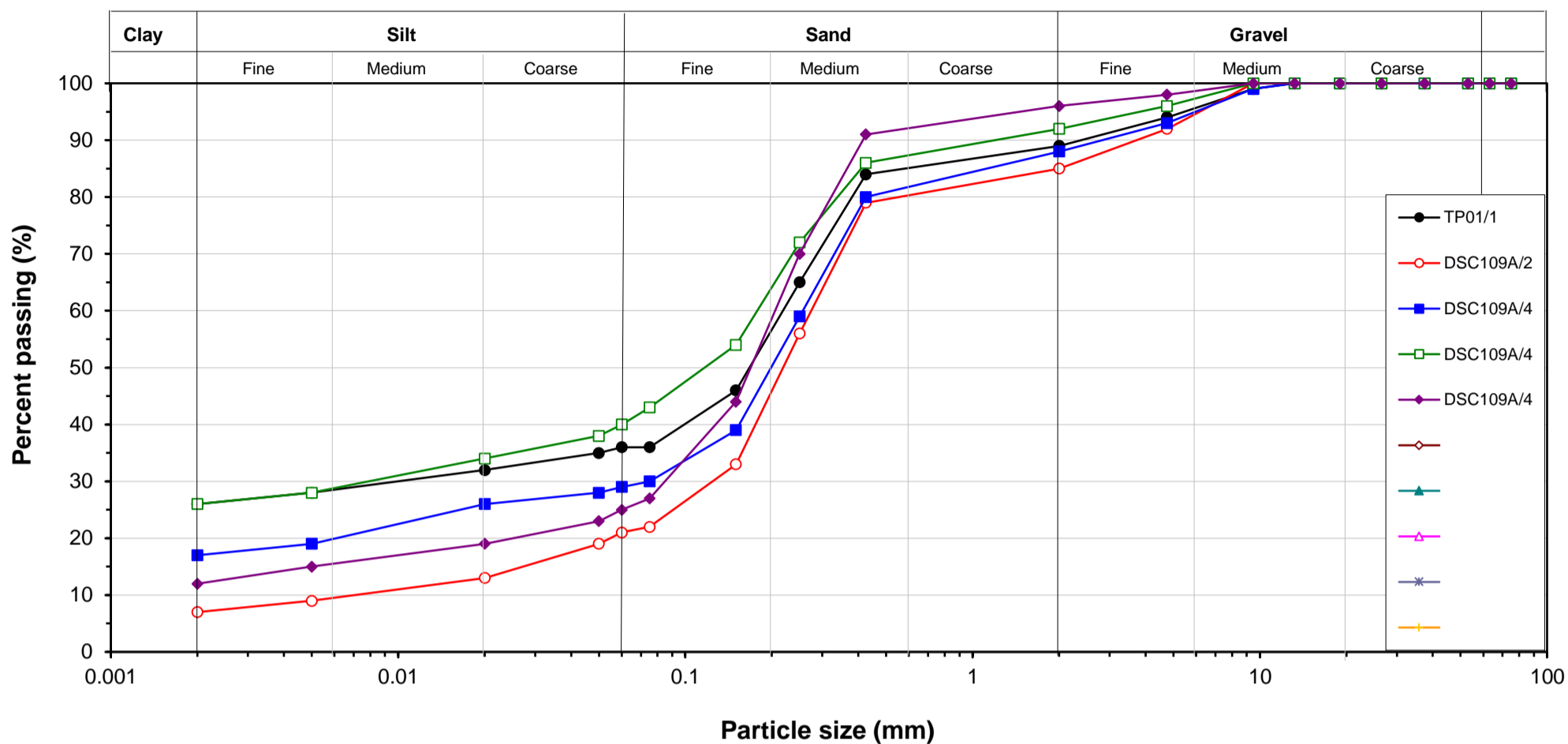
JB

Date:

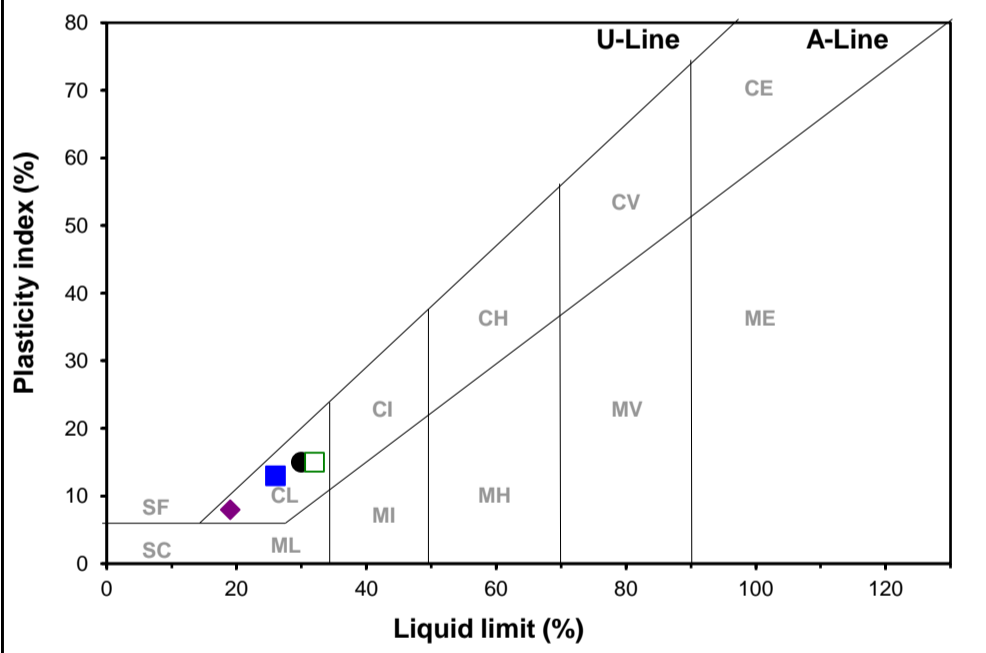
Classification Data

Hole no.			1	2	3	4	5	6	7	8	9	10
Sample Name			TP01	TP02	TP02	TP02	TP02					
Depth			TP01/1	DSC109A/2	DSC109A/4	DSC109A/4	DSC109A/4					
Description	m		3.0	0-0.35	>3	>3	>3					
			Crack Infill	Hillwash	Crk inf west	Grnl east	Sandy east					
Specific Gravity: G_s			2.640	2.640	2.640	2.640	2.640					
Grading:												
		75.0	100	100	100	100	100					
		63.0	100	100	100	100	100					
		53.0	100	100	100	100	100					
		37.5	100	100	100	100	100					
		26.5	100	100	100	100	100					
		19.0	100	100	100	100	100					
		13.2	100	100	100	100	100					
		9.5	99	100	99	100	100					
	No 4	4.75	94	92	93	96	98					
	No 10	2.00	89	85	88	92	96					
	No 40	0.425	84	79	80	86	91					
	No 60	0.250	65	56	59	72	70					
	No 100	0.150	46	33	39	54	44					
	No 200	0.075	36	22	30	43	27					
	Hydrometer	0.060	36	21	29	40	25					
		0.050	35	19	28	38	23					
		0.020	32	13	26	34	19					
		0.005	28	9	19	28	15					
		0.002	26	7	17	26	12					
Grading Properties												
D_{10}	mm			0.007								
D_{30}	mm		0.010	0.124	0.075	0.008	0.085					
D_{60}	mm		0.219	0.274	0.256	0.178	0.205					
Coefficient of Uniformity	CU		112.0	26.0	129.0	92.0	106.0					
Coefficient of Curvature	CC		0.5	5.7	11.5	0.4	19.2					
Grading Modulus	GM		0.91	1.14	1.02	0.79	0.86					
Gravel	G	%	11	15	12	8	4					
Sand	S	%	53	64	59	52	71					
Silt	M	%	10	14	12	14	13					
Clay	C	%	26	7	17	26	12					
Fines	M+C	%	36	21	29	40	25					
Atterberg Limits												
Liquid Limit	LL	%	30		26	32	19					
Plasticity Index	PI	%	15	NP	13	15	8					
Linear Shrinkage	LS	%	7.5		6.5	7.5	4.0					
Natural Moisture Content	w	%										
Dry Density	ρ_d	kg/m^3										
Plastic Limit	PL	%	15		13	17	11					
PI Whole Sample		%	13	NP	10	13	7					
Saturation	S	%										
Liquidity Index	LI											
Clay Activity	A		0.58 Inactive		0.76 Normal	0.58 Inactive	0.67 Inactive					
Vd Merwe Swell			Low	Low	Low	Low	Low					
Pidgeon Free Swell		%										
Weston Swell @ p(kPa)	50 %											
Brackley Swell @ p(kPa)	50 %											
Classification												
Matrix Description			Clayey SAND	Silty SAND	Silty SAND	Clayey SAND	Silty SAND					
British			CLS	SML	SCL	CLS	SCL					
AASHTO			A-6[1]	A-2-4[0]	A-2-6[0]	A-6[3]	A-2-4[0]					
Unified			SC	SM	SC	SC	SC					

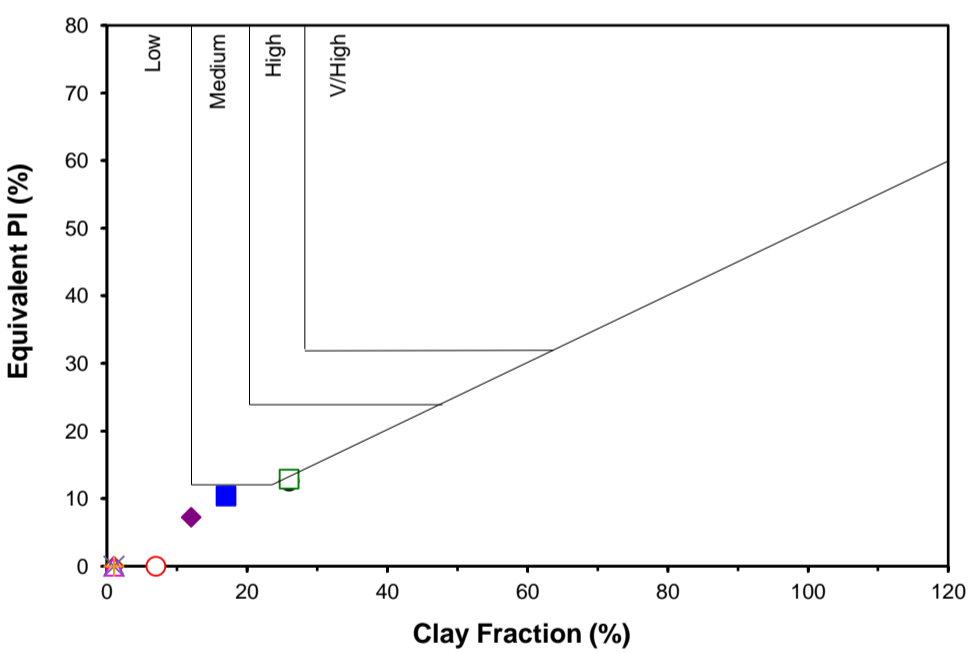
PARTICLE SIZE DISTRIBUTION



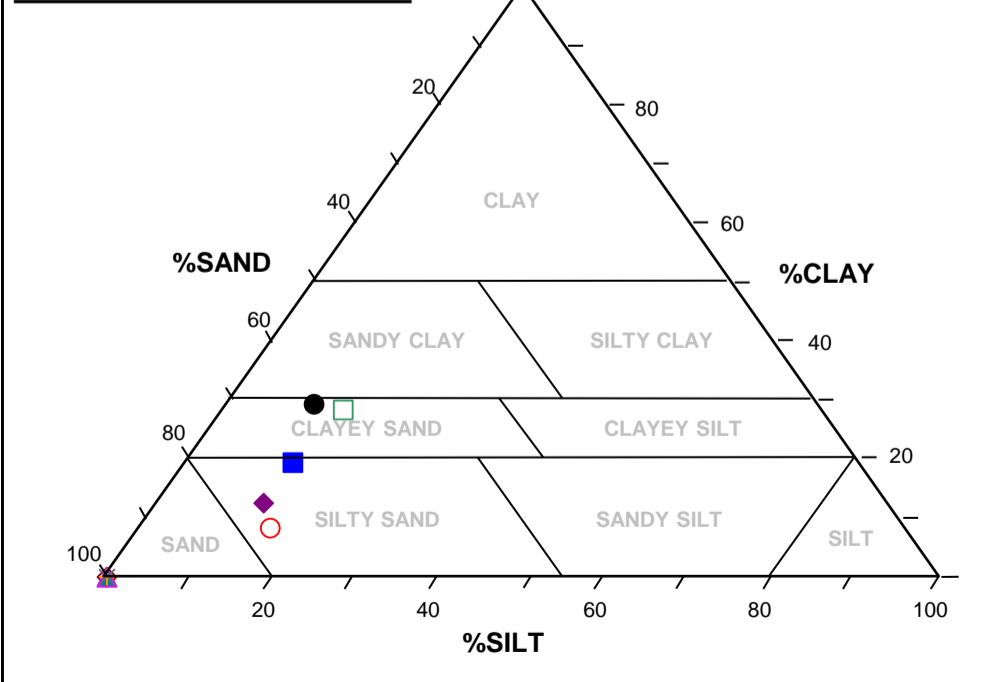
CASAGRANDE CHART



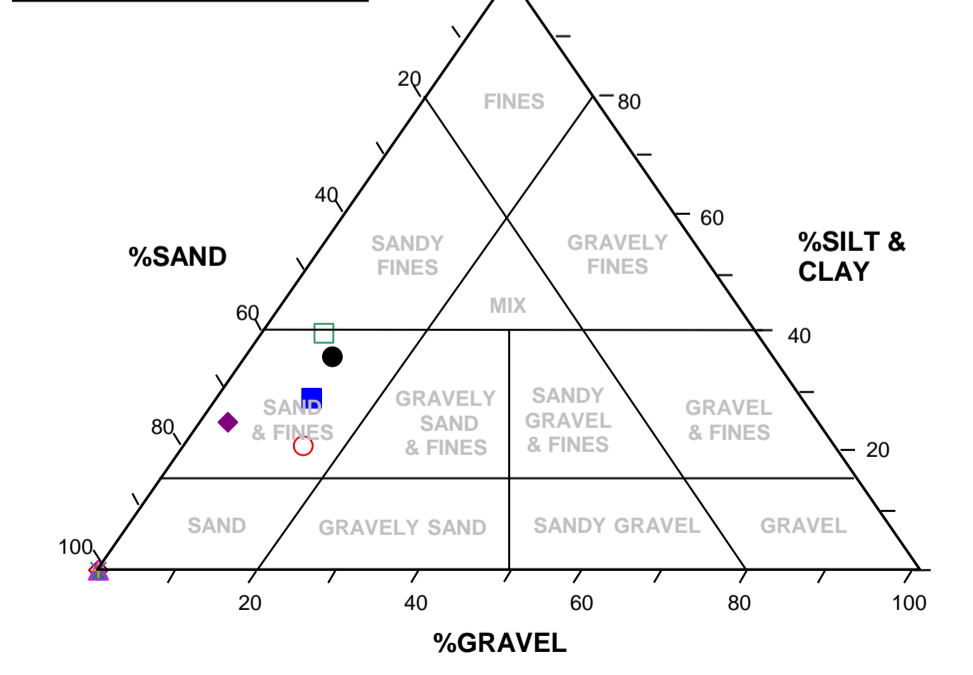
HEAVE CHART



MATRIX CLASSIFICATION



FULL CLASSIFICATION





Jones & Wagener

Consulting Civil Engineers

59 Bevan Road PO Box 1434 Rivonia 2128 South Africa
Tel: (011) 519-0200 Fax: (011) 803-1456 email: post@jaws.co.za

Client: SSE Research Project

Job:

Lab:

Tests:

Our Ref:

Set no.:

Made by:

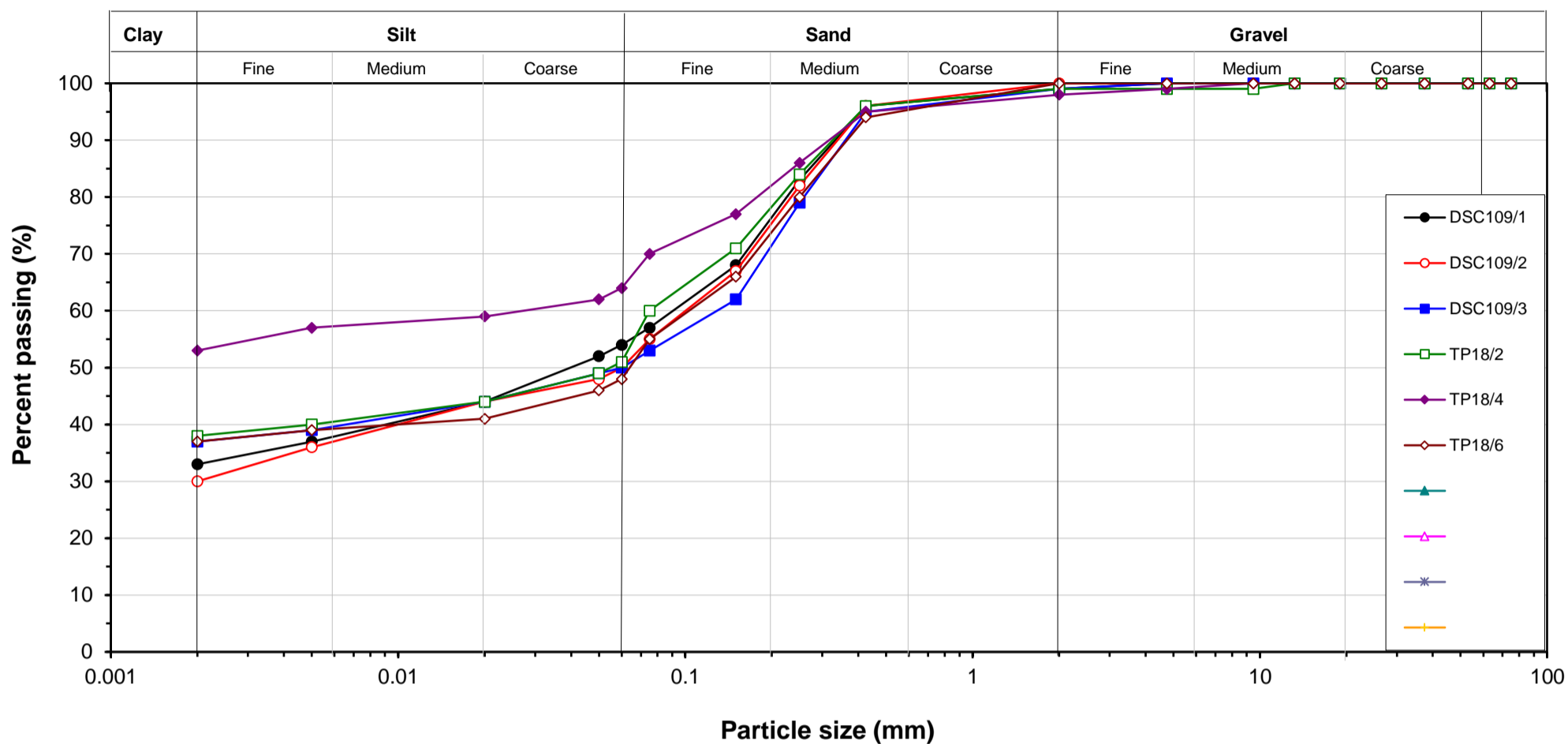
JB

Date:

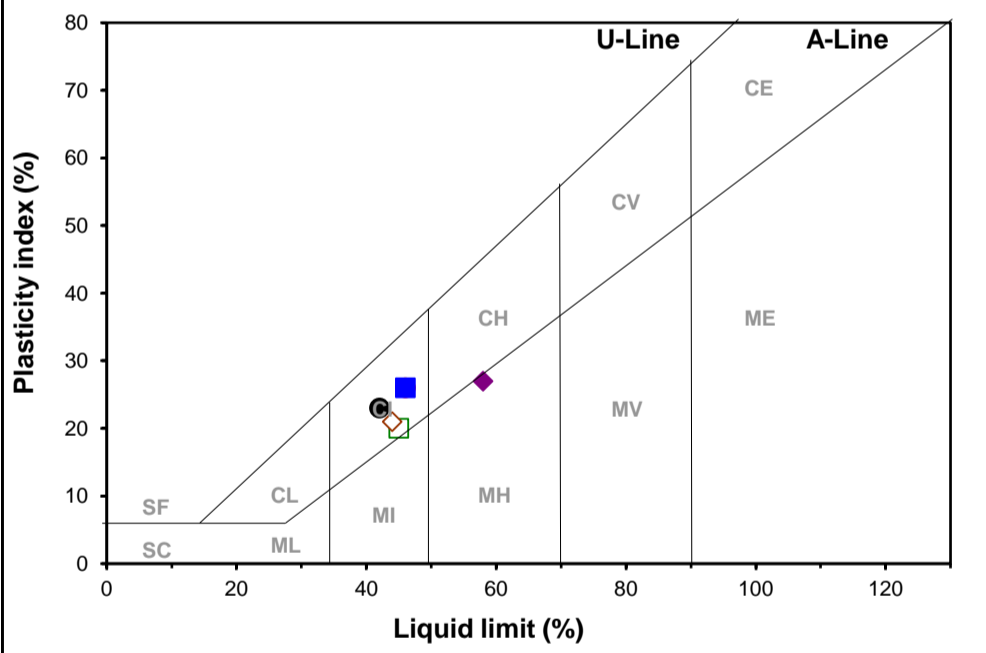
Classification Data

Hole no.	Sample Name	Depth Description	m	1	2	3	4	5	6	7	8	9	10
				TP03 DSC109/1 2.5 Res SS tun	TP03 DSC109/2 2.5 Res SS nrth	TP03 DSC109/3 0.6 Res SS	TP18 TP18/2 2.0 Res SS	TP18 TP18/4 0.5-2.0 Res SS	TP18 TP18/6 2.6 Col tun wst				
Specific Gravity:		G _s		2.640	2.640	2.640	2.640	2.640	2.640				
Grading:													
			75.0	100	100	100	100	100	100				
			63.0	100	100	100	100	100	100				
			53.0	100	100	100	100	100	100				
			37.5	100	100	100	100	100	100				
			26.5	100	100	100	100	100	100				
			19.0	100	100	100	100	100	100				
			13.2	100	100	100	100	100	100				
			9.5	100	100	100	99	100	100				
	No 4		4.75	100	100	100	99	99	100				
	No 10		2.00	99	100	99	99	98	100				
	No 40		0.425	96	96	95	96	95	94				
	No 60		0.250	83	82	79	84	86	80				
	No 100		0.150	68	67	62	71	77	66				
	No 200		0.075	57	55	53	60	70	55				
	Hydrometer		0.060	54	50	50	51	64	48				
			0.050	52	48	49	49	62	46				
			0.020	44	44	44	44	59	41				
			0.005	37	36	39	40	57	39				
			0.002	33	30	37	38	53	37				
Grading Properties													
	D ₁₀	mm											
	D ₃₀	mm		0.002									
	D ₆₀	mm	0.091	0.100	0.129	0.075	0.027	0.103					
	Coefficient of Uniformity	CU	48.0	53.0	67.0								
	Coefficient of Curvature	CC	0.0	0.0	0.0								
	Grading Modulus	GM	0.48	0.49	0.53	0.45	0.37	0.51					
	Gravel	G	%	1	0	1	1	2	0				
	Sand	S	%	45	50	49	48	34	52				
	Silt	M	%	21	20	13	13	11	11				
	Clay	C	%	33	30	37	38	53	37				
	Fines	M+C	%	54	50	50	51	64	48				
Atterberg Limits													
	Liquid Limit	LL	%	42	46	46	45	58	44				
	Plasticity Index	PI	%	23	26	26	20	27	21				
	Linear Shrinkage	LS	%	11.5	13.0	12.5	8.5	13.0	8.0				
	Natural Moisture Content	w	%										
	Dry Density	ρ _d	kg/m ³										
	Plastic Limit	PL	%	19	20	20	25	31	23				
	PI Whole Sample		%	22	25	25	19	26	20				
	Saturation	S	%										
	Liquidity Index	LI											
	Clay Activity	A		0.70 Inactive	0.87 Normal	0.70 Inactive	0.53 Inactive	0.51 Inactive	0.57 Inactive				
	Vd Merwe Swell			Medium	High	High	Medium	Low	Medium				
	Pidgeon Free Swell		%										
	Weston Swell @ p(kPa)	50 %											
	Brackley Swell @ p(kPa)	50 %											
Classification													
	Matrix Description			Sandy CLAY	Sandy CLAY	Sandy CLAY	Sandy CLAY	CLAY MH	Sandy CLAY				
	British			CIS	CIS	CIS	CIS	MH	CIS				
	AASHTO			A-7-6[1]	A-7-6[11]	A-7-6[10]	A-7-6[1]	A-7-5[17]	A-7-6[9]				
	Unified			CL	CL	CL	CL	MH/OH	CL				

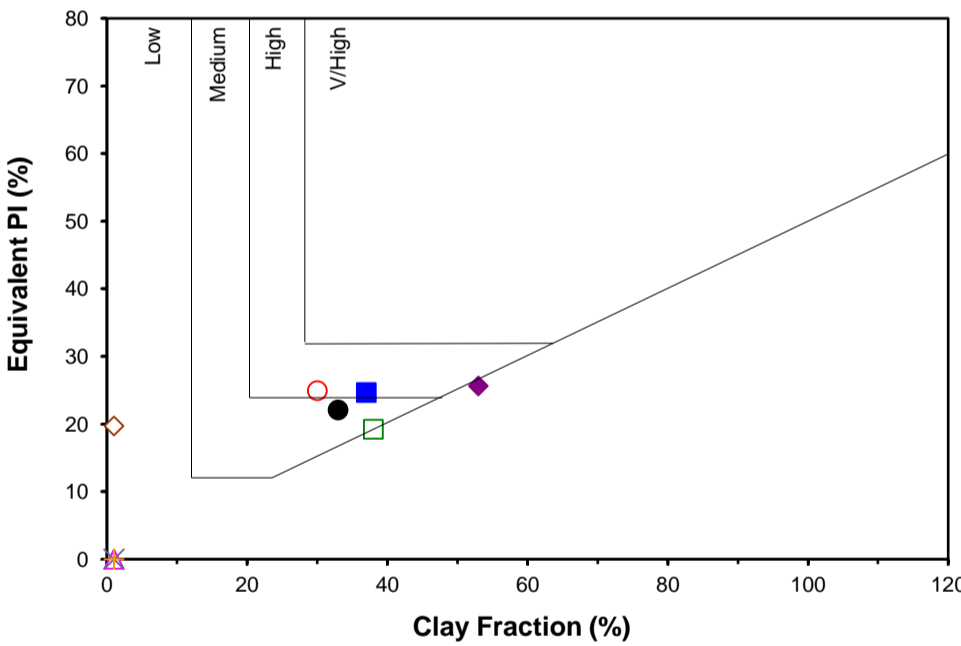
PARTICLE SIZE DISTRIBUTION



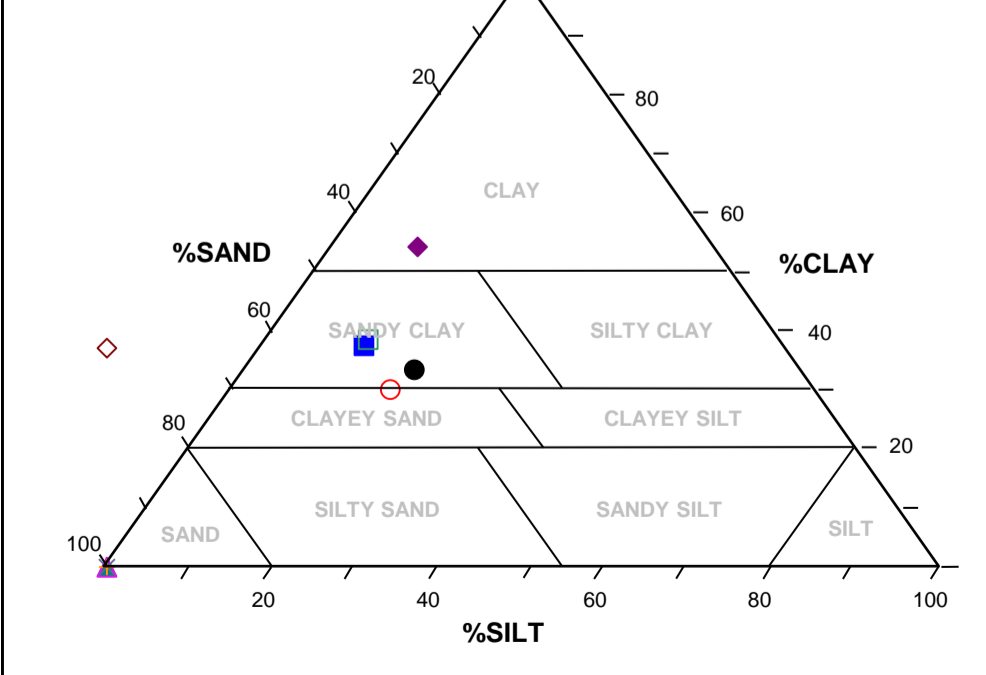
CASAGRANDE CHART



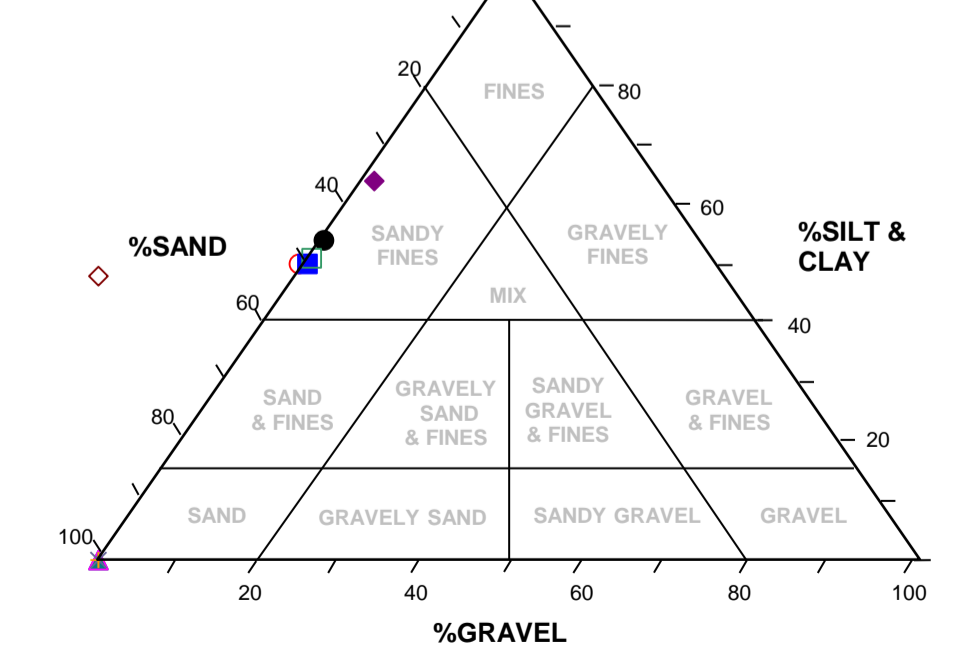
HEAVE CHART



MATRIX CLASSIFICATION



FULL CLASSIFICATION





Jones & Wagener

Consulting Civil Engineers

59 Bevan Road PO Box 1434 Rivonia 2128 South Africa
Tel: (011) 519-0200 Fax: (011) 803-1456 email: post@jaws.co.za

Client: SSE Research Project

Job:

Lab:

Tests:

Our Ref:

Set no.:

Made by:

JB

Date:

Classification Data

Hole no.			1	2	3	4	5	6	7	8	9	10
Sample Name			TP05	TP05/2	TP20							
Depth	m		TP05/1	TP05/3	TP20/1							
Description			1.2 - 3.0	0.2 - 0.4	1.3 - 3.0							
			Res SS	Hillwash	Res SS							
Specific Gravity:	G _s		2.640	2.640	2.640							
Grading:												
		75.0	100	100	100							
		63.0	100	100	100							
		53.0	100	100	100							
		37.5	100	100	100							
		26.5	100	100	100							
		19.0	100	100	100							
		13.2	100	100	100							
		9.5	100	100	100							
	No 4	4.75	97	99	89							
	No 10	2.00	94	98	87							
	No 40	0.425	90	93	83							
	No 60	0.250	77	72	74							
	No 100	0.150	63	48	63							
	No 200	0.075	53	37	52							
	Hydrometer	0.060	50	31	44							
		0.050	49	29	42							
		0.020	44	21	35							
		0.005	39	17	34							
		0.002	37	12	33							
Grading Properties												
D ₁₀	mm											
D ₃₀	mm			0.055								
D ₆₀	mm		0.122	0.194	0.124	0.075	0.027	0.103				
Coefficient of Uniformity	CU		64.0	100.0								
Coefficient of Curvature	CC		0.0	8.1								
Grading Modulus	GM		0.63	0.72	0.78							
Gravel	G	%	6	2	13							
Sand	S	%	44	67	43							
Silt	M	%	13	19	11							
Clay	C	%	37	12	33							
Fines	M+C	%	50	31	44							
Atterberg Limits												
Liquid Limit	LL	%	39	16	43							
Plasticity Index	PI	%	20	6	23							
Linear Shrinkage	LS	%	10.0	3.0	10.0							
Natural Moisture Content	w	%			15.3							
Dry Density	ρ _d	kg/m ³										
Plastic Limit	PL	%	19	10	20							
PI Whole Sample		%	18	6	19							
Saturation	S	%										
Liquidity Index	LI				-0.2							
					Brittle							
Clay Activity	A		0.54	0.50	0.70							
			Inactive	Inactive	Inactive							
Vd Merwe Swell			Low	Low	Medium	Medium	Low	Medium				
Pidgeon Free Swell		%			3.6							
Weston Swell @ p(kPa)	50 %				0.5							
Brackley Swell @ p(kPa)	50 %											
Classification												
Matrix Description			Sandy	Silty	Sandy							
British			CLAY	SAND	CLAY							
AASHTO			CIS	MLS	CIS							
Unified			A-6[7]	A-4[0]	A-7-6[8]							
			CL	SC-SM	CL							

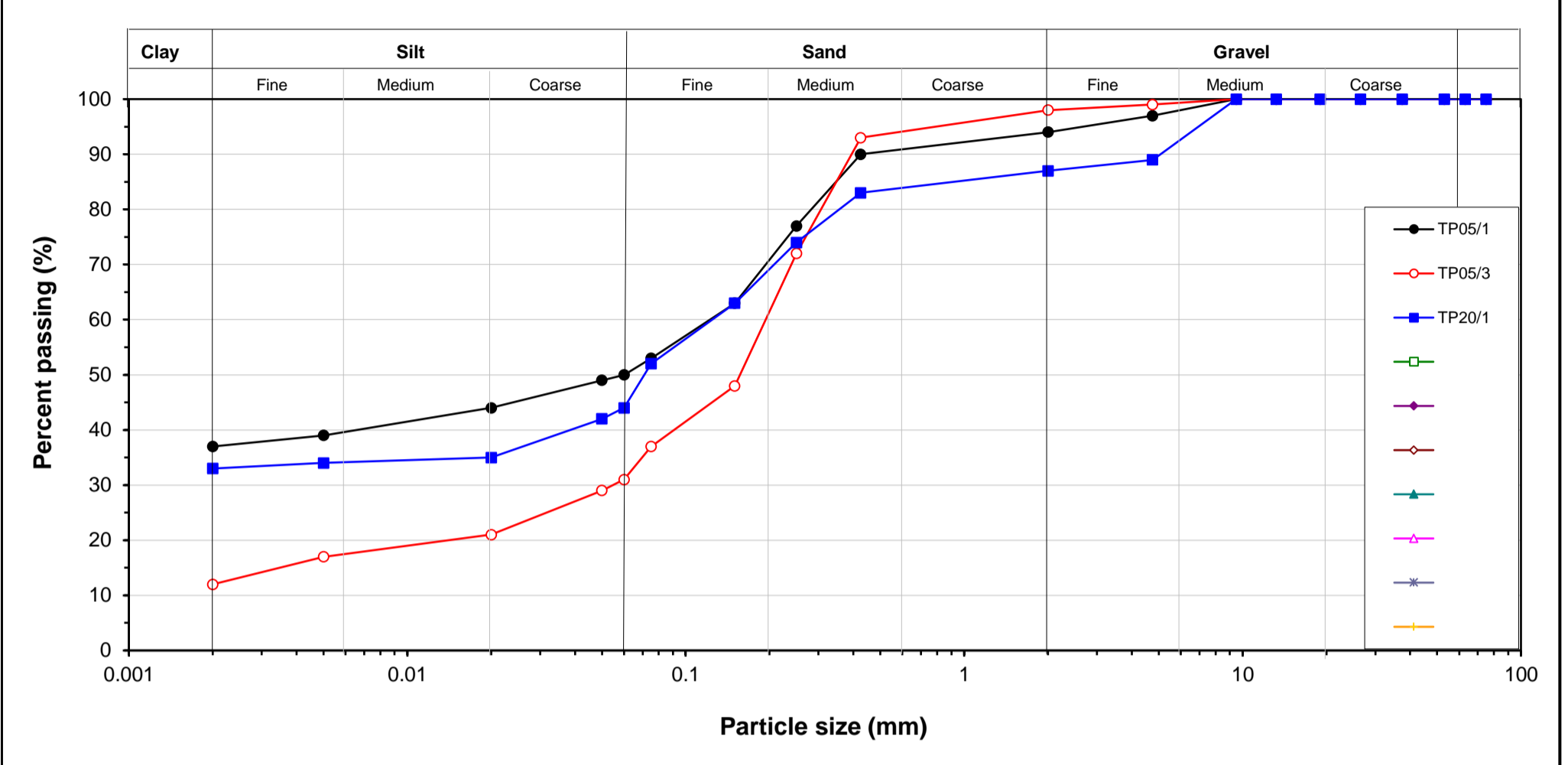


Jones & Wagener
 Consulting Civil Engineers
 59 Bevan Road PO Box 1434 Rivonia 2128 South Africa
 Tel: (011) 519-0200 Fax: (011) 803-1456 email: post@jaws.co.za

Client: SSE Research Project
 Job: _____
 Lab: _____
 Tests: _____

Our Ref: _____
 Set no.: _____
 Made by: JB
 Date: _____

PARTICLE SIZE DISTRIBUTION





Jones & Wagener

Consulting Civil Engineers
 59 Bevan Road PO Box 1434 Rivonia 2128 South Africa
 Tel: (011) 519-0200 Fax: (011) 803-1456 email: post@jaws.co.za

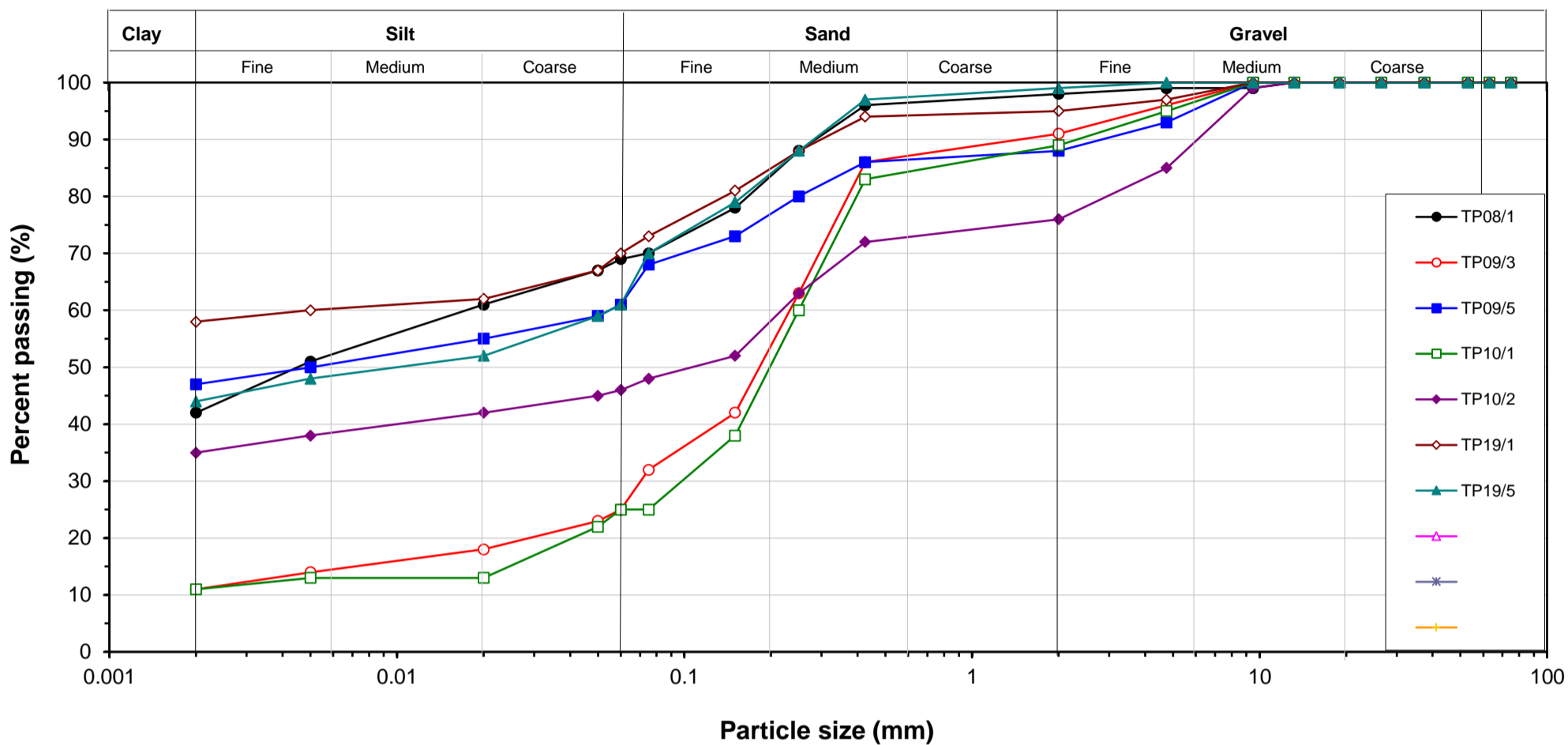
Client: _____
 Job: **SSE Research Project**
 Lab: _____
 Tests: _____

Our Ref: _____
 Set no.: _____
 Made by: **JB**
 Date: _____

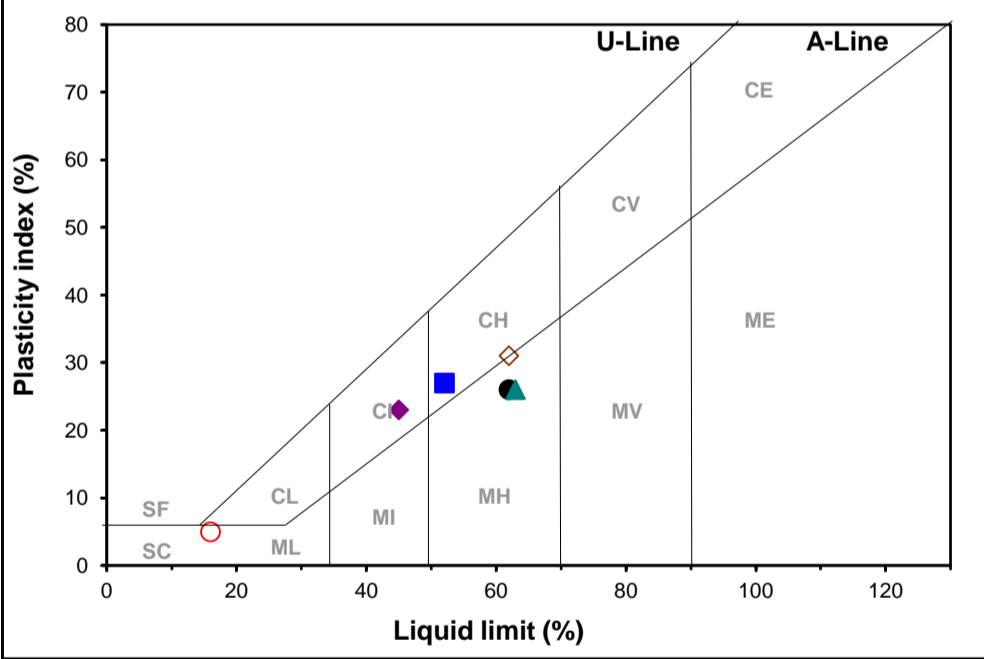
Classification Data

Hole no.			TP08	TP09	TP09	4	5	6	7	8	9	10
Sample Name			TP08/1	TP09/3	TP09/5	TP10/1	TP10/2	TP19/1	TP19/5			
Depth	<i>m</i>		2.6 - 4.1	0 - 0.4	0.8 - 1.8	0 - 0.4	0.45 - 1.3	0.5 - 1.3	3.0			
Description			Res SS SiS	Hillwash	Res SS	Hillwash	Res SS	Res SS	Res SS			
Specific Gravity:	G _s		2.640	2.640	2.640	2.640	2.640	2.640	2.640			
Grading:												
		75.0	100	100	100	100	100	100	100			
		63.0	100	100	100	100	100	100	100			
		53.0	100	100	100	100	100	100	100			
		37.5	100	100	100	100	100	100	100			
		26.5	100	100	100	100	100	100	100			
		19.0	100	100	100	100	100	100	100			
		13.2	100	100	100	100	100	100	100			
		9.5	99	100	100	100	99	100	100			
	No 4	4.75	99	96	93	95	85	97	100			
	No 10	2.00	98	91	88	89	76	95	99			
	No 40	0.425	96	86	86	83	72	94	97			
	No 60	0.250	88	63	80	60	63	88	88			
	No 100	0.150	78	42	73	38	52	81	79			
	No 200	0.075	70	32	68	25	48	73	70			
	Hydrometer	0.060	69	25	61	25	46	70	61			
		0.050	67	23	59	22	45	67	59			
		0.020	61	18	55	13	42	62	52			
		0.005	51	14	50	13	38	60	48			
		0.002	42	11	47	11	35	58	44			
Grading Properties												
D ₁₀	mm											
D ₃₀	mm			0.070		0.085						
D ₆₀	mm		0.017	0.232	0.055	0.250	0.217	0.005	0.055			
Coefficient of Uniformity	CU		9.0	118.0	28.0	125.0	111.0					
Coefficient of Curvature	CC		0.1	11.2	0.0	22.4	0.0					
Grading Modulus	GM		0.36	0.91	0.58	1.03	1.04	0.38	0.34			
Gravel	G	%	2	9	12	11	24	5	1			
Sand	S	%	29	66	27	64	30	25	38			
Silt	M	%	27	14	14	14	11	12	17			
Clay	C	%	42	11	47	11	35	58	44			
Fines	M+C	%	69	25	61	25	46	70	61			
Atterberg Limits												
Liquid Limit	LL	%	62	16	52		45	62	63			
Plasticity Index	PI	%	26	5	27	NP	23	31	26			
Linear Shrinkage	LS	%	13.0	2.5	14.0		11.5	12.0	13.0			
Natural Moisture Content	w	%						23.5				
Dry Density	ρ _d	kg/m ³										
Plastic Limit	PL	%	36	11	25		22	31	37			
PI Whole Sample		%	25	4	23	NP	17	29	25			
Saturation	S	%										
Liquidity Index	LI							-0.2				
								Brittle				
Clay Activity	A		0.62	0.45	0.57		0.66	0.53	0.59			
			Inactive	Inactive	Inactive		Inactive	Inactive	Inactive			
Vd Merwe Swell			High	Low	Low	Low	Low	High	High			
Pidgeon Free Swell		%						3.4				
Weston Swell @ p(kPa)	50 %							1.3				
Brackley Swell @ p(kPa)	50 %											
Classification												
Matrix Description			Sandy CLAY	Silty SAND	Sandy CLAY	Silty SAND	Sandy CLAY	CLAY	Sandy CLAY			
British			MH	SML	CH	SML	CIS	CH	MH			
AASHTO			A-7-5[17]	A-2-4[0]	A-7-6[15]	A-2-4[0]	A-7-6[7]	A-7-5[19]	A-7-5[17]			
Unified			MH/OH	SC-SM	CH	SM	SC	CH	MH/OH			

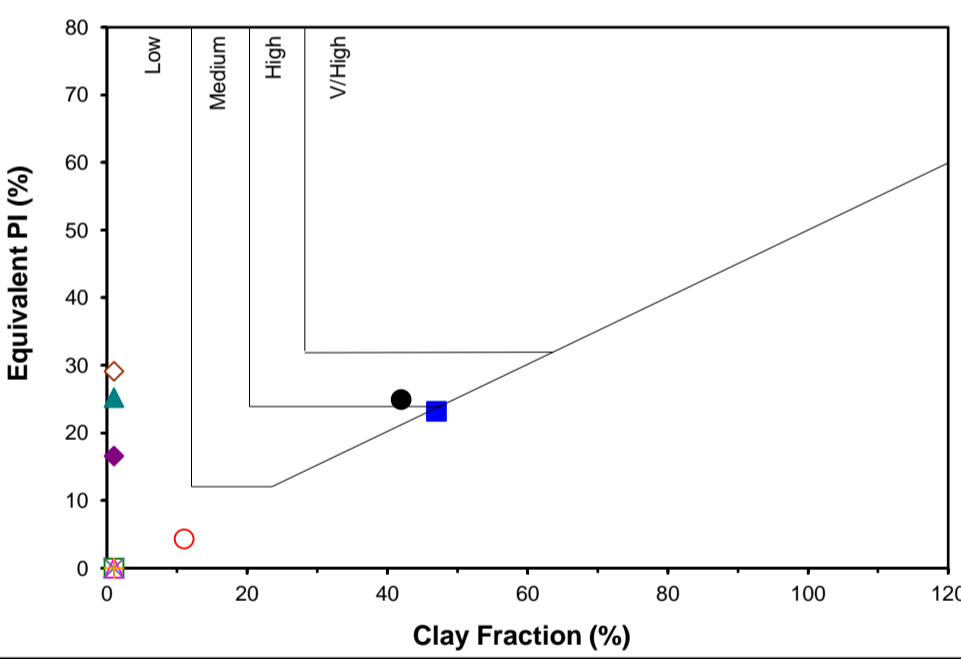
PARTICLE SIZE DISTRIBUTION



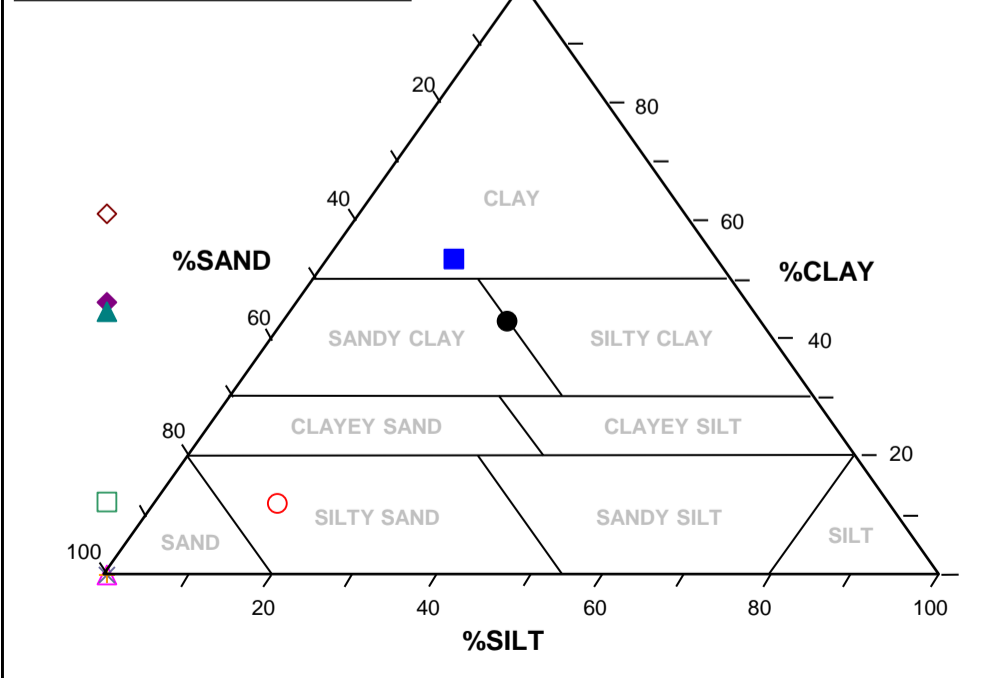
CASAGRANDE CHART



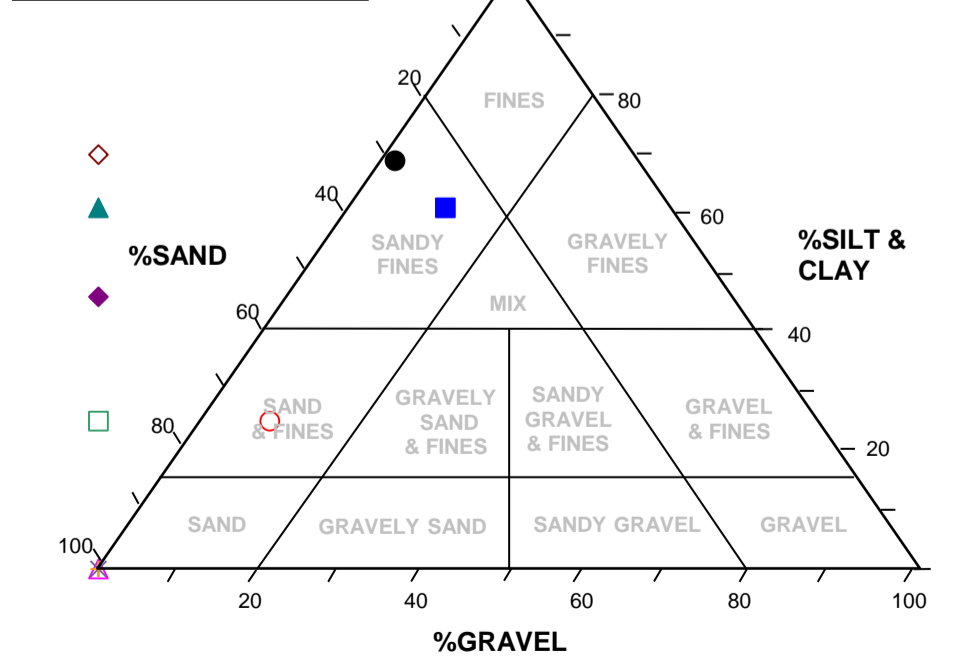
HEAVE CHART



MATRIX CLASSIFICATION



FULL CLASSIFICATION





Jones & Wagener

Consulting Civil Engineers

59 Bevan Road PO Box 1434 Rivonia 2128 South Africa
Tel: (011) 519-0200 Fax: (011) 803-1456 email: post@jaws.co.za

Client: SSE Research Project

Job:

Lab:

Tests:

Our Ref:

Set no.:

Made by:

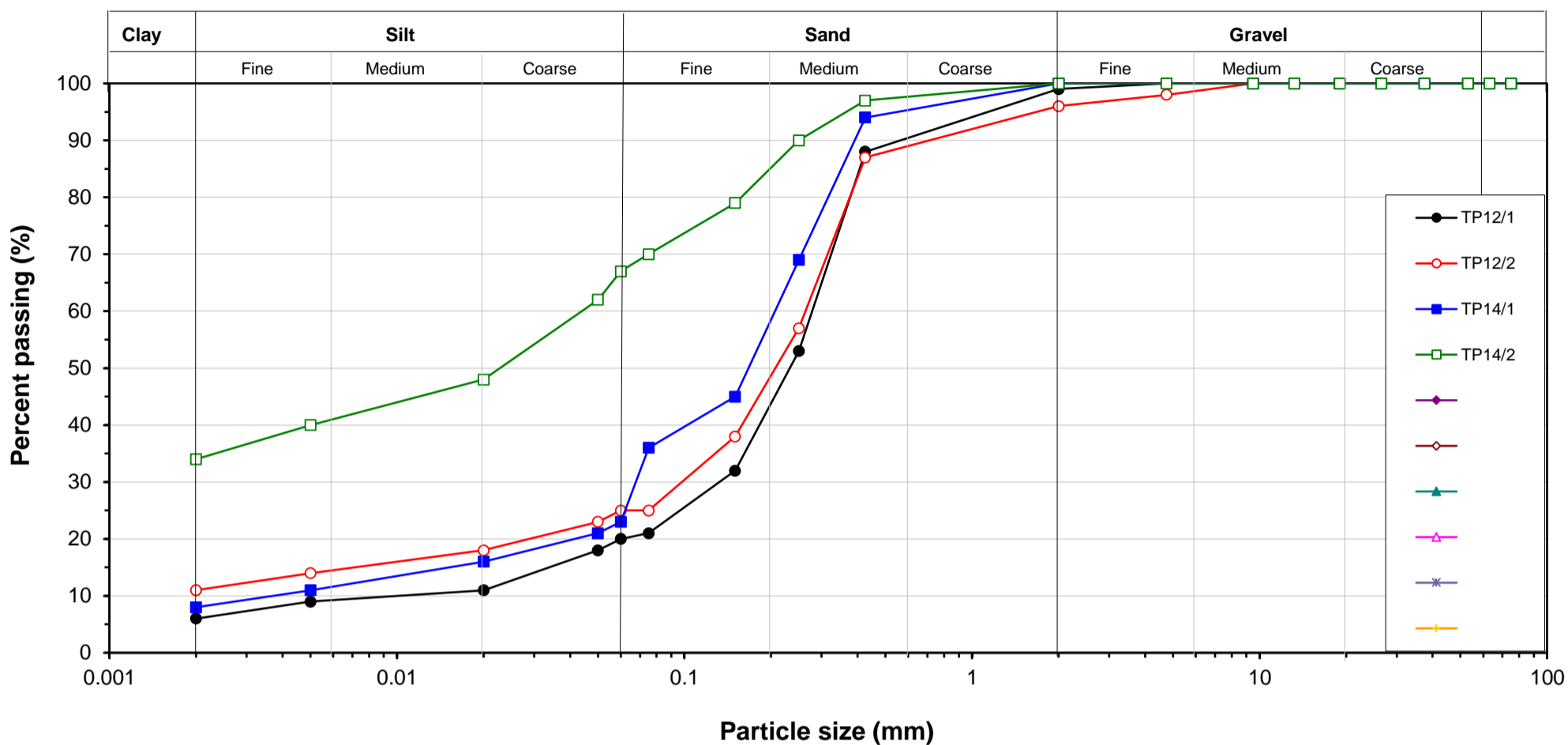
JB

Date:

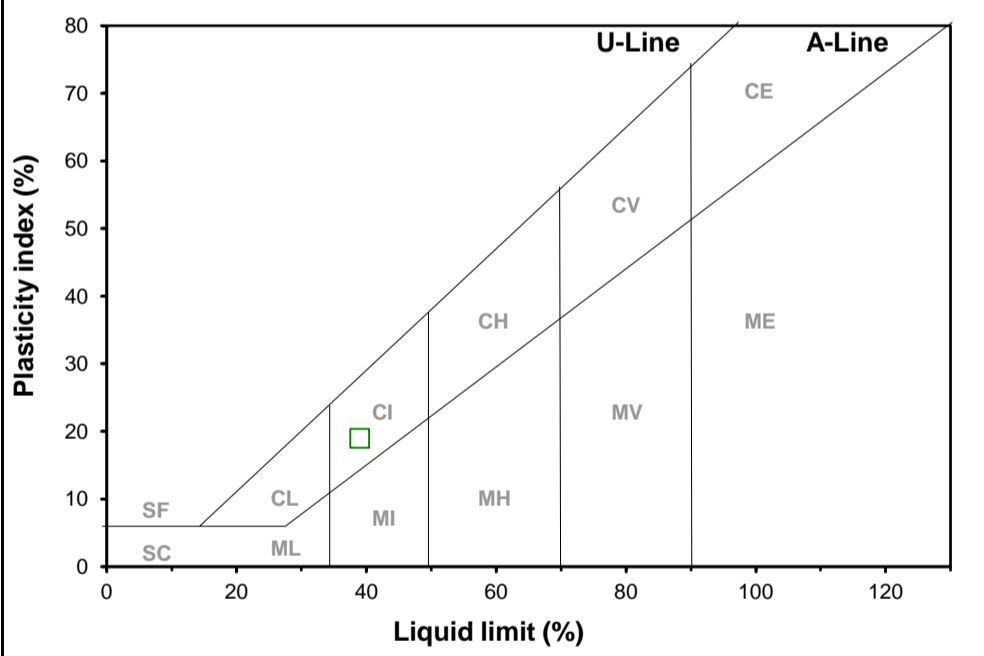
Classification Data

Hole no.	Sample Name	Depth Description	m	1	2	3	4	5	6	7	8	9	10
				TP12 TP12/1 0.35 - 0.8 Hillwash	TP12 TP12/2 0.8 - 1.3 Res SS	TP14 TP14/1 0 - 0.5 Hillwash	TP14 TP14/2 1.7 - 2.4 Res SS						
Specific Gravity:		G _s		2.640	2.640	2.640	2.640						
Grading:													
			75.0	100	100	100	100						
			63.0	100	100	100	100						
			53.0	100	100	100	100						
			37.5	100	100	100	100						
			26.5	100	100	100	100						
			19.0	100	100	100	100						
			13.2	100	100	100	100						
			9.5	100	100	100	100						
	No 4		4.75	100	98	100	100						
	No 10		2.00	99	96	100	100						
	No 40		0.425	88	87	94	97						
	No 60		0.250	53	57	69	90						
	No 100		0.150	32	38	45	79						
	No 200		0.075	21	25	36	70						
	Hydrometer		0.060	20	25	23	67						
			0.050	18	23	21	62						
			0.020	11	18	16	48						
			0.005	9	14	11	40						
			0.002	6	11	8	34						
Grading Properties													
	D ₁₀	mm		0.010		0.004							
	D ₃₀	mm		0.132	0.085	0.068							
	D ₆₀	mm		0.278	0.264	0.206	0.044	0.027	0.103				
	Coefficient of Uniformity	CU		20.0	134.0	53.0	23.0						
	Coefficient of Curvature	CC		4.6	20.9	5.8	0.0						
	Grading Modulus	GM		0.92	0.92	0.70	0.33						
	Gravel	G	%	1	4	0	0						
	Sand	S	%	79	71	77	33						
	Silt	M	%	14	14	15	33						
	Clay	C	%	6	11	8	34						
	Fines	M+C	%	20	25	23	67						
Atterberg Limits													
	Liquid Limit	LL	%				39						
	Plasticity Index	PI	%	NP	NP	NP	19						
	Linear Shrinkage	LS	%				9.5						
	Natural Moisture Content	w	%										
	Dry Density	ρ _d	kg/m ³										
	Plastic Limit	PL	%				20						
	PI Whole Sample		%	NP	NP	NP	18						
	Saturation	S	%										
	Liquidity Index	LI											
	Clay Activity	A					0.56 Inactive						
	Vd Merwe Swell			Low	Low	Low	Medium	Low	Medium				
	Pidgeon Free Swell		%										
	Weston Swell @ p(kPa)	50 %											
	Brackley Swell @ p(kPa)	50 %											
Classification													
	Matrix Description			Silty SAND	Silty SAND	Silty SAND	Sandy CLAY						
	British			SML	SML	MLS	CI						
	AASHTO			A-2-4[0]	A-2-4[0]	A-4[0]	A-6[11]						
	Unified			SM	SM	SM	CL						

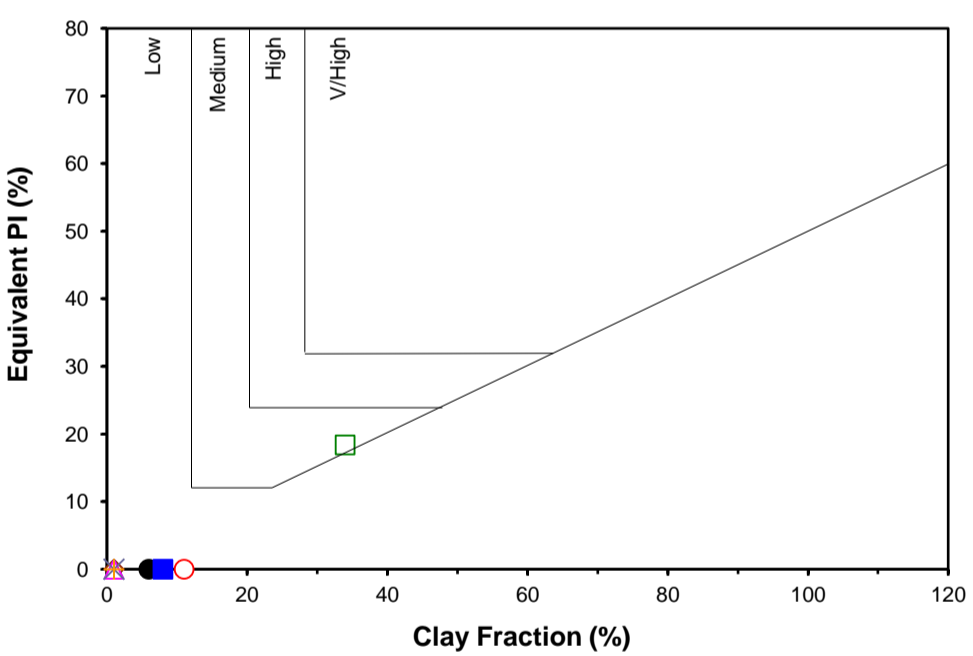
PARTICLE SIZE DISTRIBUTION



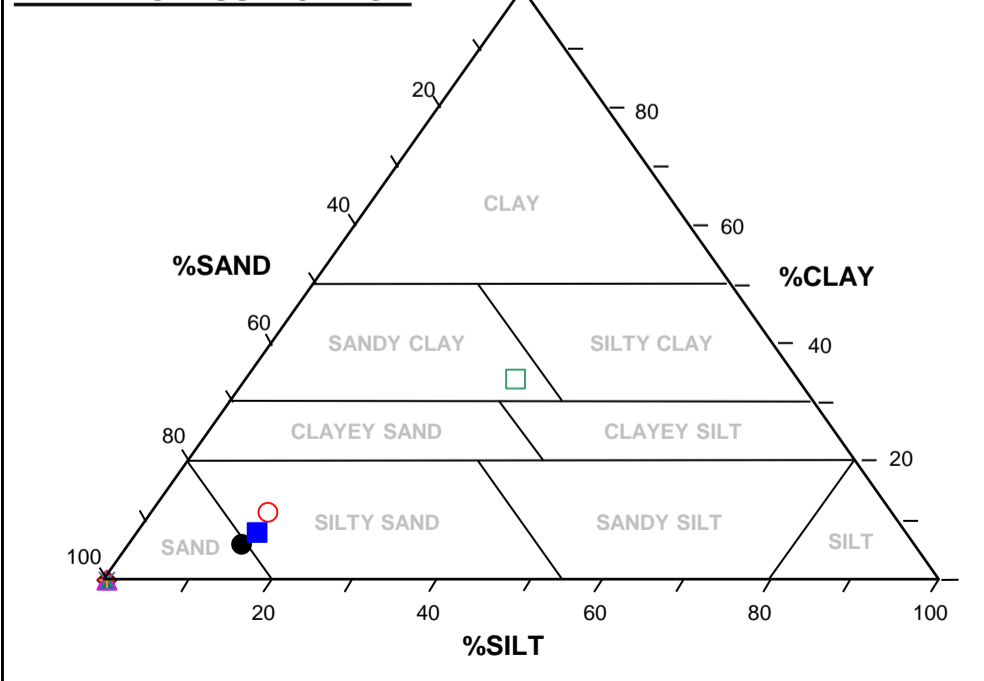
CASAGRANDE CHART



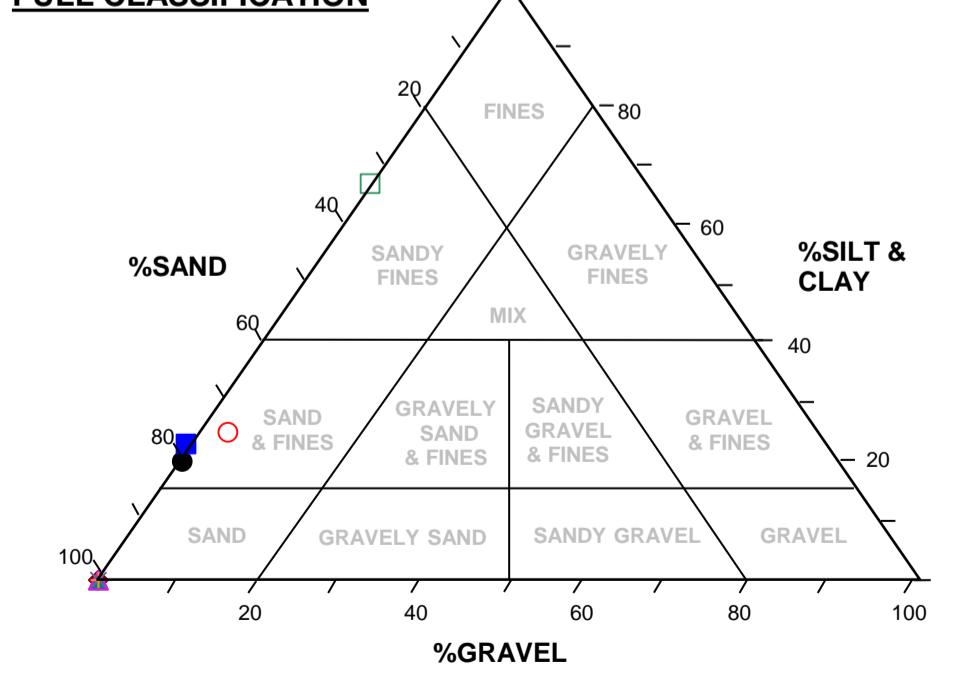
HEAVE CHART



MATRIX CLASSIFICATION



FULL CLASSIFICATION



**B.2b) DISPERSION TESTS: DOUBLE HYDROMETER, CRUMB TEST and
CHEMICAL ANALYSIS**



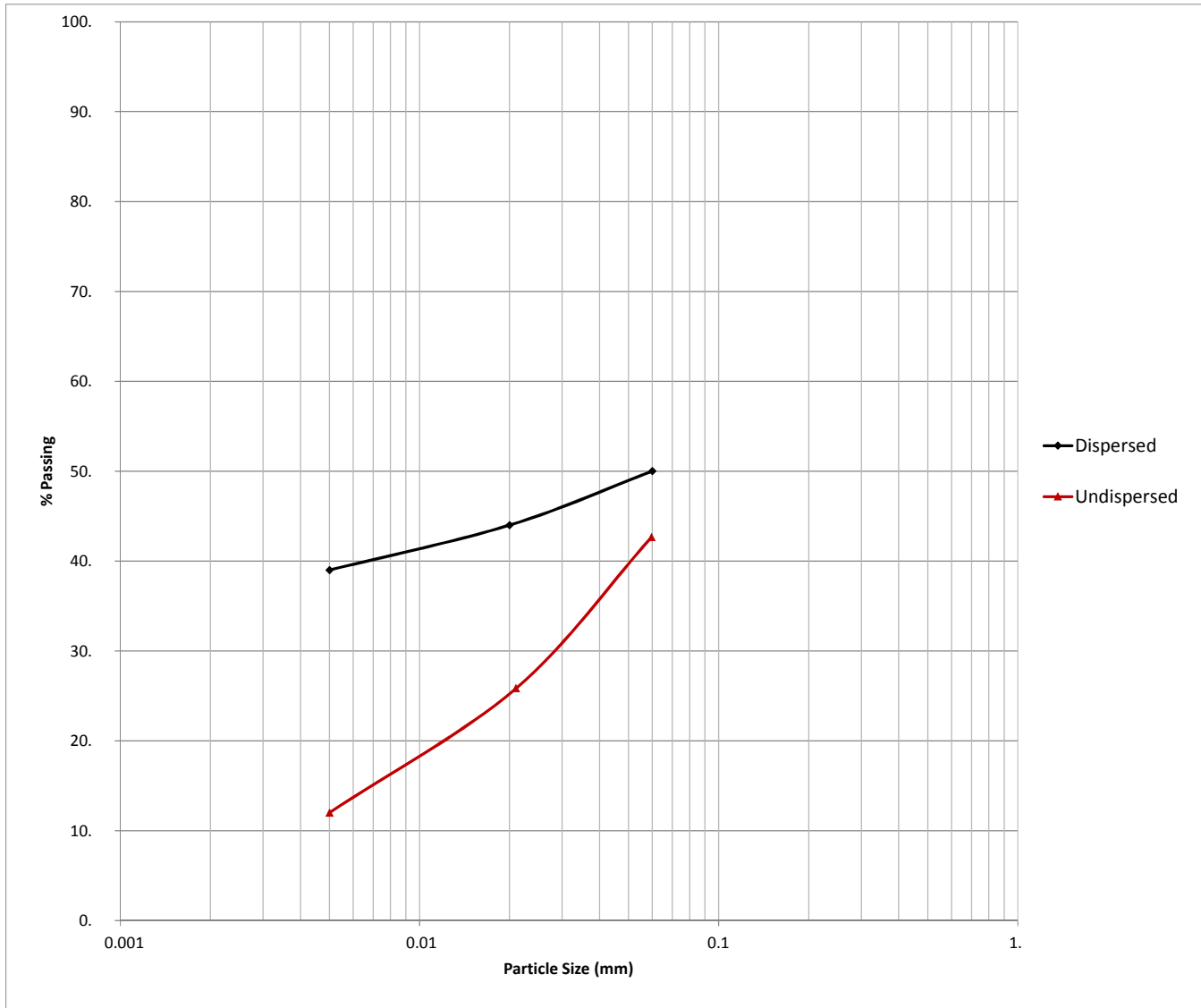
Double Hydrometer Test Result

ASTM
D4221

Client University of Pretoria
Sample no TP05/1
Lab no 7/3740

Project Sub-surface erosion research project
Depth (m) 1.2-3.0

Job no 2017-C-813
Date 2017/08/25



Dispersion:

31%



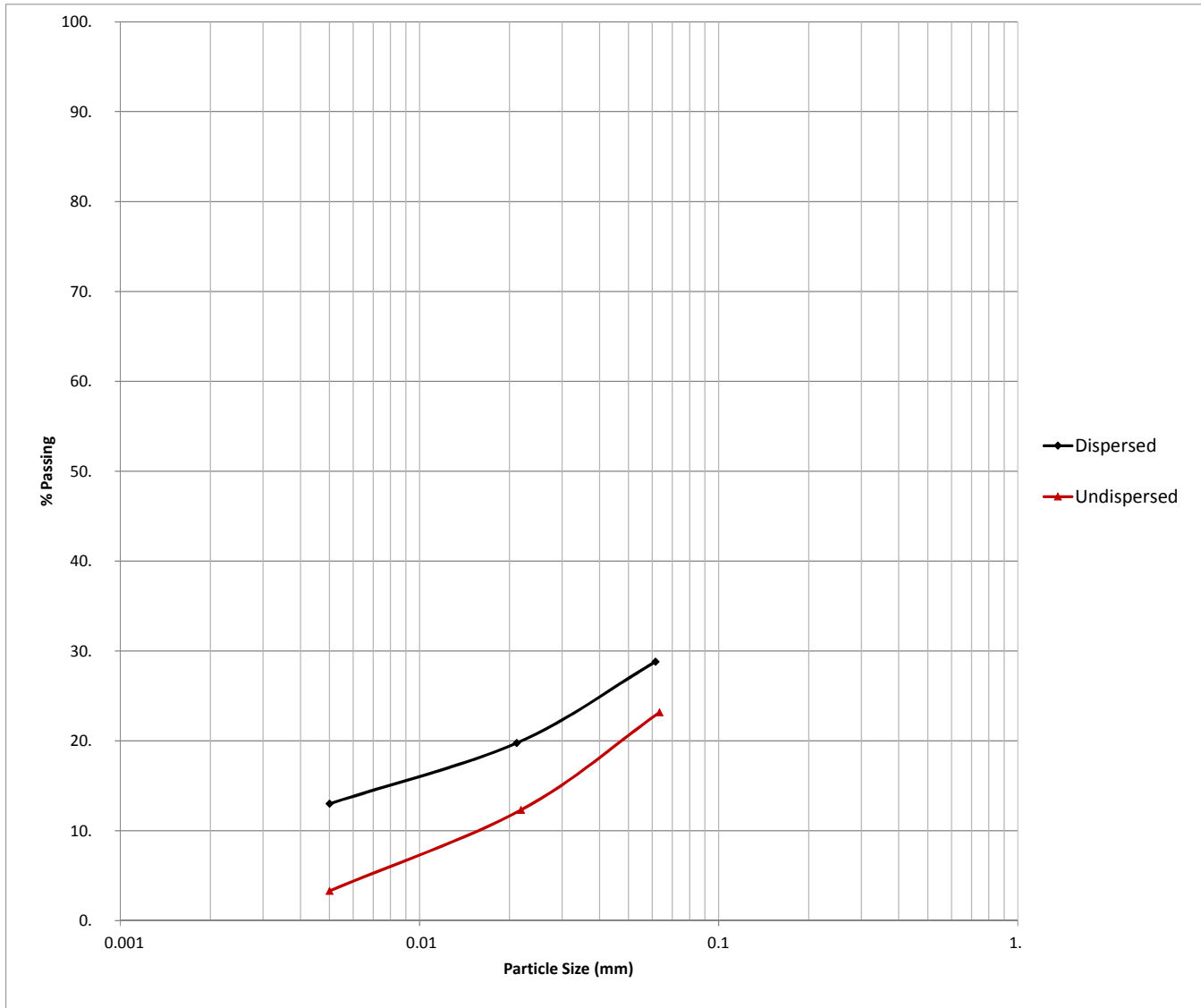
Double Hydrometer Test Result

ASTM
D4221

Client University of Pretoria
Sample no TP05/4
Lab no 7/3742

Project Sub-surface erosion research project
Depth (m) 0.2-0.4

Job no 2017-C-813
Date 2017/08/25



Dispersion:

25%



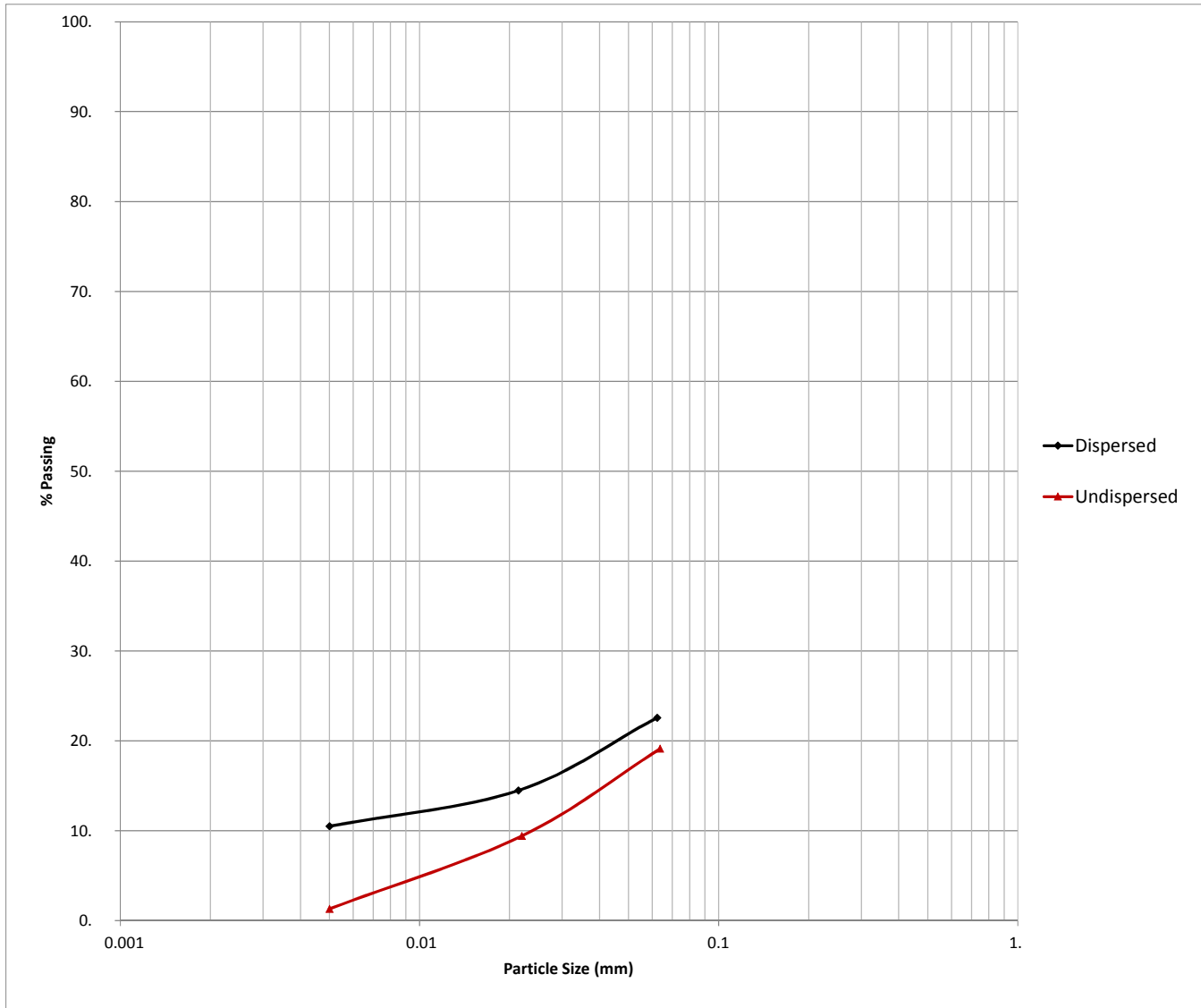
Double Hydrometer Test Result

ASTM
D4221

Client University of Pretoria
Sample no TP09/2
Lab no 7/3744

Project Sub-surface erosion research project
Depth (m) 0-0.4

Job no 2017-C-813
Date 2017/08/25



Dispersion:

12%



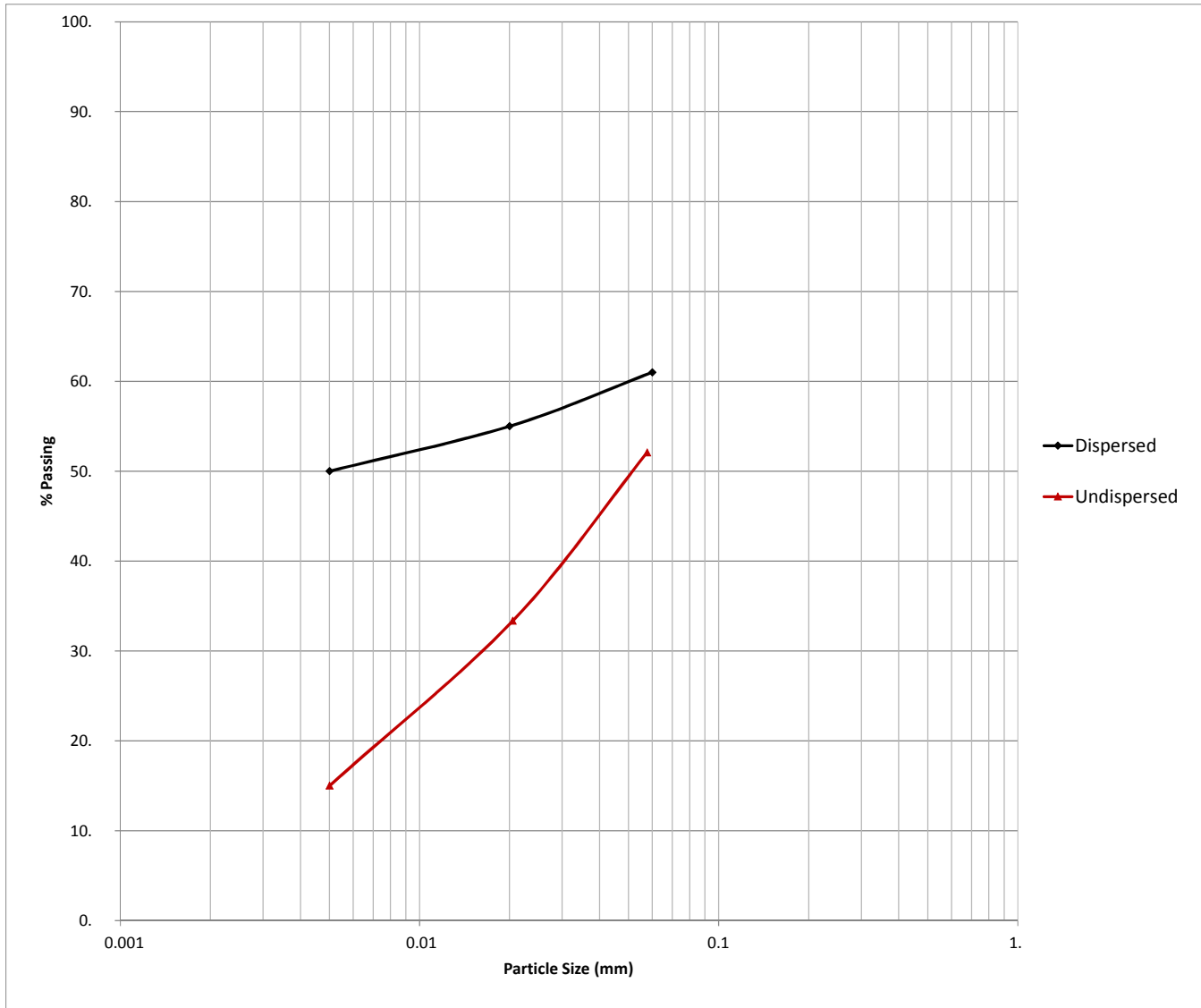
Double Hydrometer Test Result

ASTM
D4221

Client University of Pretoria
Sample no TP09/5
Lab no 7/3746

Project Sub-surface erosion research project
Depth (m) 0.8-1.8

Job no 2017-C-813
Date 2017/08/25



Dispersion:

30%



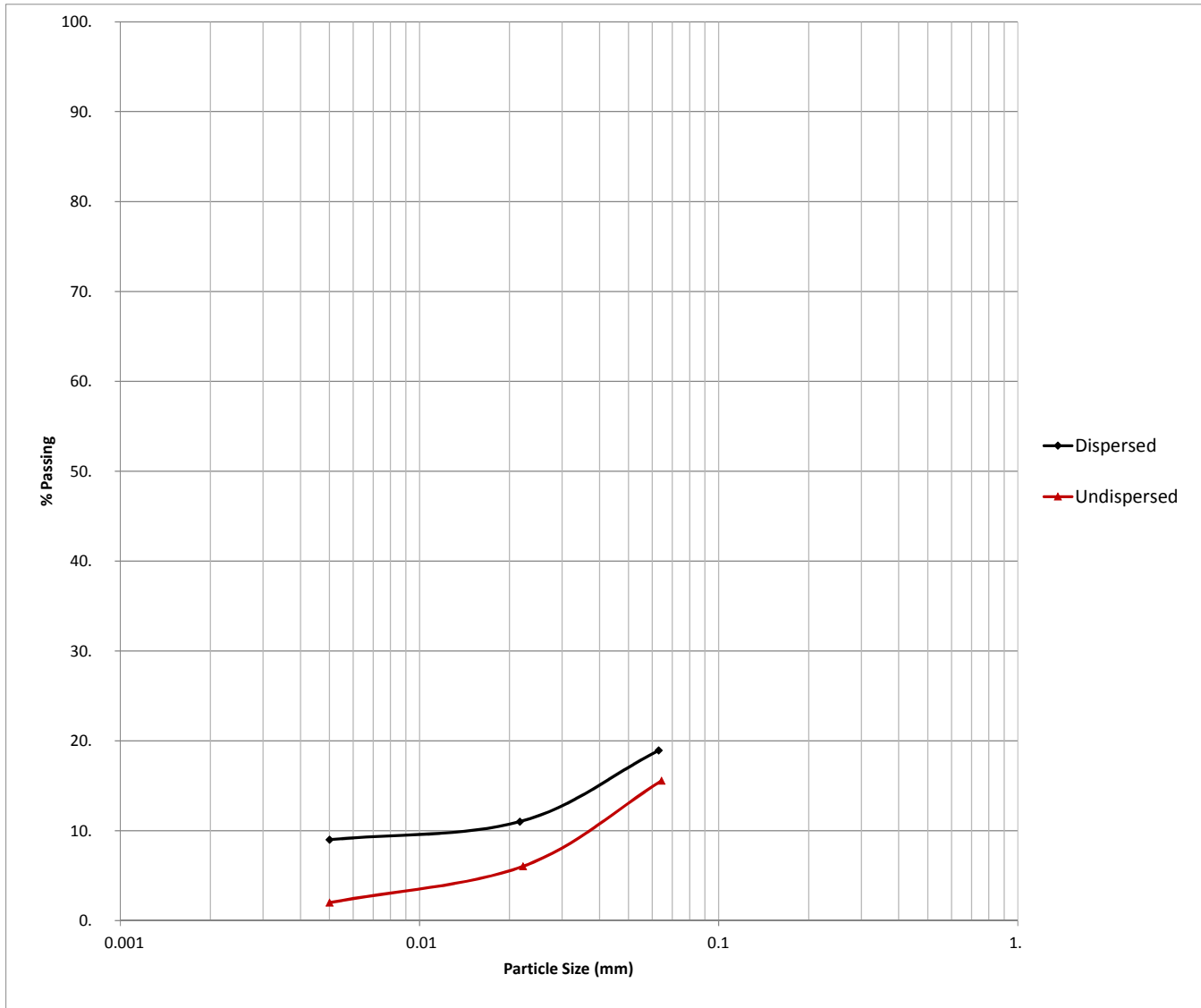
Double Hydrometer Test Result

ASTM
D4221

Client University of Pretoria
Sample no TP10/4
Lab no 7/3749

Project Sub-surface erosion research project
Depth (m) 0-0.4

Job no 2017-C-813
Date 2017/08/25



Dispersion:

22%



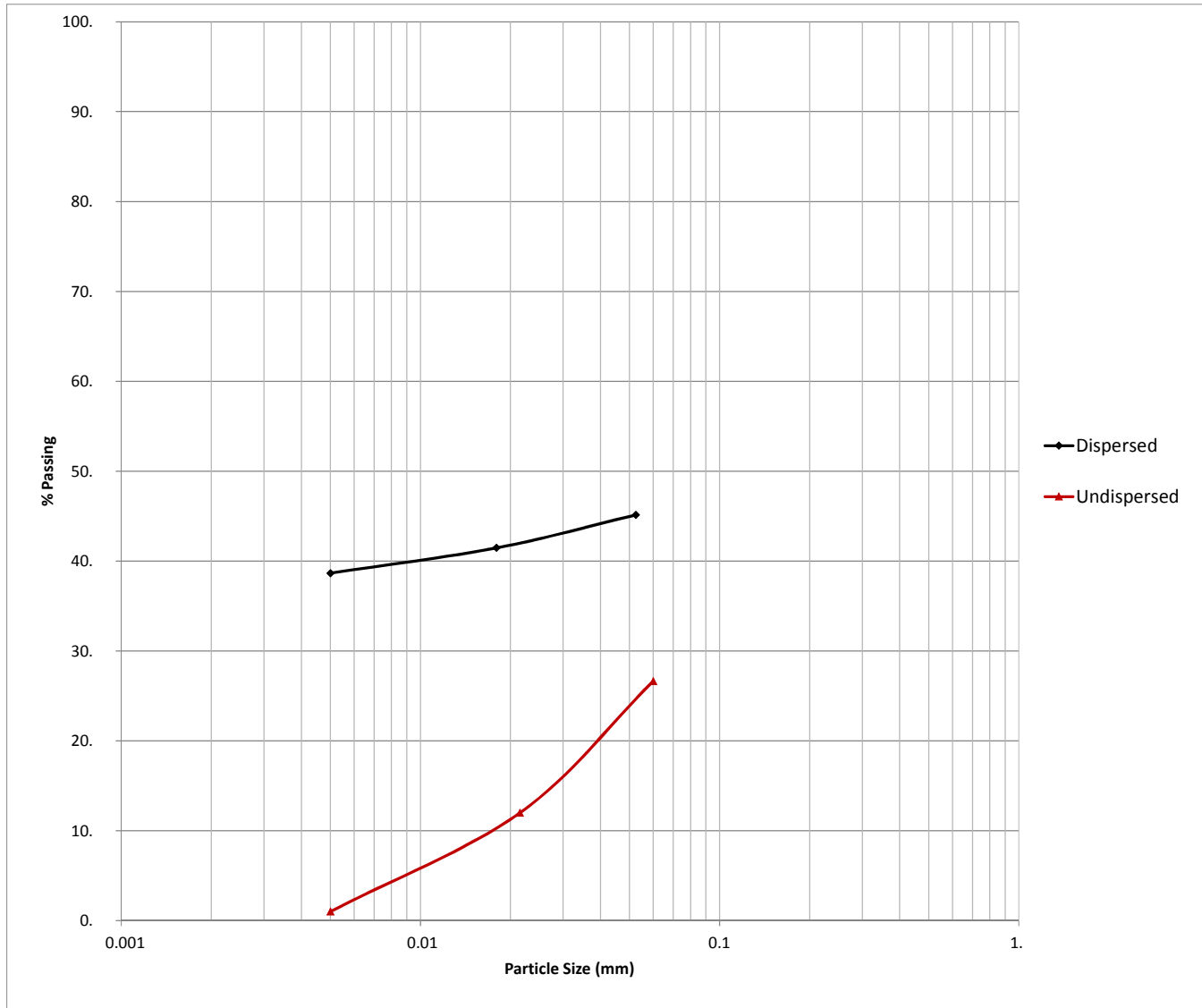
Double Hydrometer Test Result

ASTM
D4221

Client University of Pretoria
Sample no TP10/5
Lab no 7/3750

Project Sub-surface erosion research project
Depth (m) 0.45-1.3

Job no 2017-C-813
Date 2017/08/25



Dispersion:

3%



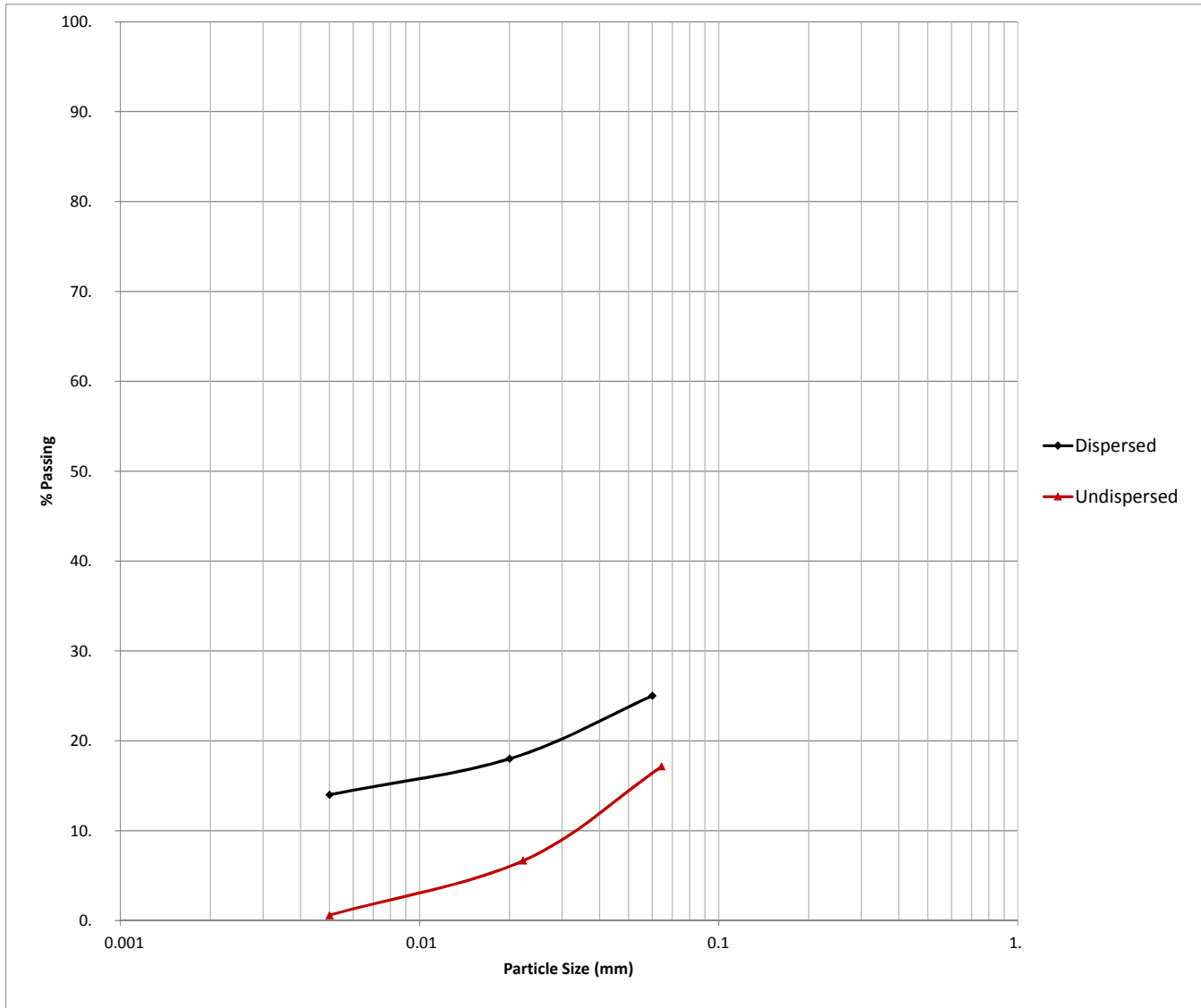
Double Hydrometer Test Result

ASTM
D4221

Client University of Pretoria
Sample no TP12/2
Lab no 7/3752

Project Sub-surface erosion research project
Depth (m) 0.8-1.3

Job no 2017-C-813
Date 2017/08/25



Dispersion:

4%

SGS MATROLAB (PTY) LTD
 - CIVIL ENGINEERING SERVICES -
 Reg.No.: 2003/021980/07 - VAT. Reg.No.: 4040210587
 a SANAS Accredited Testing Laboratory, No. T0025

256 Brander Street, Jan Niemand Park, Pretoria.
 P.O Box 912387, Silverton, 0127
 Tel. : (012) 800 1299
 Fax : (012) 800 3043
 Email : bennie.vanniekerk@sgs.com

TEST RESULTS

UNIVERSITY OF PRETORIA
 THE DIRECTOR FINANCE
 PRETORIA
 0002
 Attention: Petro Venter

Project : Subsurface Erosion Research Project

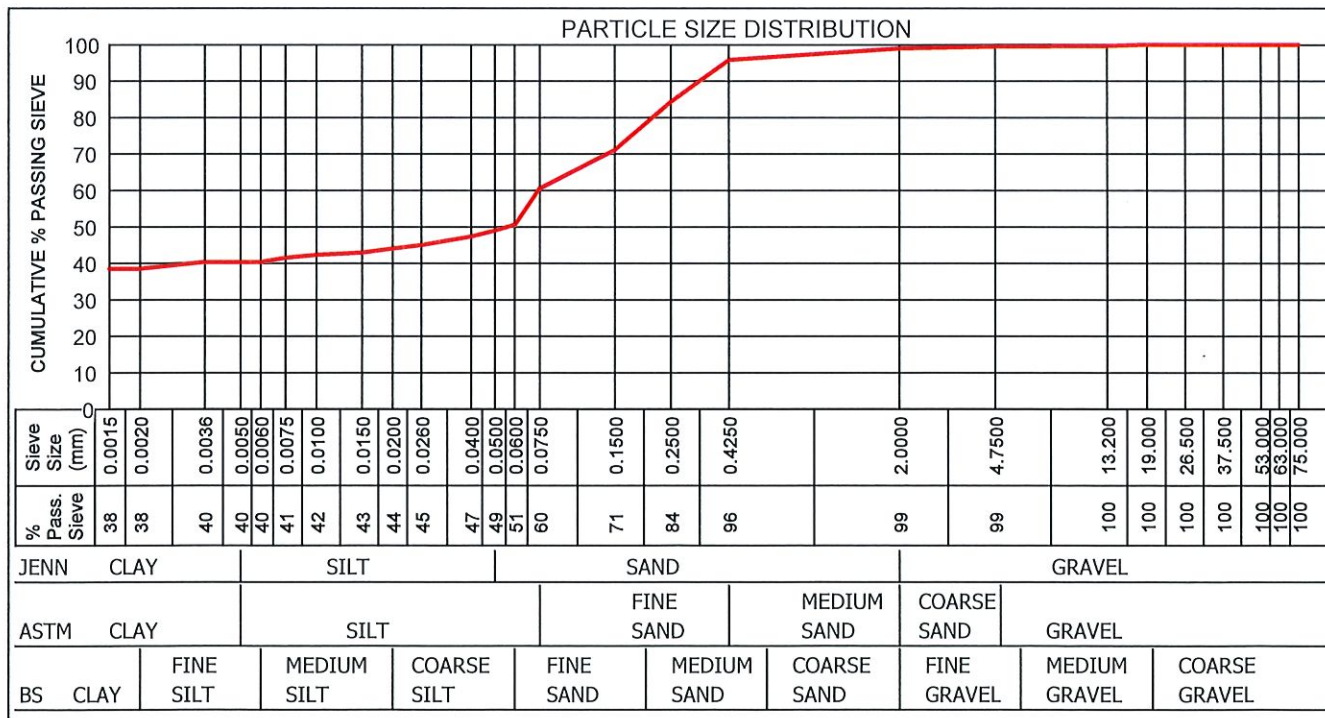
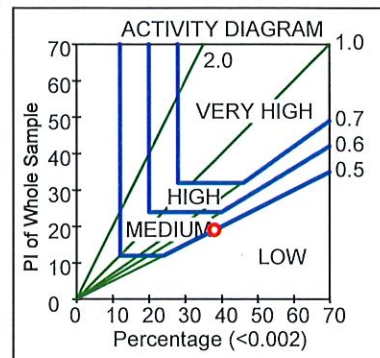
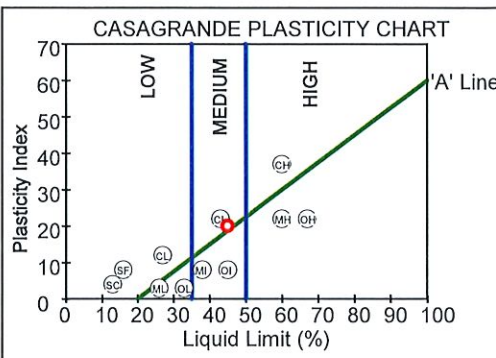
Your Ref :
 Our Ref : PL/20819
 Date Reported : 11.10.2017

FOUNDATION INDICATOR (ASTM: D422)

Sample No. : A7/2487
 Hole No. : TP 18/2
 Depth : 2500
 Liquid Limit (%) : 45
 Plasticity Index : 20
 Linear Shrinkage (%) : 8.5
 PI of Whole Sample : 19
 P.R.A. Classification : A-7-6(10)
 Unified Soil Classification: CL
 Activity : 0.50
 Heave Classification : MEDIUM
 Grading Modulus : 0.45
 Percentage (<0.002) : 38.0
 Moisture Content (%) : 18.4

Material Description : Light grey SANDY CLAY

	Clay (%)	Silt (%)	Sand (%)	Gravel (%)	Classification
Jennings	40.3	8.6	50.0	1.1	SANDY CLAY
Astm	40.3	20.2	38.9	0.6	SANDY CLAY
British Standard	38.4	12.2	48.3	1.1	SANDY CLAY



Remarks : Sampled by client.

FORM: A6

4.4.0(SGS)(2016.08.31) Technical Signatory : B.Van Niekerk / A.Verwey / S.Dewnath

MATROLAB IS NOW PART OF SGS, THE WORLD'S LEADING INSPECTION, VERIFICATION, TESTING AND CERTIFICATION COMPANY.

This document is issued by the Company under its General Condition of Service accessible at http://www.sgs.com/en/Terms_and_Conditions.aspx. Attention is drawn to the limitation of liability, indemnification and jurisdiction issues defined therein.

TEST RESULTS

UNIVERSITY OF PRETORIA
THE DIRECTOR FINANCE
PRETORIA
0002
Attention: Petro Venter

Project : Subsurface Erosion Research Project

Your Ref :
Our Ref : PL/20819
Date Reported : 11.10.2017

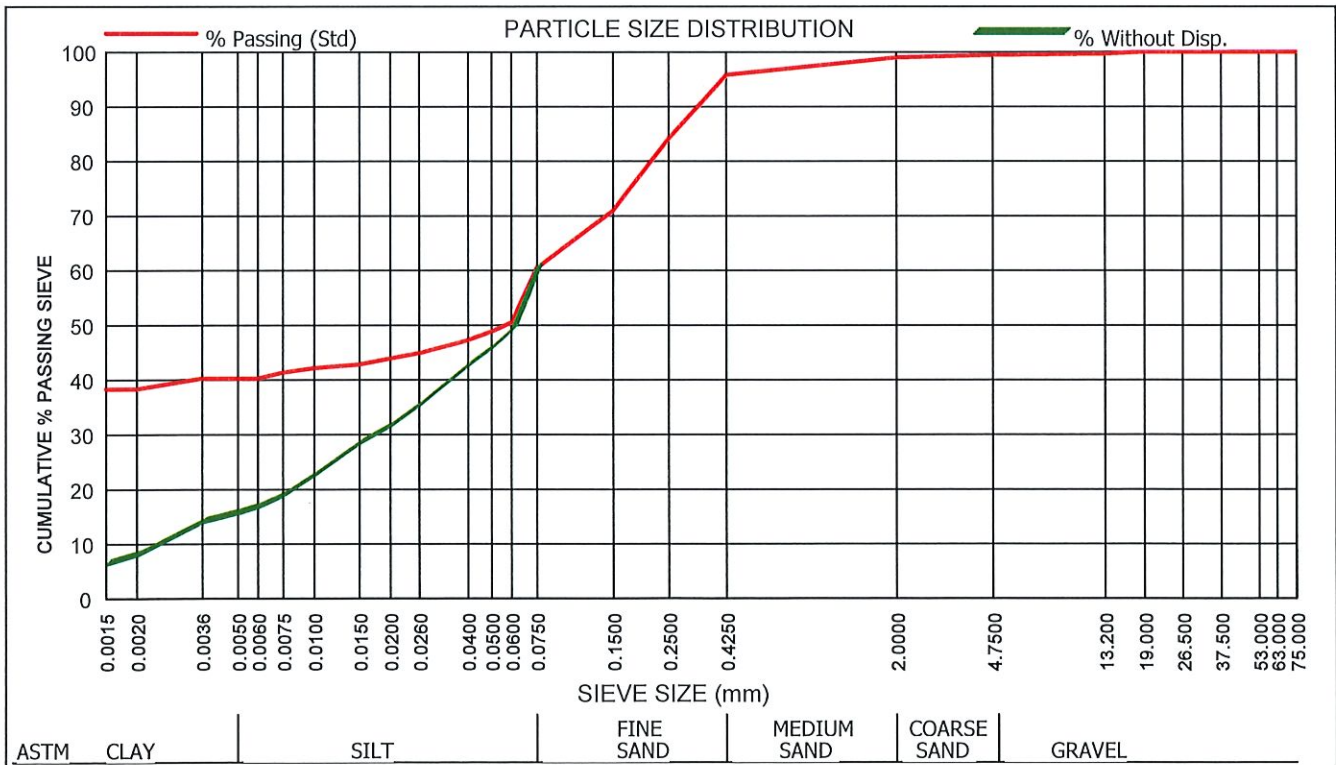
DOUBLE HYDROMETER (ASTM: D422)

Sample No. : A7/2487	Liquid Limit (%) : 5	PI of Whole Sample : 19	P.R.A. Classification : A-6(9)
Hole No. : TP18/2	Plasticity Index : 20	Grading Modulus : 0.45	Unified Soil Classifier: CL
Depth : 2500	Linear Shrinkage (%) : 8.5	Percentage (<0.002) : 38.0	Activity : 0.50
		Moisture Content (%)	Heave Classification : MEDIUM
Description : Light grey SANDY CLAY			

Dispersion (%)	Clay (%)	Silt (%)	Sand (%)	Gravel (%)	Classification
20.4	40.2	20.1	39.1	0.6	SANDY CLAY

Sieve Size (mm)	75.000	63.000	53.000	37.500	26.500	19.000	13.200	4.7500	2.0000	0.4250	0.2500	0.1500	0.0750
% Passing Sieve	100	100	100	100	100	100	100	99	99	96	84	71	60

Sieve Size (mm)	0.0600	0.0500	0.0400	0.0260	0.0200	0.0150	0.0100	0.0075	0.0060	0.0050	0.0036	0.0020	0.0015
% Passing (Std)	50.48	48.82	47.16	44.88	43.87	42.77	42.13	41.30	40.22	40.22	40.22	38.30	38.30
% Without Disp.	49.11	45.76	42.41	35.39	31.50	28.28	22.43	18.64	16.61	15.44	13.82	7.81	6.15



Remarks : Sampled by client.

FORM: A6



4.4.0(SGS)(2016.08.31)

Technical Signatory : B. Van Niekerk / A. Verwey / B. Dewnath

MATROLAB IS NOW PART OF SGS, THE WORLD'S LEADING INSPECTION, VERIFICATION, TESTING AND CERTIFICATION COMPANY.

This document is issued by the Company under its General Condition of Service accessible at http://www.sgs.com/en/Terms_and_Conditions.aspx. Attention is drawn to the limitation of liability, indemnification and jurisdiction issues defined therein.

TEST RESULTS

UNIVERSITY OF PRETORIA
 THE DIRECTOR FINANCE
 PRETORIA
 0002
 Attention: Petro Venter

Project : Subsurface Erosion Research Project

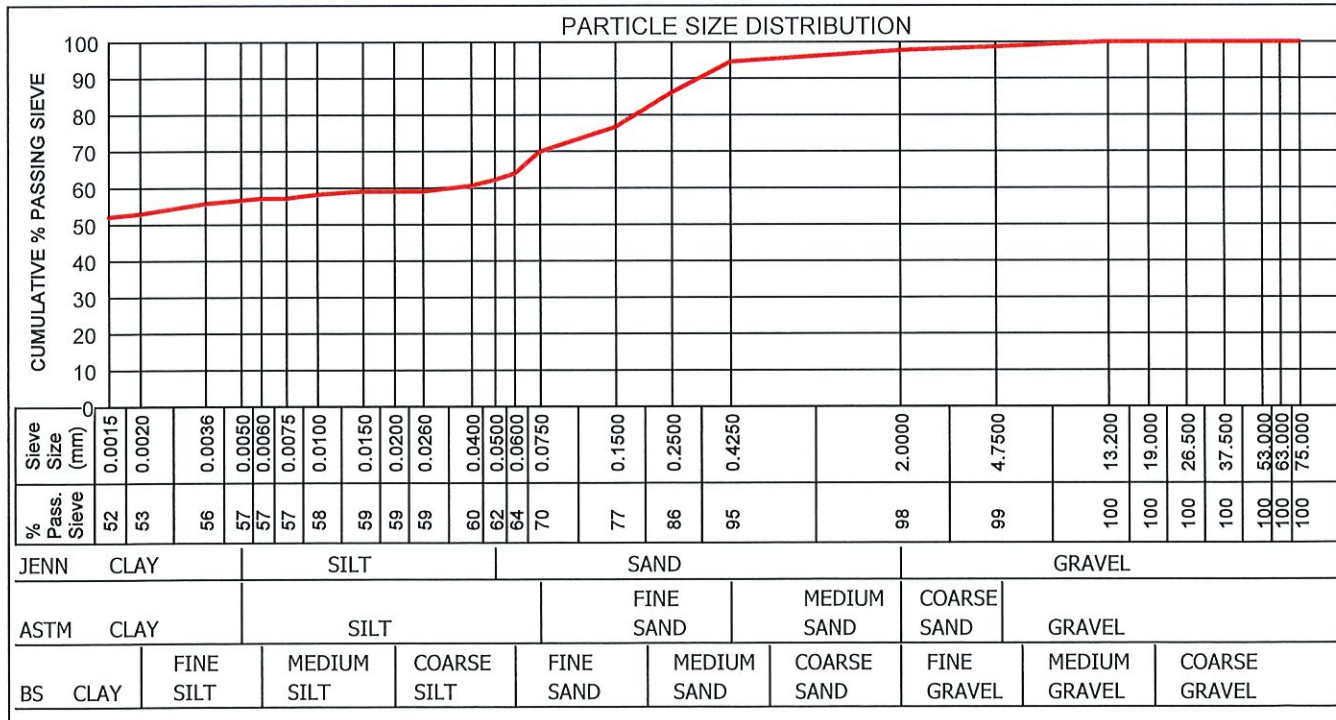
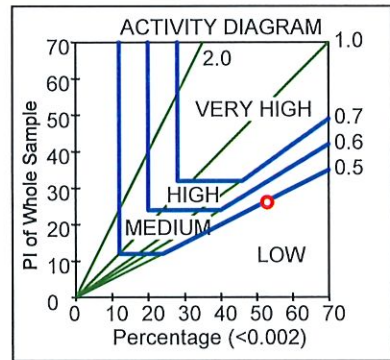
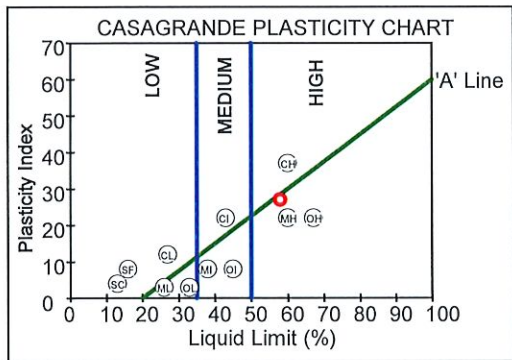
Your Ref :
 Our Ref : PL/20819
 Date Reported : 11.10.2017

FOUNDATION INDICATOR (ASTM: D422)

Sample No. : A7/2488
 Hole No. : TP 18/4
 Depth : 500-2000
 Liquid Limit (%) : 58
 Plasticity Index : 27
 Linear Shrinkage (%) : 13.0
 PI of Whole Sample : 26
 P.R.A. Classification : A-7-5(17)
 Unified Soil Classificati: OH
 Activity : 0.49
 Heave Classification : LOW
 Grading Modulus : 0.37
 Percentage (<0.002) : 53.0
 Moisture Content (%) : 24.8

Material Description : Dark yellow brown CLAY

	Clay (%)	Silt (%)	Sand (%)	Gravel (%)	Classification
Jennings	56.5	5.6	35.4	2.5	CLAY
Astm	56.5	13.2	28.9	1.4	CLAY
British Standard	52.8	11.0	33.7	2.5	CLAY



Remarks : Sampled by client.

FORM: A6

4.4.0(SGS)(2016.08.31)

Technical Signatory : B.Van Niekerk / A.Verwey / S.Dewnath

MATROLAB IS NOW PART OF SGS, THE WORLDS'S LEADING INSPECTION, VERIFICATION, TESTING AND CERTIFICATION COMPANY.

This document is issued by the Company under its General Condition of Service accessible at <http://www.sgs.com/en/Terms and Conditions.aspx>. Attention is drawn to the limitation of liability, indemnification and jurisdiction issues defined therein.

TEST RESULTS

UNIVERSITY OF PRETORIA
THE DIRECTOR FINANCE
PRETORIA
0002
Attention: Petro Venter

Project : Subsurface Erosion Research Project

Your Ref :
Our Ref : PL/20819
Date Reported : 11.10.2017

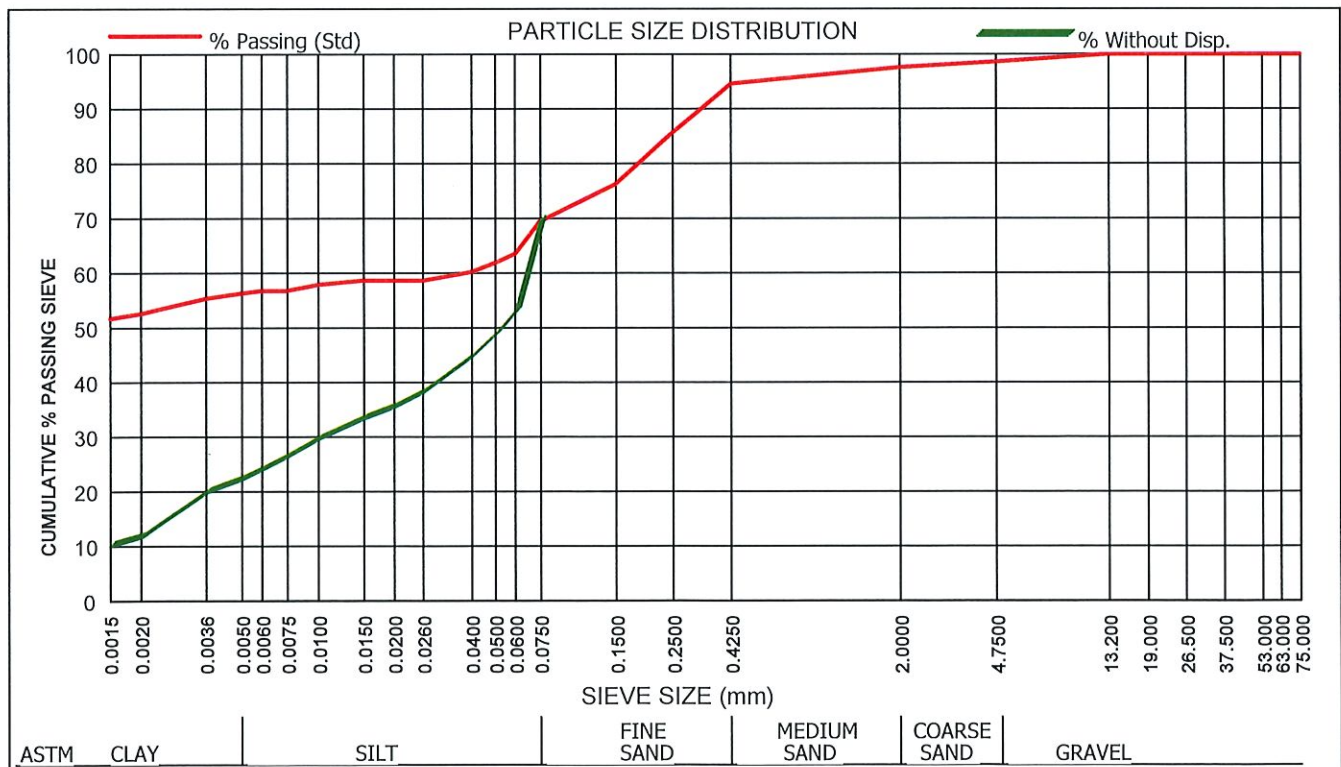
DOUBLE HYDROMETER (ASTM: D422)

Sample No. : A7/2488	Liquid Limit (%) : 58	PI of Whole Sample : 26	P.R.A. Classification : A-7-5(17)
Hole No. : TP 18/4	Plasticity Index : 27	Grading Modulus : 0.39	Unified Soil Classifier: OH
Depth : 500-2000	Linear Shrinkage (%) : 13.0	Percentage (<0.002) : 53.0	Activity : 0.49
		Moisture Content (%)	Heave Classification : LOW
Description : Dark yellow brown CLAY			

Dispersion (%)	Clay (%)	Silt (%)	Sand (%)	Gravel (%)	Classification
22.0	56.2	13.1	29.2	1.4	CLAY

Sieve Size (mm)	75.000	63.000	53.000	37.500	26.500	19.000	13.200	4.7500	2.0000	0.4250	0.2500	0.1500	0.0750
% Passing Sieve	100	100	100	100	100	100	100	99	98	95	86	76	69

Sieve Size (mm)	0.0600	0.0500	0.0400	0.0260	0.0200	0.0150	0.0100	0.0075	0.0060	0.0050	0.0036	0.0020	0.0015
% Passing (Std)	63.56	61.85	60.13	58.62	58.62	58.62	57.82	56.73	56.73	56.25	55.34	52.57	51.63
% Without Disp.	52.90	48.69	44.47	38.14	35.33	33.21	29.50	26.22	23.86	22.10	19.63	11.56	9.90



Remarks : Sampled by client.

FORM: A6

4.4.0(SGS)(2016.08.31)

Technical Signatory : B.Van Niekerk / A.Verwey / S.Dewnath

MATROLAB IS NOW PART OF SGS, THE WORLD'S LEADING INSPECTION, VERIFICATION, TESTING AND CERTIFICATION COMPANY.

This document is issued by the Company under its General Condition of Service accessible at <http://www.sgs.com/en/Terms and Conditions.aspx>. Attention is drawn to the limitation of liability, indemnification and jurisdiction issues defined therein.

SGS MATROLAB (PTY) LTD
 - CIVIL ENGINEERING SERVICES -
 Reg.No.: 2003/021980/07 - VAT. Reg.No.: 4040210587

256 Brander Street, Jan Niemand Park, Pretoria.
 P.O Box 912387, Silverton, 0127
 Tel. : (012) 800 1299
 Fax : (012) 800 3043
 Email : bennie.vanniekerk@sgs.com

a SANAS Accredited Testing Laboratory, No. T0025

TEST RESULTS

UNIVERSITY OF PRETORIA
 THE DIRECTOR FINANCE
 PRETORIA
 0002
 Attention: Petro Venter

Project : Subsurface Erosion Research Project

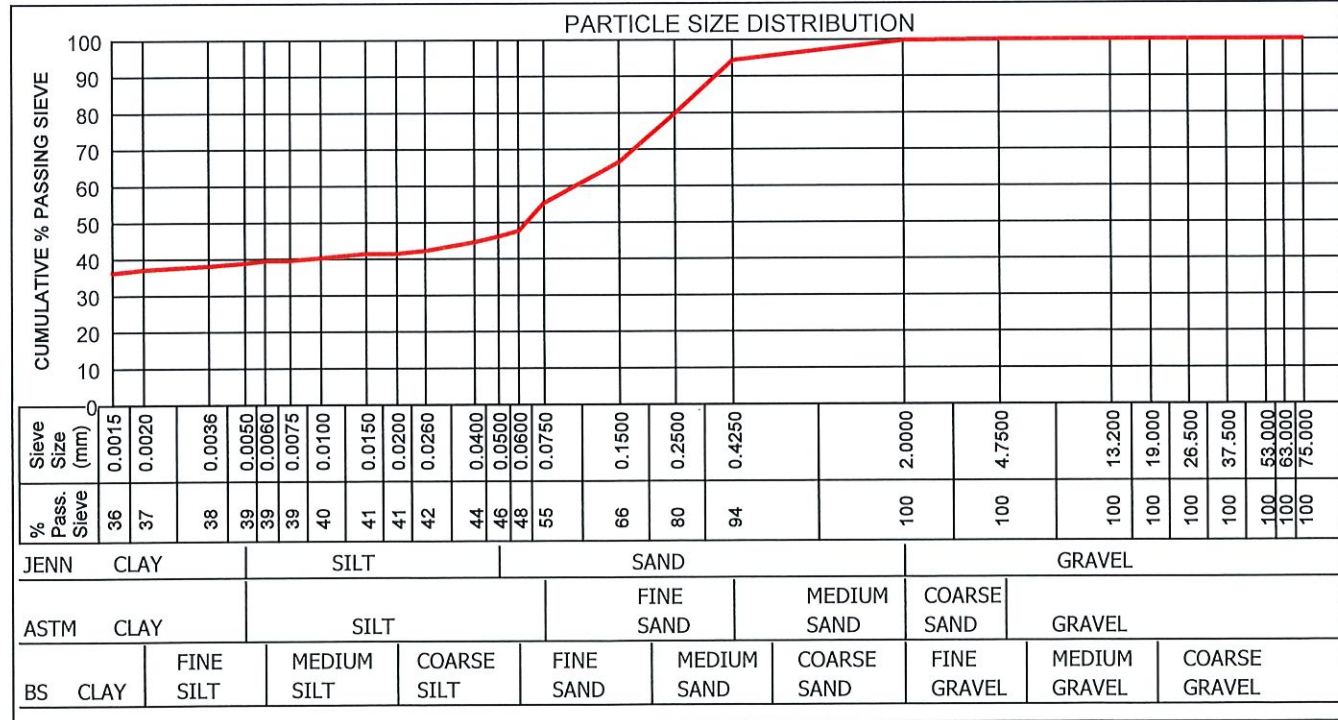
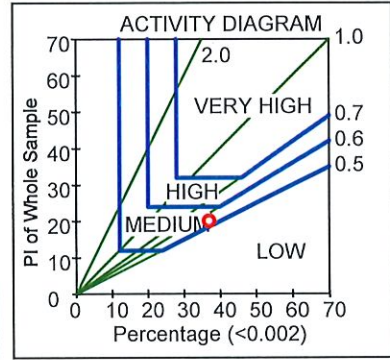
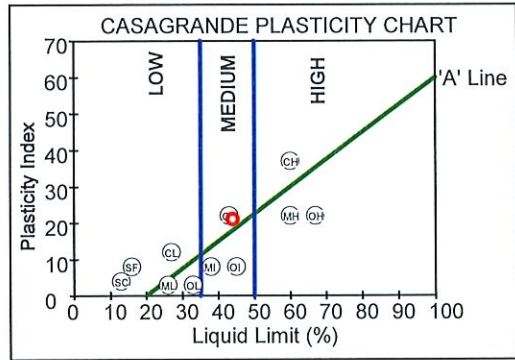
Your Ref :
 Our Ref : PL/20819
 Date Reported : 11.10.2017

FOUNDATION INDICATOR (ASTM: D422)

Sample No. : A7/2489
 Hole No. : TP 18/6
 Depth : 2550
 Liquid Limit (%) : 44
 Plasticity Index : 21
 Linear Shrinkage (%) : 8.0
 PI of Whole Sample : 20
 P.R.A. Classification : A-7-6(9)
 Unified Soil Classificati: CL
 Activity : 0.54
 Heave Classification : MEDIUM
 Grading Modulus : 0.51
 Percentage (<0.002) : 37.0
 Moisture Content (%) : 18.7

Material Description : Light brown SANDY CLAY

	Clay (%)	Silt (%)	Sand (%)	Gravel (%)	Classification
Jennings	38.8	7.2	53.7	0.4	SANDY CLAY
Astm	38.8	16.3	44.8	0.1	SANDY CLAY
British Standard	37.0	10.6	52.1	0.4	SANDY CLAY



Remarks : Sampled by client.

FORM: A6

Technical Signatory : *B. Van Niekerk / A. Verwey / S. Dornath*

4.4.0(SGS)(2016.08.31)

MATROLAB IS NOW PART OF SGS, THE WORLDS'S LEADING INSPECTION, VERIFICATION, TESTING AND CERTIFICATION COMPANY.

This document is issued by the Company under its General Condition of Service accessible at <http://www.sgs.com/en/Terms and Conditions.aspx>. Attention is drawn to the limitation of liability, indemnification and jurisdiction issues defined therein.

SGS MATROLAB (PTY) LTD
 - CIVIL ENGINEERING SERVICES -
 Reg.No.: 2003/021980/07 - VAT. Reg.No.: 4040210587
 a SANAS Accredited Testing Laboratory, No. T0025

256 Brander Street, Jan Niemand Park, Pretoria.
 P.O Box 912387, Silverton, 0127
 Tel. : (012) 800 1299
 Fax : (012) 800 3043
 Email : bennie.vanniekerk@sgs.com

TEST RESULTS

UNIVERSITY OF PRETORIA
 THE DIRECTOR FINANCE
 PRETORIA
 0002
 Attention: Petro Venter

Project : Subsurface Erosion Research Project

Your Ref :
 Our Ref : PL/20819
 Date Reported : 11.10.2017

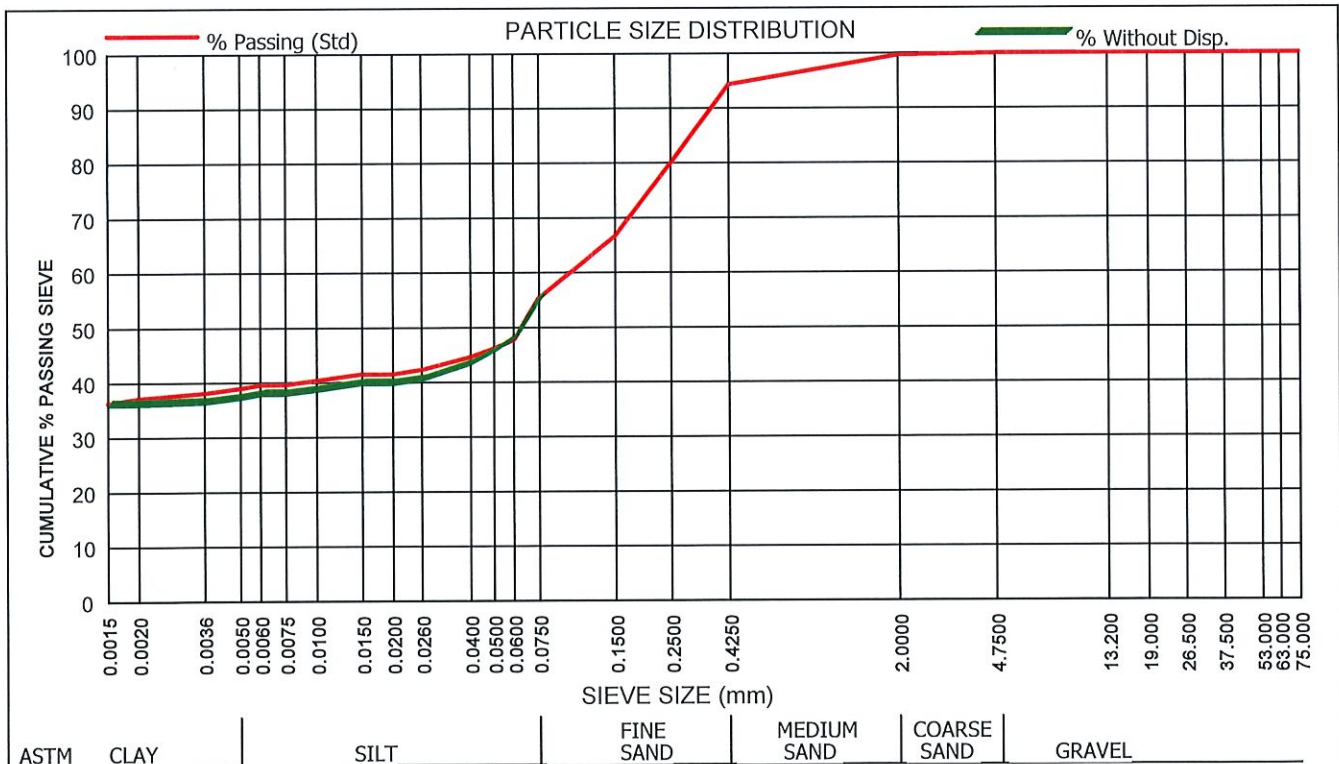
DOUBLE HYDROMETER (ASTM: D422)

Sample No. : A7/2489	Liquid Limit (%) : 44	PI of Whole Sample : 20	P.R.A. Classification : A-7-6(9)
Hole No. : TP 18/6	Plasticity Index : 21	Grading Modulus : 0.51	Unified Soil Classification: CL
Depth : 2550	Linear Shrinkage (%) : 8.0	Percentage (<0.002) : 37.0	Activity : 0.54
		Moisture Content (%)	Heave Classification : MEDIUM
Description : Light brown SANDY CLAY			

Dispersion (%)	Clay (%)	Silt (%)	Sand (%)	Gravel (%)	Classification
96.4	38.9	16.3	44.7	0.1	SANDY CLAY

Sieve Size (mm)	75.000	63.000	53.000	37.500	26.500	19.000	13.200	4.7500	2.0000	0.4250	0.2500	0.1500	0.0750
% Passing Sieve	100	100	100	100	100	100	100	100	100	94	80	67	55

Sieve Size (mm)	0.0600	0.0500	0.0400	0.0260	0.0200	0.0150	0.0100	0.0075	0.0060	0.0050	0.0036	0.0020	0.0015
% Passing (Std)	47.73	46.12	44.51	42.28	41.49	41.49	40.34	39.60	39.53	38.93	38.08	37.15	36.26
% Without Disp.	48.04	45.60	43.15	40.36	39.60	39.60	38.42	37.71	37.63	37.03	36.18	35.83	35.83



Remarks : Sampled by client.

FORM: A6

4.4.0(SGS)(2016.08.31)

Technical Signatory : B.Van Niekerk / A.Verwey / S.Dewnath

MATROLAB IS NOW PART OF SGS, THE WORLD'S LEADING
 INSPECTION, VERIFICATION, TESTING AND CERTIFICATION COMPANY.

This document is issued by the Company under its General Condition of
 Service accessible at <http://www.sgs.com/en/Terms and Conditions.aspx>
 Attention is drawn to the limitation of liability, indemnification and jurisdiction
 issues defined therein.

TEST RESULTS

UNIVERSITY OF PRETORIA
THE DIRECTOR FINANCE
PRETORIA
0002
Attention: Petro Venter

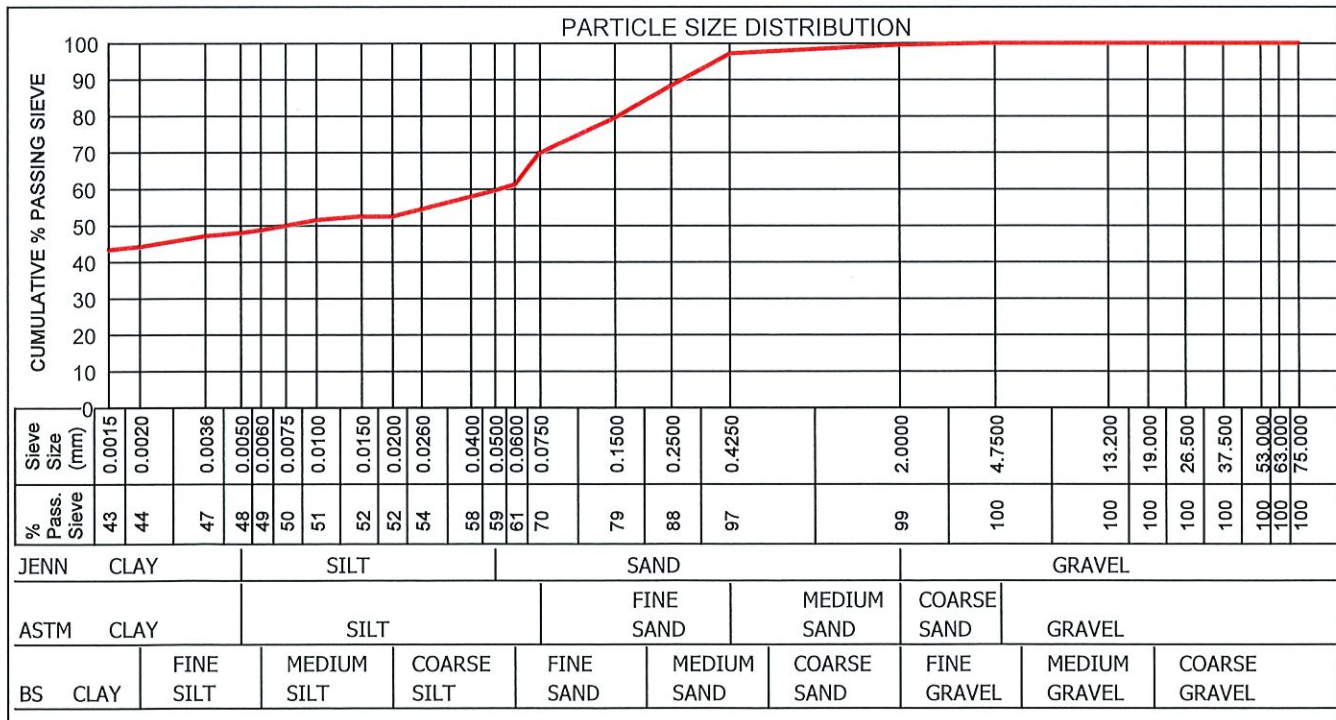
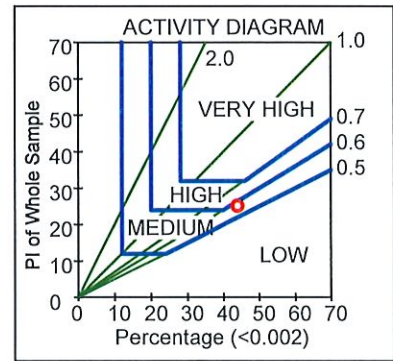
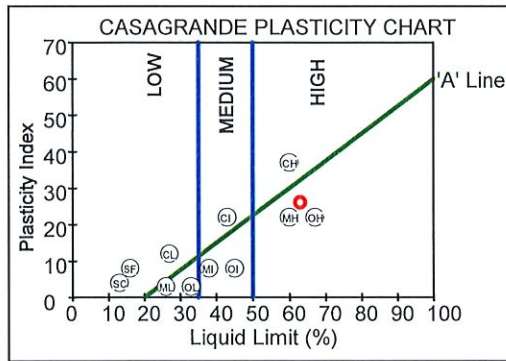
Project : Subsurface Erosion Research Project

Your Ref :
Our Ref : PL/20819
Date Reported : 11.10.2017

FOUNDATION INDICATOR (ASTM: D422)

Sample No. : A7/2491
Hole No. : TP 19/5
Depth : 3000
Liquid Limit (%) : 63
Plasticity Index : 26
Linear Shrinkage (%) : 13.0
PI of Whole Sample : 25
P.R.A. Classification : A-7-5(17)
Unified Soil Classificati: OH
Activity : 0.57
Heave Classification : MEDIUM
Grading Modulus : 0.34
Percentage (<0.002) : 44.0
Moisture Content (%) : 22.5

Material Description : Light grey brown SANDY CLAY					
	Clay (%)	Silt (%)	Sand (%)	Gravel (%)	Classification
Jennings	47.9	11.6	40.0	0.5	SANDY CLAY
Astm	47.9	21.8	30.3	0.1	SANDY CLAY
British Standard	44.1	17.1	38.3	0.5	SANDY CLAY



Remarks : Sampled by client.

FORM: A6

4.4.0(SGS)(2016.08.31)

Technical Signatory : B. Van Niekerk / A. Verwey / S. Dewnath

MATROLAB IS NOW PART OF SGS, THE WORLD'S LEADING INSPECTION, VERIFICATION, TESTING AND CERTIFICATION COMPANY.

This document is issued by the Company under its General Condition of Service accessible at http://www.sgs.com/en/Terms_and_Conditions.aspx. Attention is drawn to the limitation of liability, indemnification and jurisdiction issues defined therein.

TEST RESULTS

UNIVERSITY OF PRETORIA THE DIRECTOR FINANCE PRETORIA 0002 Attention: Petro Venter	Project : Subsurface Erosion Research Project Your Ref : Our Ref : PL/20819 Date Reported : 11.10.2017
---	---

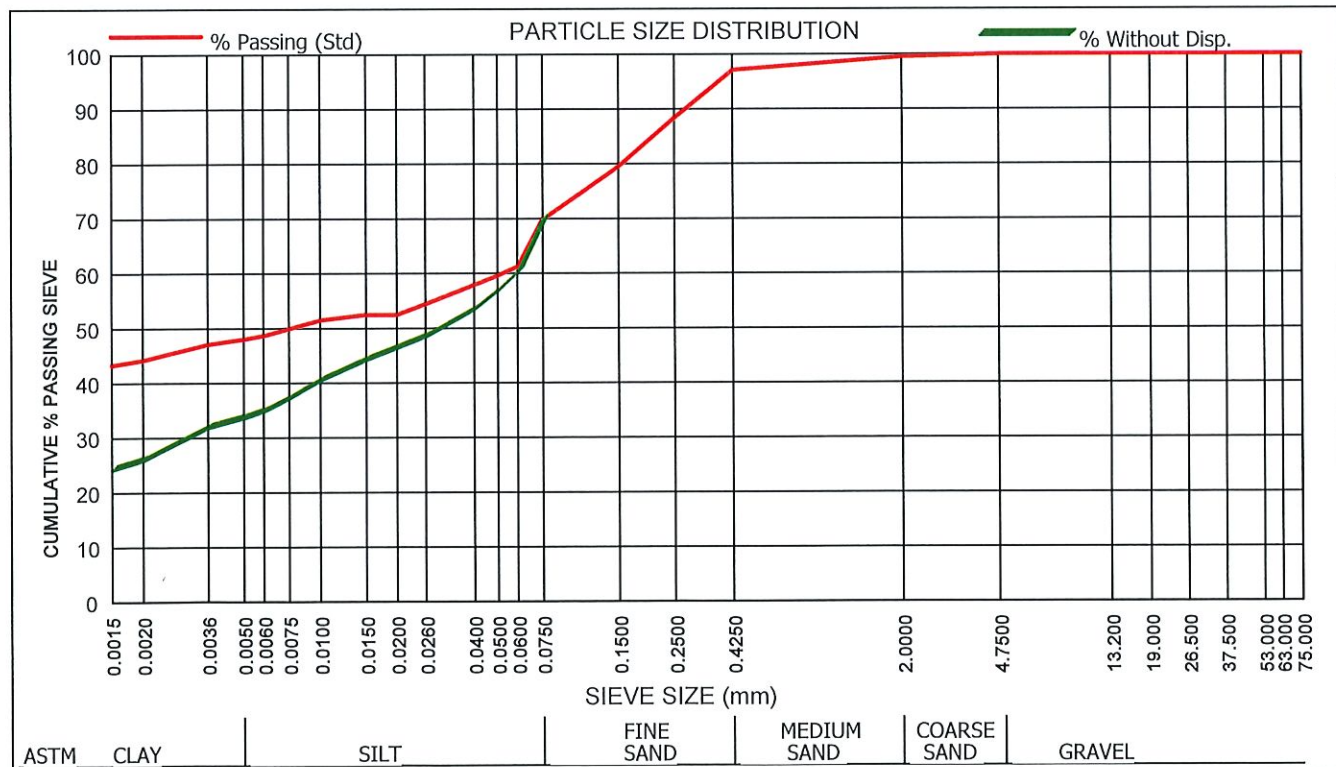
DOUBLE HYDROMETER (ASTM: D422)

Sample No. : A7/2491	Liquid Limit (%) : 63	PI of Whole Sample : 25	P.R.A. Classification : A-7-5(17)
Hole No. : TP 19/5	Plasticity Index : 26	Grading Modulus : 0.34	Unified Soil Classifier: OH
Depth : 3000	Linear Shrinkage (%) : 13.0	Percentage (<0.002) : 44.0	Activity : 0.57
		Moisture Content (%)	Heave Classification : MEDIUM
Description : Light grey brown SANDY CLAY			

Dispersion (%)	Clay (%)	Silt (%)	Sand (%)	Gravel (%)	Classification
58.3	47.9	21.8	30.3	0.1	SANDY CLAY

Sieve Size (mm)	75.000	63.000	53.000	37.500	26.500	19.000	13.200	4.7500	2.0000	0.4250	0.2500	0.1500	0.0750
% Passing Sieve	100	100	100	100	100	100	100	100	99	97	88	79	70

Sieve Size (mm)	0.0600	0.0500	0.0400	0.0260	0.0200	0.0150	0.0100	0.0075	0.0060	0.0050	0.0036	0.0020	0.0015
% Passing (Std)	61.20	59.46	57.73	54.35	52.39	52.39	51.40	49.78	48.56	47.90	47.00	44.12	43.18
% Without Disp.	60.15	56.66	53.16	48.34	46.24	43.99	40.31	36.97	34.68	33.43	31.69	25.73	23.95



Remarks : Sampled by client.

FORM: A6

4.4.0(SGS)(2016.08.31)


 Technical Signatory : B. Van Niekerk / A. Verwey / S. Dewnath

MATROLAB IS NOW PART OF SGS, THE WORLD'S LEADING INSPECTION, VERIFICATION, TESTING AND CERTIFICATION COMPANY.

This document is issued by the Company under its General Condition of Service accessible at <http://www.sgs.com/en/Terms and Conditions.aspx>. Attention is drawn to the limitation of liability, indemnification and jurisdiction issues defined therein.

SGS MATROLAB (PTY) LTD
 - CIVIL ENGINEERING SERVICES -
 Reg.No.: 2003/021980/07 - VAT. Reg.No.: 4040210587
 a SANAS Accredited Testing Laboratory, No. T0025

256 Brander Street, Jan Niemand Park, Pretoria.
 P.O Box 912387, Silverton, 0127
 Tel. : (012) 800 1299
 Fax : (012) 800 3043
 Email : bennie.vanniekerk@sgs.com

TEST RESULTS

UNIVERSITY OF PRETORIA
 THE DIRECTOR FINANCE
 PRETORIA
 0002
 Attention: Petro Venter

Project : Subsurface Erosion Research Project

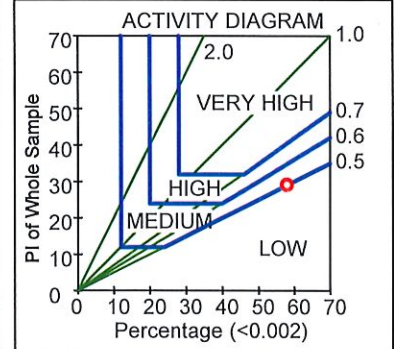
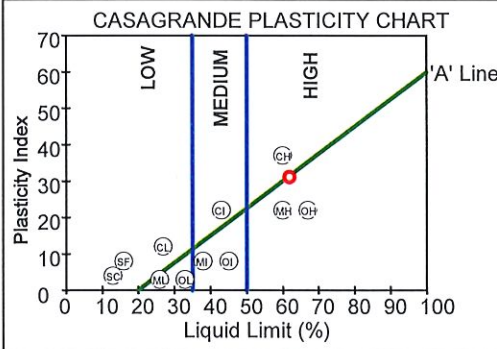
Your Ref :
 Our Ref : PL/20819
 Date Reported : 31.10.2017

FOUNDATION INDICATOR (ASTM: D422)

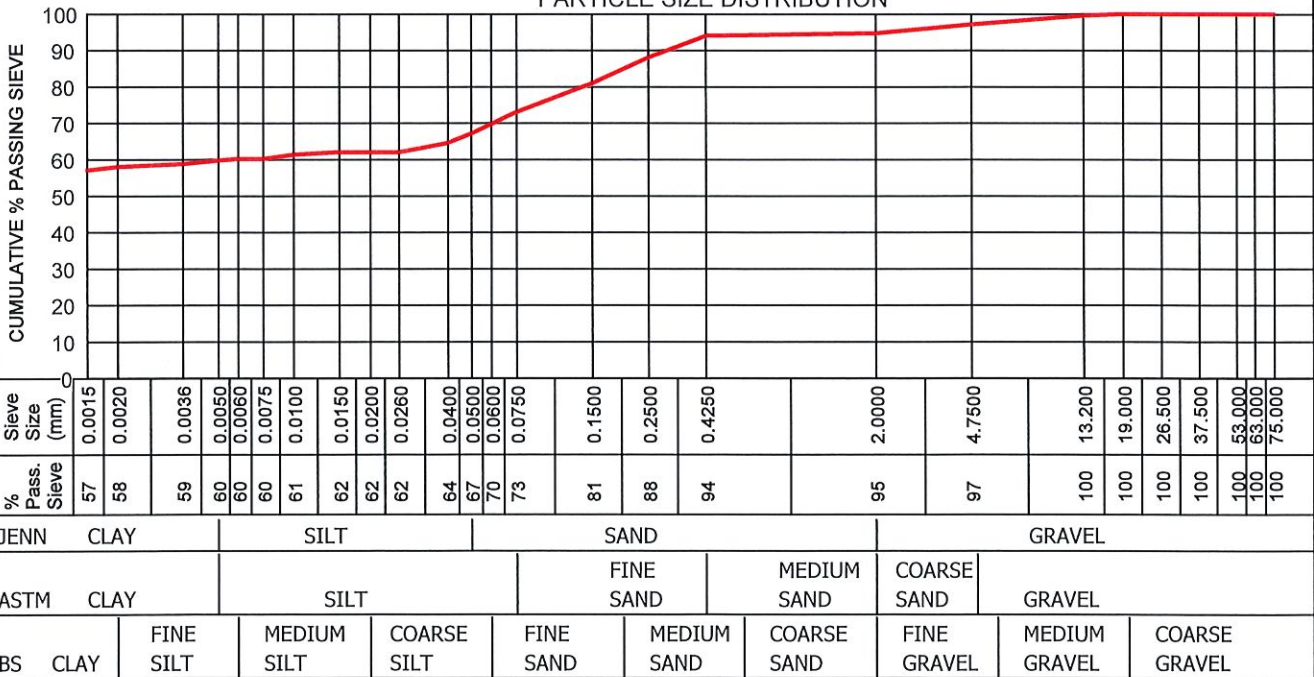
Sample No. : A7/2490
 Hole No. : TP 19/1
 Depth : 500-1300
 Liquid Limit (%) : 62
 Plasticity Index : 31
 Linear Shrinkage (%) : 12.0
 PI of Whole Sample : 29
 P.R.A. Classification : A-7-5(19)
 Unified Soil Classification: OH
 Activity : 0.50
 Heave Classification : MEDIUM
 Grading Modulus : 0.38
 Percentage (<0.002) : 58.0
 Moisture Content (%) : 23.5

Material Description : Dark yellow brown CLAY

	Clay (%)	Silt (%)	Sand (%)	Gravel (%)	Classification
Jennings	59.7	7.4	27.5	5.3	CLAY
Astm	59.7	13.2	24.1	2.9	CLAY
British Standard	58.0	11.8	24.9	5.3	CLAY



PARTICLE SIZE DISTRIBUTION



Remarks : Sampled by client.
 Replacement test report to report dated 11.10.2017.

FORM: A6

4.4.0(SGS)(2016.08.31)

Technical Signatory : B.Van Niekerk / A.Verwey / S.Dewnath

MATROLAB IS NOW PART OF SGS, THE WORLD'S LEADING INSPECTION, VERIFICATION, TESTING AND CERTIFICATION COMPANY.

This document is issued by the Company under its General Condition of Service accessible at http://www.sgs.com/en/terms_and_conditions.aspx. Attention is drawn to the limitation of liability, indemnification and jurisdiction issues defined therein.

SGS MATROLAB (PTY) LTD
- CIVIL ENGINEERING SERVICES -
Reg.No.: 2003/021980/07 - VAT. Reg.No.: 4040210587

a SANAS Accredited Testing Laboratory, No. T0025

256 Brander Street, Jan Niemand Park, Pretoria.
P.O Box 912387, Silverton, 0127
Tel. : (012) 800 1299
Fax : (012) 800 3043
Email : bennie.vanniekerk@sgs.com

TEST RESULTS

UNIVERSITY OF PRETORIA
THE DIRECTOR FINANCE
PRETORIA
0002
Attention: Petro Venter

Project : Subsurface Erosion Research Project

Your Ref :
Our Ref : PL/20819
Date Reported : 11.10.2017

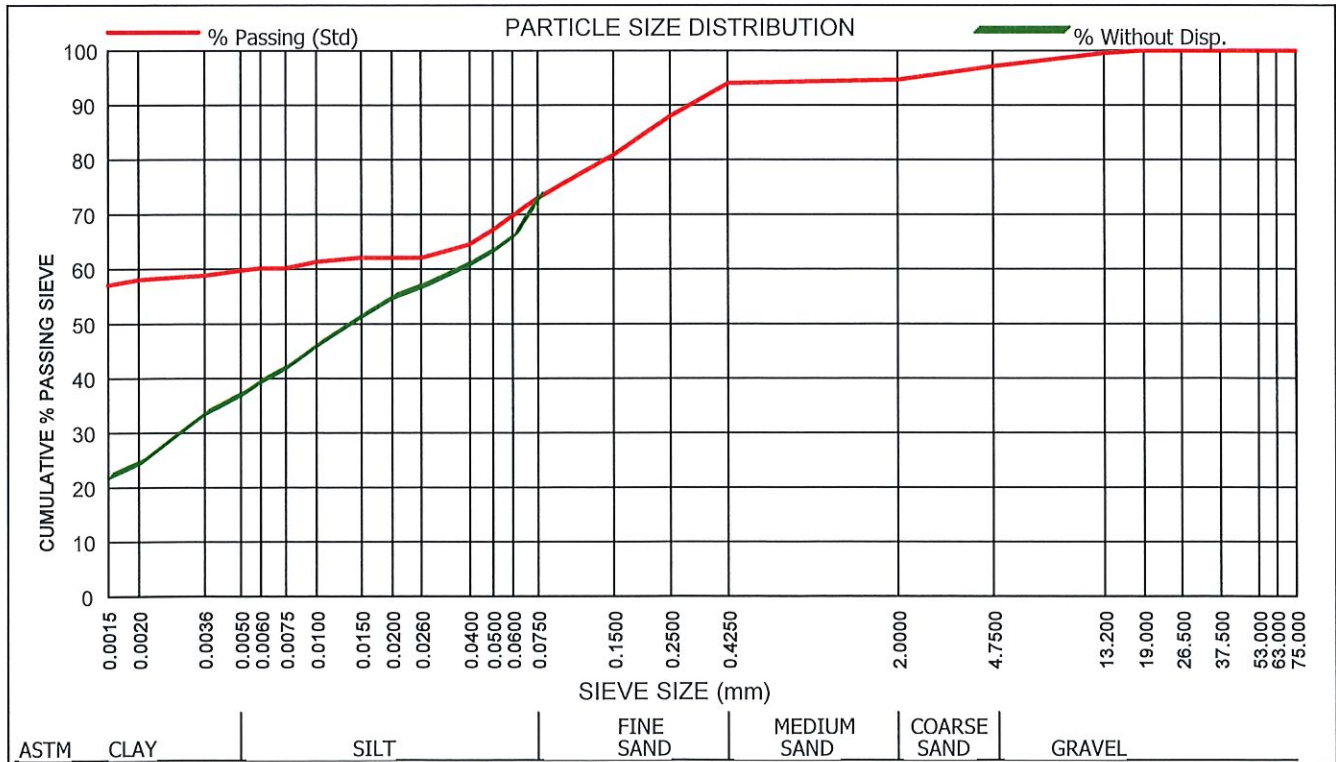
DOUBLE HYDROMETER (ASTM: D422)

Sample No. : A7/2490	Liquid Limit (%) : 62	PI of Whole Sample : 29	P.R.A. Classification : A-7-5(19)
Hole No. : TP 19/1	Plasticity Index : 31	Grading Modulus : 0.38	Unified Soil Classifier: OH
Depth : 500-1300	Linear Shrinkage (%) : 12.0	Percentage (<0.002) : 58.0	Activity : 0.50
		Moisture Content (%)	Heave Classification : MEDIUM
Description : Dark yellow brown CLAY			

Dispersion (%)	Clay (%)	Silt (%)	Sand (%)	Gravel (%)	Classification
41.8	59.7	13.2	24.1	2.9	CLAY

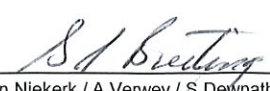
Sieve Size (mm)	75.000	63.000	53.000	37.500	26.500	19.000	13.200	4.7500	2.0000	0.4250	0.2500	0.1500	0.0750
% Passing Sieve	100	100	100	100	100	100	100	97	95	94	88	81	73

Sieve Size (mm)	0.0600	0.0500	0.0400	0.0260	0.0200	0.0150	0.0100	0.0075	0.0060	0.0050	0.0036	0.0020	0.0015
% Passing (Std)	69.80	67.14	64.49	62.04	62.04	62.04	61.32	60.16	60.16	59.72	58.81	57.99	57.03
% Without Disp.	65.81	63.20	60.59	56.54	54.53	51.09	45.82	41.67	39.21	36.75	33.29	24.21	21.61



Remarks : Sampled by client.

FORM: A6



4.4.0(SGS)(2016.08.31)

Technical Signatory : B. Van Niekerk / A. Verwey / S. Dewnath

MATROLAB IS NOW PART OF SGS, THE WORLD'S LEADING INSPECTION, VERIFICATION, TESTING AND CERTIFICATION COMPANY.

This document is issued by the Company under its General Condition of Service accessible at http://www.sgs.com/en/Terms_and_Conditions.aspx. Attention is drawn to the limitation of liability, indemnification and jurisdiction issues defined therein.

TEST RESULTS

UNIVERSITY OF PRETORIA
THE DIRECTOR FINANCE
PRETORIA
0002
Attention: Petro Venter

Project : Subsurface Erosion Research Project

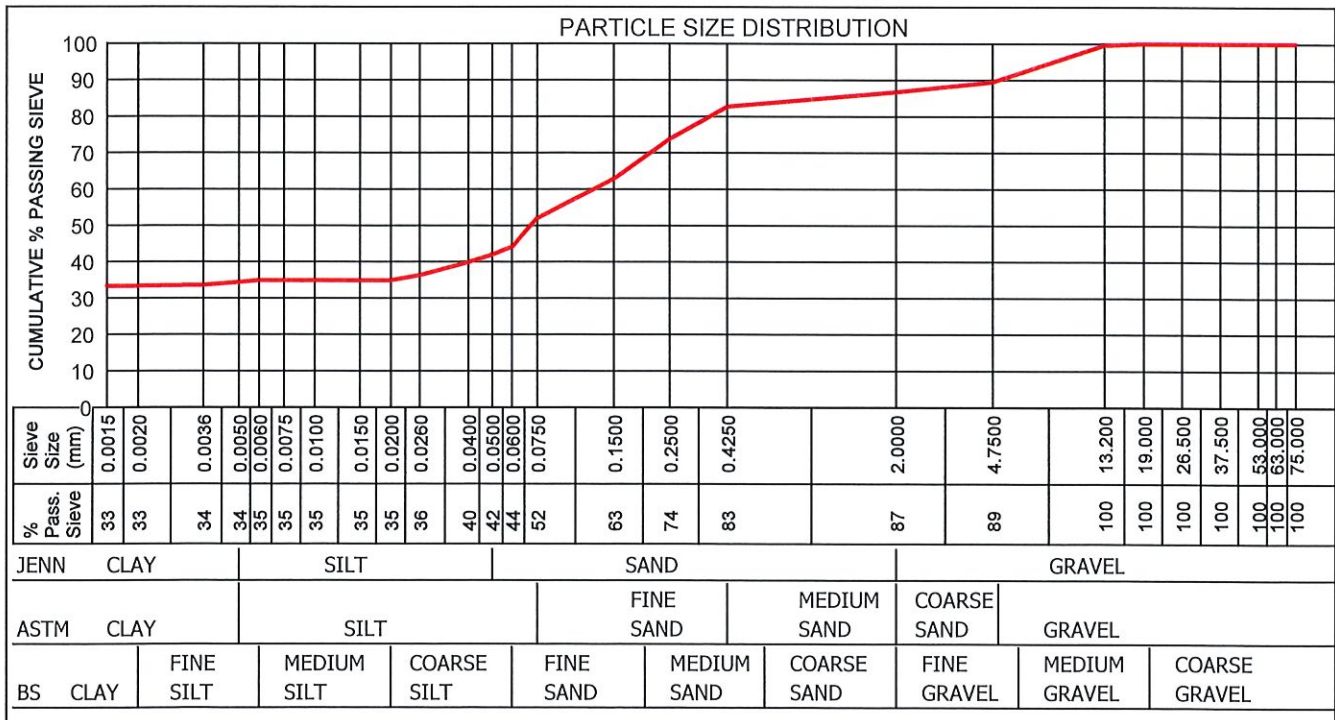
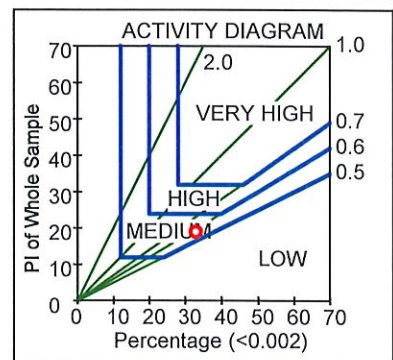
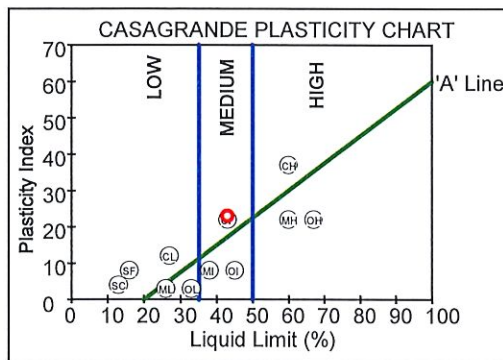
Your Ref :
Our Ref : PL/20819
Date Reported : 31.10.2017

FOUNDATION INDICATOR (ASTM: D422)

Sample No. : A7/2492
Hole No. : TP 20/1
Depth : 1300-3000
Liquid Limit (%) : 43
Plasticity Index : 23
Linear Shrinkage (%) : 10.0
PI of Whole Sample : 19
P.R.A. Classification : A-7-6(8)
Unified Soil Classification: CL
Activity : 0.58
Heave Classification : MEDIUM
Grading Modulus : 0.78
Percentage (<0.002) : 33.0
Moisture Content (%) : 15.3

Material Description : Dark yellow brown SANDY CLAY

	Clay (%)	Silt (%)	Sand (%)	Gravel (%)	Classification
Jennings	34.3	7.6	44.8	13.3	SANDY CLAY
Astm	34.3	17.5	37.6	10.6	SANDY CLAY
British Standard	33.2	10.9	42.6	13.3	SANDY CLAY



Remarks : Sampled by client.
Replacement test report to report dated 11.10.2017.

FORM: A6

4.4.0(SGS)(2016.08.31) Technical Signatory : B.Van Niekerk / A.Verwey / S.Dewnath

SGS MATROLAB (PTY) LTD
 - CIVIL ENGINEERING SERVICES -
 Reg.No.: 2003/021980/07 - VAT. Reg.No.: 4040210587

a SANAS Accredited Testing Laboratory, No. T0025

256 Brander Street, Jan Niemand Park, Pretoria.
 P.O Box 912387, Silverton, 0127
 Tel. : (012) 800 1299
 Fax : (012) 800 3043
 Email : bennie.vanniekerk@sgs.com

TEST RESULTS

UNIVERSITY OF PRETORIA THE DIRECTOR FINANCE PRETORIA 0002 Attention: Petro Venter	Project : Subsurface Erosion Research Project Your Ref : Our Ref : PL/20819 Date Reported : 11.10.2017
---	---

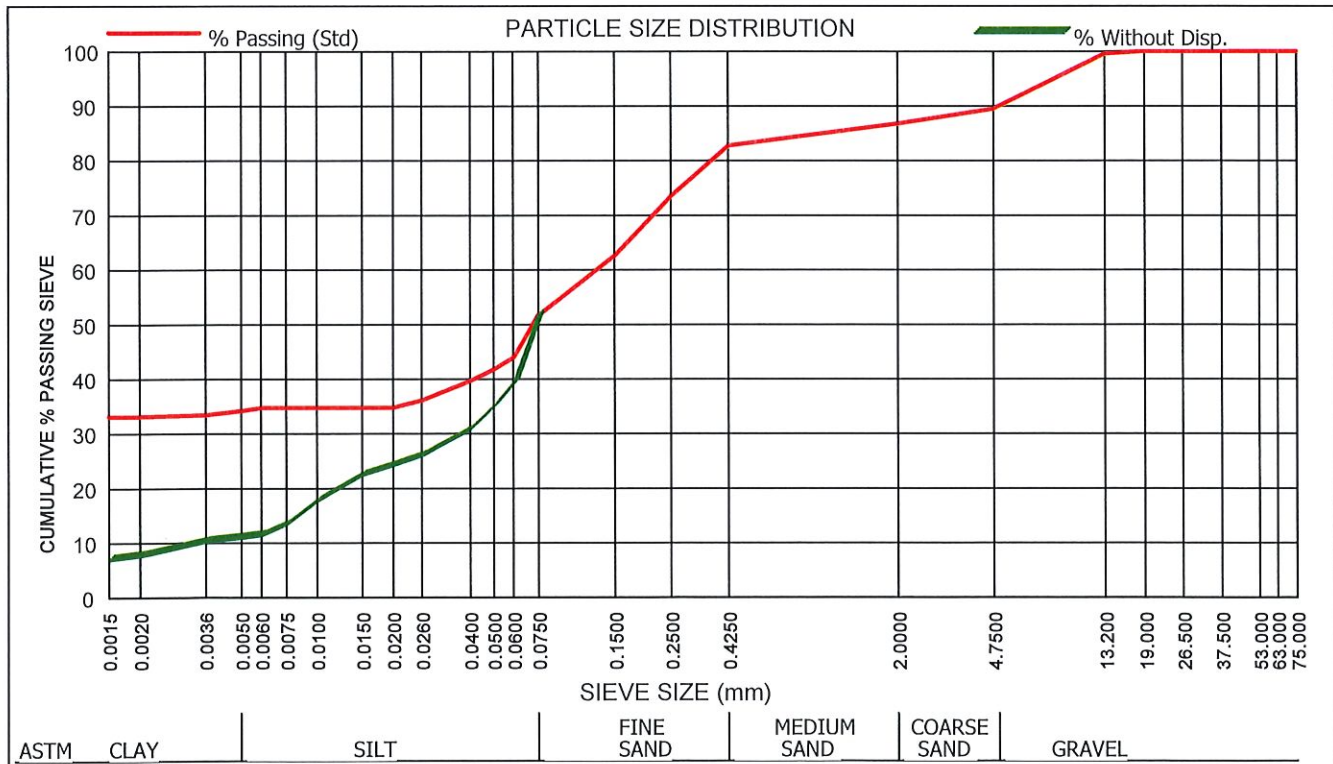
DOUBLE HYDROMETER (ASTM: D422)

Sample No. : A7/2492	Liquid Limit (%) : 43	PI of Whole Sample : 19	P.R.A. Classification : A-7-6(8)
Hole No. : TP 20/1	Plasticity Index : 23	Grading Modulus : 0.79	Unified Soil Classifier: CL
Depth : 1300-3000	Linear Shrinkage (%) : 10.0	Percentage (<0.002) : 33.0	Activity : 0.57
		Moisture Content (%)	Heave Classification : MEDIUM
Description : Dark yellow brown SANDY CLAY			

Dispersion (%)	Clay (%)	Silt (%)	Sand (%)	Gravel (%)	Classification
22.7	34.1	17.5	37.8	10.6	SANDY CLAY

Sieve Size (mm)	75.000	63.000	53.000	37.500	26.500	19.000	13.200	4.7500	2.0000	0.4250	0.2500	0.1500	0.0750
% Passing Sieve	100	100	100	100	100	100	100	89	87	83	73	62	52

Sieve Size (mm)	0.0600	0.0500	0.0400	0.0260	0.0200	0.0150	0.0100	0.0075	0.0060	0.0050	0.0036	0.0020	0.0015
% Passing (Std)	43.88	41.72	39.55	36.08	34.72	34.72	34.72	34.72	34.66	34.13	33.38	33.06	33.06
% Without Disp.	39.32	34.97	30.62	25.90	24.11	22.29	17.61	13.24	11.26	10.77	10.09	7.51	6.80



Remarks : Sampled by client.

FORM: A6

4.4.0(SGS)(2016.08.31)

Technical Signatory : *S. J. Breding*
 B. Van Niekerk / A. Verwey / S. Dewnath

MATROLAB IS NOW PART OF SGS, THE WORLD'S LEADING INSPECTION, VERIFICATION, TESTING AND CERTIFICATION COMPANY.

This document is issued by the Company under its General Condition of Service accessible at http://www.sgs.com/en/Terms_and_Conditions.aspx. Attention is drawn to the limitation of liability, indemnification and jurisdiction issues defined therein.



du Plessis
Civil Engineering

Reg. No: cc 200004833323

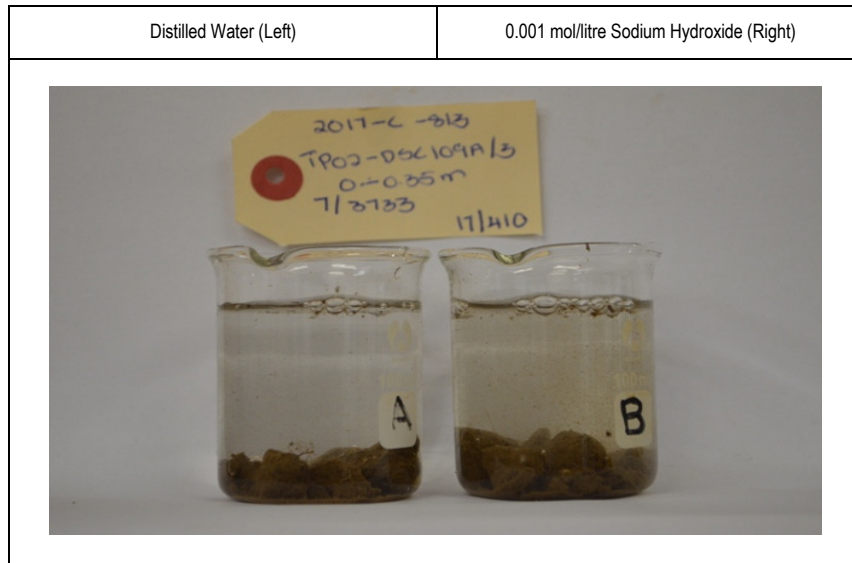
250 ORION Ave
Monument Park
0181

PO Box 26272
Monument Park
0105

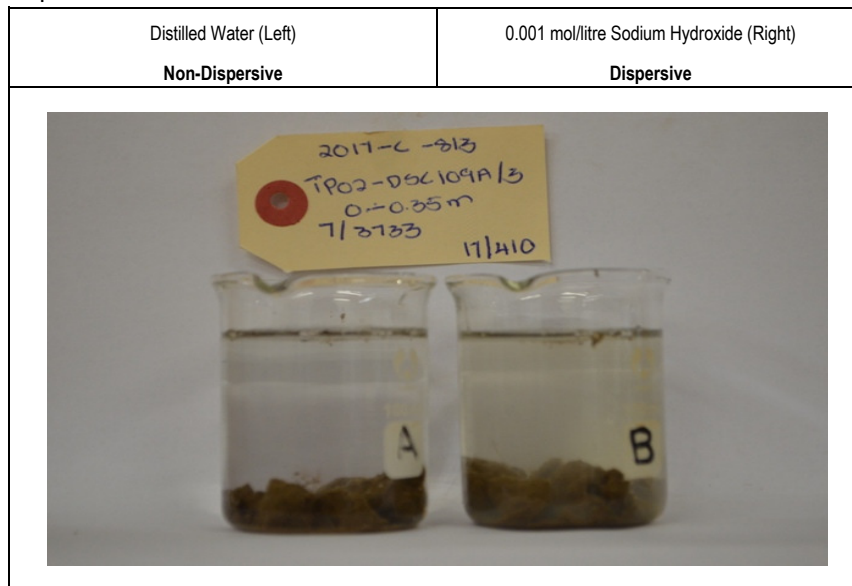
Tel/Fax 012 346 7586
Cell: 082 375 3003
bennie@geotesting.co.za

Client Name:	Geostrada	Date sampled/tested on site:	-
Client Contact:	Hennie Barnard	Sample Receive Date:	11-Aug-17
Project:	2017-C-813	Laboratory Sample Number:	17/410
Order Number:	Pending	Report Revision:	Rev 0
Laboratory Project Number:	B731	Report Date:	23-Aug-17
Client Sample Number/Reference:	TP02-DSC109A/3 (7/3733)	Tests:	Crumb Test (BS1377:Part 5:1990:6.3)
Sample Position/Depth:	0.0-0.35m	Remarks:	-

Elapsed Time: Zero Minutes



Result after Elapsed Time: 5 Minutes





BM du Plessis
Civil Engineering

Reg. No: cc 200004833323

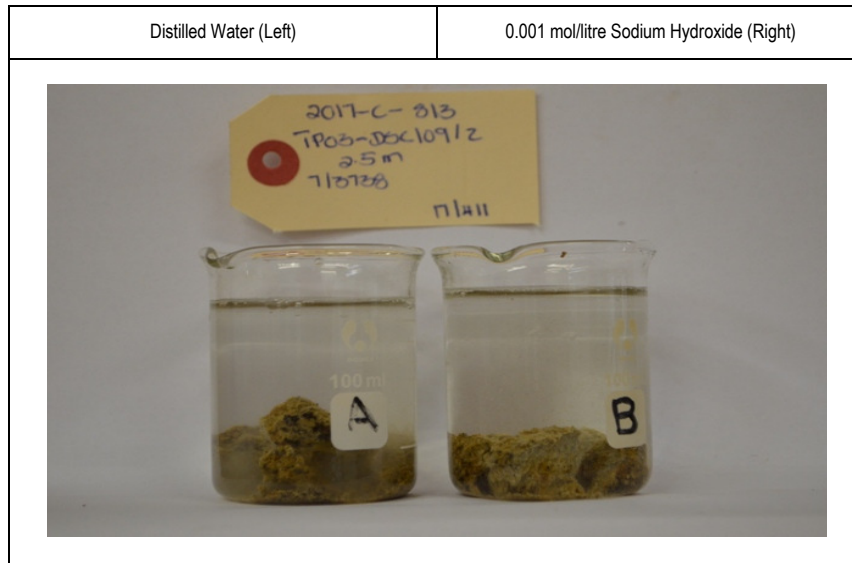
250 ORION Ave
Monument Park
0181

PO Box 26272
Monument Park
0105

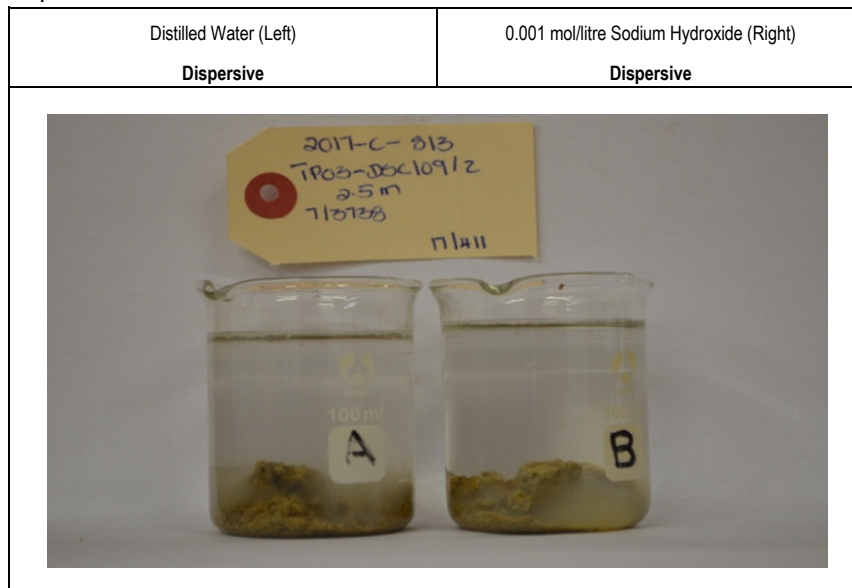
Tel/Fax 012 346 7586
Cell: 082 375 3003
bennie@geotesting.co.za

Client Name:	Geostrada	Date sampled/tested on site:	-
Client Contact:	Hennie Barnard	Sample Receive Date:	11-Aug-17
Project:	2017-C-813	Laboratory Sample Number:	17/411
Order Number:	Pending	Report Revision:	Rev 0
Laboratory Project Number:	B731	Report Date:	23-Aug-17
Client Sample Number/Reference:	TP03-DSC109/2 (7/3738)	Tests:	Crumb Test (BS1377:Part 5:1990:6.3)
Sample Position/Depth:	2.5m	Remarks:	-

Elapsed Time: Zero Minutes



Result after Elapsed Time: 5 Minutes





BM du Plessis
Civil Engineering

Reg. No: cc 200004833323

250 ORION Ave
Monument Park
0181

PO Box 26272
Monument Park
0105

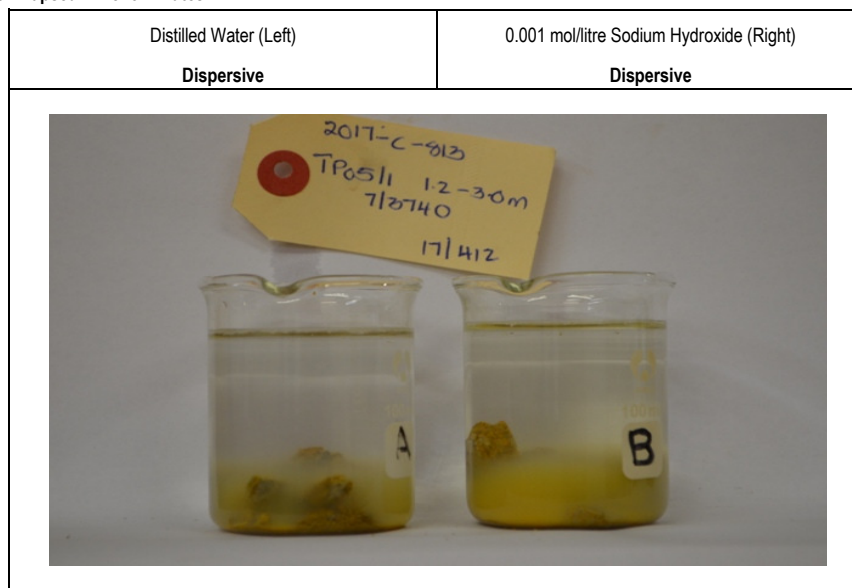
Tel/Fax 012 346 7586
Cell: 082 375 3003
bennie@geotesting.co.za

Client Name:	Geostrada	Date sampled/tested on site:	-
Client Contact:	Hennie Barnard	Sample Receive Date:	11-Aug-17
Project:	2017-C-813	Laboratory Sample Number:	17/412
Order Number:	Pending	Report Revision:	Rev 0
Laboratory Project Number:	B731	Report Date:	23-Aug-17
Client Sample Number/Reference:	TP05/1 (7/3740)	Tests:	Crumb Test (BS1377:Part 5:1990:6.3)
Sample Position/Depth:	1.2-3.0m	Remarks:	-

Elapsed Time: Zero Minutes



Result after Elapsed Time: 5 Minutes





du Plessis
Civil Engineering

Reg. No: cc 200004833323

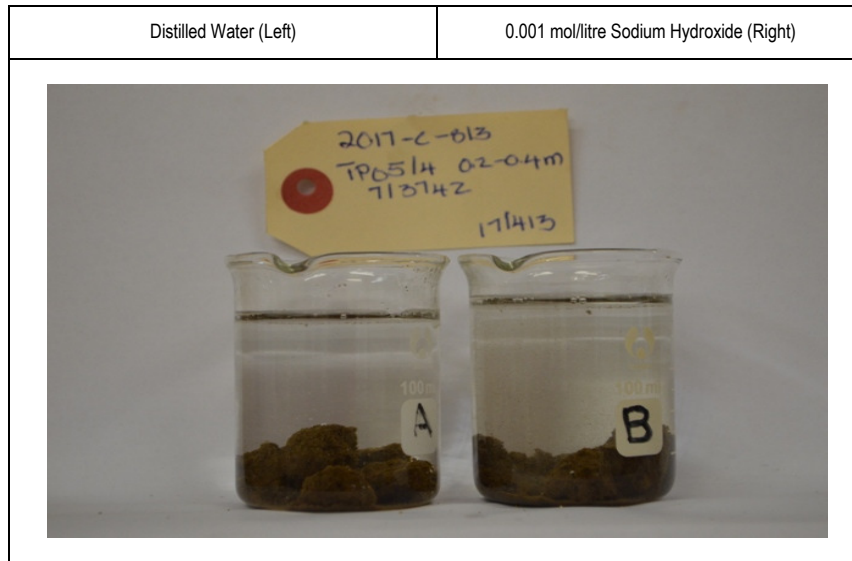
250 ORION Ave
Monument Park
0181

PO Box 26272
Monument Park
0105

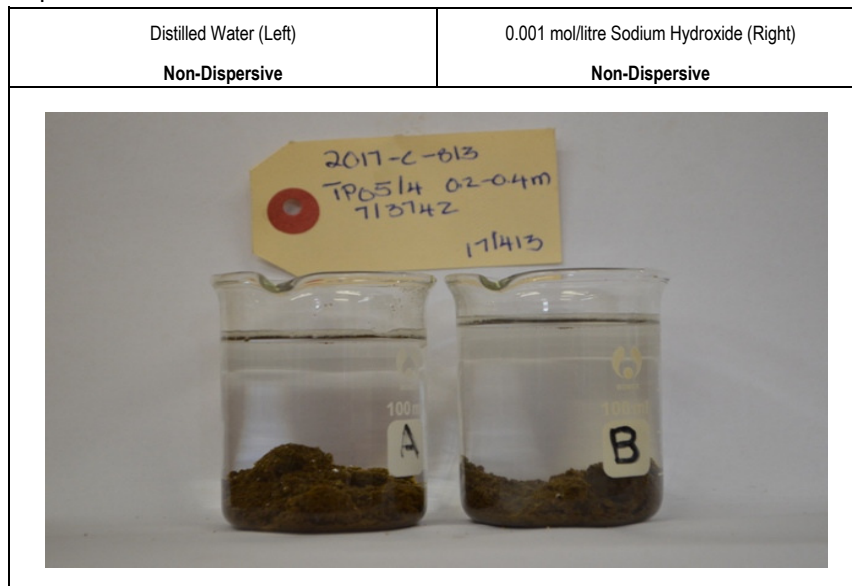
Tel/Fax 012 346 7586
Cell: 082 375 3003
bennie@geotesting.co.za

Client Name:	Geostrada	Date sampled/tested on site:	-
Client Contact:	Hennie Barnard	Sample Receive Date:	11-Aug-17
Project:	2017-C-813	Laboratory Sample Number:	17/413
Order Number:	Pending	Report Revision:	Rev 0
Laboratory Project Number:	B731	Report Date:	23-Aug-17
Client Sample Number/Reference:	TP05/4 (7/3742)	Tests:	Crumb Test (BS1377:Part 5:1990:6.3)
Sample Position/Depth:	0.2-0.4m	Remarks:	-

Elapsed Time: Zero Minutes



Result after Elapsed Time: 5 Minutes





du Plessis
Civil Engineering

Reg. No: cc 200004833323

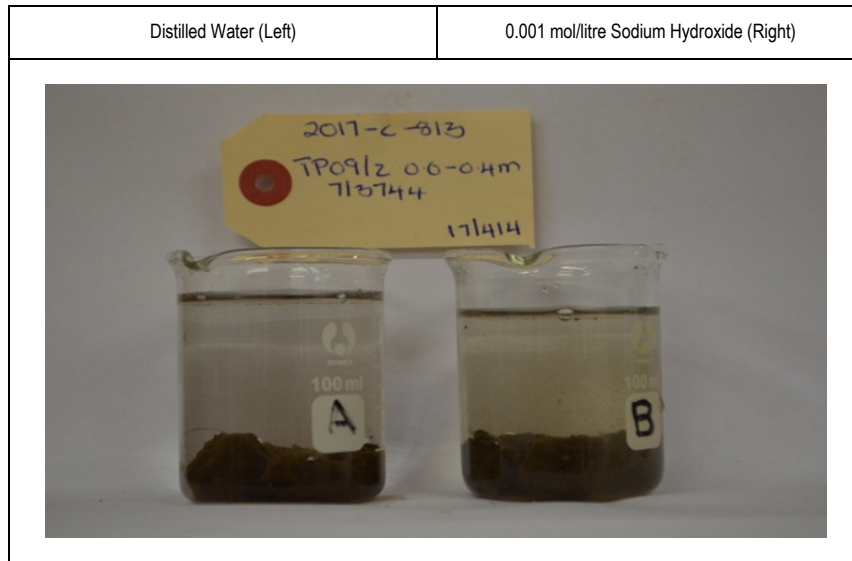
250 ORION Ave
Monument Park
0181

PO Box 26272
Monument Park
0105

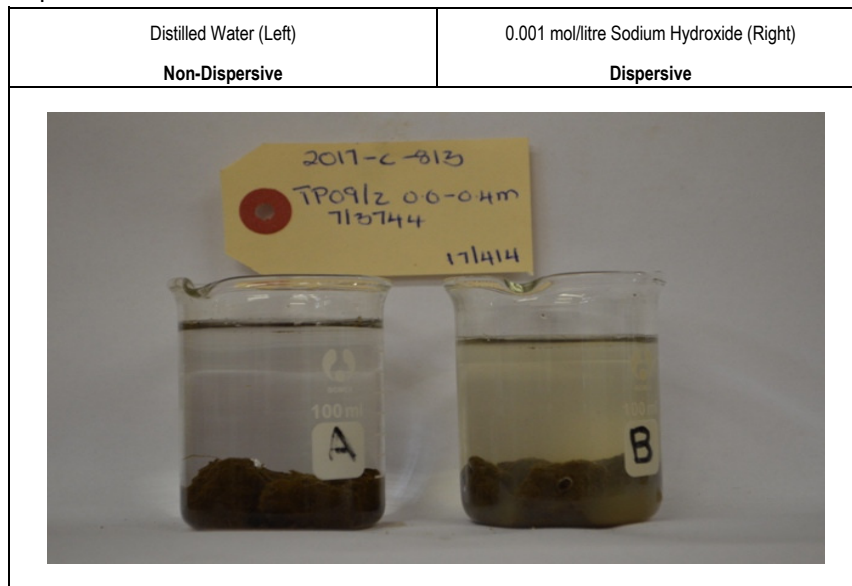
Tel/Fax 012 346 7586
Cell: 082 375 3003
bennie@geotesting.co.za

Client Name:	Geostrada	Date sampled/tested on site:	-
Client Contact:	Hennie Barnard	Sample Receive Date:	11-Aug-17
Project:	2017-C-813	Laboratory Sample Number:	17/414
Order Number:	Pending	Report Revision:	Rev 0
Laboratory Project Number:	B731	Report Date:	23-Aug-17
Client Sample Number/Reference:	TP09/2 (7/3744)	Tests:	Crumb Test (BS1377:Part 5:1990:6.3)
Sample Position/Depth:	0.0-0.4m	Remarks:	-

Elapsed Time: Zero Minutes



Result after Elapsed Time: 5 Minutes





BM du Plessis
Civil Engineering

Reg. No: cc 200004833323

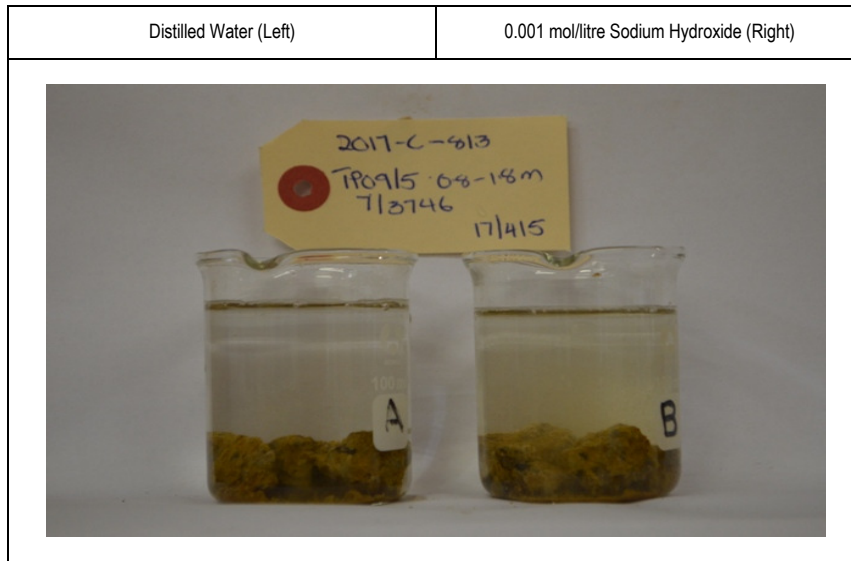
250 ORION Ave
Monument Park
0181

PO Box 26272
Monument Park
0105

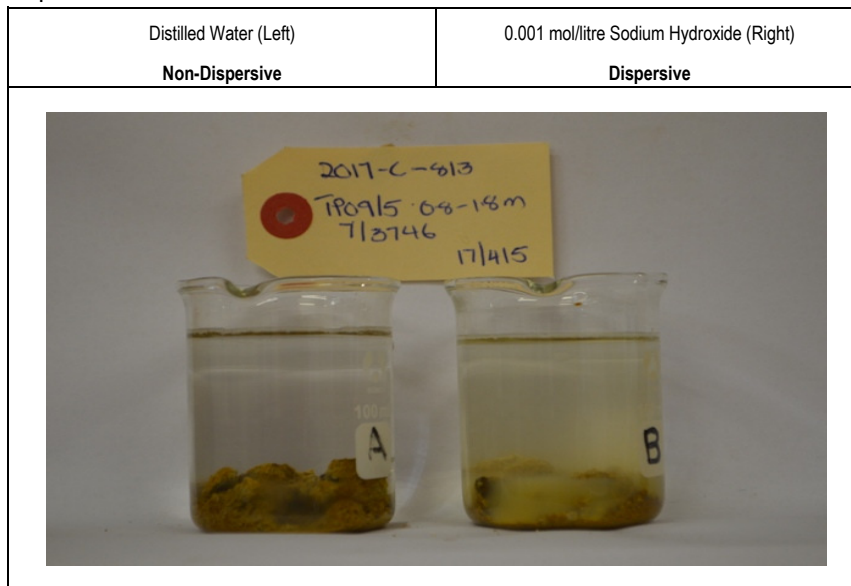
Tel/Fax 012 346 7586
Cell: 082 375 3003
bennie@geotesting.co.za

Client Name:	Geostrada	Date sampled/tested on site:	-
Client Contact:	Hennie Barnard	Sample Receive Date:	11-Aug-17
Project:	2017-C-813	Laboratory Sample Number:	17/415
Order Number:	Pending	Report Revision:	Rev 0
Laboratory Project Number:	B731	Report Date:	23-Aug-17
Client Sample Number/Reference:	TP09/5 (7/3746)	Tests:	Crumb Test (BS1377:Part 5:1990:6.3)
Sample Position/Depth:	0.8-1.8m	Remarks:	-

Elapsed Time: Zero Minutes



Result after Elapsed Time: 5 Minutes





du Plessis
Civil Engineering

Reg. No: cc 200004833323

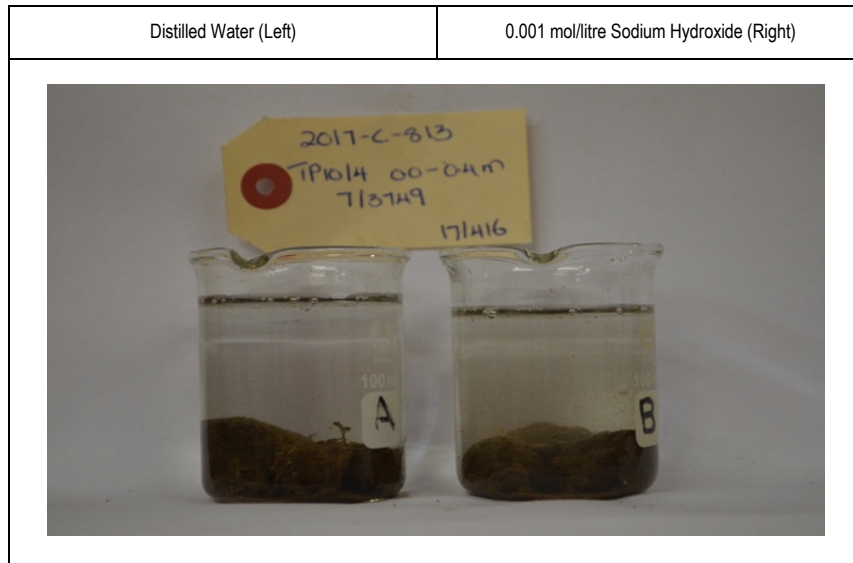
250 ORION Ave
Monument Park
0181

PO Box 26272
Monument Park
0105

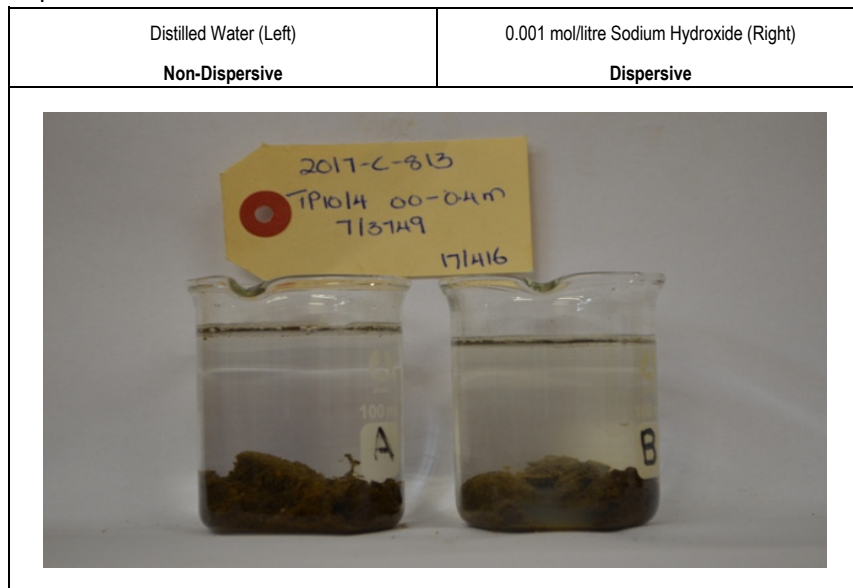
Tel/Fax 012 346 7586
Cell: 082 375 3003
bennie@geotesting.co.za

Client Name:	Geostrada	Date sampled/tested on site:	-
Client Contact:	Hennie Barnard	Sample Receive Date:	11-Aug-17
Project:	2017-C-813	Laboratory Sample Number:	17/416
Order Number:	Pending	Report Revision:	Rev 0
Laboratory Project Number:	B731	Report Date:	23-Aug-17
Client Sample Number/Reference:	TP10/4 (7/3749)	Tests:	Crumb Test (BS1377:Part 5:1990:6.3)
Sample Position/Depth:	0.0-0.4m	Remarks:	-

Elapsed Time: Zero Minutes



Result after Elapsed Time: 5 Minutes





du Plessis
Civil Engineering

Reg. No: cc 200004833323

250 ORION Ave
Monument Park
0181

PO Box 26272
Monument Park
0105

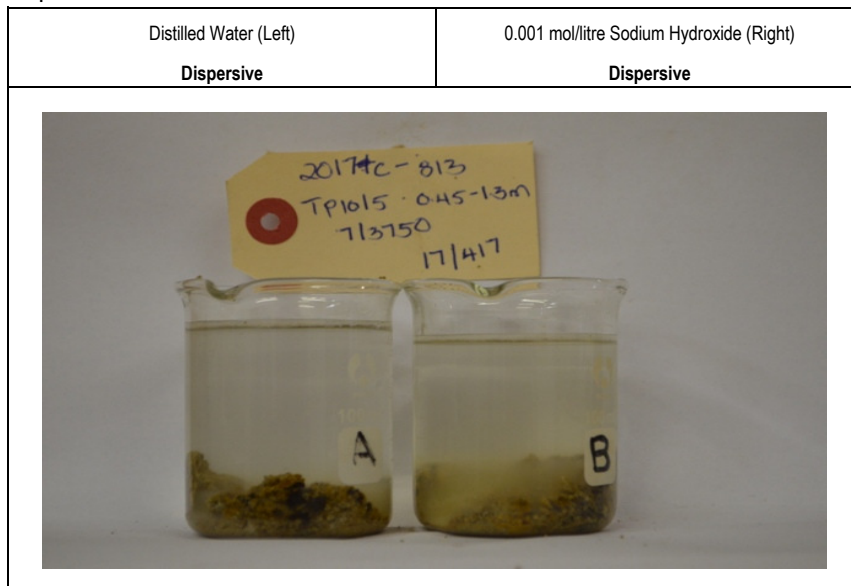
Tel/Fax 012 346 7586
Cell: 082 375 3003
bennie@geotesting.co.za

Client Name:	Geostrada	Date sampled/tested on site:	-
Client Contact:	Hennie Barnard	Sample Receive Date:	11-Aug-17
Project:	2017-C-813	Laboratory Sample Number:	17/417
Order Number:	Pending	Report Revision:	Rev 0
Laboratory Project Number:	B731	Report Date:	23-Aug-17
Client Sample Number/Reference:	TP10/5 (7/3750)	Tests:	Crumb Test (BS1377:Part 5:1990:6.3)
Sample Position/Depth:	0.45-1.3m	Remarks:	-

Elapsed Time: Zero Minutes



Result after Elapsed Time: 5 Minutes





du Plessis
Civil Engineering

Reg. No: cc 200004833323

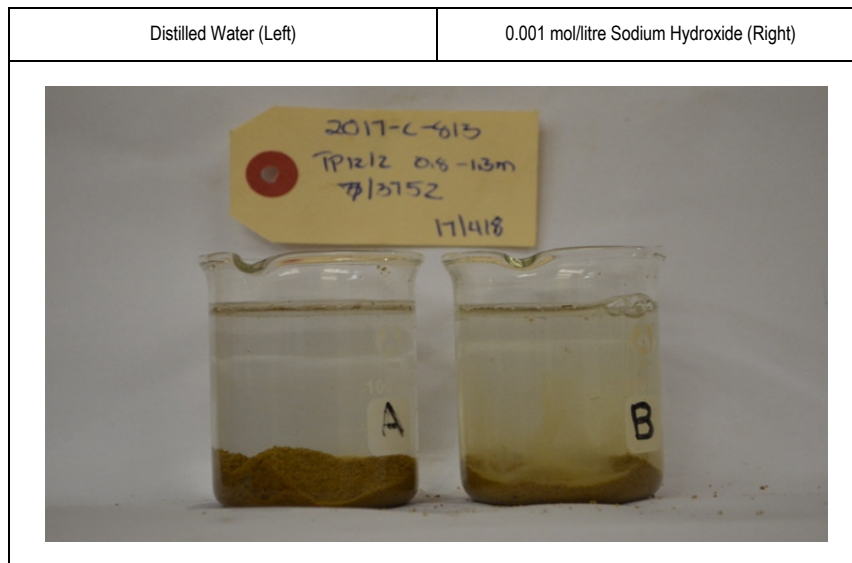
250 ORION Ave
Monument Park
0181

PO Box 26272
Monument Park
0105

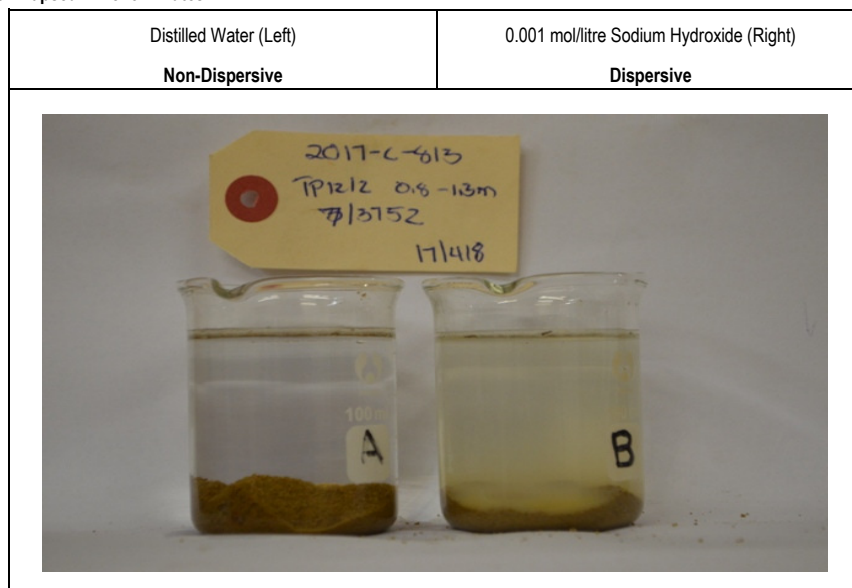
Tel/Fax 012 346 7586
Cell: 082 375 3003
bennie@geotesting.co.za

Client Name:	Geostrada	Date sampled/tested on site:	-
Client Contact:	Hennie Barnard	Sample Receive Date:	11-Aug-17
Project:	2017-C-813	Laboratory Sample Number:	17/418
Order Number:	Pending	Report Revision:	Rev 0
Laboratory Project Number:	B731	Report Date:	23-Aug-17
Client Sample Number/Reference:	TP12/2 (7/3752)	Tests:	Crumb Test (BS1377:Part 5:1990:6.3)
Sample Position/Depth:	0.8-1.3m	Remarks:	-

Elapsed Time: Zero Minutes



Result after Elapsed Time: 5 Minutes





BM du Plessis
Civil Engineering

Reg. No: cc 200004833323

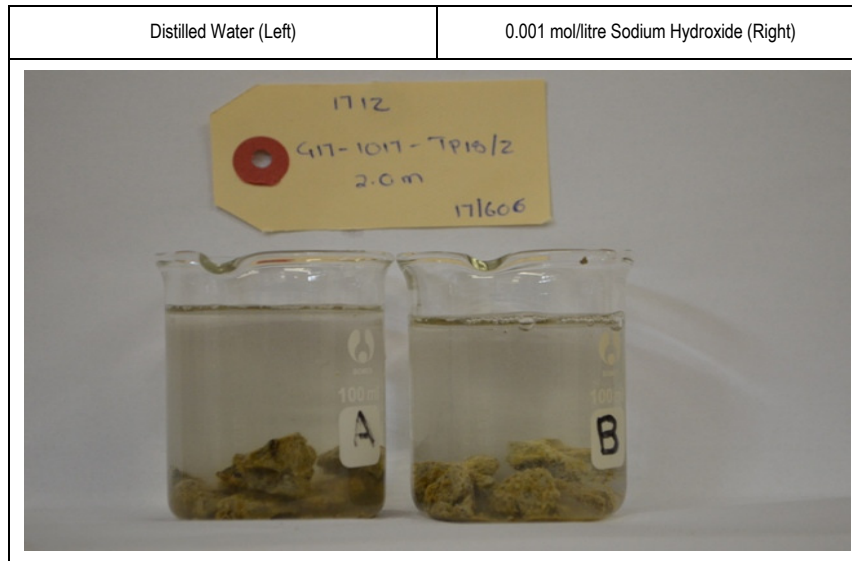
250 ORION Ave
Monument Park
0181

PO Box 26272
Monument Park
0105

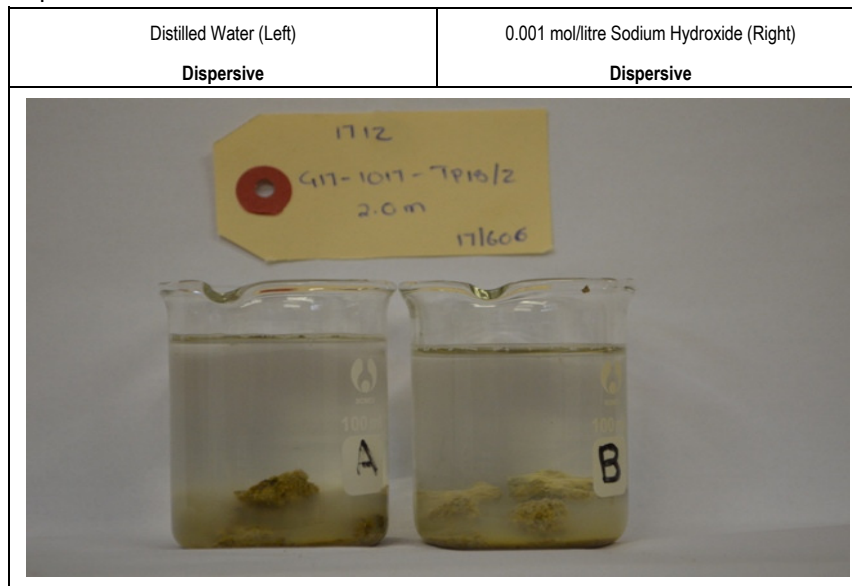
Tel/Fax 012 346 7586
Cell: 082 375 3003
bennie@geotesting.co.za

Client Name:	SGS Matrolab	Date sampled/tested on site:	-
Client Contact:	Hennie Barnard	Sample Receive Date:	05-Oct-17
Project:	1712	Laboratory Sample Number:	17/606
Order Number:	40001011	Report Revision:	Rev 1
Laboratory Project Number:	B773	Report Date:	31-Oct-17
Client Sample Number/Reference:	G17-1017 TP 18/2	Tests:	Crumb Test (BS1377:Part 5:1990:6.3)
Sample Position/Depth:	2.0m	Remarks:	-

Elapsed Time: Zero Minutes



Result after Elapsed Time: 5 Minutes





BM du Plessis
Civil Engineering

Reg. No: cc 200004833323

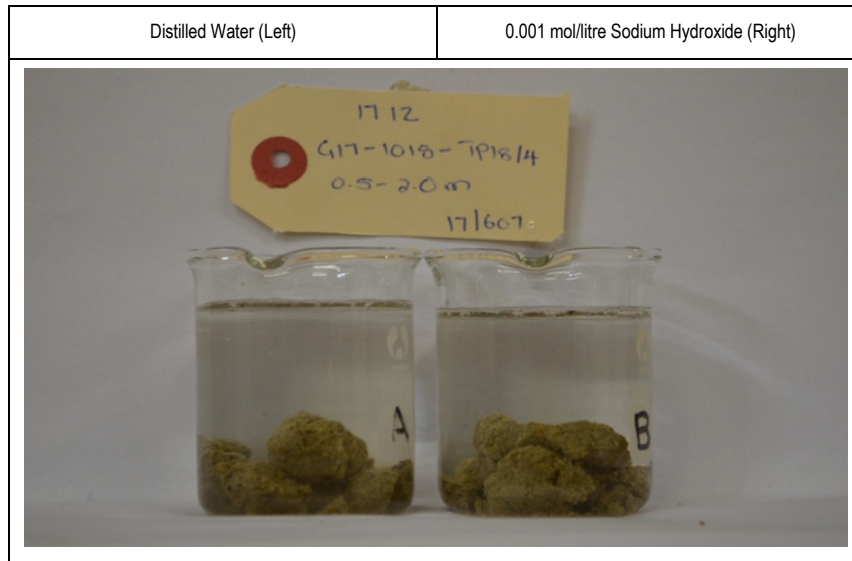
250 ORION Ave
Monument Park
0181

PO Box 26272
Monument Park
0105

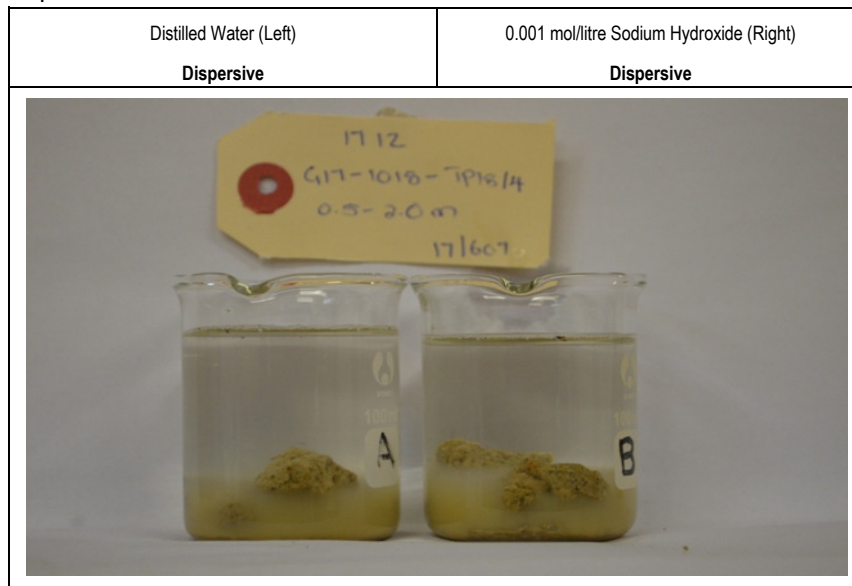
Tel/Fax 012 346 7586
Cell: 082 375 3003
bennie@geotesting.co.za

Client Name:	SGS Matrolab	Date sampled/tested on site:	-
Client Contact:	Hennie Barnard	Sample Receive Date:	05-Oct-17
Project:	1712	Laboratory Sample Number:	17/607
Order Number:	40001011	Report Revision:	Rev 1
Laboratory Project Number:	B773	Report Date:	31-Oct-17
Client Sample Number/Reference:	G17-1018 TP 18/4	Tests:	Crumb Test (BS1377:Part 5:1990:6.3)
Sample Position/Depth:	0.5-2.0m	Remarks:	-

Elapsed Time: Zero Minutes



Result after Elapsed Time: 5 Minutes





BM du Plessis
Civil Engineering

Reg. No: cc 200004833323

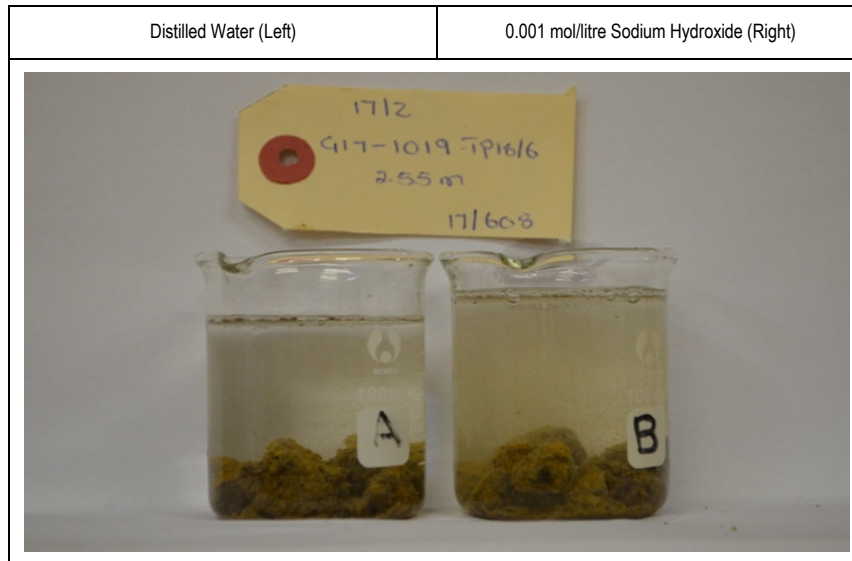
250 ORION Ave
Monument Park
0181

PO Box 26272
Monument Park
0105

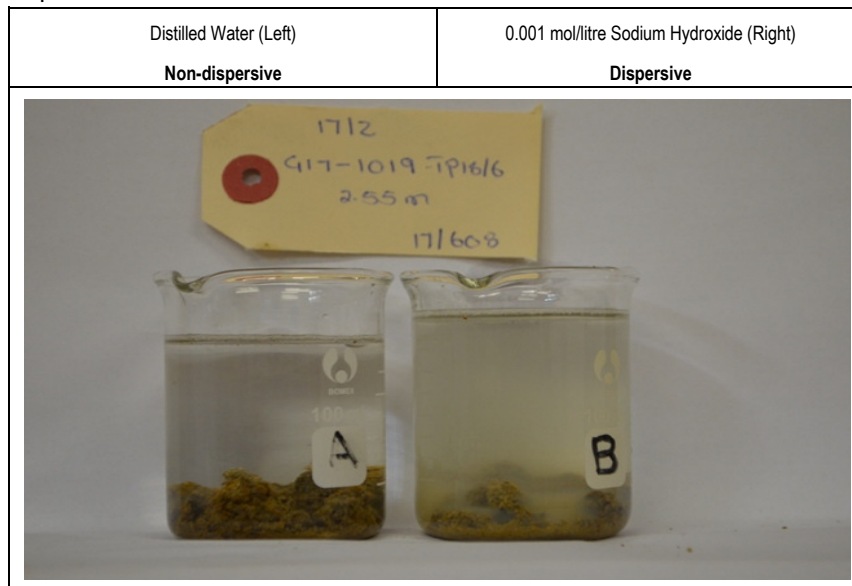
Tel/Fax 012 346 7586
Cell: 082 375 3003
bennie@geotesting.co.za

Client Name:	SGS Matrolab	Date sampled/tested on site:	-
Client Contact:	Hennie Barnard	Sample Receive Date:	05-Oct-17
Project:	1712	Laboratory Sample Number:	17/608
Order Number:	40001011	Report Revision:	Rev 1
Laboratory Project Number:	B773	Report Date:	31-Oct-17
Client Sample Number/Reference:	G17-1019 TP 18/6	Tests:	Crumb Test (BS1377:Part 5:1990:6.3)
Sample Position/Depth:	2.55m	Remarks:	-

Elapsed Time: Zero Minutes



Result after Elapsed Time: 5 Minutes





du Plessis
Civil Engineering

Reg. No: cc 200004833323

250 ORION Ave
Monument Park
0181

PO Box 26272
Monument Park
0105

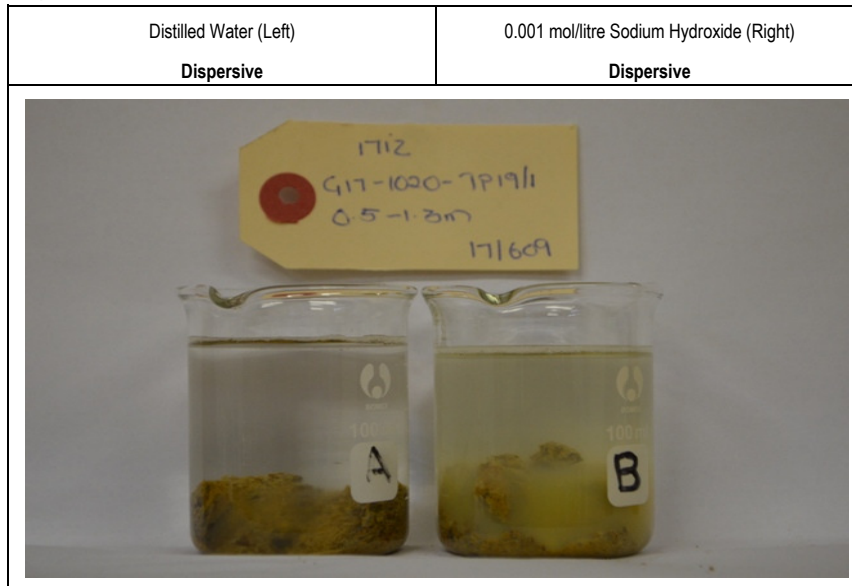
Tel/Fax 012 346 7586
Cell: 082 375 3003
bennie@geotesting.co.za

Client Name:	SGS Matrolab	Date sampled/tested on site:	-
Client Contact:	Hennie Barnard	Sample Receive Date:	05-Oct-17
Project:	1712	Laboratory Sample Number:	17/609
Order Number:	40001011	Report Revision:	Rev 1
Laboratory Project Number:	B773	Report Date:	31-Oct-17
Client Sample Number/Reference:	G17-1020 TP 19/1	Tests:	Crumb Test (BS1377:Part 5:1990:6.3)
Sample Position/Depth:	0.5-1.3m	Remarks:	-

Elapsed Time: Zero Minutes



Result after Elapsed Time: 5 Minutes





BM du Plessis
Civil Engineering

Reg. No: cc 200004833323

250 ORION Ave
Monument Park
0181

PO Box 26272
Monument Park
0105

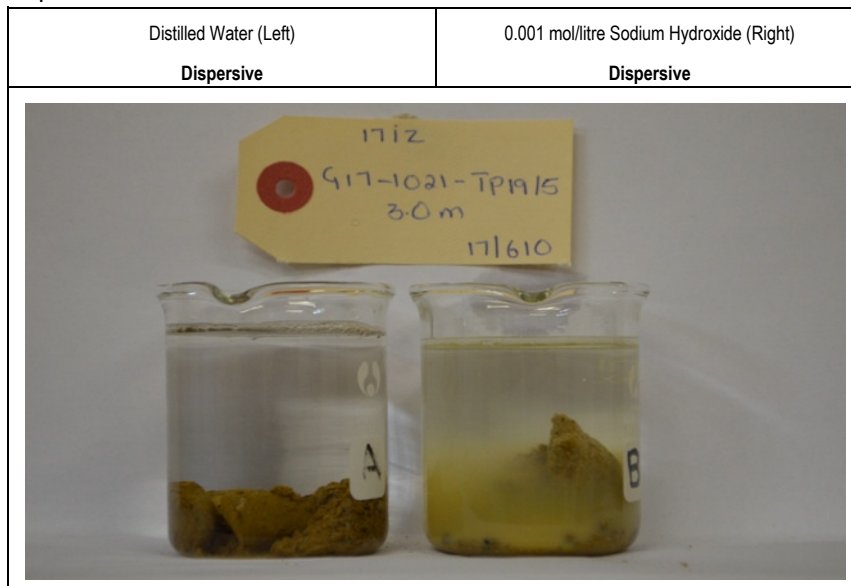
Tel/Fax 012 346 7586
Cell: 082 375 3003
bennie@geotesting.co.za

Client Name:	SGS Matrolab	Date sampled/tested on site:	-
Client Contact:	Hennie Barnard	Sample Receive Date:	05-Oct-17
Project:	1712	Laboratory Sample Number:	17/610
Order Number:	40001011	Report Revision:	Rev 1
Laboratory Project Number:	B773	Report Date:	31-Oct-17
Client Sample Number/Reference:	G17-1021 TP 19/5	Tests:	Crumb Test (BS1377:Part 5:1990:6.3)
Sample Position/Depth:	3.0m	Remarks:	-

Elapsed Time: Zero Minutes



Result after Elapsed Time: 5 Minutes





BM du Plessis
Civil Engineering

Reg. No: cc 200004833323

250 ORION Ave
Monument Park
0181

PO Box 26272
Monument Park
0105

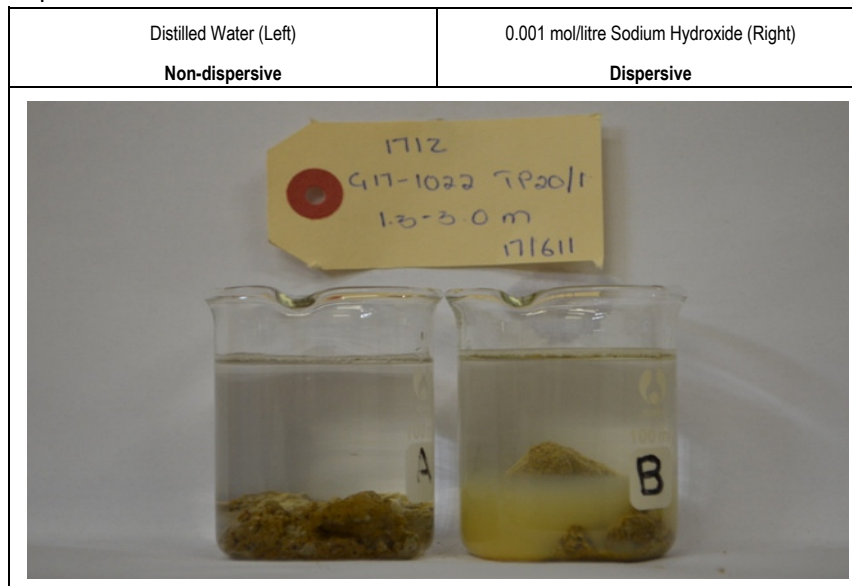
Tel/Fax 012 346 7586
Cell: 082 375 3003
bennie@geotesting.co.za

Client Name:	SGS Matrolab	Date sampled/tested on site:	-
Client Contact:	Hennie Barnard	Sample Receive Date:	05-Oct-17
Project:	1712	Laboratory Sample Number:	17/611
Order Number:	40001011	Report Revision:	Rev 1
Laboratory Project Number:	B773	Report Date:	31-Oct-17
Client Sample Number/Reference:	G17-1022 TP 20/1	Tests:	Crumb Test (BS1377:Part 5:1990:6.3)
Sample Position/Depth:	1.3-3.0m	Remarks:	-

Elapsed Time: Zero Minutes



Result after Elapsed Time: 5 Minutes



MAATSKAPPY: Aurecon SA (Pty) Ltd t.a GeoStrada
 ADRES: PO Box 11126 Hatfield 0028
 ADRES:
 POSKODE:
 TELEFOON NO: Hennie, Cynthia

NAAM: Aurecon SA (Pty) Ltd t.a GeoStrada
 PLAAS:
 EPOS: hennieb@geostrada.co.za, cynthiak
 FAKS: 27124303548
 BESTEL: 200,087 2017-C-813

DATUM:

		Ammonium Assetaat																				
Lab No	Verwysings no	pH(KCl)	Bray I	K	Na	Ca	Mg	UIT H+	%Ca	%Mg	%K	%Na	SUUR.V	Ca:Mg	(Ca+Mg)/K	Mg:K	S-Waarde	Na:K	T	Digtheid	S AmAC	KUV
		-	mg/kg	mg/kg	mg/kg	mg/kg	mg/kg	cmol(+)/kg	%	%	%	%	%	1.5-4.5	10.0-20.0	3.0-4.0	cmol(+)/kg	-	cmol(+)/kg	g/cm3	mg/kg	
16310	7/3740 2017-C-813	6.13	5	304	34	1238	684	0.00	48.65	44.07	6.12	1.15	0.00	1.10	15.15	7.20	12.72	0.19	12.72	1.02	28.51	8.04
16311	7/3742 2017-C-813	5.22	1	112	11	604	230	0.00	57.62	36.02	5.46	0.90	0.00	1.60	17.15	6.60	5.24	0.17	5.24	1.33	4.55	4.39
16312	7/3750 2017-C-813	5.76	1	449	136	2283	961	0.00	54.27	37.46	5.46	2.82	0.00	1.45	16.81	6.87	21.04	0.52	21.04	1.26	1.79	7.11
16313	7/3744 2017-C-813	4.75	13	232	6	373	118	0.00	53.98	28.04	17.17	0.81	0.00	1.93	4.78	1.63	3.46	0.05	3.46	1.42	2.70	2.34
16314	7/3749 2017-C-813	4.18	12	160	4	175	49	0.03	50.48	23.18	23.55	0.91	1.87	2.18	3.13	0.98	1.71	0.04	1.74	1.26	6.29	2.40
16315	7/3752 2017-C-813	4.33	1	30	15	240	101	0.25	49.58	34.12	3.19	2.64	10.48	1.45	26.25	10.70	2.17	0.83	2.42	1.20	35.33	1.88
16316	7/3733 2017-C-813	6.19	6	106	8	453	143	0.00	60.48	31.32	7.28	0.93	0.00	1.93	12.62	4.30	3.74	0.13	3.74	1.16	8.32	2.30
16317	7/3738 2017-C-813	7.29	2	650	457	1820	1318	0.00	38.64	45.87	7.06	8.43	0.00	0.84	11.97	6.50	23.55	1.19	23.55	0.92	5.88	6.27
16318	7/3746 2017-C-813	6.20	2	514	44	2058	728	0.00	57.93	33.59	7.39	1.08	0.00	1.72	12.38	4.54	17.76	0.15	17.76	1.15	11.43	5.61

		Versadigde Pasta													
Lab No	Verwysings no	Ca	Mg	K	Na	Fe	Mn	Cu	Zn	S	B	EG	PO4	SO4	NAV
		mg/l	mg/l	mg/l	mg/l	mg/l	mg/l	mg/l	mg/l	mg/l	mg/l	mS/m	mg/l	mg/l	-
16310	7/3740 2017-C-813	9.21	5.71	6.22	6.53	7.18	0.03	0.00	0.01	16.42	0.00	17.13	0.33	49.26	0.42
16311	7/3742 2017-C-813	12.72	9.72	22.36	1.96	97.00	0.85	0.08	0.17	7.36	0.05	10.65	1.86	22.08	0.10
16312	7/3750 2017-C-813	5.63	8.13	16.61	4.02	66.49	0.32	0.05	0.12	2.50	0.02	4.94	0.60	7.50	0.25
16313	7/3744 2017-C-813	2.42	2.25	16.67	0.89	27.66	0.46	0.03	0.06	2.60	0.02	5.05	1.86	7.80	0.10
16314	7/3749 2017-C-813	2.13	1.48	8.70	1.16	15.25	0.30	0.01	0.04	1.52	0.01	4.74	1.20	4.56	0.15
16315	7/3752 2017-C-813	12.34	5.88	3.08	7.40	4.51	0.04	0.00	0.01	21.58	0.01	18.22	0.45	64.74	0.43
16316	7/3733 2017-C-813	6.27	4.47	16.38	1.79	52.12	0.30	0.04	0.12	6.30	0.02	7.27	2.22	18.90	0.13
16317	7/3738 2017-C-813	2.34	5.40	8.07	2.25	43.22	0.17	0.03	0.07	0.26	0.01	1.62	0.57	0.78	0.18
16318	7/3746 2017-C-813	6.30	2.98	5.49	5.34	6.44	0.03	0.00	0.01	10.06	0.00	10.92	0.45	30.18	0.44

SOILANALYSIS REPORT




TEL: 0828890133 / 0828890139

FAX: 086 243 4281

COMPANY: Geostrada
 ADDRESS: 993 Park street
 ADDRESS: Hatfield
 CODE: 83
 TEL NO: 012 427 3071

NAME: Project : DATE: 8/14/17
 EMAIL: Hennie Barnard <HennieB@geostrada.co.za>
 FAX: 012 427 3050
 Job NO: 200.087 2017-C-813

Lab No	Ref No	Position	Depth(m)	pH (H ₂ O)	Conductivity	Na	Mg	CEC	ESP	EMgP	Sat. Paste Extract			
											me/100gsoil (cmol+)/kg	me/100gsoil (cmol+)/kg	cmol(+)/kg	Na
					mS/m						me/l	me/l	me/l	
16310	7/3740 2017-C-813			6.93	17.13	0.15	5.47	6.70	2.19	81.689	0.28	0.46	0.46	0.42
16311	7/3742 2017-C-813			6.02	10.65	0.05	1.84	3.66	1.29	50.314	0.09	0.64	0.78	0.10
16312	7/3750 2017-C-813			6.56	4.94	0.59	7.69	5.91	10.04	130.14	0.17	0.28	0.65	0.25
16313	7/3744 2017-C-813			5.55	5.05	0.03	0.95	1.95	1.43	48.54	0.04	0.12	0.18	0.10
16314	7/3749 2017-C-813			4.98	4.74	0.02	0.39	2.01	0.79	19.56	0.05	0.11	0.12	0.15
16315	7/3752 2017-C-813			5.13	18.22	0.06	0.81	1.56	4.10	51.75	0.32	0.62	0.47	0.43
16316	7/3733 2017-C-813			6.99	7.27	0.03	1.14	1.92	1.80	59.58	0.08	0.31	0.36	0.13
16317	7/3738 2017-C-813			8.09	1.62	1.99	10.54	5.22	38.04	201.94	0.10	0.12	0.43	0.18
16318	7/3746 2017-C-813			7.00	10.92	0.19	5.82	4.68	4.11	124.43	0.23	0.32	0.24	0.44


 NF REEDERS

MAATSKAPPY: **SGS Matrolab (Pty)LTD**
 ADRES: **257 Henning str**
 ADRES: **Jan Niemand Park**
 POSKODE: **0186**
 TELEFOON NO:

NAAM:
 PLAAS:
 EPOS:
 FAKS:
 BESTEL:

DATUM:

		Ammonium Assetaat																				
Lab No	Verwysings no	pH(KCl)	Bray I	K	Na	Ca	Mg	UIT H+	%Ca	%Mg	%K	%Na	SUUR.V	Ca:Mg	(Ca+Mg)/K	Mg:K	S-Waarde	Na:K	T	Digtheid	S AmAC	KUV
		-	mg/kg	mg/kg	mg/kg	mg/kg	mg/kg	cmol(+)/kg	%	%	%	%	%	1.5-4.5	10.0-20.0	3.0-4.0	cmol(+)/kg	-	cmol(+)/kg	g/cm3	mg/kg	
63670	University of Pretoria TP18/2 G17_1017	7.04	1	636	511	1715	1150	0.00	39.25	43.14	7.44	10.17	0.00	0.91	11.07	5.80	21.85	1.37	21.85	0.99	6.07	15.76
63671	University of Pretoria TP18/4 G17_1018	5.28	1	591	93	1409	709	0.00	47.71	39.32	10.23	2.74	0.00	1.21	8.51	3.84	14.77	0.27	14.77	1.13	20.17	9.60
63672	University of Pretoria TP18/6 G17_1019	6.71	1	560	431	1545	990	0.00	40.35	42.38	7.48	9.79	0.00	0.95	11.05	5.66	19.14	1.31	19.14	1.19	2.55	7.47
63673	University of Pretoria TP19/1 G17_1020	5.73	1	648	104	2374	924	0.00	55.06	35.15	7.69	2.10	0.00	1.57	11.73	4.57	21.55	0.27	21.55	1.06	32.05	15.76
63674	University of Pretoria TP19/5 G17_1021	6.51	1	629	248	3257	1134	0.00	57.60	32.89	5.69	3.82	0.00	1.75	15.89	5.78	28.27	0.67	28.27	1.11	3.26	16.58
63675	University of Pretoria TP20/1 G17_1022	5.72	1	268	28	1195	637	0.00	49.80	43.48	5.70	1.01	0.00	1.15	16.36	7.62	12.00	0.18	12.00	1.16	104.66	7.47

		Versadigde Pasta													
Lab No	Verwysings no	Ca	Mg	K	Na	Fe	Mn	Cu	Zn	S	B	EG	PO4	SO4	NAV
		mg/l	mg/l	mg/l	mg/l	mg/l	mg/l	mg/l	mg/l	mg/l	mg/l	mS/m	mg/l	mg/l	-
63670	University of Pretoria TP18/2 G17_1017	22.31	51.80	79.92	22.66	51.31	1.00	0.37	0.73	3.27	0.82	8.05	6.13	9.80	0.60
63671	University of Pretoria TP18/4 G17_1018	3.38	1.64	4.51	6.90	7.45	0.00	0.01	0.01	6.29	0.02	7.67	0.86	18.86	0.77
63672	University of Pretoria TP18/6 G17_1019	18.42	42.54	64.31	20.61	51.31	1.00	0.28	0.56	2.69	0.60	8.46	5.25	8.06	0.60
63673	University of Pretoria TP19/1 G17_1020	6.10	2.23	4.17	9.55	2.22	0.00	0.00	0.00	10.38	0.00	11.49	0.74	31.14	0.84
63674	University of Pretoria TP19/5 G17_1021	3.58	3.12	5.89	12.35	15.56	0.03	0.01	0.03	4.81	0.02	9.13	0.59	14.42	1.15
63675	University of Pretoria TP20/1 G17_1022	14.99	7.95	4.45	3.96	0.14	0.00	0.00	0.00	22.88	0.00	17.69	0.35	68.64	0.21

SOILANALYSIS REPORT



TEL: 0828890133 / 0828890139

FAX: 086 243 4281

COMPANY: SGS Matrolab (Pty)LTD
 ADDRESS: 257 Henning str
 ADDRESS: Jan Niemand Park
 CODE: 0186
 TEL NO:

NAME: Auke Keijser DATE: 10/9/17
 EMAIL: auke.keijser@sgs.com
 FAX: 012 427 3050
 ORDER NO: PO40000951,0

Lab No	Ref No	Position	Depth(m)	pH (H ₂ O)	Conductivity	Sat. Paste Extract								
						Na me/100gsoil (cmol(+)/kg)	Mg me/100gsoil (cmol(+)/kg)	CEC cmol(+)/kg	ESP	EMgP	Na me/l	Ca me/l	Mg me/l	SAR
63670	University of Pretoria TP18/2 G17_1017			7.71	8.05	2.22	9.20	15.76	14.10	58.39	0.99	1.12	4.14	0.61
63671	University of Pretoria TP18/4 G17_1018			5.95	7.67	0.40	5.67	9.6	4.21	59.05	0.30	0.17	0.13	0.77
63672	University of Pretoria TP18/6 G17_1019			7.38	8.46	1.87	7.92	7.47	25.09	105.99	0.90	0.92	3.40	0.61
63673	University of Pretoria TP19/1 G17_1020			6.40	11.49	0.45	7.39	15.76	2.87	46.91	0.42	0.30	0.18	0.85
63674	University of Pretoria TP19/5 G17_1021			7.18	9.13	1.08	9.08	16.58	6.51	54.74	0.54	0.18	0.25	1.17
63675	University of Pretoria TP20/1 G17_1022			6.39	17.69	0.12	5.09	7.47	1.62	68.19	0.17	0.75	0.64	0.21
63676	JN1701 Grey material G17_0992			7.44	95.00	0.18	5.40	7.88	2.34	68.59	0.42	6.38	3.61	0.19
63677	JN1701 Red Material bag 1 G17_0993			6.45	43.50	0.27	6.58	15.14	1.76	43.44	0.35	2.16	1.41	0.26
63678	Bag2 G17_0994			7.02	91.30	0.34	5.79	10.83	3.10	53.48	0.45	6.25	3.50	0.20

NF REEDERS

B.2c) XRF AND XRD TESTS



UNIVERSITEIT VAN PRETORIA
UNIVERSITY OF PRETORIA
YUNIBESITHI YA PRETORIA

Faculty of Natural & Agricultural Sciences

XRD & XRF Facility

Department of Geology

Pretoria 0002, South Africa

Direct Telephone (012) 420-2137

Direct Telefax: (012) 362 5219

E-Mail: jeanette.dykstra@up.ac.za

<http://www.up.ac.za/academic/science>

CLIENT: Jacobus Breyl

PO NUMBER: t.b.c.

DATE: 2017-10-27

ANALYSIS: XRF

ANALYSIS: The samples were roasted at 1000° C to determine Loss On Ignition (LOI).
1g Roasted sample was then placed together with 6g of Li₂B₄O₇ into a Pt/Au crucible and fused
The ARL PerformX Sequential XRF instrument was used for the analyses.
Analyses were executed using the Quantas software.
The software analyse for all elements in the periodic table between Na and U, but only elements
found above the detection limits were reported.
The results were also monitored and filtered to eliminate the presence of some of the flux, wetting
and oxidising agents elements.

Blank and certified reference materials are analysed with each batch of samples and the columns in bold represent one of these.

	SARM49		TP01	TP02	TP02	TP02	TP02	TP03	TP03	TP03	TP03	TP05	TP05	TP09	TP09	TP10	TP10	TP18	TP18	TP19	TP19	TP19	TP20
	Certified	Analysed	1	109A4-1	109A4-2	109A4-3	109A-2	109-1	109-2	109-3	109-4	4	5	2	4	4	5	4	5	1	2	3	1
SiO ₂	99.6	99.70	72.40	80.20	85.80	75.20	91.50	73.00	73.70	71.00	73.40	88.50	73.40	86.50	56.00	85.10	64.20	70.40	75.50	58.70	64.10	74.00	67.50
TiO ₂	0.01	0.00	0.55	0.40	0.28	0.51	0.41	0.55	0.52	0.51	0.41	0.38	0.56	0.44	0.55	0.43	0.69	0.62	0.58	0.59	0.59	0.69	0.51
Al ₂ O ₃	0.05	0.01	11.00	8.13	5.69	10.10	3.66	11.70	10.80	13.80	6.38	4.91	11.70	3.90	20.60	3.57	16.70	12.30	11.40	19.40	13.90	10.10	13.80
Fe ₂ O ₃	0.05	0.01	8.42	4.08	2.45	4.76	1.69	5.77	5.00	5.24	7.31	2.13	6.86	4.97	10.10	6.66	7.12	7.52	5.22	8.75	10.40	4.93	9.44
MnO	0.01	0.00	0.09	0.06	0.03	0.08	0.04	0.07	0.09	0.05	0.18	0.04	0.05	0.09	0.10	0.05	0.11	0.12	0.09	0.05	0.27	0.20	0.07
MgO	0.05	0.01	0.43	0.33	0.34	0.58	<0.01	0.54	0.68	0.38	1.82	0.19	0.33	0.15	0.68	<0.01	1.02	0.64	0.52	0.66	0.84	1.32	0.19
CaO	0.01	0.01	0.25	0.29	0.36	0.43	0.12	0.42	0.35	0.25	2.14	0.09	0.22	0.09	0.44	0.04	0.53	0.53	0.25	0.39	0.44	0.67	0.18
Na ₂ O	0.05	0.02	<0.01	<0.01	0.38	0.40	0.34	<0.01	0.12	<0.01	<0.01	<0.01	<0.01	<0.01	<0.01	<0.01	0.00	<0.01	<0.01	<0.01	<0.01	<0.01	<0.01
K ₂ O	0.01	0.01	1.08	1.03	1.07	1.19	0.71	1.53	1.36	1.09	0.86	0.79	1.20	0.79	1.61	0.77	1.76	1.33	1.41	1.50	1.57	1.33	0.94
Cr ₂ O ₃	0	0.00	0.04	0.02	0.02	0.04	0.05	0.12	0.20	0.20	0.09	0.04	0.06	0.04	0.04	0.07	0.04	0.05	0.04	0.17	0.26	0.21	0.05
NiO	0	0.01	0.04	<0.01	<0.01	<0.01	0.02	0.40	0.51	0.46	0.08	<0.01	0.04	0.03	0.03	0.03	0.02	0.03	0.04	0.45	0.63	0.59	<0.01
V ₂ O ₅	0	0.00	0.03	0.03	<0.01	0.01	<0.01	0.00	0.02	0.02	<0.01	0.01	0.03	<0.01	0.03	0.03	0.05	0.03	0.03	0.03	0.03	0.02	0.02
ZrO ₂	0	0.01	0.06	0.05	0.05	0.05	0.08	0.06	0.05	0.05	0.06	0.08	0.06	0.08	0.04	0.07	0.05	0.06	0.06	0.04	0.05	0.06	0.06
SO ₃			<0.01	<0.01	0.07	0.08	0.08	<0.01	<0.01	<0.01	0.01	<0.01	<0.01	<0.01	<0.01	<0.01	<0.01	<0.01	<0.01	<0.01	<0.01	<0.01	<0.01
LOI	0	0.10	5.52	5.27	3.42	6.51	1.04	5.79	6.56	6.88	7.20	2.74	5.41	2.87	9.62	3.04	7.61	6.26	4.66	9.17	6.84	5.28	7.14
Total	100	99.89	99.91	99.89	99.96	99.94	99.73	99.94	99.94	99.93	99.94	99.88	99.93	99.93	99.83	99.86	99.90	99.87	99.81	99.91	99.91	99.41	99.91

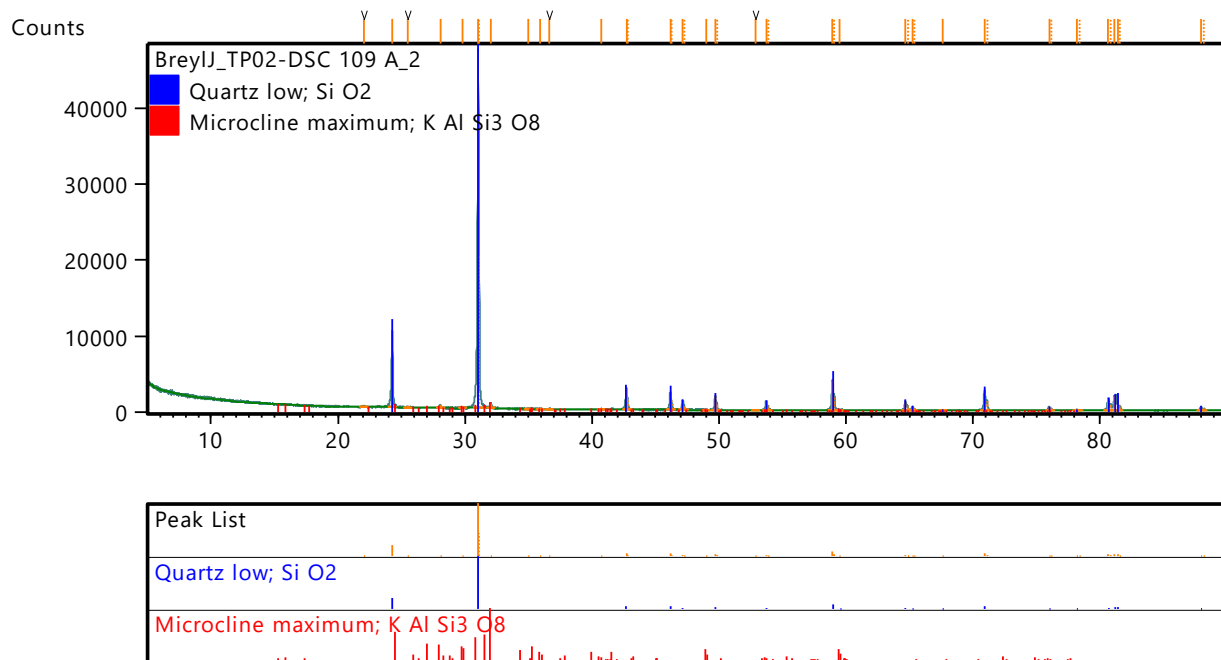
If you have any further queries, kindly contact the laboratory.

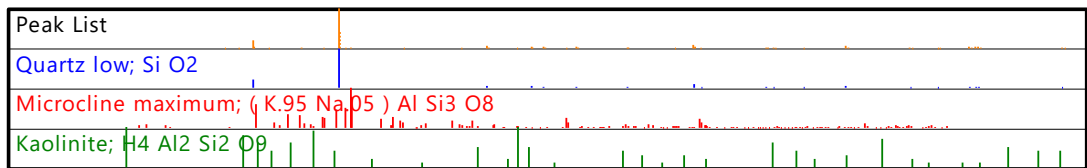
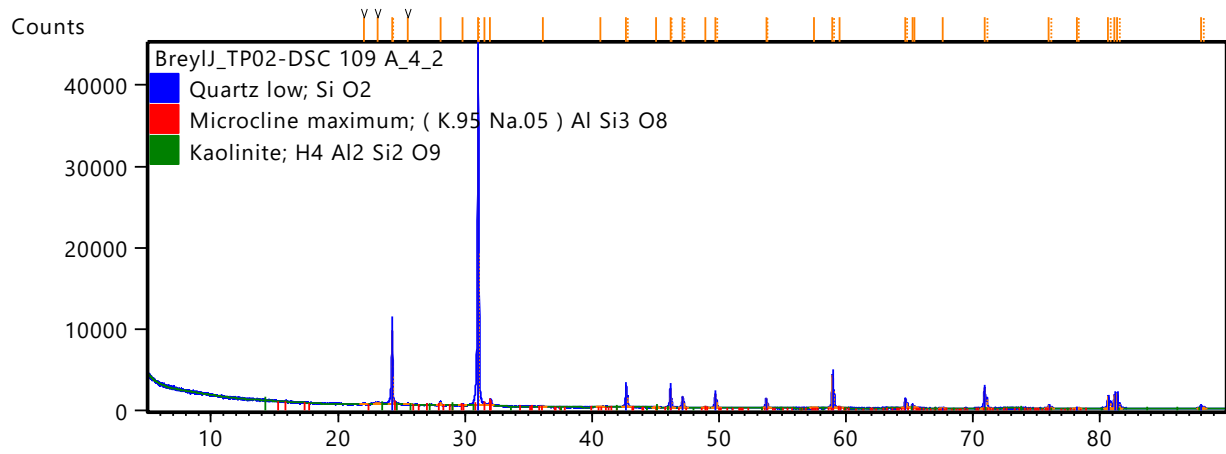
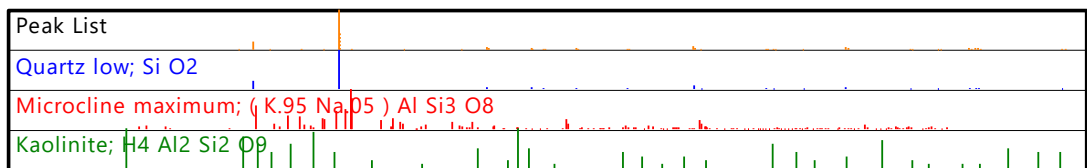
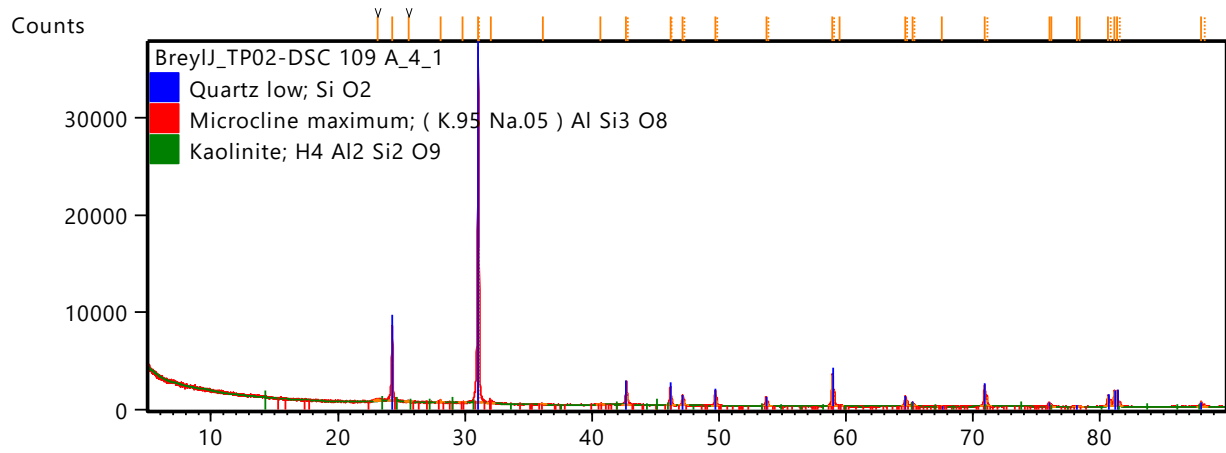
Analyst: J.E. Dykstra
XRF Analyst

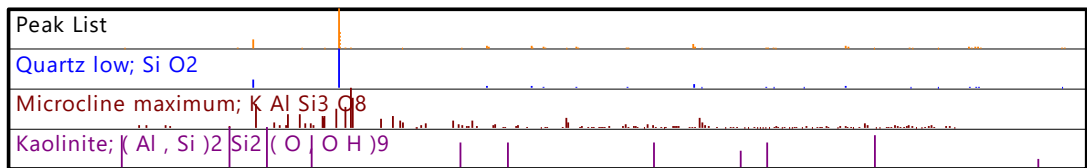
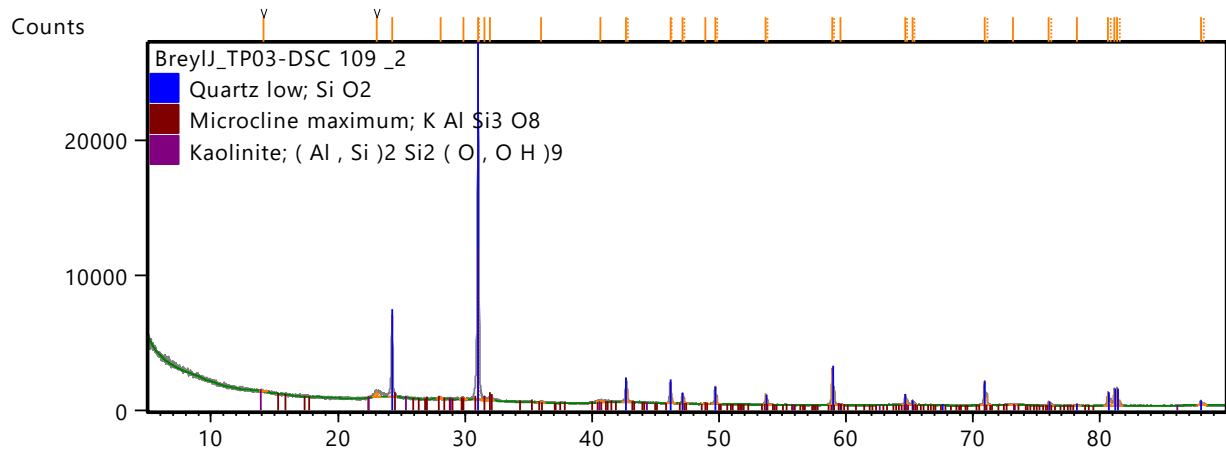
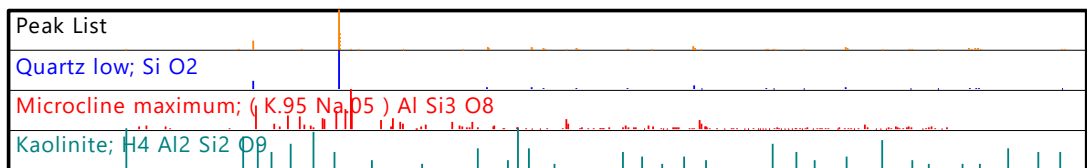
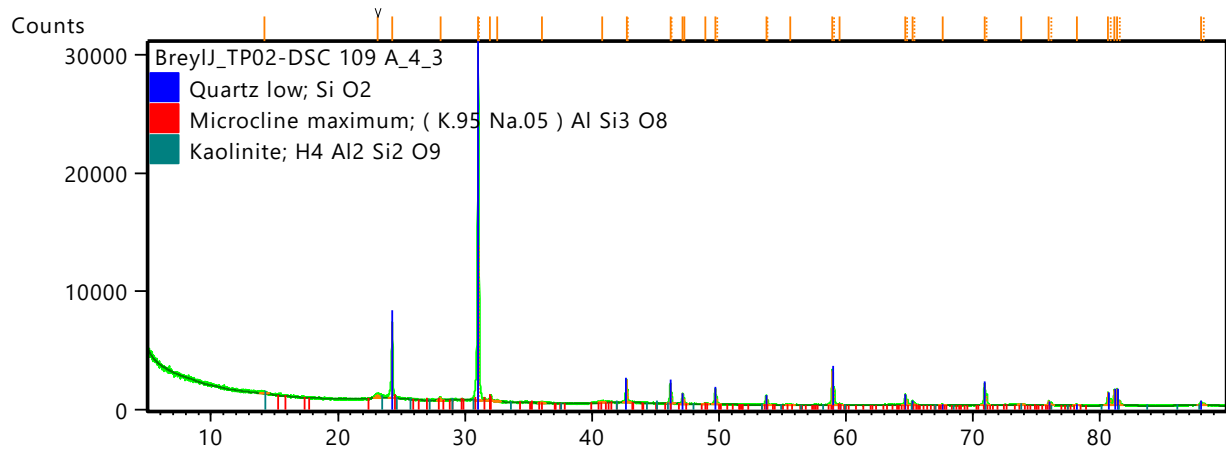
The samples were prepared according to the standardized Panalytical backloading system, which provides nearly random distribution of the particles.

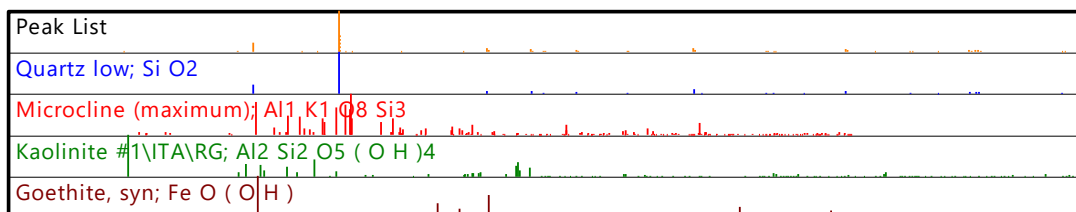
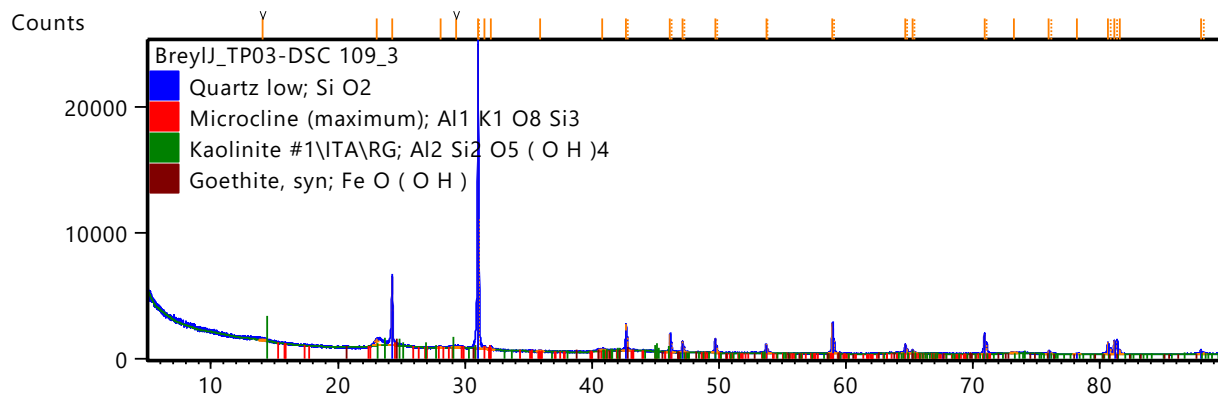
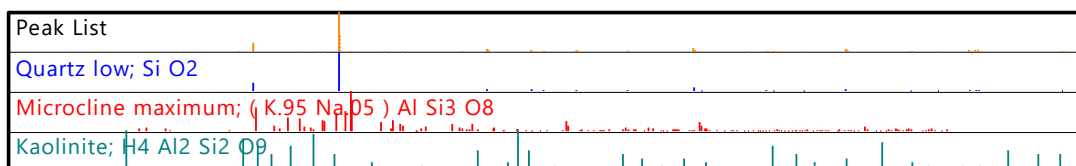
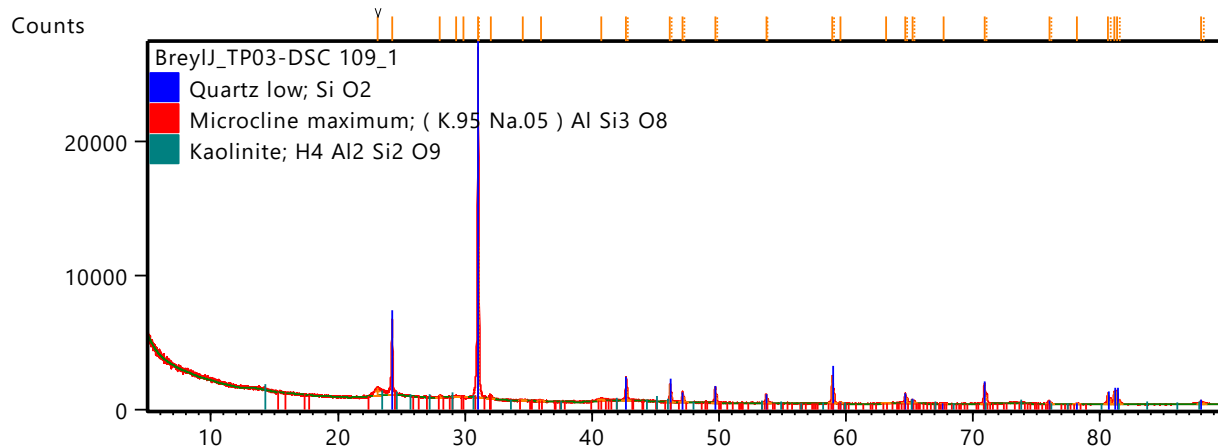
The sample were analyzed using a PANalytical X'Pert Pro powder diffractometer in $\theta-\theta$ configuration with an X'Celerator detector and variable divergence- and fixed receiving slits with Fe filtered Co-K α radiation ($\lambda=1.789\text{\AA}$). The phases were identified using X'Pert Highscore plus software.

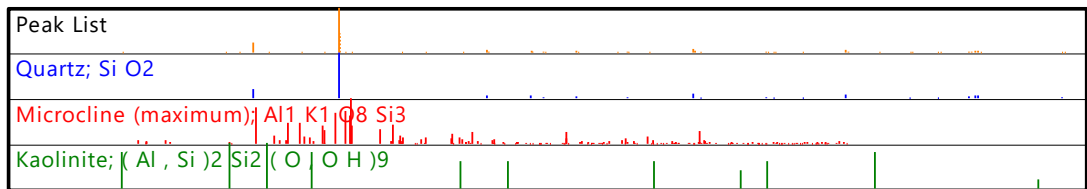
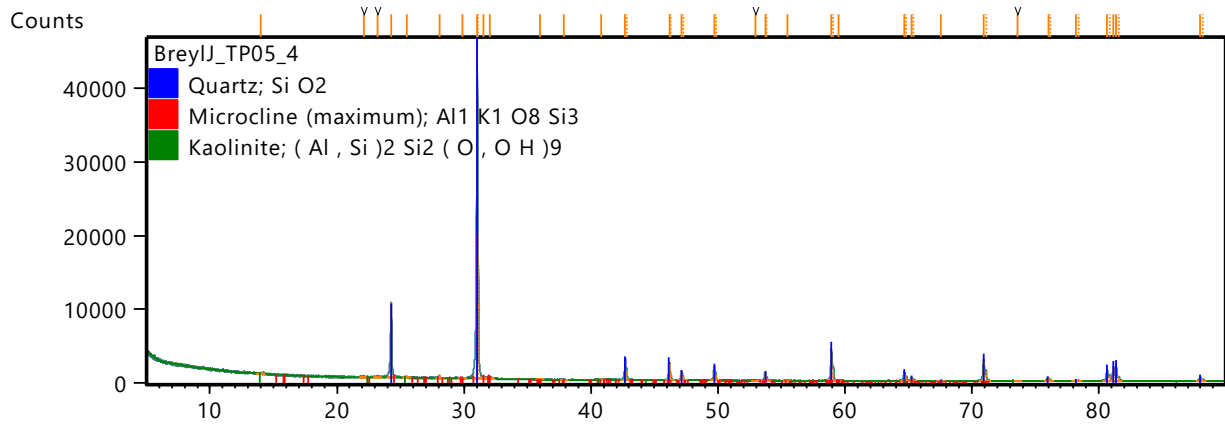
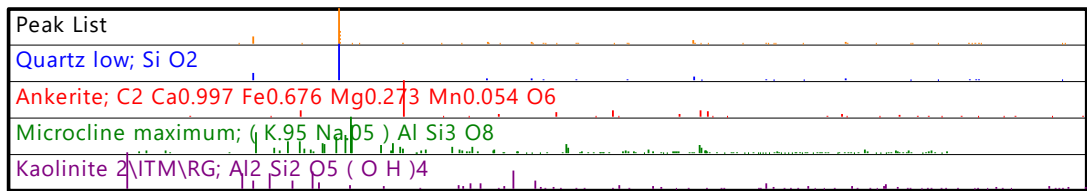
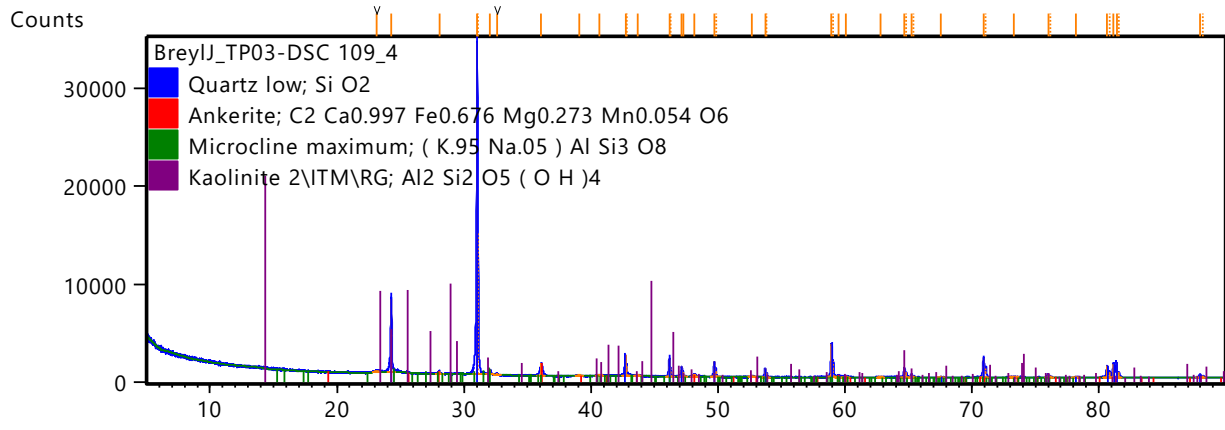
The relative phase amounts (weight%) were estimated using the Rietveld method (Autoquan Program).

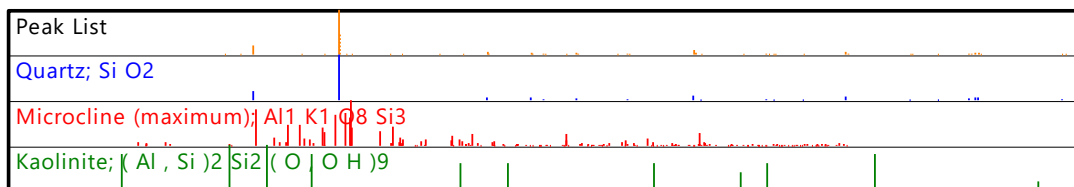
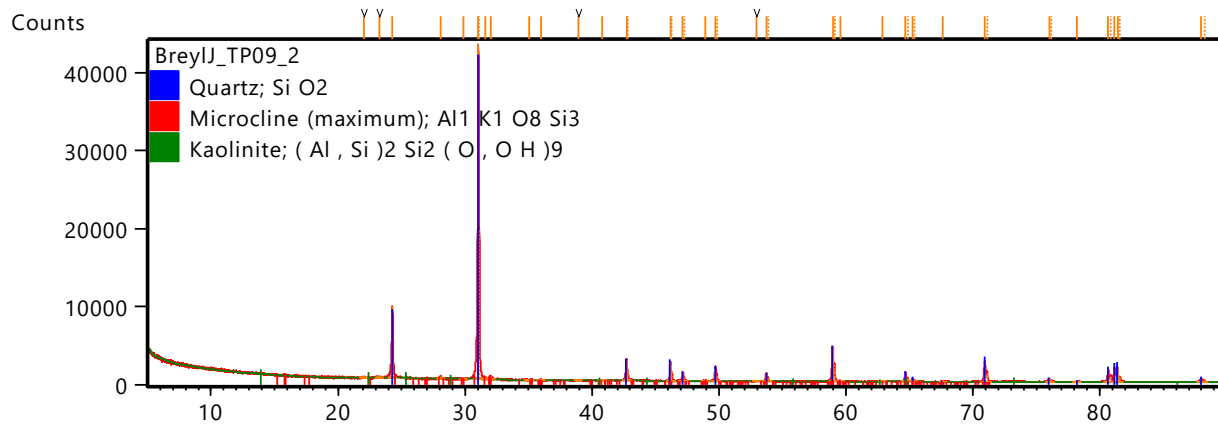
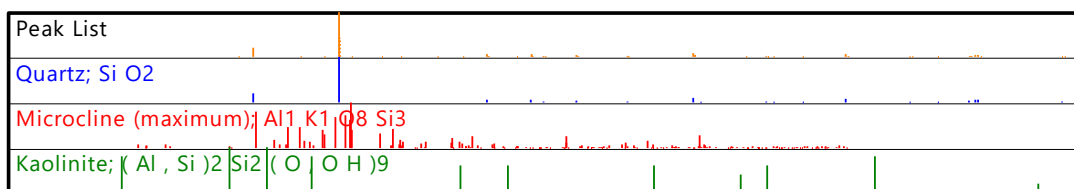
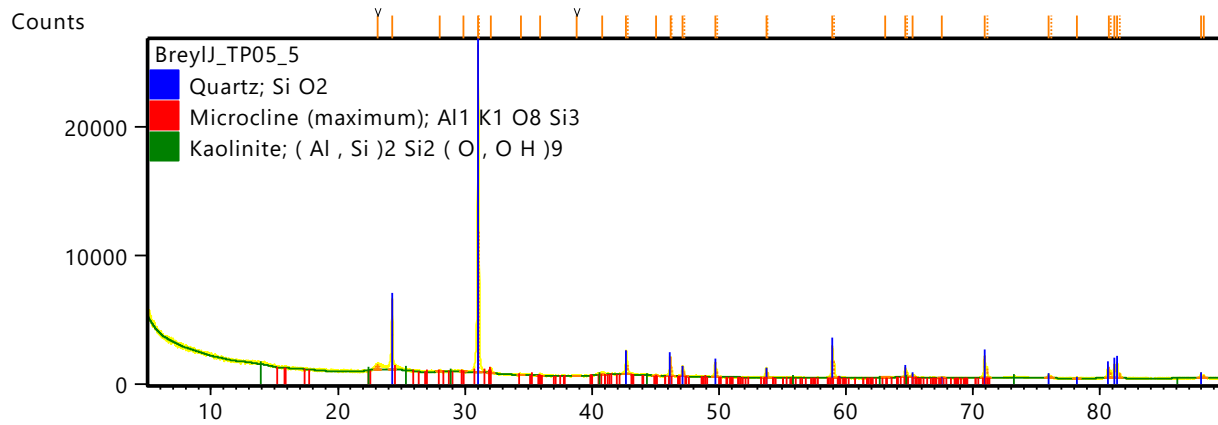


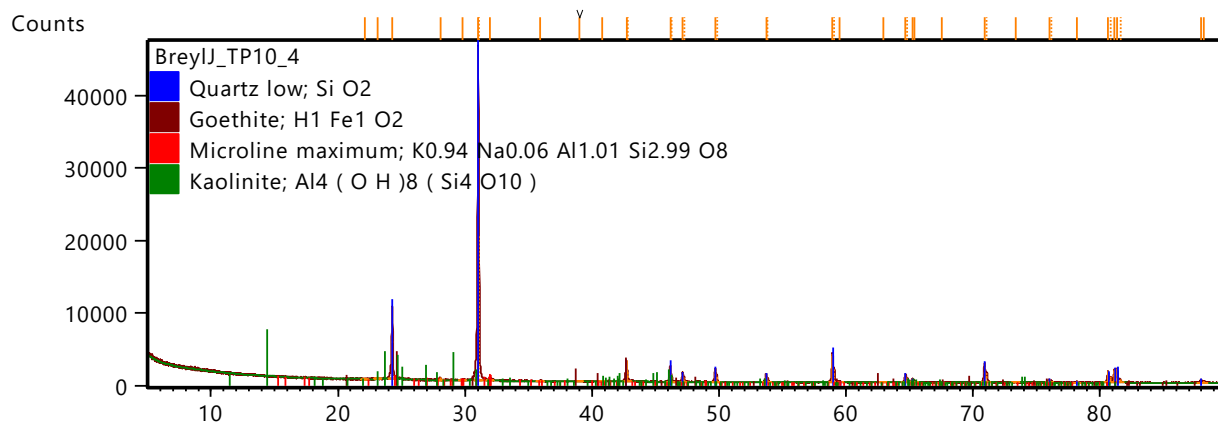
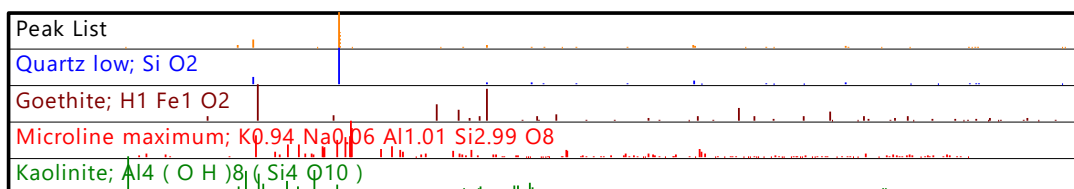
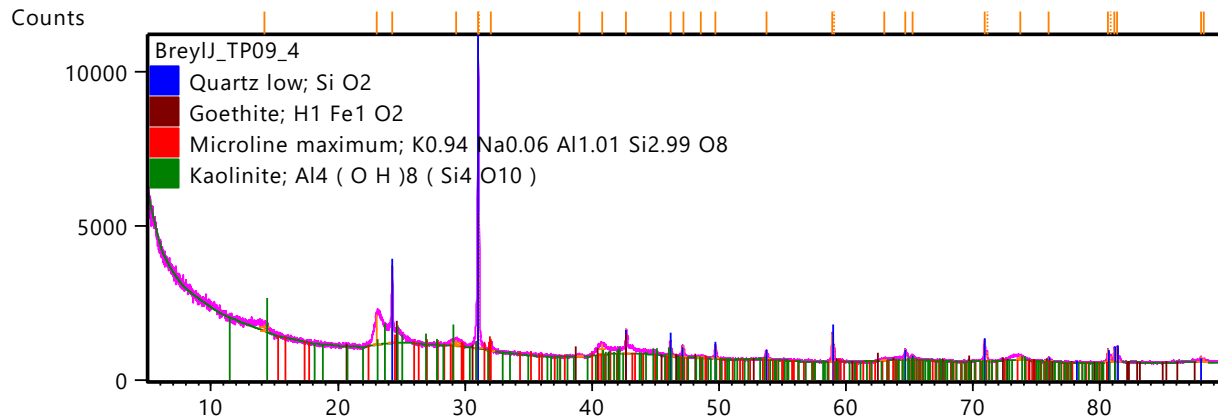


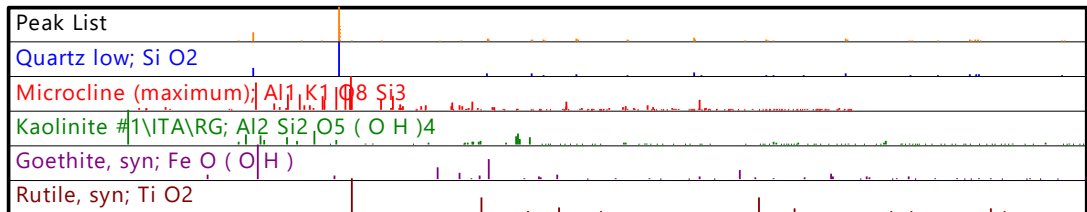
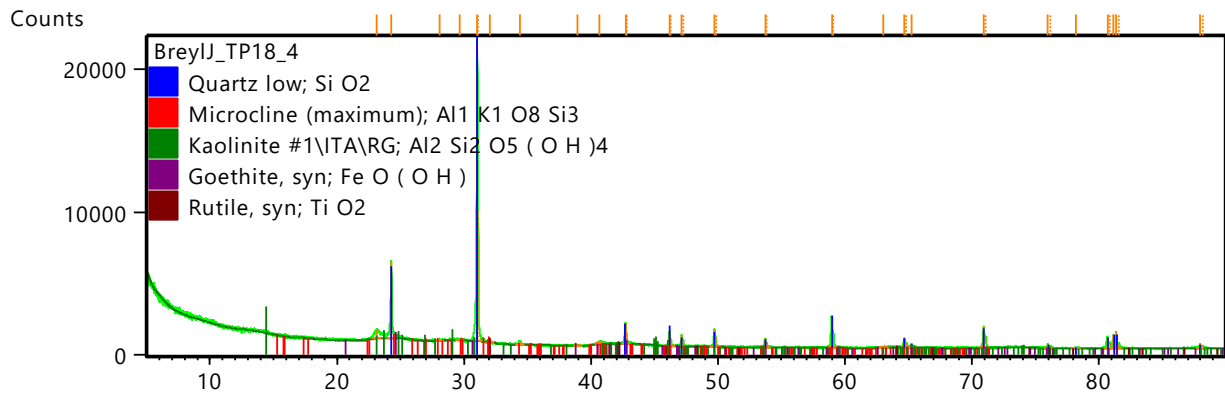
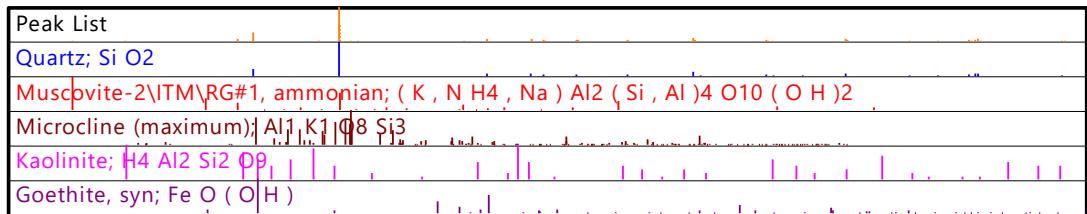
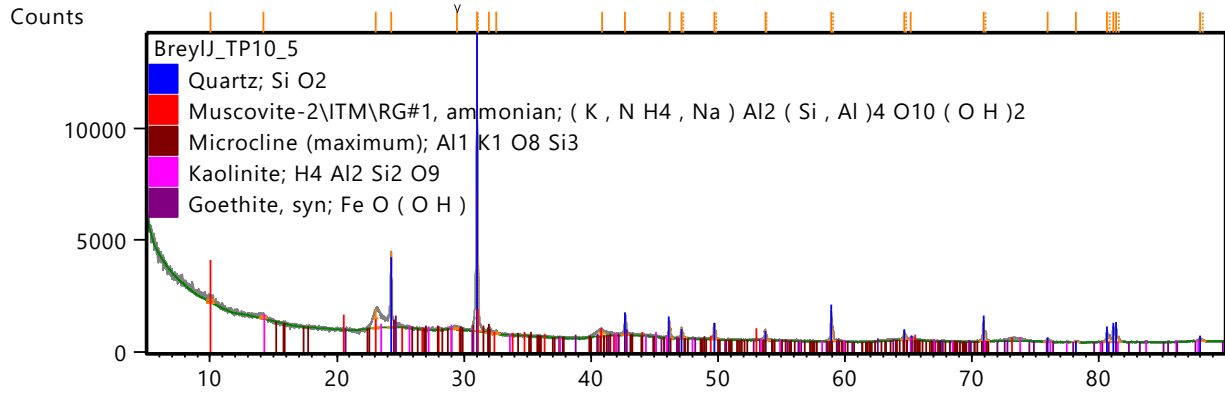


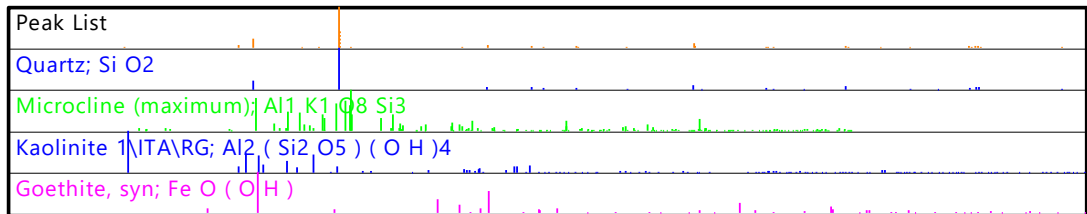
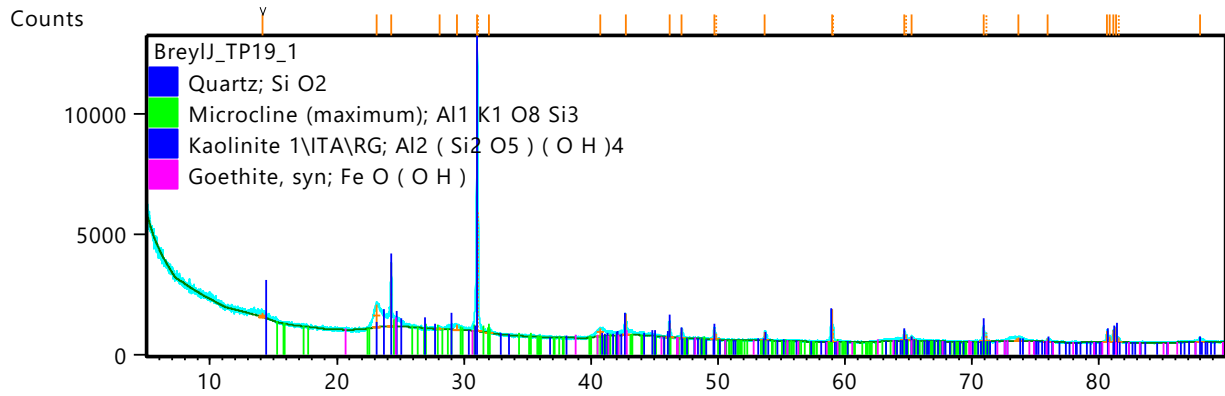
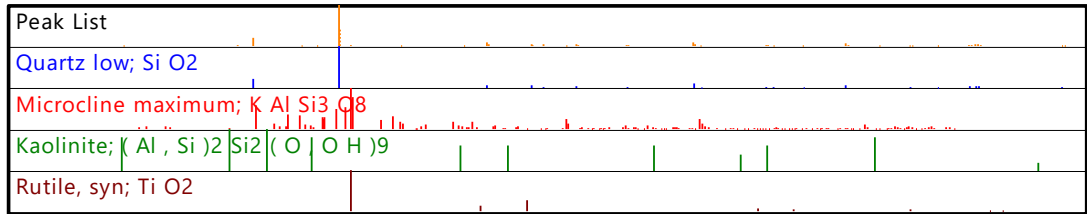
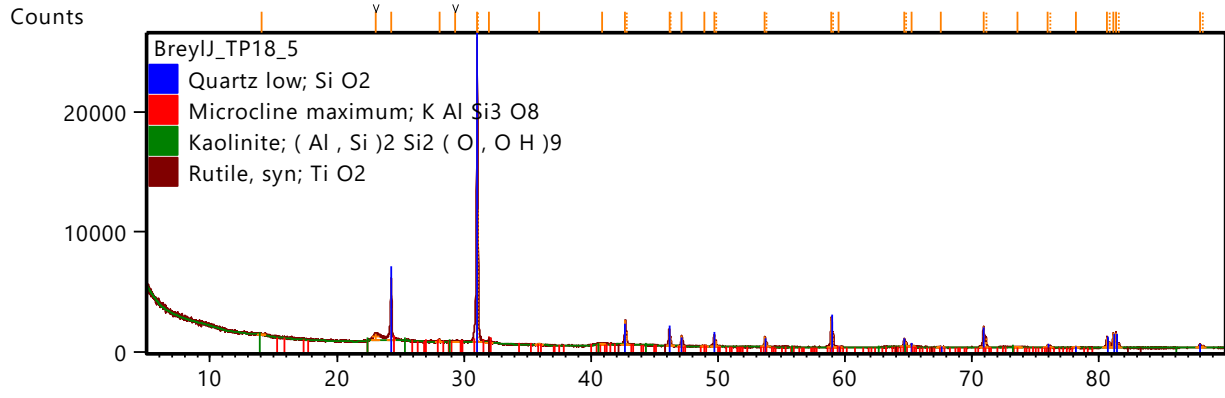


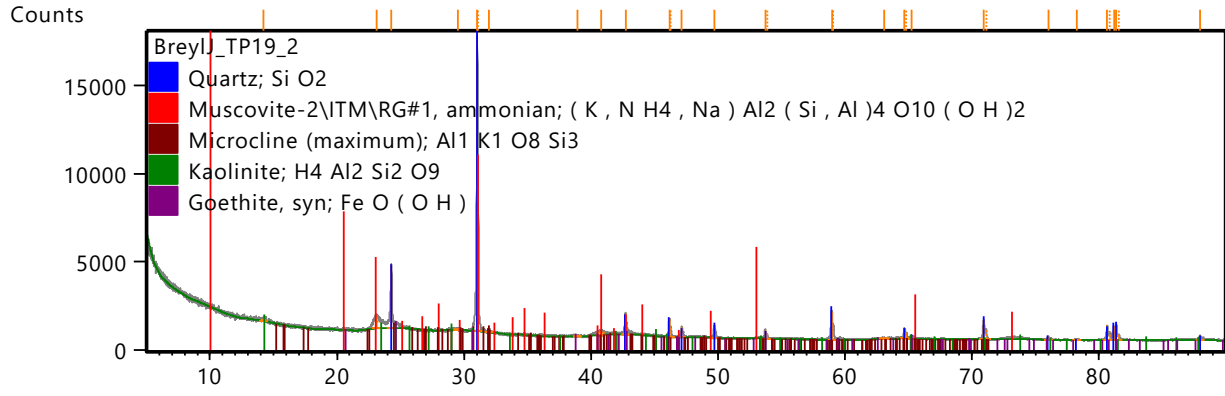




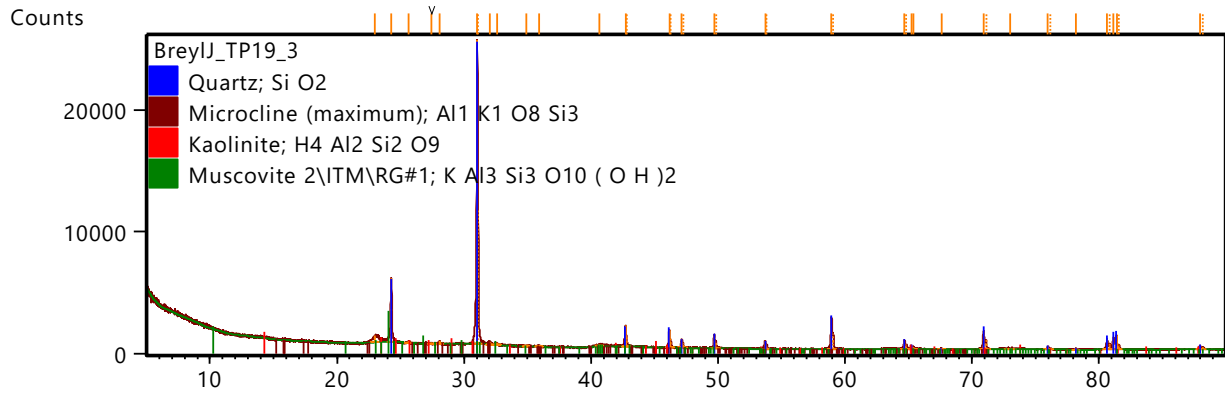




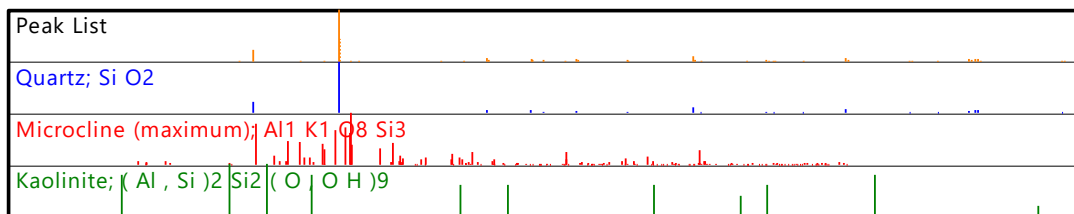
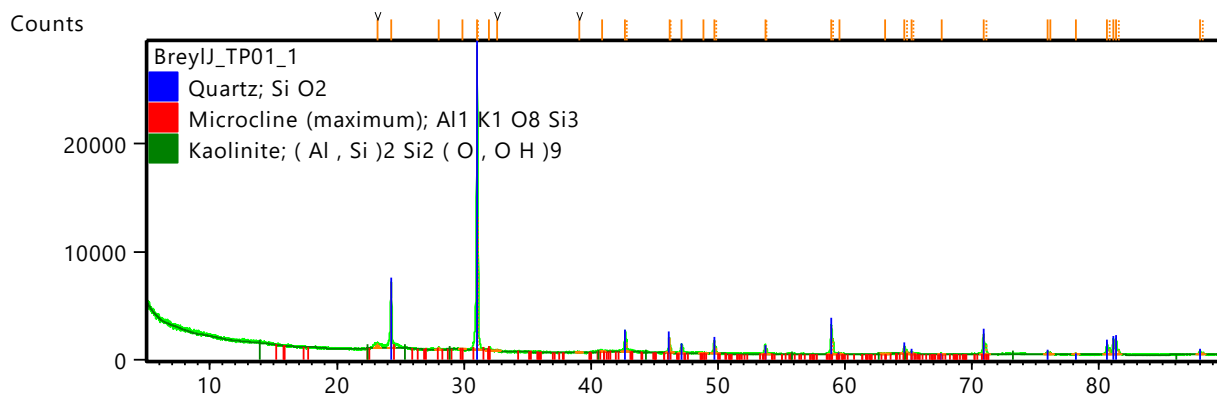
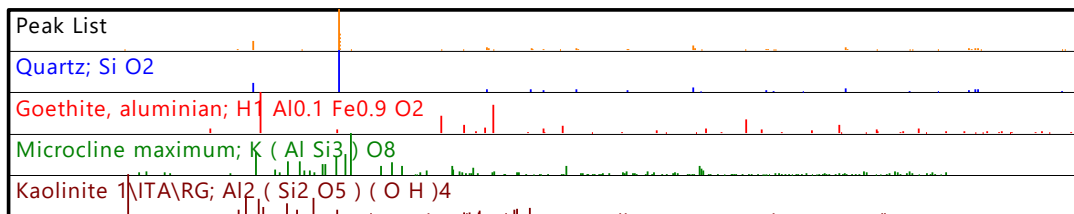
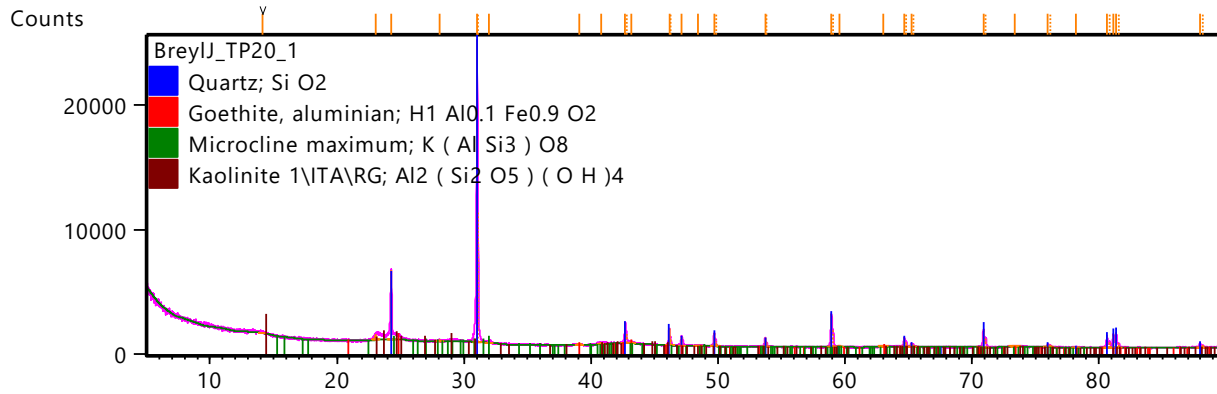




Peak List
Quartz; Si O2
Muscovite-2\ITM\RG#1, ammonian; (K , N H4 , Na) Al2 (Si , Al)4 O10 (O H)2
Microcline (maximum); Al1 K1 O8 Si3
Kaolinite; H4 Al2 Si2 O9
Goethite, syn; Fe O (O H)



Peak List
Quartz; Si O2
Microcline (maximum); Al1 K1 O8 Si3
Kaolinite; H4 Al2 Si2 O9
Muscovite 2\ITM\RG#1; K Al3 Si3 O10 (O H)2



Quantitative Results:

TP02-DSC 109A_2		TP02_DSC 109A_4-1		TP02_DSC 109A_4-2		TP02_DSC 109A_4-3	
	weight%		weight%		weight%		weight%
Microcline	1.9	Kaolinite	7.13	Kaolinite	5.01	Kaolinite	12.46
Quartz	98.1	Microcline	2.54	Microcline	4.77	Microcline	3.59
		Quartz	90.33	Quartz	90.22	Quartz	83.94
TP03DSC 109_2		TP03DSC 109_1		TP03DSC 109_3		TP03DSC 109_4	
	weight%		weight%		weight%		weight%
Kaolinite	13.02	Kaolinite	15.71	Goethite	4.95	Ankerite	9.56
Microcline	4.12	Microcline	4.69	Kaolinite	16.96	Kaolinite	7.14
Quartz	82.86	Quartz	79.6	Microcline	4.28	Microcline	3.39
				Quartz	73.81	Quartz	79.92
TP05_4		TP05_5		TP09_2		TP09_4	
	weight%		weight%		weight%		weight%
Kaolinite	4.02	Kaolinite	15.66	Kaolinite	3.97	Goethite	8.44
Microcline	2.29	Microcline	4.83	Microcline	3.14	Kaolinite	43.52
Quartz	93.69	Quartz	79.51	Quartz	92.89	Microcline	4.66
						Quartz	43.38
TP10_4		TP10_5		TP18_4		TP18_5	
	weight%		weight%		weight%		weight%
Goethite	7.51	Goethite	2.17	Goethite	4.2	Kaolinite	17.06
Kaolinite	2.19	Kaolinite	15.93	Kaolinite	19.17	Microcline	4.62
Microcline	1.11	Microcline	9.98	Microcline	4.9	Quartz	77.11
Quartz	89.19	Muscovite	11.94	Quartz	70.07	Rutile	1.21
		Quartz	59.98	Rutile	1.66		
TP19-1		TP19-2		TP19-3		TP20-1	
	weight%		weight%		weight%		weight%
Goethite	5.43	Goethite	4.36	Kaolinite	11.47	Goethite	8.14
Kaolinite	28.3	Kaolinite	19.1	Microcline	3.65	Kaolinite	17.85
Microcline	7.61	Microcline	2.46	Muscovite	7.92	Microcline	4.53
Quartz	58.66	Muscovite	11.38	Quartz	76.96	Quartz	69.48
		Quartz	62.7				
TP01_1							
	weight%						
Goethite	4.76						
Kaolinite	22.7						
Microcline	3.43						
Quartz	69.11						

B.2d) CONSOLIDATED UNDRAINED TRIAXIAL TESTS

STRESS PATHS

TP18/4

Project:

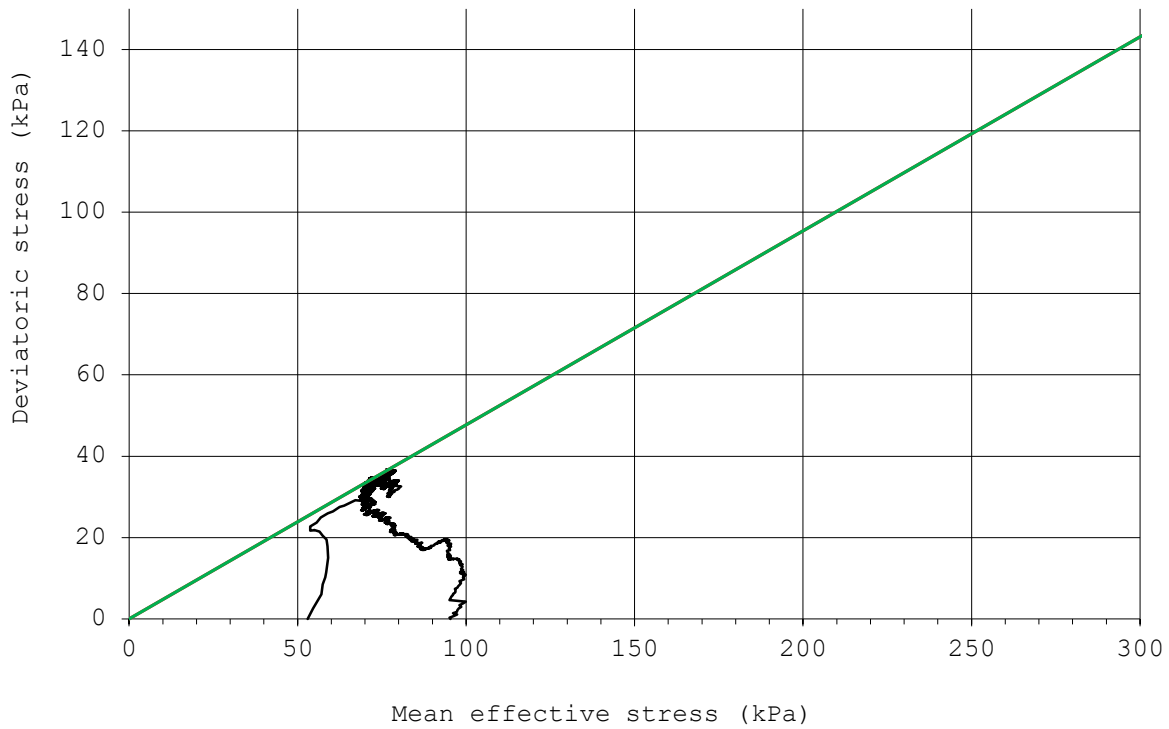
Sub-surface erosion

Sampling position:

0.5 - 2.0m

c'_{peak} (kPa) : 0
 ϕ'_{peak} (degrees) 28

$c'_{failure}$ (kPa) : 0
 $\phi'_{failure}$ (degrees) 28



CONSOLIDATED UNDRAINED TRIAXIAL TEST
WITH BASE PORE PRESSURE MEASUREMENT

P.O. Box 14679
Hatfield 0028



Tel: (012) 420-3124
sw.jacobsz@up.ac.za

STRESS PATHS

TP19/1

Project:

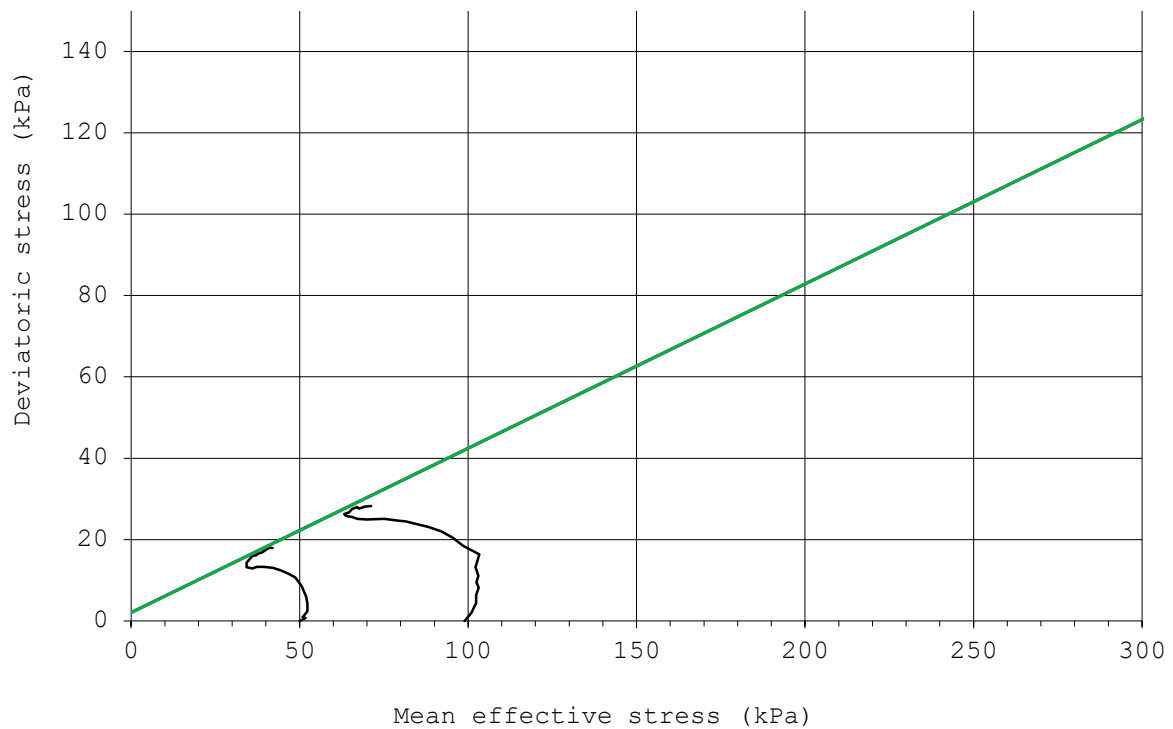
Sub-surface erosion

Sampling position:

0.5m - 2m

c'_{peak} (kPa) : 2
 ϕ'_{peak} (degrees) : 24

$c'_{failure}$ (kPa) : 2
 $\phi'_{failure}$ (degrees) : 24



CONSOLIDATED UNDRAINED TRIAXIAL TEST
WITH BASE PORE PRESSURE MEASUREMENT

P.O. Box 14679
Hatfield 0028



Tel: (012) 420-3124
sw.jacobsz@up.ac.za

STRESS PATHS

TP20/1

Project:

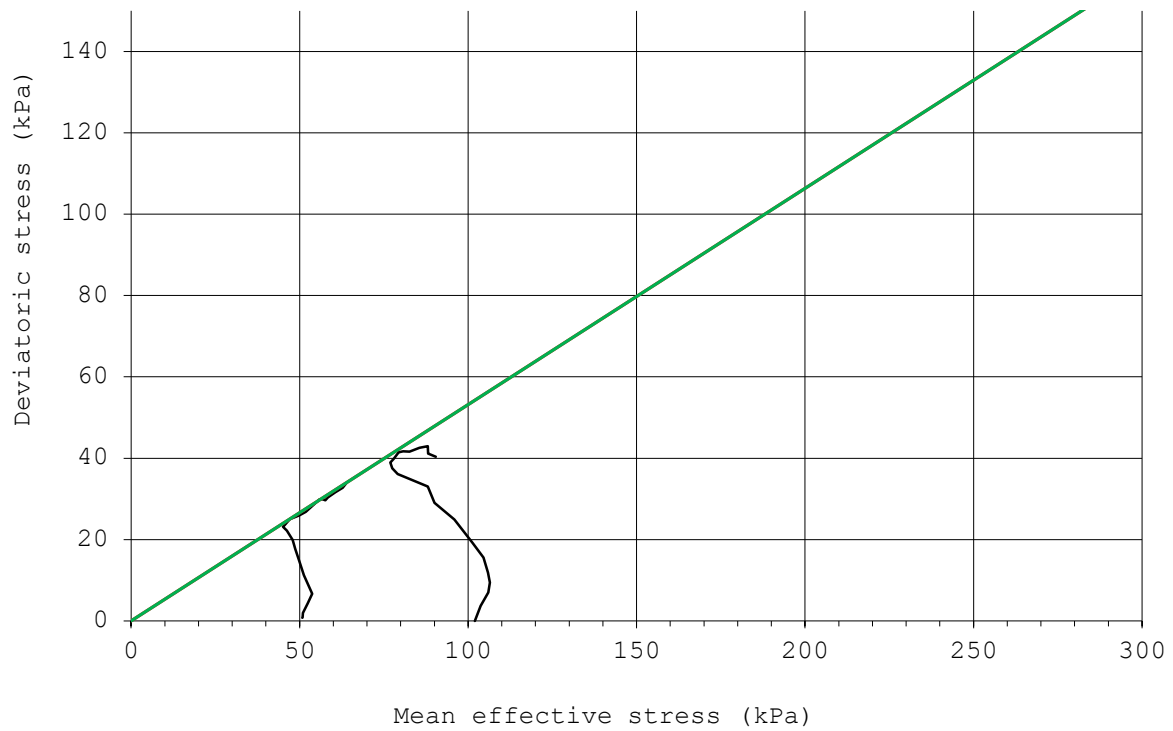
Sub-surface erosion

Sampling position:

1.3 - 3.0m

c'_{peak} (kPa) : 0
 ϕ'_{peak} (degrees) 32

$c'_{failure}$ (kPa) : 0
 $\phi'_{failure}$ (degrees) 32



CONSOLIDATED UNDRAINED TRIAXIAL TEST
WITH BASE PORE PRESSURE MEASUREMENT

P.O. Box 14679
Hatfield 0028



Tel: (012) 420-3124
sw.jacobsz@up.ac.za

B.2e) TRAXIAL PERMEABILITY TESTS

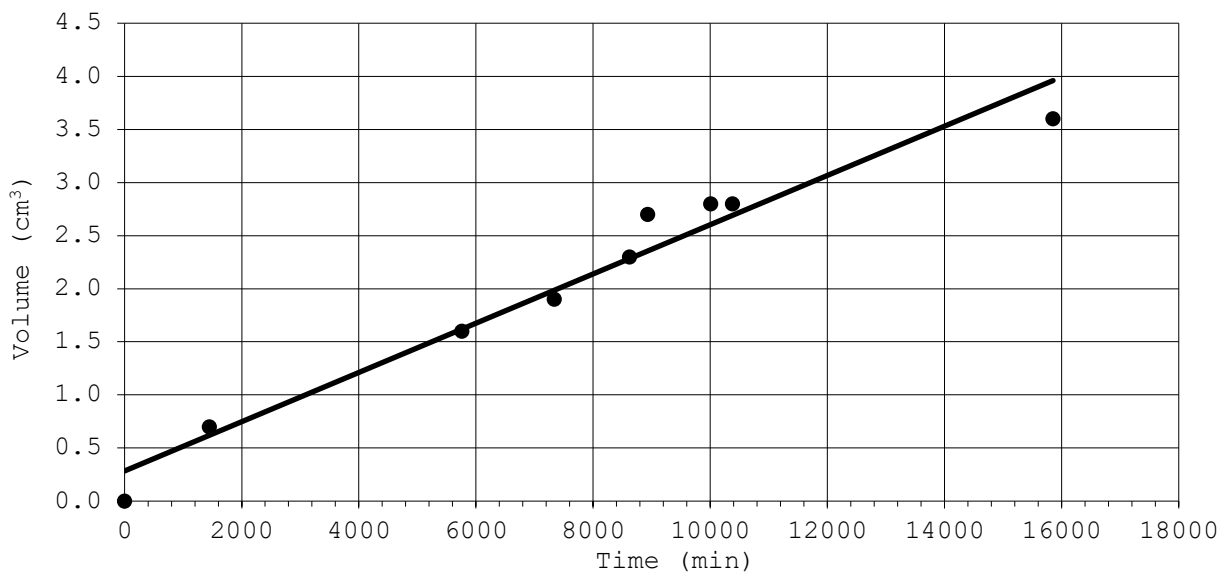
PERMEABILITY STAGE

Project: Sub-surface erosion
Sampling position: 0.5 - 2.0m
Sample no: TP18-4 Block 4/14 100kPa

Volumetric strain prior to permeability stage (%): 3.87
 Flow direction: upwards

Time (min)	Cell press. (kPa)	Pore press. bottom (kPa)	Back press. top (kPa)	Vol. (cm ³)	Vol. change (cm ³)	Flow rate (cm ³ /s)	Perm. (cm/s)
0	300	205	195	0.0			
1445	300	205	195	0.7	0.7	8.1E-06	2.3E-08
5760	300	205	195	1.6	0.9	3.5E-06	9.8E-09
7336	300	205	195	1.9	0.3	3.2E-06	9.0E-09
8623	300	205	195	2.3	0.4	5.2E-06	1.5E-08
8930	300	205	195	2.7	0.4	2.2E-05	6.2E-08
10006	300	205	195	2.8	0.1	1.5E-06	4.4E-09
10380	300	205	195	2.8	0.0	0.0E+00	0.0E+00
15853	300	205	195	3.6	0.8	2.4E-06	6.9E-09

Average Permeability (cm/s): 1.1E-08



TRIAxIAL PERMEABILITY TEST

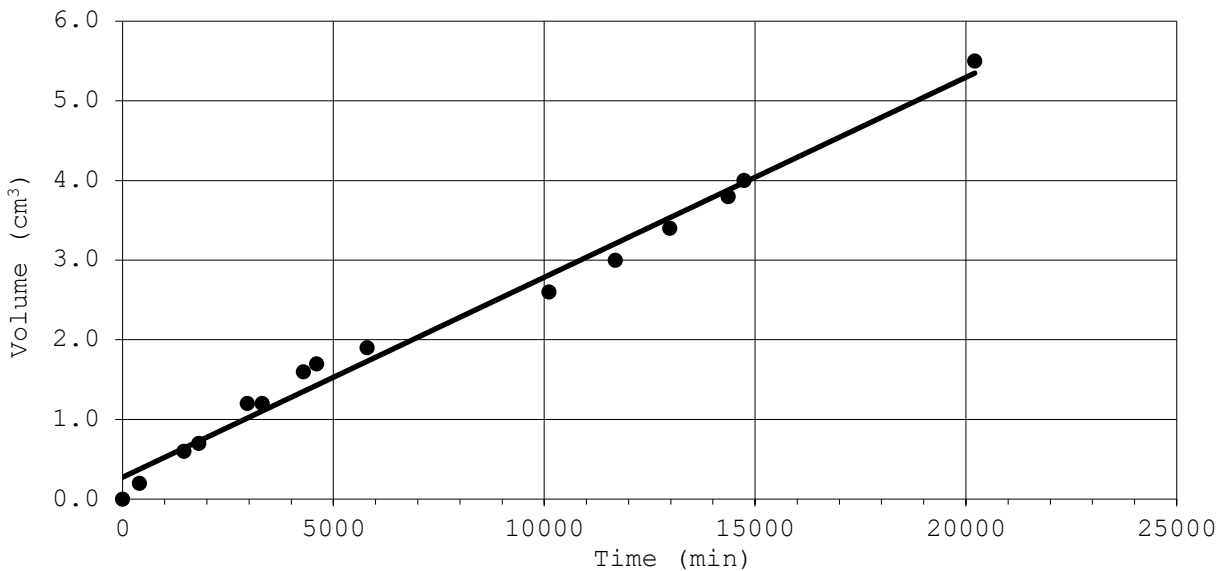
PERMEABILITY STAGE

Project: Sub-surface erosion
Sampling position: 0.5m - 2m
Sample no: TP19-1 Block 1/6 100kPa

Volumetric strain prior to permeability stage (%): 2.78
 Flow direction: upwards

Time (min)	Cell press. (kPa)	Pore press. bottom (kPa)	Back press. top (kPa)	Vol. (cm ³)	Vol. change (cm ³)	Flow rate (cm ³ /s)	Perm. (cm/s)
0	400	305	295	0.0			
397	400	305	295	0.2	0.2	8.4E-06	2.4E-08
1455	400	305	295	0.6	0.4	6.3E-06	1.8E-08
1807	400	305	295	0.7	0.1	4.7E-06	1.3E-08
2960	400	305	295	1.2	0.5	7.2E-06	2.1E-08
3307	400	305	295	1.2	0.0	0.0E+00	0.0E+00
4284	400	305	295	1.6	0.4	6.8E-06	1.9E-08
4597	400	305	295	1.7	0.1	5.3E-06	1.5E-08
5797	400	305	295	1.9	0.2	2.8E-06	7.9E-09
10107	400	305	295	2.6	0.7	2.7E-06	7.7E-09
11688	400	305	295	3.0	0.4	4.2E-06	1.2E-08
12973	400	305	295	3.4	0.4	5.2E-06	1.5E-08
14359	400	305	295	3.8	0.4	4.8E-06	1.4E-08
14736	400	305	295	4.0	0.2	8.8E-06	2.5E-08
20210	400	305	295	5.5	1.5	4.6E-06	1.3E-08

Average Permeability (cm/s): 1.2E-08



TRIAXIAL PERMEABILITY TEST

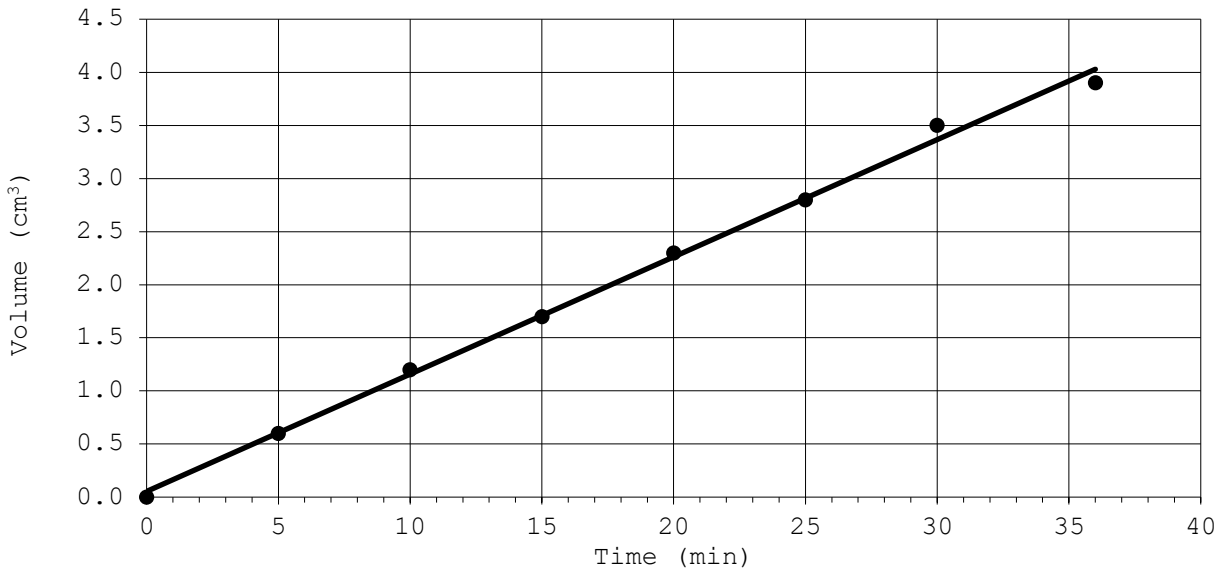
PERMEABILITY STAGE

Project: Sub-surface erosion
Sampling position: 1.3 - 3.0m
Sample no: TP20-1 Block 2/14 100kPa

Volumetric strain prior to permeability stage (%): 1.76
 Flow direction: upwards

Time (min)	Cell press. (kPa)	Pore press. bottom (kPa)	Back press. top (kPa)	Vol. (cm ³)	Vol. change (cm ³)	Flow rate (cm ³ /s)	Perm. (cm/s)
0	300	205	195	0.0			
5	300	205	195	0.6	0.6	2.0E-03	8.5E-06
10	300	205	195	1.2	0.6	2.0E-03	8.5E-06
15	300	205	195	1.7	0.5	1.7E-03	7.1E-06
20	300	205	195	2.3	0.6	2.0E-03	8.5E-06
25	300	205	195	2.8	0.5	1.7E-03	7.1E-06
30	300	205	195	3.5	0.7	2.3E-03	1.0E-05
36	300	205	195	3.9	0.4	1.1E-03	4.7E-06

Average Permeability (cm/s): 7.9E-06



TRIAxIAL PERMEABILITY TEST